LBL--31855

DE93 001537

NUCLEAR SCIENCE DIVISION

Annual Report for 1991

Division Director
T. J. M. Symons

Deputy Division Director
Janis M. Dairiki

Editor
W. D. Myers

Lawrence Berkeley Laboratory
University of California
Berkeley, California 94720, USA

This work was supported by the Director, Office of Energy Reserach, Office of High Energy and Nuclear Physics, Division of Nuclear Physics and by the Office of Basic Energy Sciences, Division of Nuclear Sciences, of the U.S. Department of Energy under Contract No. DE-AC03-76SF00098

Table of Contents

Introduction and Overviews

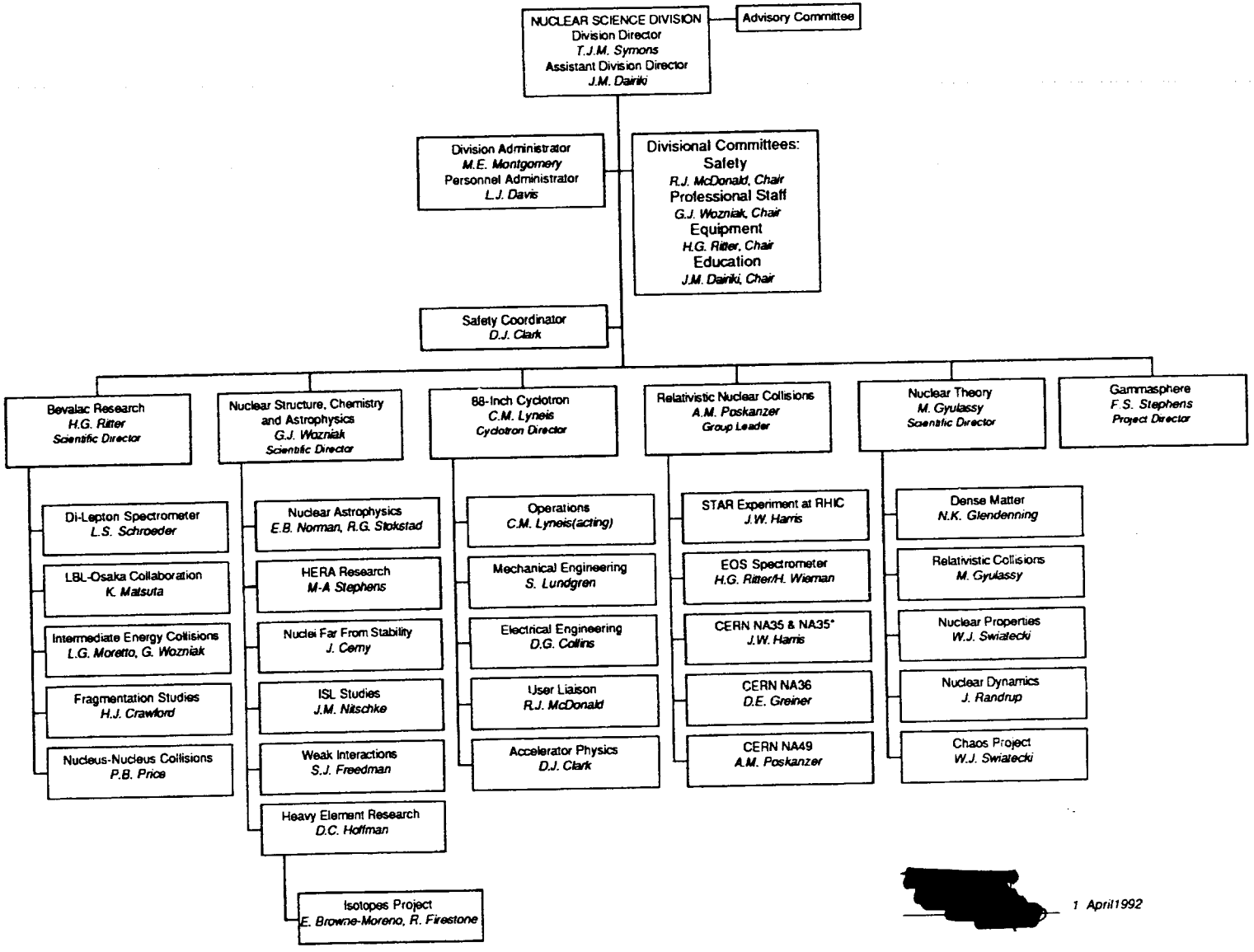
NUCLEAR SCIENCE DIVISION
Division Director
T.J.M. Symons
Assistant Division Director
J.M. Dairiki
Advisory Committee
Division Administrator
M.E. Montgomery
Personnel Administrator
L.J. Davis
Divisional Committees:
Safety
R.J. McDonald, Chair
Professional Staff
G.J. Wozniak, Chair
Equipment
H.G. Ritter, Chair
Education
J.M. Dairiki, Chair
Safety Coordinator
D.J. Clark
Bevalac Research
H.G. Ritter
Scientific Director
Nuclear Structure, Chemistry and Astrophysics
G.J. Wozniak
Scientific Director
88-Inch Cyclotron
C.M. Lyneis
Cyclotron Director
Relativistic Nuclear Collisions
A.M. Poskanzer
Group Leader
Nuclear Theory
M. Gyulassy
Scientific Director
Gammasphere
F.S. Stephens
Project Director
Di-Lepton Spectrometer
L.S. Schroeder
LBL-Osaka Collaboration
K. Matsuta
Intermediate Energy Collisions
L.G. Moretto, G. Wozniak
Fragmentation Studies
H.J. Crawford
Nucleus-Nucleus Collisions
P.B. Price
Nuclear Astrophysics
E.B. Norman, R.G. Stokstad
HERA Research
M-A Stephens
Nuclei Far From Stability
J. Cerny
ISL Studies
J.M. Nitschke
Weak Interactions
S.J. Freedman
Heavy Element Research
D.C. Hoffman
Isotopes Project
E. Browne-Moreno, R. Firestone
Operations
C.M. Lyneis(acting)
Mechanical Engineering
S. Lundgren
Electrical Engineering
D.G. Collins
User Liaison
R.J. McDonald
Accelerator Physics
D.J. Clark
STAR Experiment at RHIC
J.W. Harris
EOS Spectrometer
H.G. Ritter/H. Wieman
CERN NA35 & NA35*
J.W. Harris
CERN NA36
D.E. Greiner
CERN NA49
A.M. Poskanzer
Dense Matter
N.K. Glendenning
Relativistic Collisions
M. Gyulassy
Nuclear Properties
W.J. Swiatecki
Nuclear Dynamics
J. Randrup
Chaos Project
W.J. Swiatecki

1 April1992

Introduction

T.J.M. Symons

This report describes the activities of the Nuclear Science Division for the year ending December 31, 1991. This was a period during which several important decisions were taken at the National level which will have long term consequences for our programs.

The first was the decision taken in August 1991 to start fabrication of the Gammasphere detector following a successful cost, schedule and management review. Gammasphere is a large new gamma-ray detector array which will be the centerpiece of the nuclear structure program in the United States. Completion of the detector is scheduled in 1994 to be followed by an initial running period at the 88-Inch Cyclotron. However, activities in preparation for the arrival of Gammasphere are already well under way at building 88 and first operation with a partial array is expected in January 1993.

Later in the same month, the Program Advisory Committee at Brookhaven National Laboratory recommended approval of the STAR experiment at the relativistic heavy ion collider (RHIC). This new detector involving participants from twenty four institutions will be a major component of the experimental program at RHIC. STAR was conceived within the Nuclear Science Division and much of the initial design work has been done here. Although RHIC is not scheduled to operate until 1997, it will require a major effort by all of the collaborators to bring the detector into operation at that time.

On a less happy note, the Department of Energy organized a high level panel chaired by Professor Charles Townes to give advice on scientific priorities during the next decade. As a result of this committee's report and of recommendations by the Nuclear Science Advisory Committee, a decision was taken to phase out nuclear physics funding at the Bevalac two years earlier than had been planned. This will have a major impact on several of our research projects, especially the EOS time projection chamber and dilepton spectrometer.

These three decisions set the direction for the Nuclear Science Division's activities in nuclear structure and relativistic heavy ion research. In addition, we have a growing program in nuclear astrophysics and fundamental interactions with major participation in the Sudbury Neutrino Observatory. Together these three major projects, Gammasphere, STAR and SNO will provide the backbone of our program for several years to come.

In the short term, however, much exciting research is being done, using our accelerators here at LBL and also using facilities at Michigan State University and at CERN. We also have a very lively program in nuclear theory and an innovative group working on nuclear data evaluation.

Finally, as always it is a pleasure to acknowledge the enthusiasm and hard work of the staff and visitors who have contributed to this report, and of Bill Myers who edited it.

Low-Energy Research Program

G. J. Wozniak

The Nuclear Science Division's efforts in the broad area of low-energy nuclear physics include studies of nuclear structure, chemistry, astrophysics, weak interactions, and heavy-ion reaction mechanisms. Main themes are the effects of high angular momentum, extremes in isospin and nuclear charge (the heaviest elements) and exotic modes of decay. Following an overview of the highlights of this research, recent developments at the 88-Inch Cyclotron, where a significant portion of this work has been carried out, are mentioned.

The focus of studies in high-spin nuclear structure continues to be on superdeformed nuclei. During the last several years, many new superdeformed bands (SD) have been discovered at the Cyclotron. A major effort has been undertaken to map out the boundaries of superdeformation in the region around A ~190, where about 25 SD bands have been experimentally observed. With the discovery of a SD band in ^{198}Pb, this region of superdeformation has been extended to N = 116. Many of these bands show similar moments of inertia and "identical" transition energies. With discovery that a nucleus may contain more than one superdeformed band, an intensive effort has been undertaken to find examples of such multiple SD bands. The more powerful Gammasphere array will greatly facilitate the study of weakly populated SD bands and allow the investigation of superdeformation in new regions previously inaccessible with HERA.

The study of the transuranic elements has three aspects - the reaction mechanisms by which they are produced, the chemistry of the short-lived atoms, and the properties of their nuclear decay. Recently, Hoffman and collaborators have been investigating the chemical properties of the heaviest elements. The chemistry of high-Z atoms is influenced by the effects of relativity on the valence electrons which could affect their chemical properties. Several experiments on the chemistry of ^{261}Rf (element number 104) have been conducted. Their results show that Rf behaves similarly to the group IV element Zr. Radiochemical techniques were essential to the discovery of the two new isotopes, ^{252}Bk and ^{253}Bk. A new non-accelerator program to study the chemical behavior of plutonium in groundwater has also been undertaken.

The mechanisms by which heavy ions react is a subject of broad interest that is approached in many different ways at the Cyclotron and by using other accelerators as well. Beams of ^{63}Cu at 12.6 MeV/nucleon have been used in reverse kinematics with light targets of ^{12}C and ^{27}Al to investigate the conditional barriers for fission and the production of complex fragments. These studies (by the Moretto/Wozniak group) are also carried out with higher energy, heavier beams at the K1200 Cyclotron and the Bevalac. Fragmentation of the target has been studied using radiochemical techniques and a wide range of

bombarding energies at the Cyclotron and at several other accelerators by the Loveland and Seaborg groups. The Stokstad/Chan group has used much lighter projectiles, such as ^{16}O and ^{20}Ne at 32 MeV/nucleon to produce projectile-like nuclei with excitation energies up to about 5 MeV/nucleon and to observe their decay into as many as five fragments.

The spectroscopy of nuclei far from stability begins with the production and identification of a new nuclide, proceeds to the measurement of its mass and decay properties, and ultimately to the study of its (or its daughter's) level structure. The new isotopes ^{252}Bk and ^{253}Bk mentioned above were observed recently at the 88-Inch Cyclotron. The OASIS group has studied neutron-deficient nuclei in the region Z=54-71. Using their on-line isotope separator, the decay properties of ^{155}Lu, ^{155}Yb, ^{155}Tm, ^{151}Er, and ^{151}Ho have been investigated. In a study of the α emitters above N = 82, isomer excitation energies and precise α-branching ratios were measured. Lighter and shorter-lived proton-rich nuclei are studied at the 88-Inch Cyclotron by the Cerny group. Recently they produced the nucleus ^{39}Ti and observed its β-delayed two-proton decay. The heaviest member of the T_z = -3/2, A = 4n+1 series, ^{65}Se has been produced and its β-delayed proton emission observed.

An experimental result that has aroused very wide interest has been the Norman group's study of the β-decay spectrum of ^{14}C. This was measured with a Ge detector that had been doped with ^{14}C. At the upper end of the spectrum, in the region around 140 keV, the spectrum deviates from the standard prediction in a manner that is consistent with the emission of a neutrino of mass (~17 keV) with a probability of (~1)%. Similar results have been reported by other investigators using Si or Ge detectors. However, magnetic spectrometer measurements have not seen such an effect. To see whether this could be due to some unknown property of crystalline solid state devices, a high-pressure ionization chamber has been constructed which is capable of handling both solid and gaseous radioactive sources.

During the last year a new group was formed, under the leadership of Prof. Stuart Freedman, to study weak interactions. The discovery that certain neutral atoms can be easily cooled and manipulated with laser light provides the exciting opportunity to study nuclear-beta decay with unprecedented precision. In traps, atoms are essentially free, so a trap is like an atomic beam, but without the unpleasant limitations arising from motion along the beam axis. Moreover, trapped atoms can easily be polarized without the limitation of wall relaxation inevitable when atoms are stored in cells. The β-decay asymmetry of ^{21}Na will be measured for the purpose of studying the structure of the charge-changing weak currents and to test the hypothesis that the weak interaction should be represented by a purely left-handed theory at the most fundamental level. Previously, the trapping of cold ^{23}Na as been demonstrated. Currently a more sophisticated trapping apparatus is being constructed to do further tests on stable sodium. Work is in progress at producing ^{21}Na from the (p, α) reaction on

^{24}Mg. An atomic beam of ^{21}Na will be extracted from an oven, cooled with laser light, and then trapped using the techniques developed with stable sodium.

The Nuclear Science Division (NSD) is involved in two major construction projects in low-energy nuclear physics. The Sudbury Neutrino Observatory is a heavy-water neutrino detector to be located more than a mile underground in a mine in Sudbury, Ontario. The U.S. is providing a portion of the funding for this project. The NSD is designing the structure to support the approximately ten thousand phototubes that will record Cherenkov light from neutrino-induced reactions. In addition, the NSD group has assumed major responsibility for limiting contamination due to low-level background radioactivity. The second major project is Gammasphere, which will be built and initially operated at the 88-Inch Cyclotron for the international nuclear-structure community. Gammasphere will consist of 110 Compton-suppressed Ge detectors and will be the major new detector facility for the low-energy community.

In February of 1991, the Glenn T. Seaborg Institute for Transactinium Science was jointly established by LBL and LLNL. The Institute will be devoted to the study of the transactinium elements with special emphasis on education and training of the future generations of scientists in heavy-element research. Prof. Darleane Hoffman has been appointed as the first Director.

The 88-Inch Cyclotron is a national facility and experiments in nuclear science are allocated beam time on the basis of recommendations made by a Program Advisory Committee. Although a separate and more complete overview of the operation of this facility is contained in this report, several significant developments will be mentioned here. The continued technical development of the Cyclotron is essential to the future of the low-energy research program of the Division. The significant developments in this area are threefold. The development of high-temperature ovens for the ECR source has expanded the range of metallic ion beams. The introduction of an electron gun as a supplementary source of electrons for the ECR source is new and shows promise for improving both performance and operation. The successful testing of the Advanced ECR source indicates that it will provide heavier beams at significantly higher energies.

Nuclear Science Division Personnel and Collaborators in Low-Energy Nuclear Research

Many of the experiments described in the following one-page contributions to this annual report involve collaborations among NSD personnel and scientists from other institutions. The nature and extent of these collaborations varies widely — from single experiments to programs that have continued for decades. Although the following list containing NSD personnel and collaborating scientists and their institutions cannot convey this variety, it will give recognition to the important role of collaborative work in low-energy nuclear science. The

membership of the large collaborations, which are now constructing Gammasphere and the Sudbury Neutrino Observatory, has not been included. Also, the work of groups using the low-energy national facilities without collaboration from NSD scientists has not been covered in this annual report.

Graduate students and undergraduate students are indicated by an asterisk and double asterisks, respectively. Leaders of the NSD groups are indicated in **bold face**. The period covered is approximately 1991.

High Energy Resolution Array

R.M. Diamond, F.S. Stephens, M.A. Deleplanque, F. Azaiez, J. Burde, W. Korten, A.O. Macchiavelli, J.R.B. Oliveira, J.A. Becker[1], M.J. Brinkman[2], J.A. Cizewski[2], P.M. Davidson[5], G.D. Dracoulis[5], J.E. Draper[3], C. Duyar[3], B. Fabricius[5], E.A. Henry[1], J.C. Hill[4], H. Hubel[6], W.H. Kelly[4], H. Kluge[7], A. Kuhnert[1], E. Rubel[3], D.T. Vo[4], T.F. Wang[1], P. Willsau[6], F.K. Wohn[4]

1. Lawrence Livermore National Laboratory, Livermore, CA, USA
2. Rutgers University, New Brunswick, NJ, USA
3. University of California, Davis, CA, USA
4. Iowa State University, Ames, CA, USA
5. Australian National University, Australia
6. Bonn University, Germany
7. Hahn-Meitner Institute, Berlin, Germany

Heavy Element Nuclear and Radiochemistry

D.C. Hoffman, G.T. Seaborg, K.R. Czerwinski*, R. Gaylord**, A. Ghiorso, K.E. Gregorich, H.L. Hall[1], T.M. Hamilton*, N.J. Hannink*, C.D. Kacher*, B.A. Kadkhodayan*, S.A. Kreek*, M.R. Lane*, D.M. Lee, M.P. Neu*, M.J. Nurmia, A. Türler[3], W.D. Loveland[2], A. Bilewicz[4]

1. Lawrence Livermore National Laboratory, Livermore, CA
2. Oregon State University
3. Postdoctoral Fellow
4. Department of Radiochemistry, Institute of Nuclear Chemistry and Technology, Warsaw, Poland

OASIS

J.M. Nitschke, R.M. Chasteler*, R.B. Firestone, P.A. Wilmarth, Y.A. Akovali[1], F.T. Avignone III[2], J. Bergman[3], J. Bennett**[4], J.L. Feng**[5], R. Ghanadan**[6], J. Gilat[7], A.L. Goodman[8], G.G. Howes[9], W.H. Kelly[10], M.O. Kortelahti[11], J.I. McIntyre[12], P. Möller[13], C.M. Skluzacek**[14], A.A. Shihab-Eldin[15], D.C. Sousa[16], K.S. Toth[1], K.S. Vierinen[17]

1. ORNL, Oak Ridge, TN, USA
2. University of So. Carolina, SC, USA
3. San Francisco State University, San Francisco, CA, USA
4. Vanderbilt University, Nashville, TN, USA
5. Harvard College, Cambridge, MA, USA
6. University of Maryland, College Park, MD, USA
7. Soreq Nuclear Research Center, Yavne, Israel
8. Tulane University, New Orleans, LA, USA
9. Occidental College, Los Angeles, CA, USA
10. Iowa State University, Ames, IA, USA
11. University of Jyväskylä, Jyväskylä, Finland
12. The College of William and Mary, Williamsburg, VA, USA
13. Lund University, Lund, Sweden
14. Carleton College, Northfield, MN, USA
15. Kuwait Institute for Scientific Research, Kuwait
16. Eastern Kentucky University, Richmond, KY, USA
17. University of Helsinki, Helsinki, Finland

Exotic Nuclei: RAMA

J. Cerny, J.C. Batchelder*, D.M. Moltz, T.J. Ognibene*, M. Rowe*, G. Rose**, E. Wang**

Heavy-Ion Reactions at Low and Intermediate Energies

Y. Chan, R.G. Stokstad, J.A. Scarpaci, J. Suro Perez[1]

1. Instituto de Física, UNAM, México

Nuclear Astrophysics

E.B. Norman, R.G. Stokstad, Y.D. Chan, A. Garcia, R.M. Larimer, K.T. Lesko, I. Zlimen, M.T.F. da Cruz[1], M.M. Hindi[2], F.E. Wietfeldt*, E. Kong**, H. Leung**

1. (University of Sao Paulo)
2. (Tennessee Technological University)

Bevalac Research Program

L.S. Schroeder

The Bevalac still maintains its unique position in the U.S. heavy ion program by providing beams spanning the periodic table (protons to uranium) from the low energy region of 30 MeV/nucleon to relativistic energies of 1-2 GeV/nucleon. With these beams a program of fundamental research in nuclear science, atomic physics and cosmic-rays, as well as biology and medicine, is carried out under one roof. With the closure of the Bevalac for nuclear science now projected to be in the period FY93 or FY94, emphasis continues to be placed on those experiments which will provide the deepest insights into the nuclear matter equation of state.

The central focus of the Bevalac's research program continues to be the production and study of extreme conditions in nuclear matter. Early experiments with the Plastic Ball and Streamer Chamber provided the first definitive evidence for "collective flow" of nuclear matter at high temperatures (50-100 MeV) and nuclear densities (2-4 times normal) created in the central collision of two heavy nuclei. These experiments allow us to study the thermodynamic and transport properties of nuclear matter, and, from this, the nuclear matter equation of state (EOS), a quantity of fundamental importance in nuclear physics and of relevance to the understanding of the extreme conditions existing inside neutron stars. The EOS time projection chamber (TPC), the next generation 4π detector, has just completed its construction phase and is beginning operation for physics. EOS will expand on existing 4π measurements and provide new capabilities for complete event analysis of the central collisions of the heaviest nuclei.

Dileptons (e^+e^- pairs) continue to be used as fundamental probes of extreme conditions. Because of their relatively weak interaction with matter, leptons are used to study the hot, dense stage of the collision process. Theoretical calculations continue to indicate that dilepton production should be a sensitive probe of pionic annihilation in nuclear matter, with the potential of measuring the propagation of pions in hot nuclear matter. Subthreshold particle production, experimentally accessible because of the high beam currents available at the Bevalac, plays an important role in the understanding of cooperative phenomena in the nuclear medium.

In the energy range of 30-150 MeV/nucleon the interactions of heavy beams are used to study nuclear matter at high temperatures and excitations, but at below-normal densities. These experiments provide a vehicle for studying the nuclear matter equation of state through the process of multifragmentation. Through the characterization of nuclear interactions at these energies and their distribution between direct and sequential fragmentation processes, possible insights into the liquid-gas phase transition are sought.

Distant or grazing collisions between nuclei provide enormous potential for creating nuclear fragments with extreme numbers of neutrons and protons. The combination of Bevalac beams, energy variability and unique experimental facilities allows studies of nuclear species out to the proton and neutron driplines. The production of radioactive beams and measurements of their ground-state properties were pioneered at the Bevalac by several groups from Japan. Initial work involved the measurement of the radii of light neutron-rich nuclei, culminating in the observation of the "neutron halo" associated with ^{11}Li. Present work in this area continues to concentrate on measurements of the correlations between nuclear fragments from these exotic nuclei and to play a world-wide leadership role in defining new directions for this line of research.

A variety of experiments in other disciplines is carried out at the Bevalac. Cosmic-ray scientists from around the world use the Bevalac to calibrate their detectors for flights on high altitude balloons and satellites. Virtually all the heavy-ion detectors which have flown on satellites in the last ten years have been calibrated at the Bevalac (some both before and after retrieval from orbit). The availability of all nuclear species at variable energies, on a demand basis, makes the Bevalac a unique national resource for this type of work. Atomic physicists study the extreme conditions presented by 1- and 2-electron uranium ions to test our understanding of quantum electrodynamics (QED).

Following are the named collaborations in which the Nuclear Science Divisions participates. The spokespersons are indicated in **bold face**.

DLS Collaboration

S. Beedoe[1], M. Bougteb[2], J. Carroll[1], T. Hallman[1], L. Heibronn, H.Z. Huang, G. Igo[1], P. Kirk[4], G. Krebs, L. Madansky[3], F. Manso[2], H.S. Matis, D. Miller[5], J. Miller, C. Naudet, J. Porter, G. Roche[2], **L. Schroeder**, P.A. Seidl, W. K. Wilson, Z.F. Wang[4], R. Welsh[3], A. Yegneswaran[6]

1. University of California at Los Angeles, Los Angeles, CA, USA
2. Université de Clermont II, Aubière, France
3. The Johns Hopkins University, Baltimore, MD, USA
4. Louisiana State University, Baton Rouge, LA, USA
5. Northwestern University, Evanston, IL, USA
6. CEBAF, Newport News, VA, USA

EOS Collaboration

F. Bieser, F. P. Brady[1], D. Cebra, A. D. Chacon[3], J. Chance, Y. Choi[2], S. Costa[5], J. Elliot[2], M. Gilkes[2], A. Hirsch[2], E. Hjort[2], **D. Keane**[4], U. Lynen[6], H. S. Matis, M. McMahan, C. McParland, W. Mueller[6], G. Odyniec, D. L. Olson, M. D. Partlan[1], N. Porile[2], R. Potenza[5], G. Rai, J. Rasmussen, **H. G. Ritter**, J. L. Romero[1], H. Sann[6], **R. Scharenberg**[2], A. Scott[4], Y. Shao[4], B. Srivastava[2], T.J.M. Symons, P. Warren[2], **H. H. Wieman**, K. Wolf[3]

1. U.C. Davis, Davis, CA, USA
2. Purdue University, West Lafayette, IN, USA
3. Texas A&M University, College Station, TX, USA
4. Kent State University, Kent, OH, USA
5. INFN Catania, Italy
6. GSI Darmstadt, Germany

Intermediate Energy Collaboration

L. G. Moretto, G. J. Wozniak, N. Colonna, M. Justice, W. Skulski, D. Delis, K. Hanold, Kin Tso, A. Veek, M. Colonna[1], P. Roussel-Chomaz[2], Q. C. Sui[3], B. Libby[4], Mehdi Varasten, Veronique Pascalon, M. A. McMahan[5], A. C. Mignerey[4], A. Moroni[6], I. Iori[6], A. Pantaleo[7], L. Fiore[7], D. Bowman[8], G. Peaslee[8], W. Lynch[8], B. Tsang[8], K. Gelbke[8], D. Morrissey[8], B. Sherrill[8],

1. INFN-LNS, Catania, Italy
2. Saclay, 91191, Gif-sur-Yvette, Cedex France
3. Institute of Atomic Energy, Beijing, China
4. University of Maryland, College Park, Maryland, 20742
5. Accelerator & Fusion Research Division, LBL
6. INFN and Department of Physics, University of Milano, Milano, Italy
7. INFN, 70100, Bari, Italy
8. Michigan State University, East Lansing, MI

Janus Collaboration

K. Crowe, J. Rasmussen, R. Bossingham, T. Case, Y. Dardenne[1], W. McHarris[1]

1. Michigan State University, East Lansing, MI, USA

Secondary Radioactive Beams Collaboration

K. Matsuta, J. R. Alonso, G. F. Krebs, T. J. M. Symons, H. H. Wieman, D. L. Olson, W. Christie, L. Greiner, A. Ozawa[1], Y. Nojiri[1], **T. Minamisono**[1], M. Fukuda[1], A. Kitagawa[1], S. Momota[1], T. Ohtsubo[1], S. Fukuda[1], Y. Matsuo[1], H. Takechi[1], I. Minami[1], K. Sugimoto[1], **I. Tanihata**[2], K. Yoshida[2], T. Kobayashi[2], T. Suzuki[2], S. Shimoura[3], K. Omata[4], O. Testard[5]

1. Osaka University, Toyonaka, Osaka 560, Japan
2. RIKEN, Wako, Saitama 351-01, Japan
3. University of Tokyo, Bunkyo-ku, Tokyo 113, Japan
4. INS, University of Tokyo, Tanashi,Tokyo 188, Japan
5. Saclay, 91191 GIF-sur-YVETTE, Cedex, France

Subthreshold Kaons and Antiproton Collaboration

V. Perez-Mendez, S. N. Kaplan, J. Drewery, **A. Shor**[1], J. Tserruya[1], S. Trentalang[2], G. Igo[2], P. Kirk[3], Z. Wang[3]

1. Weizmann Institute of Science, Rehovot, Israel
2. University of California Los Angeles, Los Angeles, CA, USA
3. Louisiana State University, Baton Rouge, LA, USA

Nuclear & Astrophysics Collaboration

P.J. Lindstrom, **H.J. Crawford**[1], J. Engelage[1], I. Flores[1], L. Greiner[1], S. Costa[2],R. Potenza[2], C. Chen[3], C. Tull[3], C. Knott[4], J. Waddington[4], W.R. Webber[5], O. Testard[6], A. Soutoul[6]

1. UCSSL, Berkeley, CA, USA
2. INFN-LNS, Catania, Italy
3. Louisiana State University, Baton Rouge, LA, USA
4. University of Minnesota, Minneapolis, MN, USA
5. New Mexico State University, Albuquerque, NM, USA
6. Saclay, 91191 GIF-sur-YVETTE, Cedex France

Ultrarelativistic Research Program

A.M. Poskanzer

The Nuclear Science Division at LBL has played a seminal role in defining the forefront of relativistic heavy ion physics since the field's inception and continues to maintain its leadership role. An important step for the Division in adjusting to the evolution of the field to higher energies and larger experiments was the consolidation of many small projects into the Relativistic Nuclear Collisions Group, to provide a focus for future activities. In the past year approval has been won for the major experiment with Pb beams, called NA49, at the CERN Super Proton Synchrotron, and for construction of STAR, one of two major experiments to be built at the Brookhaven Relativistic Heavy Ion Collider. After the close of the Bevalac these two experiments will be the focus of LBL's relativistic activities through the end of the century.

The STAR Collaboration now has 135 scientists from 23 institutions. The spokesperson and thirty of the scientists are from LBL. STAR is an experiment to study particle production and high transverse momentum jet production at midrapidity to identify the phase transition from normal nuclear matter to quark matter. A measurement of the produced particles at midrapidity provides the opportunity to select on events with extreme values of temperature (particle spectrum), flavor (strangeness content), shape (particle momenta) and size (two-particle correlations). The experiment will contain a Time Projection Chamber (TPC) located inside a superconducting solenoidal magnet for tracking, momentum analysis and particle identification. Time-of-flight detectors surrounding the main TPC will extend particle identification to higher momenta. A silicon vertex tracker near the interaction region will distinguish primary and secondary vertices, and improve the tracking and momentum resolution. Segmented electromagnetic calorimeters will be implemented in an azimuthally symmetric geometry outside the magnetic field for jet identification and triggering. External TPCs around the beam line will extend the multiplicity and charge-sign measurements to more forward and backward angles.

At the CERN SPS the emphasis of the present program of 200 GeV/nucleon ^{32}S-induced reactions is to explore the possibilities of producing a phase transition from hadronic matter to a quark-gluon plasma in central collisions of heavy ions at these energies. The NA36 TPC Collaboration has finished data-taking and is now producing physics results for lambdas and kaons. The LBL contingent of WA80 has switched to NA35. As their final WA80 task they did an intermittency analysis of the streamer tube data. LBL closed down its emulsion scanning effort last year and this year is closing down the film and CCD scanning program. Thus, LBL has effected a consolidation so that it is participating in only one active CERN data-taking experiment: NA35. Its TPC is the first such detector to operate in a magnetic field free region with pad readout only. LBL is building and installing 6000 additional channels of modern EOS-style electronics. This is a

step on the way to a much larger contribution from LBL of integrated electronics for the main TPC for the 1994 NA49 Pb-beams experiment. This experiment will consist of two dipole magnets in series in either a sweeper-rebender or sweeper-sweeper configuration, a large volume TPC with 90,000 channels for tracking and particle identification of charged particles, the NA35 TPCs on one side for the wide-angle pions, two high-resolution intermediate-size TPCs to detect neutral strange particle decays, and a time-of-flight wall to complete the hadron identification scheme. This combination of detectors should allow enough coverage to do event-by-event physics for the first time at a CERN experiment.

At the Brookhaven AGS the Nuclear Science Division is participating with the UC Space Sciences Laboratory in a search for rare negative particle production in Si + Au collisions. The main purpose is to study the space-time evolution of the reaction through coalescence yields.

Following are the named collaborations in which the Nuclear Science Division participates. The spokespersons are indicated in **bold face.**

WA80 Collaboration

R. Albrecht[1], T.C. Awes[2], P. Beckmann[3,9], F. Berger[4], M.A. Bloomer, D. Bock[4], R. Bock[1], G. Claesson[5], G. Clewing[4], R. Debbe[6], L. Dragon[4,10], A. Eklund[5], R.L. Ferguson[2], S. Fokin[7], A. Franz[2,9], S. Garpman[5], R. Glasow[4], H.Å. Gustafsson[5], H.H. Gutbrod[1], O. Hansen[6], M. Hartig[4], G. Hölker[4], J. Idh[5], M. Ippolitov[7], P. Jacobs, K.H. Kampert[4], K. Karadjev[7], B.W. Kolb[1], A. Lebedev[7], H. Löhner[3], I. Lund[1,11], V. Manko[7], B. Moskowitz[6], F.E. Obenshain[2], A. Oskarsson[5], I. Otterlund[5], T. Peitzmann[4], F. Plasil[2], A.M. Poskanzer, M. Purschke[4], H.-G. Ritter, B. Roters[4], S. Saini[2], **R. Santo**[4], H.R. Schmidt[1], K. Söderström[5], S.P. Sørensen[2,8], K. Steffens[4], P. Steinhäuser[4], E. Stenlund[5], D. Stüken[4], A. Twyhues[4], A. Vinogradov[7], and G.R. Young[2]

1. Gesellschaft für Schwerionenforschung, Darmstadt, Germany
2. Oak Ridge National Laboratory, Oak Ridge, TN, USA
3. KVI, University of Groningen, Gronigen, Netherlands
4. University of Münster, Münster, Germany
5. University of Lund, Lund, Sweden
6. Brookhaven National Laboratory, Upton, NY, USA
7. Kurchatov Institute, Kurchatov Square, Moscow, USSR
8. University of Tennessee, Knoxville, TN, USA
9. now at: CERN, Geneva, Switzerland
10. now at: Mercedes-Benz, Stuttgart, Germany
11. now at: KVI, University of Groningen, Gronigen, Netherlands

NA35 Collaboration

J. Bächler[7], J. Bartke[4], H. Bialkowska[11], M. Bloomer, R. Bock[5], R. Brockmann[5], P. Buncic[12], S.I. Chase, J. Cramer[14], I. Derado[9], V. Eckardt[9], J. Eschke[6], C. Favuzzi[2], D. Ferenc[12], B. Fleischmann[5], P. Foka[5] , M. Fuchs[5], M. Gazdzicki[10], E. Gladysz[4], O. Hansen[6,13], J.W. Harris, W. Heck[6], M. Hoffmann[7], P, Jacobs, S. Kabana[6], K. Kadija[3,12], A. Karabarbounis[1], R. Keidel[8], J. Kosiec[6], M. Kowalski[9], A. Kühmichel[6], M. Lahanas[6], J.Y. Lee[6], M. LeVine[6,13], A. Ljubicic, Jr.[12], S. Margetis[6], R. Morse, E. Nappi[2], G. Odyniec, G. Paic[5,12], A.D. Panagiotou[1], A. Petridis[1], A. Piper[8], F. Posa[2], A. Poskanzer, F. Pühlhofer[8], G. Rai, W. Rauch[9], R. Renfordt[6], W. Retyk[10], D. Röhrich[6], G. Roland[6], H. Rothard[6], K. Runge[7], A. Sandoval[5], J. Schambach, E. Schmidt[6], N. Schmitz[9], E. Schmoetten[7], I. Schneider[6], **P. Seyboth**[11], J. Seyerlein[9], E. Skrzypczak[10], P. Spinelli[2], P. Stefanski[4], R. Stock[6], H. Ströbele[6], L. Teitelbaum, S. Tonse, T. Trainor[14], G. Vasileiadis[1], M. Vassiliou[1], G. Vesztergombi[9], D. Vranic[12], S. Wenig[6]

1. Department of Physics, University of Athens, Athens, Greece
2. Dipartimento di Fisica, Università di Bari and INFN Bari, Bari, Italy
3. CERN, Geneva, Switzerland
4. Institute of Nuclear Physics, Cracow, Poland
5. Gesellschaft für Schwerionenforschung (GSI), Darmstadt, Germany
6. Fachbereich Physik der Universität, Frankfurt, Germany
7. Fakultät für Physik der Universität Freiburg, Germany
8. Fachbereich Physik der Universität, Marburg, Germany
9. Max-Planck-Institut für Physik u. Astrophysik, München, Germany
10. Institute for Experimental Physics, University of Warsaw, Warsaw, Poland
11. Institute for Nuclear Studies, Warsaw, Poland
12. Rudjer Boskovic Institute, Zagreb, Yugoslavia
13. Department of Physics, Brookhaven National Laboratory, Upton, NY, USA
14. Nuclear Physics Laboratory, University of Washington, Seattle, WA, USA

NA36 Collaboration

E. Andersen[1], P.D. Barnes[7], R. Blaes[9], H. Braun[9], J.M. Brom[9], M. Cherney[6], M. Cohler[11], B. de la Cruz[5], G.E. Diebold[7], B. Dulny[4], C. Fernández[8], G. Franklin[7], C. Garabatos[8], J.A. Garzón[8], W.M. Geist[9], **D.E. Greiner**, C. Gruhn, M. Hafidouni[9], J. Hrubec[10], P.G. Jones[2,†], E. Judd[2], J.P.M. Kuipers[11], M. Ladrem[9], P. Ladrón de Guevara[5], G. Løvhøiden[1], J. MacNaughton[10], A. Michalon[9], M.E. Michalon-Mentzer[9], J. Mosquera[8], Z. Natkaniec[4], J.M. Nelson[2], G. Neuhofer[10], C.Perez de los Heros[5], M. Pló[8], P. Porth[10], B. Powell[3], B. Quinn[7], A. Ramil[8], J.L. Riester[9], H. Rohringer[10], I. Sakrejda, T. Thorsteinsen[1], J. Traxler[10], C. Voltolini[9], A. Yañez[8] and R. Zybert[2].

1. University of Bergen, Dept. of Physics, Bergen, Norway

2. University of Birmingham, Dept. of Physics, Birmingham, UK
3. CERN, Geneva, Switzerland
4. Instytut Fizyki Jadrowej, Krakow, Poland
5. CIEMAT, Div. de Física de Partículas, Madrid, Spain
6. Creighton University, Department of Physics, Omaha, Nebraska, USA
7. Carnegie-Mellon University, Dept. of Physics, Pittsburgh PA, USA
8. Universidad de Santiago, Dpto. Física de Partículas, Santiago de Compostela, Spain
9. Centre de Recherches Nucléaires, IN2P3-CNRS/Université L. Pasteur, Strasbourg, France
10. Institut für Hochenergiephysik (HEPHY), Wien, Austria
11. University of York, Dept. of Physics, York, UK

† Present address: Lawrence Berkeley Laboratory, Berkeley CA, USA

NA49 Collaboration

J. Bächler[7], J. Bartke[4], H. Bialkowska[11], M. Bloomer, R. Bock[5], R. Brockmann[5], P. Buncic[12], S.I. Chase, J. Cramer[14], I. Derado[9], V. Eckardt[9], J. Eschke[6], C. Favuzzi[2], D. Ferenc[12], H.G. Fischer[3], B. Fleischmann[5], P. Foka[5] , M. Fuchs[5], M. Gazdzicki[10], E. Gladysz[4], O. Hansen[6,13], J.W. Harris, W. Heck[6], M. Hoffmann[7], P, Jacobs, P.G. Jones, E. Judd[15], S. Kabana[6], K. Kadija[3,12], A. Karabarbounis[1], R. Keidel[8], J. Kosiec[6], M. Kowalski[9], A. Kühmichel[6], M. Lahanas[6], J.Y. Lee[6], M. LeVine[6,13], A. Ljubicic, Jr.[12], S. Margetis[6], R. Morse, E. Nappi[2], J.M. Nelson[15], G. Odyniec, G. Paic[5,12], A.D. Panagiotou[1], A. Petridis[1], A. Piper[8], F. Posa[2], A. Poskanzer, F. Pühlhofer[8], G. Rai, W. Rauch[9], R. Renfordt[6], W. Retyk[10], D. Röhrich[6], G. Roland[6], H. Rothard[6], K. Runge[7], A. Sandoval[5], J. Schambach, E. Schmidt[6], N. Schmitz[9], E. Schmoetten[7], I. Schneider[6], P. Seyboth[11], J. Seyerlein[9], E. Skrzypczak[10], P. Spinelli[2], P. Stefanski[4], **R. Stock**[6], H. Ströbele[6], L. Teitelbaum, T. Trainor[14], G. Vasileiadis[1], M. Vassiliou[1], G. Vesztergombi[9], D. Vranic[12], S. Wenig[6], H. Wieman, R. Zybert[15]

1. Department of Physics, University of Athens, Athens, Greece
2. Dipartimento di Fisica, Università di Bari and INFN Bari, Bari, Italy
3. CERN, Geneva, Switzerland
4. Institute of Nuclear Physics, Cracow, Poland
5. Gesellschaft für Schwerionenforschung (GSI), Darmstadt, Germany
6. Fachbereich Physik der Universität, Frankfurt, Germany
7. Fakultät für Physik der Universität Freiburg, Germany
8. Fachbereich Physik der Universität, Marburg, Germany
9. Max-Planck-Institut für Physik u. Astrophysik, München, Germany
10. Institute for Experimental Physics, University of Warsaw, Warsaw, Poland
11. Institute for Nuclear Studies, Warsaw, Poland
12. Rudjer Boskovic Institute, Zagreb, Yugoslavia

13. Department of Physics, Brookhaven National Laboratory, Upton, NY, USA
14. Nuclear Physics Laboratory, University of Washington, Seattle, WA, USA
15. University of Birmingham, Dept. of Physics, Birmingham, UK

STAR Collaboration

B.D. Anderson[2], F. Bieser, M.A. Bloomer, F.P. Brady[7], W.J. Braithwaite[10], A. Breskin[13], P. Buncic[14], D.D. Carmony[3], J. Carroll[8], D.A. Cebra, A.D. Chacon, S.I. Chase, M.G. Cherney[1], Y. Choi[3], W. Christie, H.J. Crawford[6], J.G. Cramer[10], W. Dominik[11], J.E. Draper[7], W.R. Edwards, J.M. Engelage[6], D. Ferenc[14], Z. Fraenkel[13], M. Gazdzicki[11], V. Ghazikhanian[8], M. Green, D. Greiner, L. Greiner[6], C. Gruhn, E. Gulmez[8], T.J. Hallman[8], **J.W. Harris**, A.S. Hirsch[3], E. Hjort[3], H. Huang, G.J. Igo[8], P.M. Jacobs, P. Jones, K. Kadija[14], D. Keane[2], S. Kleinfelder, P.J. Lindstrom, L. Madansky[5], R. Madey[2], H.S. Matis, C. McParland, T. Moore, R. Morse, C.J. Naudet, T. Noggle, G. Odyniec, D.L. Olson, G. Paic[14], M.D. Partlan[7], T. Pawlak[12], W. Peryt[12], J. Pluta[12], N.T. Porile[3], A.M. Poskanzer, D. Prindle[10], G. Rai, J. Rasson, R.E. Renfordt[9], H.-G. Ritter, D. Roehrich[9], J.L. Romero[7], I. Sakrejda, J. Schambach, R.P. Scharenberg[3], L.S. Schroeder, Y.P. Shao[2], D. Shuman, B. Srivastava[3], R. Stock[9], R. Stone, H. Stroebele[9], T.J.M. Symons, M.L. Tincknell[3], T.A. Trainor[10], S. Trentalange[8], I. Tserruya[13], D.Vranic[14], J.W. Watson[2], R.C. Welsh[5], S. Wenig[9], C. Whitten, Jr.[8], H. Wieman, W.K. Wilson, K.L. Wolf[4]

1. Creighton University, Omaha, NE, USA
2. Kent State University, Kent, OH, USA
3. Purdue University, West Lafayette, IN, USA
4. Texas A & M University, College Station, TX, USA
5. The Johns Hopkins University, Baltimore, MD, USA
6. U.C. Berkeley, Space Science Laboratory, Berkeley, CA, USA
7. U.C. Davis, Davis, CA, USA
8. U. C. Los Angeles, Los Angeles, CA, USA
9. University of Frankfurt, Frankfurt, Germany
10. University of Washington, Seattle, WA, USA
11. Warsaw University, Warsaw, Poland
12. Warsaw University of Technology, Warsaw, Poland
13. Weizmann Institute of Science, Rehovot, Israel
14. Zagreb-Boskovic Institute, Zagreb, Yugoslavia

Nuclear Theory Program

M. Gyulassy

The goal of the nuclear theory program at LBL is to develop precise theoretical tools and methods necessary for the proper analysis and interpretation of experiments involving atomic nuclei. These include nuclear reactions at low to ultrarelativistic energies, and lepton-nucleus and hadron-nucleus reactions. In addition, the program aims at adding breadth to the Division's overall nuclear research program by concentrated effort also in nuclear astrophysics, macroscopic nuclear models, QCD and hadrodynamic theories of ultra-dense matter and phase transitions, order-to-chaos transition in nuclei and selected DOE research and development projects such as on neurocomputing methods for pattern recognition.

Nuclear Data Evaluation Program

R.B. Firestone and E. Browne

The Isotopes Project compiles, evaluates, and disseminates nuclear structure and radioactive-decay data for basic and applied research, and for diverse technical applications. Since 1979, the project has coordinated its efforts with the national and the international nuclear data networks, and is responsible for the evaluation of properties of nuclei with mass numbers A=167 to 194. This responsibility includes preparing data in computerized form for entry into the Evaluated Nuclear Structure Data File (ENSDF).

Spectroscopic data from radioactive decay and nuclear reactions -- after verification of completeness, correctness, and self-consistency -- serve as input data for determining recommended adopted values of specific nuclear properties. These "best values", deduced with the aid of statistical procedures, the application of systematics, and the use of nuclear models, constitute the main scientific contribution of the data evaluation effort. The project's data and corresponding bibliographic references are both computer retrievable and available in published form.

Comprehensive evaluations, produced from ENSDF, are subsequently published in the journal Nuclear Data Sheets. Concurrent with evaluation of data, the Isotopes Project develops methods and computer codes for data analysis. These include minimization procedures for deducing best values from various sets of data, and data-verification codes for assuring correctness and uniformity. The project has a continuing interest in methods for propagation of the experimental uncertainties reported for nuclear properties. Their application in nuclear data evaluation leads to uniform and rigorous interpretation of the data, and results in consistently reliable recommended values.

The Isotopes Project produced seven editions of the Table of Isotopes from 1940 to 1978, the sixth and seventh in book form. Each edition provided a comprehensive and critical evaluation of the known nuclear properties deduced from radioactive decay and reaction data. The project is also responsible for the production of the Table of Radioactive Isotopes, first published in 1986. This book provides a concise source of recommended data derived from ENSDF, and is tailored to the needs of applied users in industry, biology, medicine, and other fields. It has also proved itself as an indispensable reference for nuclear physicists and chemists in basic research. The Isotopes Project is preparing an 8th edition of the Table of Isotopes for completion in 1993. This book will primarily emphasize nuclear structure and decay data. The 8th edition of the Table of Isotopes is planned to be updated regularly and provided, on various computer media, for remote printing. Future editions are expected to be published on approximately a 5-year cycle.

The Isotopes Project is also responsible for developing an electronic version of the Table of Isotopes to display nuclear data on personal computers and workstations. This program will provide a chart-of-the-nuclides graphical interface to the ENSDF file including full searching capabilities for all data, graphical and tabular display of information, calculation utilities, and access to the Nuclear Structure Reference library (NSR). A preliminary version of this program, supporting menu-driven access to the numerical data in ENSDF, will be released in 1992 and a complete version is expected around 1994.

The Isotopes Project serves a broad user community, and plays an active role in promoting the science of nuclear data evaluation. It has developed, and makes available, an extensive computerized database of nuclear structure and radioactive decay information (LBL/ENSDF) based on ENSDF.

Publications

1. V.S. Shirley, Nuclear Data Sheets **64**, 505 (1991).
2. E. Browne, Nuclear Data Sheets **62**, (1991).
3. R.B. Firestone, Nuclear Data Sheets **62**, 101 (1991).
4. R.B. Firestone, Nuclear Data Sheets **62**, 159 (1991).
5. V.S. Shirley, Nuclear Data Sheets **64**, 205 (1991).
6. R.B. Firestone, J. Gilat, J.M. Nitschke, P.A. Wilmarth, and K.S. Vierinen, Phys. Rev. C**43**, 1066 (1991).
7. K.S. Toth, J.M. Nitschke, K.S. Vierinen, P.A. Wilmarth, R.B. Firestone, and M.O. Kortelahti, Nucl. Instr. and Meth. Phys. Res. **B56**, 484 (1991).

88-Inch Cyclotron Operations

C.M. Lyneis, D.J. Clark, D. Collins, A. Guy, R.-M. Larimer, S.A. Lundgren, R.J. McDonald, and Z. Xie

The 88-Inch Cyclotron is operated by the Nuclear Science Division as a national facility in support of U.S. Department of Energy programs in basic nuclear science. Written proposals for experiments in nuclear science are evaluated by a Program Advisory Committee on the basis of the science proposed. Current members are C.D. Goodman (IUCF), R. Janssens (ANL), R.W. Hoff (LLNL), R.L. McGrath (SUNY), and L. Sobotka (Wash. U.). The current membership of the Users' Executive Committee is J.M. Alexander (SUNY), J.A. Becker (LLNL), K.E. Gregorich (LBL), W.D. Loveland (Oregon State University, chairman) and H.R. Weller (Duke University).

Research at the Cyclotron is conducted by scientists from many institutions in addition to those from LBL and the University of California at Berkeley. During FY91, the Cyclotron was used by 120 scientists from 18 institutions. About 60% of the total beam time was used by scientists from institutions other than LBL. The Cyclotron also plays an important role in the education and training of young scientists at the undergraduate, graduate, and postdoctoral stages of their careers.

The central component of this facility is a sector-focused, variable-energy cyclotron that has been upgraded by the addition of an Electron Cyclotron Resonance (ECR) high-charge-state ion source. This versatile combination produces heavy ion beams from helium to oxygen with energies up to 32 MeV/nucleon. For heavier ions the maximum energy per nucleon decreases with increasing mass. Typical ions and maximum energy are argon at 17 MeV/u, krypton at 8 MeV/u, and xenon at 5 MeV/u. Most metallic ions and all other gaseous ions up to mass 150 either have been accelerated or can be developed with energies high enough for nuclear physics experiments. Light ions — p, d, ^{3}He and ^{4}He — are produced up to total energies of 55, 65, 135, and 130 MeV, respectively. Polarized proton and deuteron beams at intensities of up to 0.5 microampere are also available. Beams directly from the ECR source at up to 10 keV per charge state can be delivered by a transport system on the vault roof to any one of three target stations for atomic physics research.

Accelerator Use

In FY92 the Cyclotron is operating 14.5 eight-hour shifts per week for research and one shift for routine maintenance each week. The Cyclotron operating efficiency continues to benefit from the ECR source. There are long periods of steady operation, and only one operator per shift is required. The range of ions available from the ECR source has continued to expand. Table 1 summarizes the time distribution for FY91. The Machine Operation Summary shows that

Cyclotron reliability was very high, with only 5% of the operating time being lost to unscheduled maintenance.

Ions and Energies

The Cyclotron fed by the ECR source provides a wide range of ions, energies, and intensities in support of the experimental program at the 88-Inch Cyclotron. Using the low and high temperature ovens in the LBL ECR, most elements can be accelerated . A partial list of beams, energies, and intensities is given in Table 2. In addition to those listed, many isotopic beams such as ^{26}Mg, ^{29}Si, ^{30}Si, ^{34}S, ^{37}Cl, ^{65}Cu, and ^{70}Ge can be produced from natural feed. Other isotopes such as ^{3}He, ^{13}C, ^{15}N, ^{18}O, ^{22}Ne, ^{44}Ca, ^{48}Ca, ^{54}Fe and ^{235}U can be run economically from enriched isotopes because of the high efficiency of the ECR source.

The beams developed and listed in Table 2 are generally developed as needed by the wide range of experiments proposed by the users of the 88-Inch Cyclotron. Heavy element radiochemistry experiments require several eμA of beams up to mass 48 at 6–8 MeV/nucleon. The study of ℓ-delayed proton emission and of light proton-rich nuclei requires a few eμA of ^{3}He at 40–110 MeV, and carbon, silicon, and sulfur at 6–7 MeV/nucleon. The nuclear astrophysics group typically uses beams of protons, deuterons, ^{3}He and ^{4}He at energies of 8–25 MeV/nucleon. A wide range of ion species, particularly of neutron-rich isotopes, is used for the study of high spin states using the HERA detector array. Groups studying heavy ion reaction mechanisms and complex fragmentation of highly excited nuclei use higher energy beams such as nitrogen and oxygen at 32 MeV/nucleon, neon at 26 MeV/nucleon, silicon at 22 MeV/nucleon, and argon and copper at 13 MeV/nucleon.

ECR Ion Source Development [1, 2, 3]

Two types of ovens, a low and a high temperature type, are used to produce beams from solid materials in the LBL ECR source. The ovens are located outside the plasma, so their vapor feed rates depend only on their temperatures. This is an advantage over wire or rod feed. At the 1 eμA level at the source, the charge states from the oven beams are similar to those from gases in the same mass range, indicating that the oven feed systems have been well optimized. In the present configuration two ovens can be loaded at one time so that rapid changes between beams can be made during an experiment. The low temperature oven operates up to 700 degrees C and produces beams of lithium, sodium, magnesium, phosphorus, potassium, calcium, titanium, iodine and bismuth. The high temperature oven has a resistance-heated tantalum crucible, operating up to 2000 degrees C. Beams produced with this oven include beryllium, boron, aluminum, scandium, chromium, iron, nickel, copper, germanium, silver, lanthanum, terbium and uranium. The long term stability is excellent. During this year we had the first full runs with beams of boron, iron, and nickel beams. They were for outside users with the HERA facility.

Previously these beams were used only on short tests or for atomic physics. Also a germanium beam was run for the first time, ^{70}Ge from natural feed for a HERA experiment.

The key to new capabilities at the 88-Inch Cyclotron is the construction of a new Advanced Electron Cyclotron Resonance (AECR) source. Phase II of this AIP project is nearing completion. The AECR operates at 14.5 GHz and produces beams of greater intensity and higher charge states than are now available using the LBL ECR. During FY90 construction of a new horizontal beam line which connects the AECR to the cyclotron was completed. The first AECR beams were injected into the cyclotron in June of 1990 and since then a variety of ion species from the AECR have been accelerated. The cyclotron accelerated bismuth to 954 MeV using a Bi^{38+} beam from the AECR. An electron gun, which injects 10 to 150 eV electrons into the plasma chamber has been developed to increase the production of high charge state ions.

88-Inch Cyclotron User Support

The liaison scientists of the 88Users' Group provide information, assistance, and coordination to all users of the 88-Inch Cyclotron. These scientists are also the main contact between the Cyclotron operations staff and outside users. Presently, the outside user community includes both industrial users who purchase beam time for their own proprietary use and scientific users.

The 88Users' Group is also responsible for the development and maintenance of experimental facilities at the Cyclotron and for making these facilities attractive to a diverse group of users from around the world. The 88Users' Group supports the Users Association and its Executive Committee which conveys users' needs to the 88-Inch Cyclotron management via monthly telephone conference calls. 88Users, through the Users Association, sponsors an annual users meeting and the liaison scientist publishes a users newsletter.

88-Inch Cyclotron Computer Support

The low-energy computer support effort is aimed at developing and maintaining general software for experimental data acquisition and on-line diagnostics at the 88-Inch Cyclotron. The goal is to provide high-level, vax-based interactive data acquisition and analysis software for the general use of all groups, and to support the daily operation of the computer hardware.

Applied Research

The 88-Inch Cyclotron is a major source of heavy-ion beams for the testing of computer chips and other solid-state components such as charge-coupled devices (CCDs) for the U.S. space program. Because of the ability to change from one beam to another one in a matter of minutes (e.g., from nitrogen to argon to

krypton) it is possible to establish quickly the energy deposition level at which a single event upset (SEU) will occur. The availability of proton beams (used for studying radiation effects on CCDs) has further increased the demand for this use of the Cyclotron. The wide variety of ions and energies available from the cyclotron has made it an excellent source of calibration ions for spacecraft particle detector experiments.

The Aerospace Corporation and the Jet Propulsion Laboratory (JPL) each have installed specially instrumented scattering chambers on dedicated beam lines. Their investment in these testing facilities is substantial. Future advances in device technology such as smaller size and greater complexity will result in ever greater sensitivity to SEU phenomena. This continuing trend in technology indicates a long-term need for access to the 88-Inch Cyclotron by more organizations involved in national and international space programs. Accelerator time used for the above purposes is charged to the industrial and government users on a cost recovery basis. Presently we are designing a new SEU test facility in coordination with the Aerospace Corporation and JPL.

Safety

The DOE Tiger Team visited LBL in January 1991. Although there were a number of "findings" at the Cyclotron, they were in the category of least significance (Category III) and the 88-Inch Cyclotron continued to operate throughout the Tiger Team inspection. In preparation for this visit and since that time, much effort has been dedicated by the 88-Inch Cyclotron operations group to improving safety and conduct of operations at the cyclotron facility. A comprehensive self-assessment of health and safety problems in the building was done, and 1200 items were found needing correction. To correct these, safety shutdown days were scheduled and regular walk-thrus were done, so that 81% of them have now been corrected. Operating Safety Procedures and other procedures needed for safe operation of various systems in the building were written. A radiation safety committee was appointed to review the problems of radiation safety in the building. Gates to control access to radiation areas around the cyclotron vault and caves were installed. Increased control of building access was achieved by keeping the entrance doors locked, having a secretary to monitor each entry, and requiring escorts for visitors. All these steps have increased the level of safety and good conduct of operations at the facility, but have taken a great deal of operations effort.

Gammasphere

In January, 1991 it was decided by DOE that Gammasphere would be constructed and operated initially at the 88-Inch Cyclotron. We are preparing to house the Gammasphere detector in Cave 4C. Design work is underway to determine what physical modifications are needed to accommodate the detector. The beam transport and beam diagnostic systems to Cave 4C are being reviewed

to improve the transport efficiency and make rapid tuning of the beam line possible. Additional funding has been requested to increase the operating level of the Cyclotron to accommodate the increased demands for beam time associated with early implementation of Gammasphere.

References

1. Z. Xie, C.M. Lyneis, R.S. Lam and S.A. Lundgren, Rev. Sci. Instrum. 62 (3) 775 (1991).
2. C.M. Lyneis, Z. Xie, D.J. Clark, R.S.I am and S.A. Lundgren, Proceedings of the 10th International Workshop on ECR Ion Sources, Knoxville, Nov. 1990.
3. D. J. Clark, C. M. Lyneis and Zuqi Xie, Conf. Record of the 1991 IEEE Particle Accelerator Conference, San Francisco, CA, May 1991, p. 2796.

Table 1. FY 91

Accelerator Operation Summary

Machine Operation (Hours)	
Research	2498
Tuning	469
Unscheduled Shutdowns	140
Scheduled Shutdowns	5653
Electrical Energy Consumption (GWH)	5.4

Experiment Summary

Beam Utilization for Research (Hours)	
Nuclear Research	1876
Other Research	622
Total	2498
Number of Nuclear Science Experiments	40
Number of Scientists Participating in Research	120
Institutions Represented	
Universities	10
Other DOE National Laboratories	1
Industrial and Other Organizations	7
Percentage of Beam Time	
In-House Staff	40
Universities	20
DOE National Laboratories	20
Other Institutions	20
Total	100

Table 2. 88-Inch Cyclotron Beam List

Ion	Charge State	External Beam (eμA)	E/A Range or Max (MeV/u)
p	1	100-5	.2-55
p (pol.)	1	.7-.4	6-50
d	1	100-5	.3-32
d (pol.)	1	.7-.4	5-32
^{3}He	2	100-5	1-47
^{4}He	2	100-5	1-32
^{7}Li	2	.5	11
	3	.03	26
^{9}Be	2	.5	7
	3	.3	15
	4	.2	28
^{12}C	4	10	6
	4	5.0	16
	5	.1	24
	6	.01	32
^{14}N	5	5.0	18
	6	.15	26
	7	.01	32
^{16}O	5	10	9
	5	5	14
	6	3.0	20
	7	.1	27
	8	.03	32
^{19}F	6	2	9
	6	1	14
	7	.6	19
^{20}Ne	6	5	8
	6	2.0	13
	7	.4	17
	8	.1	22
	9	.02	28
^{24}Mg	6	1.5	9
	7	.7	12
	8	2	16
	9	1	20
	10	.03	24
^{28}Si	6	2.0	6
	7	1.0	9
	8	.7	11
	9	.5	14
	10	.2	18
	11	.05	22
^{31}P	8	.5	9
	10	.1	15
^{32}S	7	3.5	7
	8	2.0	9
	9	1.0	11
	10	.4	14
	11	.1	17
	12	.02	20
	13	.003	23
^{35}Cl	9	.4	9
	10	.1	11
	11	.02	14
	12	.005	16
^{39}K	9	4	7
	10	2	9
	11	1	11
	12	.02	13
^{40}Ar	9	3.0	7
	10	1.5	9
	11	.6	11
	12	.4	13
	13	.09	15
	14	.015	17
^{40}Ca	9	1.5	7
	10	1.0	9
	11	.8	11
	12	.4	13
	13	.06	15
	14	.006	17
^{63}Cu	15	.1	8
	19	.03	13
^{84}Kr	17	.2	6
	19	.08	7
	20	.04	8
^{129}Xe	23	.01	4
	27	.01	6
^{159}Tb	30	.005	5
^{238}U	21	.010	.7
	30	.001	2.2

The listed currents are based on natural isotopic source feed, except for ^{3}He. Beam intensity on target will vary according to beam line optics, collimation and energy resolution requirements. Other elements run include ^{11}B, ^{23}Na, ^{27}Al, ^{45}Sc, ^{48}Ti, ^{52}Cr, ^{56}Fe, ^{58}Ni, ^{70}Ge, ^{107}Ag, ^{127}I, ^{139}La, and ^{209}Bi. Many isotopes of these, including ^{44}Ca, ^{48}Ca and ^{235}U have also been run. These and other ions have energies and intensities similar to those in the table in the same mass range. Beam energies down to below 0.3 MeV/u are available.

Group Lists

Group Lists

Following are the lists of people in the Nuclear Science Division groups. The lists were not produced in any systematic way and their accuracy is not guaranteed.
At the end of each list are the long-term visitors with their home institutions in parenthesis.
*graduate student.
**undergraduate student.
group leader in bold face.

Administrative Staff
Montgomery, Meredith E.
Cozean, Anne
Davis, Linda J.
Erickson-Weber, Kathleen
Hodges, Robin
Lofdahl, Joy
Phillips, Barbara
Pouncey, Tonya S.
Smith-Burnett, Wanda J.
Sterling, Catherine J.
For Glenn T. Seaborg ,
Associate Director at Large:
Whyte, Sherrill L.
Jackson, June
Ludwig, Janice

Exotic Nuclei: RAMA
J.C. Batchelder*
J. Cerny
D.M. Moltz
T.J. Ognibene*
M. Rowe*
Garry Rose**
Eric Wang**

OASIS
R.M. Chasteler*
R.B. Firestone
J. M. Nitschke
P.A.Wilmarth

High-Spin Studies
F. Azaiez
M.A. Deleplanque
R.M. Diamond
W. Korten
J.R.B. Oliveira
F.S. Stephens
J. Burde (Hebrew University of Jerusalem, Israel)
J.E. Draper (UC, Davis)
E. Rubel* (UC, Davis)
C. Duyar* (UC, Davis)

Heavy-Ion Reactions at Low and Intermediate Energies
Y. Chan
J.A. Scarpacci
R.G. Stokstad
J. Suro Perez* (Instituto de Física, UNAM, México)

Nuclear Astrophysics and Fundamental Symmetries
Y. D. Chan
A. Garcia
R. M. Larimer
K. T. Lesko
E. B. Norman
R. G. Stokstad
I. Zlimen
M. T. F. da Cruz (University of Sao Paulo)
M. M. Hindi (Tennessee Technological University)
F. E. Wietfeldt*
E. Kong**
H. Leung**

Nuclear Astrophysics/Radioisotope Detection
S. Carlson
F. Crawford
H. Marvin*
R.A. Muller
C. Pennypacker
S. Perlmutter
C. Smith*
L. Wang*

Heavy Element Nuclear and Radiochemistry
D.C. Hoffman
G.T. Seaborg
K.R. Czerwinski*
R. Gaylord**
A. Ghiorso
K.E. Gregorich
H.L. Hall (Lawrence Livermore National Laboratory,Livermore, CA)
T.M. Hamilton*
N.J. Hannink*
C.D. Kacher*
B.A. Kadkhodayan*
S.A. Kreek*
M.R. Lane*
D.M. Lee
M.P. Neu*
M.J. Nurmia
A. Türler (Postdoctoral Fellow)
W.D. Loveland (Oregon State University)
A. Bilewicz (Department of Radiochemistry, Institute of Nuclear Chemistry and Technology, Warsaw, Poland)

Isotopes Project
E. Browne
R.B. Firestone
J. Z. James
V.S. Shirley
C.M. Baglin (Morgan Hill, CA)
B. Singh (McMaster University, Canada)
C.A. Stone (San Jose State University)

Intermediate Energy
M. Colonna
N. Colonna
D. N. Delis*
K. Hanold*
M. Justice*
L. G. Moretto
V. Pascalon*
P. Roussel-Chomaz
W. Skulski*
Q. C. Sui
K. Tso*
G. J. Wozniak
B. Libby* (University of Maryland)
A. Veek*
M. Varasten**

Bevalac Computers
R.A. Belshe
C. McParland
W.H. Rathbun
S. Jacobson
E. Yee

DLS
S. Beedoe
N. Eddy **
H. Z. Huang
H. S. Matis
C. Naudet
R. J. Porter*
L.S. Schroeder
P. A. Seidl
W. K. Wilson
J. Carroll (UCLA)
G. Roche (Université de Clermont II, France)

Janus
D. Armstrong
R. Bossingham
T. Case*
K. Crowe
Y. Dardennes* (Michigan State University)

Transfer Reactions and Rotational Inelastic Scattering
J.O. Rasmussen
S. Y. Chu* (Yale)
R. Donagelo (Brazil)

Plastic Track Detectors
P.B. Price
D.M. Lowder
D. Snowden-Ifft
Y.D. He
T. Miller
A. Richards
A. Westphal
W.T. Williams

Secondary Radioactive Beams
K. Matsuta
A. Ozawa*
K. Yoshida

Subthreshold Kaons and Antiprotons
J. Drewery
S.N. Kaplan
V. Perez-Mendez

Nuclear and Astrophysics
C. Chen (LSU)
S. Costa (Catania, Italy)
H.J. Crawford (UCSSL)
J. Engelage (UCSSL)
I. Flores (UCSSL)
L. Greiner (UCSSL)
C. Knott (University of Minnesota)
R. Potenza (Catania, Italy)
C. Tull (LSU)

Relativistic Nuclear Collisions
Fred Bieser
Matt Bloomer
Dan Cebra
Scott Chase*
Santa Chatterji
Bill Christie
Erwin Friedlander
Doug Greiner
Chuck Gruhn
John Harris
Peter Jacobs
Pete Lindstrom
Howard Matis
Richard Morse
Grazyna Odyniec
Doug Olson
Art Poskanzer
Gulshan Rai
Hans-Georg Ritter
Jo Schambach
Iwona Sakrejda
Larry Teitelbaum*
Shaheen Tonse
Jean Marie Walker
Howard Wieman
John Wolf
A. Dean Chacon (Texas A&M)
Salvo Costa (Catania)
Tim Hallman (UCLA)
Eric Hjort (Purdue)
Declan Keane (Kent State)
Louis Lerman* (Philipps)
Martin Partlan* (UC Davis)
Alan Scott* (Kent State)
Yiping Shao* (Kent State)

Theory
G. Batko
S. Chapman
N.K. Glendenning
T. Guhr
M. Gyulassy
C. Jarzynski
W.D. Myers
J. Randrup
M. Redlich
W.J. Swiatecki
X.N. Wang
F. Weber (Max Kade & DFG Fellow/U. Munich, Germany)
G.F. Burgio (INFN Fellow/Italy)
J. Casado (Fulbright Scholar/Santiago, Spain)
P. Chomaz (IN2P3/Orsay, France)
H. Frisk (NFR/Nordita)
M. Grabiak (Feodor Lynen Fellow)
E. Medeiros (CNPq/CBPF, Rio de Janeiro, Brazil)
M. Thoma (DFG/TU Munich, Germany)
T. Vetter (DAAD/U. Giessen, Germany)

Low Energy Experiments

Observation of a Superdeformed Band in ^{192}Pb*

E.A. Henry,[†] A. Kuhnert,[†] J.A. Becker,[†] M.J. Brinkman,[†] T.F. Wang,[†] J.A. Cizewski,[‡] W. Korten, F. Azaiez,[a] M.A. Deleplanque, R.M. Diamond, J.E. Draper,[b] W.H. Kelly,[c] A.O. Macchiavelli, and F.S. Stephens

We have identified a new superdeformed (SD) band and assigned it to ^{192}Pb, extending the region where superdeformation is known in the Hg, Tl, and Pb nuclei near A = 190. The ^{173}Yb(^{24}Mg,5n) reaction with beam energies of 128 and 132 MeV was used to produce ^{192}Pb. Data were acquired with the HERA spectrometer at the Lawrence Berkeley Laboratory 88-Inch Cyclotron. A channel-by-channel search of the data revealed at least nine mutually coincident transitions extending from 262 to 570 keV (Fig. 1). The relative intensity pattern of the transitions in the band is shown in the inset. The assignment of this new band to ^{192}Pb is based on excitation function data and coincidences of the band members with known ^{192}Pb transitions. A gamma-ray spectrum generated by double gating on three- and higher-fold events (Fig. 1) shows the 855-keV ($2^+ - 0^+$), 503-keV ($4^+ - 2^+$), and 566-keV ($6^+ - 4^+$) transitions in ^{192}Pb. Transitions in ^{193}Pb, such as the 521-keV (19/2,21/2 - 17/2) transition, are not observed in this double-gated spectrum. The method of Becker et al.[1] has been used to determine the spins of the levels in this SD band. The assignment to ^{192}Pb limits the spins to integer values. Spins of 10 or 11 are equally probable for the level populated by the 262-keV transition.

This work extends the region of superdeformation near A = 190 to ^{192}Pb. The increase in spin of the lowest observed SD band member in ^{192}Pb compared to ^{194}Pb suggests that ^{192}Pb is near the edge of the SD band region. In Pb, the SD bands do not show identical transition energies when compared among themselves; this is in contrast to a number of cases in the Hg and Tl nuclei. Finally, SD bands are now known in four even mass Pb nuclei, but a SD band has yet to be found in an odd mass Pb nucleus.

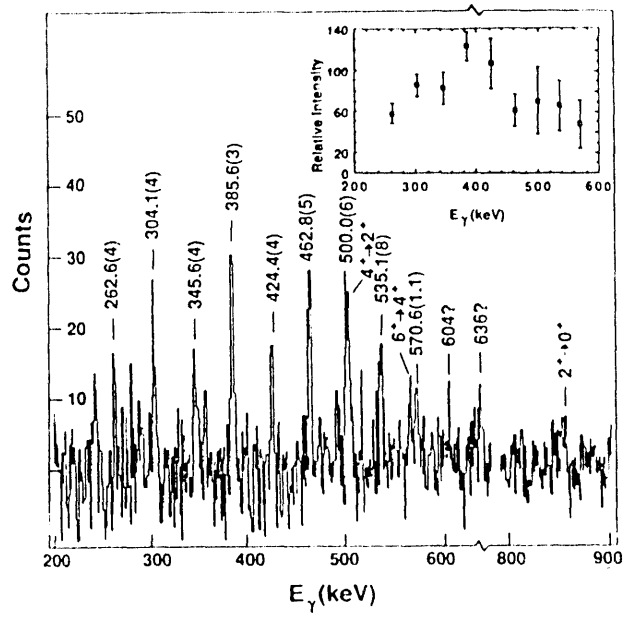

Fig. 1. A spectrum of the SD band produced in the ^{173}Yb(^{24}Mg,5n) reaction at 132 MeV, and assigned to ^{192}Pb. This spectrum is obtained by double gating three- and higher-fold events. SD band transitions are indicated by their energy. Known transitions in ^{192}Pb are indicated by the spin and parity of the levels they connect. The SD band transition intensities include internal conversion (inset).

*Condensed from Z. Phys. A 388, 469 (1991).

† Lawrence Livermore National Laboratory, Livermore, CA 94550.

‡Rutgers University, New Brunswick, NJ 08855.

[a]Permanent address: CEN-BF, IN2P3, Le Haut-Vigneau--33170 Gradigan, France.

[b]Permanent address: Univ. of Cal., Davis, CA 95616.

[c]Permanent address: Iowa State University, Ames, IA 50011.

[1]J. A. Becker, et al., Nucl. Phys. A520, 187c (1990); and to be published.

Superdeformation in the A ~ 190 Mass Region and Shape Coexistence in ^{194}Pb*

M. J. Brinkman,† J. A. Cizewski,† J. A. Becker,‡ E. A. Henry,‡ A. Kuhnert,‡ T. F. Wang,‡ S. W. Yates,‡ M. A. Stoyer,‡ R. M. Diamond,§ F. S. Stephens,§ M. A. Deleplanque,§ A. O. Machiavelli,§ and J. E. Draper§

In the first decades of this century it was believed that the atomic nucleus was a point-like mass that could be completely described by its mass and electrical charge. Currently we know that the nucleus is a many-body system composed of a number of strongly interacting nucleons. While progressing from the early 20th view to the present day, however, it has been found that many of the properties of the nucleus are intimately connected to its physical extent, i.e., the size and shape of the nucleus. Nothing emphasizes this fact more than studies of superdeformation (i.e., nuclei near the limit of large deformation) and shape-coexistence (i.e., nuclei exhibiting distinct nuclear shapes at similar energies and angular momenta).

Within the past three years, worldwide experimental effort has focussed on the neutron-deficient mercury, lead, and thallium nuclei near A ~ 194, as an exceptionally fruitful area for the study of superdeformation, and more recently shape coexistence. A recent collaboration comprised of Rutgers University, Lawrence Livermore National Laboratory, and Lawrence Berkeley Laboratory, has extensively studied the neutron-deficient mercury and lead nuclei with masses near A ~ 194, discovering or independently co-discovering 18 superdeformed rotational bands (out of the 27 such structures known in this mass region) in 9 distinct nuclei (out of the total 13 nuclei known to support superdeformation in this region).

This work was a doctoral dissertation for M. J. Brinkman of Rutgers University. It discusses the superdeformed nuclei in A ~ 190 mass region focussing on the neutron-deficient lead and mercury nuclei which Rutgers University and Lawrence Livermore National Laboratory took a lead role in analyzing. Separate sections detailed what is known about the physics of the population, the intra-band region, and the depopulation of superdeformed rotational cascades in the A ~ 190 mass region.

In addition a discussion of the near-yrast states in ^{194}Pb up to a spin of ~35 $\hbar$ is provided. This work confirms, and in a number of cases corrects, what is already known about this nucleus[1]. In particular, structures characteristic of non-collective oblate and prolate and collective near-oblate and prolate excitations are discussed. The presence of all of the classical modes of low-energy nuclear excitations in ^{194}Pb make it one of the best examples of nuclear shape-coexistence known.

Footnotes and References

*M. J. Brinkman, *Superdeformation in the A ~ 190 Mass region and Shape Coexistence in ^{194}Pb*, unpublished dissertation, Rutgers University, Oct. 1991.

† Rutgers University, New Brunswick, NJ 08903.
‡Lawrence Livermore National Laboratory, Livermore, CA 94550.
§Nuclear Science Division, Lawrence Berkeley Laboratory, Berkeley, CA 94720.

1. B. Fant et al., Jour. Phys. G17 (1991) 319.

Superdeformation in ^{198}Pb

T.F. Wang†, J.A. Becker†, E.A. Henry†, A Kuhnert†, S.W. Yates‡, M.J. Brinkman†, J.A. Cizewski‡, F. A. Azaiez, M.A. Deleplanque, R.M Diamond, J.E. Draper, W.H. Kelly, W. Korten, A.O. Macchiavelli, E. Rubel, F.S. Stephens, and Y.A. Akovali§

Three-dimensional Hartree-Fock calculations and cranked Strutinsky calculations all predict well-developed secondary minima in the nuclear energy surface throughout the A ~194 mass region. In fact, about 25 SD bands have been experimentally observed, and many of these SD bands show similar moments of inertia, and "identical" transition energies. Hence, it is important to map out the boundaries of superdeformation.

We have extended the region of superdeformation to N = 116. Fig. 1 shows the single-gated coincidence spectrum for the ^{198}Pb SD band populated via the ^{154}Sm(^{48}Ca,4n)^{198}Pb reaction at E(^{48}Ca) = 205 MeV. About 280 million coincidence events were recorded at both E(^{48}Ca) = 205 and 210 MeV. The isotopic identification was based on the excitation function behavior with different H and K cuts at the two energies.

Spin assignments of the members of SD bands were obtained from least squares fits to the expression:

$$I + 1/2 = 2\alpha\omega + 4/3\beta\omega^3. \qquad (1)$$

With the choice $\omega = dE/dI = E_\gamma/2$, I is the intermediate spin of the transition I + 1 → I - 1. The 303.8-keV γ ray is assigned as $I_i \rightarrow I_f = 14 \rightarrow 12$ transition.

An interesting feature deduced of the SD bands in ^{194,196,198}Pb is shown in Fig. 2. While many of the even-even nuclei have similar dynamic moment of inertia, $J^{(2)}$, the $J^{(2)}$(^{198}Pb) and $J^{(2)}$(^{196}Pb) are different than $J^{(2)}$(^{194}Pb), although all three nuclei have almost the same moment of inertia, 2α. It is possible that the pairing does not change as much with frequency in ^{196,198}Pb than ^{194}Pb. Another interesting feature is that alignment of the ^{198}Pb SD band with increasing ħω does not saturate at a "quantized" value with respect to the reference ^{192}Hg SD band in contrast to many other SD bands in this region.

Footnotes and References

†Lawrence Livermore National Laboratory, Livermore, CA 94550.
‡Rutgers University, New Brunswick, NJ 08903.
§Oak Ridge National Laboratory, Oak Ridge, TN 37380.

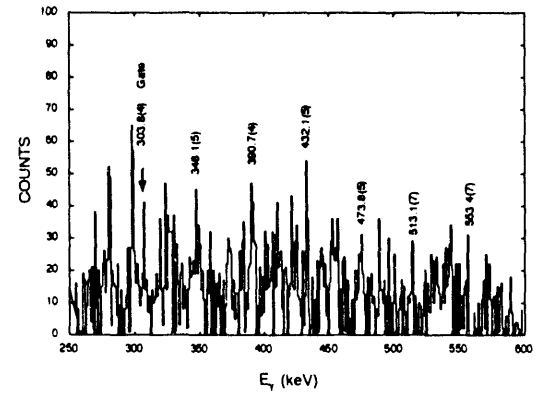

Fig. 1. Single-gated coincidence spectrum for the ^{198}Pb SD band; transition energies with errors are shown.

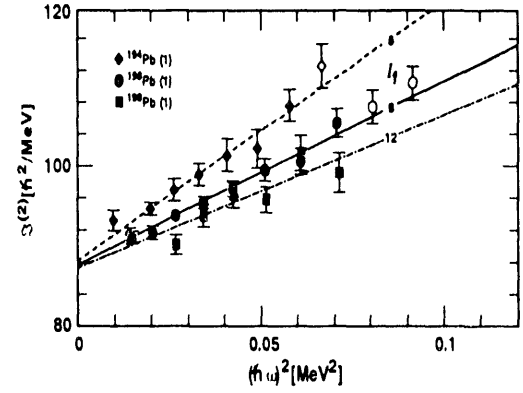

Fig. 2. The dynamic moment of inertia of ^{194,196,198}Pb SD bands as a function of $(\hbar\omega)^2$. The lines are calculated from the parameters α and β obtained with integer values of I_f obtained with Eq.(1).

Partial Level Scheme of ^{198}Pb

T.F. Wang[†], J.A. Becker[†], E.A. Henry[†], A.Kuhnert[†], M.A. Stoyer[†], S.W. Yates[‡], M.J. Brinkman[†], J.A. Cizewski[‡], F. A. Azaiez, M.A. Deleplanque, R.M Diamond, J.E. Draper, W.H. Kelly, W. Korten, A.O. Macchiavelli, E. Rubel, F.S. Stephens, and Y.A. Akovali[§]

Neutron-deficient Pb isotopes with a closed proton shell have long been good candidates for studies of nuclear excitations involving only a few active particles. In fact, low-lying structure in these isotopes can be described reasonably well in terms of two- and four- quasiparticle excitations. One long standing question is the possible onset of collective structures at high angular momentum in these isotopes.

We have observed two dipole collective bands in ^{198}Pb via the ^{154}Sm(^{48}Ca,4n)^{198}Pb reaction at E(^{48}Ca) = 205 MeV. Both thin target (a stack of three ~ 0.5 mg/cm^2 ^{154}Sm foils) and backed-target (~ 1mg/cm^2 ^{154}Sm, evaporated onto ~ 12 mg/cm^2 Pb) bombardments were made. About ~ 200 million double coincidence events were collected for each target. The results from the thin-target were used to identify the sequence of the two newly observed bands in ^{198}Pb. Backed-target results were used to establish the connection between the new levels and the known low-lying isomeric states in ^{198}Pb, and to suggest the possible location of previously unobserved isomeric states.

Fig. 1 shows the partial level scheme of ^{198}Pb deduced from present study. The identification of the 322-, 323- keV doublet is based on a channel by channel projection of the 2-D coincidence matrix, and verified by coincidence gates on other band members. Directional correlation analysis shows that most of the transitions are $\Delta I = 1$. Assuming pure M1 character of the dipole transitions, possible level spin-parity are shown.

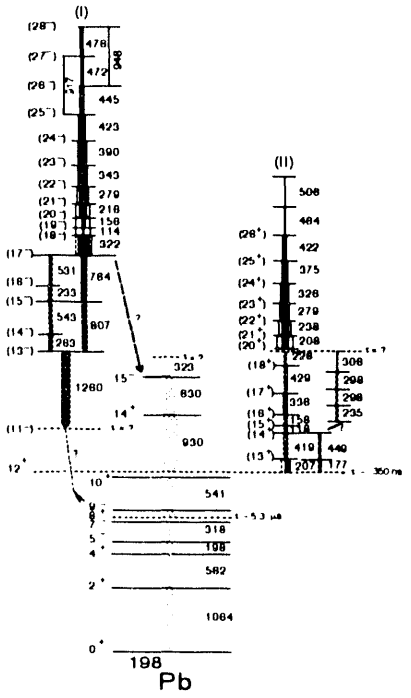

Fig. 1 Partial Level scheme of ^{198}Pb. Previously observed transitions are shaded in light gray, newly established low-lying transitions are in dark gray, and the proposed dipole collective structures are in black. Dashed-lines represent suggested locations of the isomeric states. The intensities above 12' isomer are based on the γ-ray intensities observed in thin target measurement. Transition intensities below the 10' state cannot be determined from the present study. Spin assignments are no better than ±2 ħ.

Footnotes and References

†Lawrence Livermore National Laboratory, Livermore, CA 94550.

‡Rutgers University, New Brunswick, NJ 08903.

§Oak Ridge National Laboratory, Oak Ridge, TN 37380.

Lifetimes of Dipole Collective bands in ^{198}Pb

T.F. Wang[†], J.A. Becker[†], E.A. Henry[†], A.Kuhnert[†], M.A. Stoyer[†], S.W. Yates[‡], M.J. Brinkman[†], J.A. Cizewski[‡], F. A. Azaiez, M.A. Deleplanque, R.M Diamond, J.E. Draper, W.H. Kelly, W. Korten, A.O. Macchiavelli, E. Rubel, F.S. Stephens, and Y.A. Akovali[§]

We have measured lifetimes of states in two dipole collective bands[1] in ^{198}Pb using Doppler-shift-attenuation method (DSAM). The ^{154}Sm(^{48}Ca,4n)^{198}Pb reaction at E(^{48}Ca) = 205 MeV was used to populate the band members. Two backed targets were used,~ 1mg/cm^2 ^{154}Sm, evaporated onto ~ 12 mg/cm^2 Pb or Au. About ~ 200 million double coincidence events were collected for each target.

The lifetime analysis was made with coincidence data from the Au- and Pb- backed targets sorted into forward, "90°", and backward matrices. Doppler-shifted lineshapes were observed for transitions in both bands for transition energies between ~300 keV and ~500 keV. Lifetimes were extracted using a Monte-Carlo Code. Results for both bands for Au and Pb backed are summarized in Table I.

The relatively large (~1-2 W.u.) B(M1) strength among band members suggests that these are high-K bands. The dynamic moment of inertia of both bands $\mathcal{J}^{(2)}$ ~ 25$\hbar^2$ MeV^{-1}, about 1/3 of the kinematic moment of inertia, suggests a large amount of aligned angular momentum. The alignment estimated to be ~14(3) $\hbar$, and it is presumably from the alignment of $i_{13/2}$ neutrons. The M1 transition rate can be estimated from the relation:

$B(M1)=(3/4\pi)K^2(g_k-g_r)^2 \langle IK10|I-1,K\rangle$, (1)

where g_r is the collective g-factor (~Z/A). Using g_k = 0.96 for the $\pi(h_{9/2}\otimes i_{13/2})_{11}$- configuration, the reduced M1 transition probability calculated for K=11, I=26 is ~ 1.8 W.u., in qualitative agreement with the measured transition strengths of the two bands. The deformation consistent with the properties of the two bands is $|\beta_2|$ ~ 0.1. This value is in reasonable agreement with the predicted oblate minimum at β_2 ~ -0.15 by Bengtsson and Nazarewicz[2].

Footnotes and References

1) See "Partial Level Scheme of ^{198}Pb" by T.F. Wang et al., in this Annual Report.

2) R. Bengtsson and W. Nazarewicz, Z. Phys. **A334**, 269 (1989).

†Lawrence Livermore National Laboratory, Livermore, CA 94550.

‡Rutgers University, New Brunswick, NJ 08903.

§Oak Ridge National Laboratory, Oak Ridge, TN 37380.

		Pb-BACKING				Au-BACKING		
	E_γ (keV)	τ (ps)	B(M1) (W.u.)	B(E2) (W.u.)		τ (ps)	B(M1) (W.u.)	B(E2) (W.u.)
BAND (I)	343	1.12(39)	0.53 $^{+0.29}_{-0.14}$			1.15(24)	0.52 $^{+0.14}_{-0.09}$	
	390	0.84(15)	0.67 $^{+0.20}_{-0.12}$			0.79(14)	0.55 $^{+0.12}_{-0.08}$	
	423	0.41(16)	0.85 $^{+0.54}_{-0.24}$			0.50(11)	0.70 $^{+0.20}_{-0.13}$	
	445	0.19(7)	1.6 $^{+0.9}_{-0.4}$			0.29(4)	1.1 $^{+0.2}_{-0.1}$	
	472	0.29(10)	0.72 $^{+0.66}_{-0.23}$	11.3 $^{+10.3}_{-3.6}$		0.15(5)	1.3 $^{+1.0}_{-0.4}$	20.6 $^{+15.9}_{-6.3}$
	917							
	478	0.31(11)	0.67 $^{+0.54}_{-0.21}$			0.23(7)	0.9 $^{+0.7}_{-0.3}$	
	948			9.7 $^{+7.9}_{-3.1}$				13.3 $^{+10.2}_{-4.4}$
BAND (II)	326	0.60(19)	1.1 $^{+0.5}_{-0.3}$			0.55(22)	1.2 $^{+0.8}_{-0.4}$	
	375	0.31(9)	1.6 $^{+0.6}_{-0.4}$			0.40(17)	1.2 $^{+0.8}_{-0.3}$	
	422	0.18(5)	2.0 $^{+0.8}_{-0.4}$			0.22(7)	1.6 $^{+0.7}_{-0.4}$	
	464	0.088(18)	4.0 $^{+1.5}_{-0.9}$			0.129(47)	2.1 $^{+1.2}_{-0.6}$	
	508	0.050(14)	4.4 $^{+1.7}_{-1.0}$			0.054(17)	4.0 $^{+2.0}_{-1.0}$	

Table 1. Results from the DSAM Fits to both bands, with data sets from Pb and Au backed targets.

Oblate Collectivity in ^{197}Pb*

A. Kuhnert †, M.A. Stoyer †, J.A. Becker †, E.A. Henry †, M.J. Brinkman †, S.W. Yates ‡, T.F. Wang,† J.A. Cizewski §, F. Azaiez, M.A. Deleplanque, R.M. Diamond, J.E. Draper, W.H. Kelly, W. Korten, A.O. Macchiavelli, and F.S. Stephens

The data from the fusion reactions ^{176}Yb(^{26}Mg,5n) at 135 MeV,and ^{154}Sm(^{48}Ca,5n) at 210 MeV beam energy, respectively, revealed several sequences of up to twenty strong dipole transitions. Two of these bands, one regularly and one irregularly spaced, have been unambiguously assigned to ^{197}Pb. Fig. 1 shows a partial level scheme for ^{197}Pb including the regular band. Their most likely decay pattern into the low-lying states was determined from the data (see fig. 1), although no linking transitions have been found so far. The DCO and γ-ray yield ratios for the detectors close to 30° and close to 90° suggest ΔI=1 for the main transitions in these bands. For the irregular structure one has to assume M1 electron conversion to obtain a consistent intensity balance within this band. This argument does not hold strictly for the regular band. However, we have assumed M1 transitions for the regular band also, because the observed intensities of the low-lying band members and their decay into the quasiparticle states are most consistent with this assumption. Additionally several of the ΔI=2 crossover transitions have been observed in both bands.

Lower limits for the bandhead excitation energies and angular momenta have been deduced from the experimental data. A reasonable estimate for the excitation energies is E_x > 3.8 MeV for the regular band, and E_x > 3.3 MeV for the irregular band (see fig. 1). The spins of the lowest states in these bands are most likely I≈33/2±2 ħ (regular) , and I≈ 31/2±2 ħ (irregular).

Based on our model calculations we suggest the regular band to be an oblate collective band built on a $\pi(1/2^+[400]^{-2}; 9/2^-[505]; 13/2^+[606])_{11^-} \otimes \nu(fp)^4 (i_{13/2})^{-3})$ state. The corresponding $\pi(11^-)$ state is seen in ^{196}Pb[1]. It has a g-factor of + 0.96(8) [2], and therfore a large magnetic moment perpendicular to the rotation axis of the nucleus and consequently strong M1 transitions. We expect an oblate state in ^{197}Pb, with the above mentioned configuration, close to an excitation energy of E_x=3.1 MeV. The irregular band shows the characteristics of a collective band. However, it is not a typical collective band because of the strong irregularities seen in a I versus ħω plot. We cannot give a detailed explanation for the mechanism leading to this irregular band, but from our quasiparticle Routhian calculations we suggest it is most likely a triaxial rotational band, i.e. γ ≈ −100°, built on the same general configuration described above.

† Lawrence Livermore National Laboratory, Livermore, CA 94550.

‡ University of Kentucky, Lexington, KY 40506.

§ Rutgers University,New Brunswick, NJ 08903.

*A. Kuhnert et al., submitted to *Phys. Rev. C.*

1. B. Fant et al., J. Phys. G Nucl. Part. Phys. 17, 319 (1991).

2.J. Penninga et al., Nucl. Phys. A471, 535 (1987).

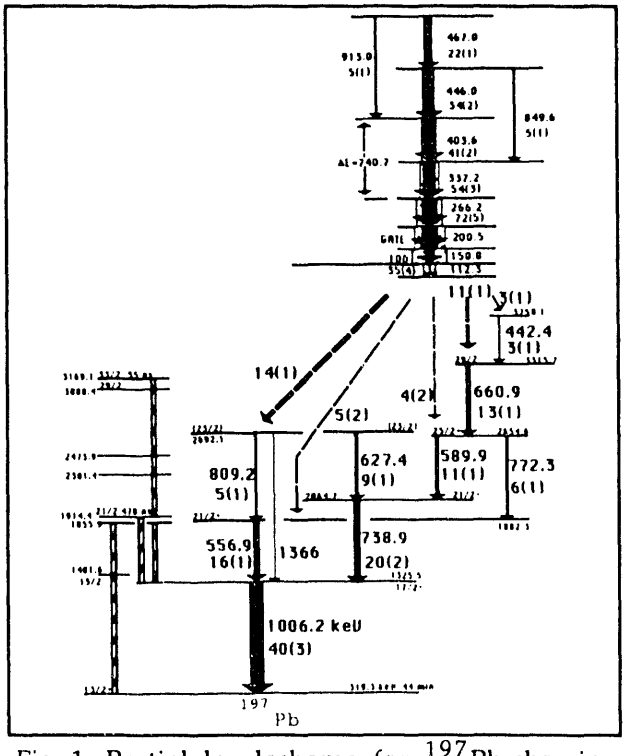

Fig. 1 Partial levelscheme for ^{197}Pb showing the most likely population of the low-lying levels by the regular band. The energies are in keV.

Inertia of Superdeformed Nuclei near $A = 194$

J. A. Becker, E. A. Henry*, A. Kuhnert*, T. F. Wang*, and S. W. Yates*, J. A. Cizewski†, M. J. Brinkman†, R .M. Diamond, F .S. Stephens, J. E. Draper‡, W. Korten, M. A. Deleplanque, A. O. Macchiavelli, F. Azaiez, and W. H. Kelly*

The notion that reliable spin assignments may be made for superdeformed (SD) bands in the $A = 194$ region based on expectations of the rotational model was introduced by Becker and coworkers,[1] in their study of superdeformation in ^{192}Hg. All experimental evidence suggests that the SD band members in this mass region are nuclear states characterized by the dynamics of an extremely good quantum rotor, and so this notion has been applied to 25 SD bands in 13 nuclei near $A = 194$. The transition energies were fit to the power series expansion of I in odd-powers of $E_\gamma/2$, $I + 1/2 = \alpha\omega + \beta\omega^3$, where $E_\gamma/2 = \hbar\omega$, and to the expression for transition energy, $E_\gamma = E(I+2) - E(I)$, where $E(I) = AI(I+1) + B(I(I+1))^2 + C(I(I+1))^3$. The leading order term of both fitting equations is just the expression for the transition energy of the quantum rotor: $E_\gamma(I + 1 \rightarrow I - 1) = 4A(I + 1/2)$, which can be seen with the substitutions $E_\gamma = 2\hbar\omega$ and $2\alpha = \hbar^2/(2A)$. The fitting was done with the assumption that all SD transitions are $L = 2$, and thus the fitting produces inertial parameters and a baseline spin, I_f. Excellent fits were obtained for 25 bands over an angular momentum range of at least $18\hbar$. The parameter I_f is (half)integer within $\pm 0.1\ \hbar$ for 18 of the 25 bands. Results are generally similar for the two fitting equations, and I_f is identified with level spin. Estimates based on cranked shell model calculations suggest that an error of no more than $\sim 1/2\ \hbar$ is expected in identifying I_f with I for orbitals likely to be involved.

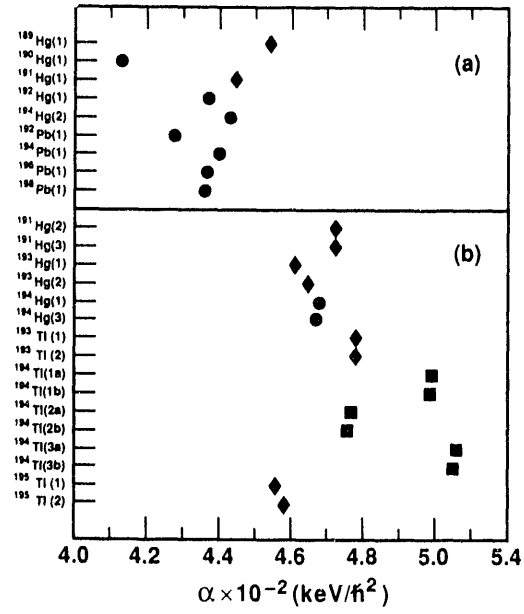

Fig. 1. The parameter α for bands without an observed signature partner (a), and for bands with a signature partner (b). Values for even-even, odd-A, and odd-odd nuclei are symbolized by ○, ◇, and □, respectively. Errors are less than the size of the plotting symbol.

Values of α calculated with (half)integer I_f corresponding to the least-squares minima are illustrated in Fig. 1 and they show some correlations. Bands identified as signature partners with small signature splitting have values of α equal within 1/4% or less (except for ^{193}Hg), supporting that identification. Values of α are distinct for the yrast and excited bands, and values of α for bands with and without observed signature partners show a clustering. The small change in α with ^{A}Z is consistent with values predicted using the results of fully self-consistent microscopic Hartree-Fock calculations.

Footnotes and References

*Lawrence Livermore National Laboratory.
†Rutgers University.
‡UC Davis.

[1] Becker, et al., Phys. Rev. C 41, R9(1990).

Lifetimes of Superdeformed States in ^{194}Pb

P. Willsau†, H. Hubel†, F. Azaiez, M.A. Deleplanque, R.M. Diamond, W. Korten, A.O. Macchiavelli, F.S. Stephens, H. Kluge††, F. Hannachi‡, J.C. Bacelar, J.A. Becker°, M.J. Brinkman°, E.A. Henry°, A.Kuhnert°, T.F. Wang°, J.A. Draper°°, E. Rubel°°*

The superdeformed (SD) rotational bands that have been found in the mass-190 region, in contrast to the mass-150 region, all show very similar dynamical moments of inertia $J^{(2)}$ that rise by about 40% over the observed frequency range. This might be caused by an increase in deformation or by a gradual alignment or loss of pairing correlations. This question can be answered in part by lifetime measurements which give the reduced transition probabilities. These in turn give the transition quadrupole moments, Q_t, via the rotational model. Since the transitions between the SD states have lifetimes of picoseconds down to a fraction of a picosecond, the Doppler-shift attenuation method (DSAM) can determine some of them. Such a measurement has been made[1] for ^{192}Hg, yielding $Q_t \approx 19$ barns and confirming a large, constant deformation. The present experiment is a similar measurement for the SD states in ^{194}Pb. The reaction used was ^{150}Sm(^{48}Ca, 4n) ^{194}Pb at the 88-Inch Cyclotron on a 1.1 mg/cm^2 foil with a 10mg/cm^2 gold backing. The gamma rays were detected with the 20 Compton-suppressed Ge detectors of HERA.

The five SD transitions above 380 keV show lineshapes for which a DSAM analysis could be performed. A Monte Carlo simulation program, which included a subroutine to solve the Bateman system of coupled differential equations for the decays of the states involved, was used. The intensities of the SD and of contaminant transitions, as well as the quadrupole moments, were simultaneously treated as free parameters in a least-squares fit to the experimental lineshapes. Only spectra from the backward detectors were clean enough for analysis, and side-feeding could be neglected in the region analyzed.

The values of Q_t derived from the lifetimes are shown in Fig. 1. Within the experimental uncertainties, they are constant at ≈ 20 barns. The dashed curve indicates the moments necessary to yield the observed increase in $J^{(2)}$ in ^{194}Pb if it were due only to centrifugal stretching. Since the experimental transition moments are essentially constant (as in the previous investigation[1] in ^{192}Hg), the deformation must be constant and the increase in $J^{(2)}$ is due to either an increasing alignment or decreasing pairing, or most likely to both.

Footnotes and References

† ISK, Universitat Bonn, D-5300 Bonn, Germany
†† HMI D-1000 Berlin, Germany
‡ CSNSM, F-91405 Orsay, France
* KVI, 9747 AA Groningen, The Netherlands
° LLNL,Livermore, CA, 94550
°° University of California, Davis, CA 95611

1. E.F. Moore et al., Phys. Rev. Lett. 64, 3127 (1990)

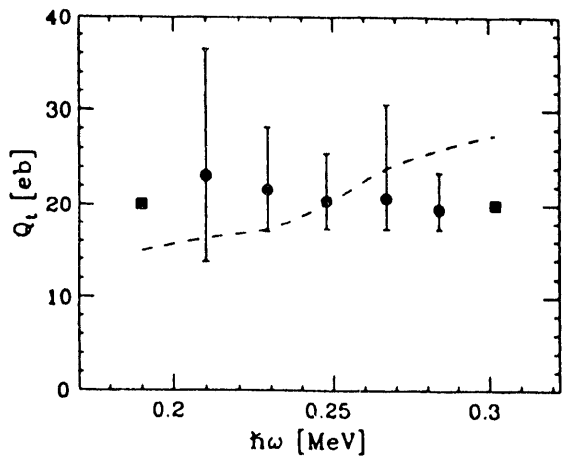

Fig. 1. Experimental Q_t of SD states in ^{194}Pb *vs.* rotational frequency. Dashed curve calculated assuming rise in $J^{(2)}$ due to centrifugal stretching.

Experimental Determination of Resolving Power of HERA Using Four-Fold Coincident Events*

M. J. Brinkman,†§ J. A. Becker,† E. A. Henry,† A. Kuhnert,† R. M. Diamond,‡ F. S. Stephens,‡ M. A. Deleplanque,‡ A. O. Machiavelli,‡ J. E. Draper,‡ and J. A. Cizewski§

The next generation of large multi-detector arrays for gamma-ray spectroscopic studies (i.e., GAMMASPHERE and EUROGAM) are currently being constructed. These arrays have been designed to maximize the collection of high multiplicity events and to optimize their resolving power[1].

The resolving power of an array is a direct measure of the ease with which one can extract information about gamma-rays of interest by gating on gamma rays in coincidence. The resolving power of the array manifests itself as an increase in the peak-to-background ratio of the gamma ray of interest as successively more stringent gating conditions are applied.

We have measured the resolving power of the High Energy-Resolution Array, located at the Lawrence Berkeley Laboratory's 88-Inch Cyclotron facility, through three increases in the gating requirements. The data used was collected following the $^{176}Yb(^{22}Ne,6n)^{192}Hg^{*}$ reaction at E(^{22}Ne) = 122 MeV. This data was chosen because it is known to contain a 17 member superdeformed rotational band, populated at ~2% of the total ^{192}Hg cross-section.

To avoid possible selection bias we created a data set containing only events in which four or more Ge detectors fired in coincidence. Following this we measured the peak-to-background ratio of the ^{192}Hg superdeformed band through three increases in the gating condition. The improvement in the peak-to-background ratio was ~125, allowing one to study the superdeformed band without the necessity of background subtraction (see figure 1).

Footnotes and References

*M. J. Brinkman et al., *Proceedings of the Conference on Capture Gamma-Ray Spectroscopy and Related Topics*, AIP Conference Proceedings 238, October 1990, Pacific Grove, CA.

† Lawrence Livermore National Laboratory, Livermore, CA 94550.

‡Nuclear Science Division, Lawrence Berkeley Laboratory, Berkeley, CA 94720.

§Rutgers University, New Brunswick, NJ 08903.

1. M. A. Deleplanque and R. M. Diamond, eds., *GAMMASPHERE-A National Gamma-Ray Facility, a Proposal*, (1988).

2. J. A. Becker, N. Roy, E. A. Henry, M. A. Deleplanque, C. W. Beausang, R. M. Diamond, J. E. Draper, F. S. Stephens, J. A. Cizewski, and M. J. Brinkman, *Phys. Rev.* **C41** (1990) R9.

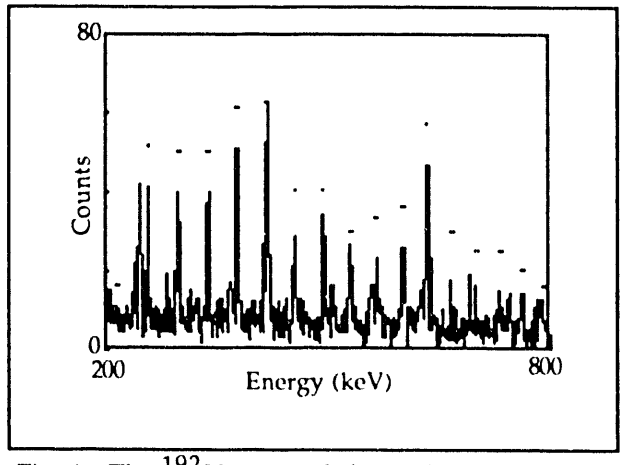

Fig. 1. The ^{192}Hg superdeformed band obtained by requiring three gamma-ray energies in all four-fold coincident events to lie within distinct gates set on the superdeformed band members. The members of the superdeformed band are denoted by •.

Shape Coexistence from the Structure of the Yrast Band in ^{174}Pt*

G.D. Dracoulis†, B. Fabricius†, A.E. Stuchbery†, A.O. Macchiavelli, W. Korten, F. Azaiez§, E.Rubel††, M.A. Deleplanque, R.M. Diamond, and F.S. Stephens

In the region of the closed shell Z=82, and around neutron number N=102, the coexistence of near-spherical and well deformed shapes at low spin and low excitation energy is well known. As one moves away towards smaller proton numbers, the ground state becomes well deformed, and only in more neutron-deficient nuclei does the ground state become spherical again.

The coexistence of a near-spherical band and a more deformed band in the same excitation energy and spin regions results in an yrast sequence that presents an irregularity in the region where the two bands cross. This has been observed in a number of nuclei in that mass region. In the Pt nuclei, this irregularity was hardly visible in ^{176}Pt. The present paper reports on the study of ^{174}Pt with the goal of seeing a clear transition between the two bands in that nucleus.

The nucleus ^{174}Pt was produced at the 88-Inch Cyclotron via the ^{107}Ag(^{70}Ge,2np) reaction at 303 MeV, favored in this case because of the neutron deficiency of the product.

The level scheme obtained is shown in Fig.1, together with alignment plots for this and the two neighboring even-Pt isotopes. The irregularity is much the clearest in ^{174}Pt, corresponding to a crossing between a weakly deformed ground state band and a well-deformed band in the 2-6 spin region.

These results are in general agreement with the systematics of that region, but the detailed mechanism producing the band crossing is not well understood.

Footnotes and References

*Condensed from Phys. Rev. C44, R1246 (1991)

† Australian National University, Australia

‡University of California, Davis, CA 95616

§Institut de Physique Nucleaire, Orsay, France

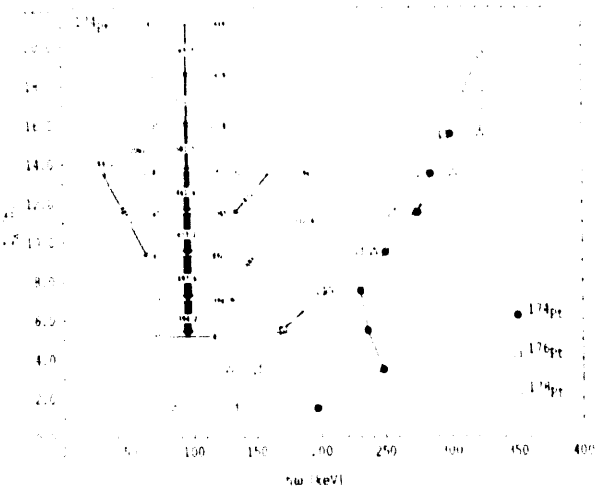

Fig. 1. Level scheme observed for the nucleus ^{174}Pt, and alignment plots for the three neighboring even Pt isotopes.

Electromagnetic properties of Tungsten Nuclei*

C.Y. Wu**, D. Cline**, E.G. Vogt†, W.J. Kernan††, T. Czosnyka#, K.G. Helmer**, R.W. Ibbotson**, A.E. Kavka##, B. Kotlinski**, and R.M. Diamond

The tungsten nuclei, near a prolate-oblate shape transition, are good cases for studying the coupling of β and γ vibrations, as the β and γ bands are low-lying and at nearly the same excitation energies. But both model calculations and experimental results give contradictory results. Some indicate strong coupling by a large (5-10 fold) reduction in the static quadrupole moments of the 2^+ states in these bands and large deviations from the Alaga rule for their decay. But others suggest weak coupling.

The present experiment studied the electromagnetic properties of $^{182,184}W$ by Coulomb excitation using 561 MeV ^{136}Xe ions from the LBL SuperHILAC and 235 MeV ^{58}Ni ions from the BNL Tandem. Four position-sensitive parallel-plate avalanche counters (PPAC) detected the scattered and recoiling particles in kinematic coincidence, and eight Compton-suppressed Ge's surrounding the PPAC's detected the coincident γ rays. A total of ≈1600 and ≈1900 independent γ-ray yields for ^{182}W and ^{184}W, respectively, were used to extract the relevant electromagnetic matrix elements using the semiclassical Coulomb-excitation least-squares search code GOSIA. States with spins up to 18^+ for the ground-state band and to 16^+ and 6^+ for the γ and β bands, respectively, were included in the analysis.

Some 35 E2 and 4 M1 matrix elements for ^{182}W, and a similar set for ^{184}W, were determined for states to spin 16^+ and 12^+ of the ground and γ bands, respectively. (The results for the static matrix elements of the latter are shown in Fig. 1.) From these data it is found that their interaction is well described by a weak coupling between them. Furthermore, three-band mixing calculations indicate that the coupling between the β- and γ-vibrational bands is also weak, which disagrees with the prediction of the pairing-plus-quadrupole model[1], but is in agreement with calculations on tungsten nuclei by references 2. and 3.

Footnotes and References

* Condensed from Nucl. Phys. A533, 359 (1991)

**NSRL, University of Rochester, Rochester, NY 14627
†Munich University, D-8046 Garching, Germany
††Physics Department, SUNY, Stony Brook, NY 11794
#Warsaw University, 02-097 Warsaw Poland
##Uppsala University, S-75121 Uppsala, Sweden

1. K. Kumar and M. Baranger, Nucl. Phys. A122, 273 (1968)
2. P.O. Hess, J. Maruhn and W. Greiner, J of Phys. G7, 737 (1981)
3. P.O. Duval and B.R. Barrett, Phys. Rev. C23, 493 (1981)

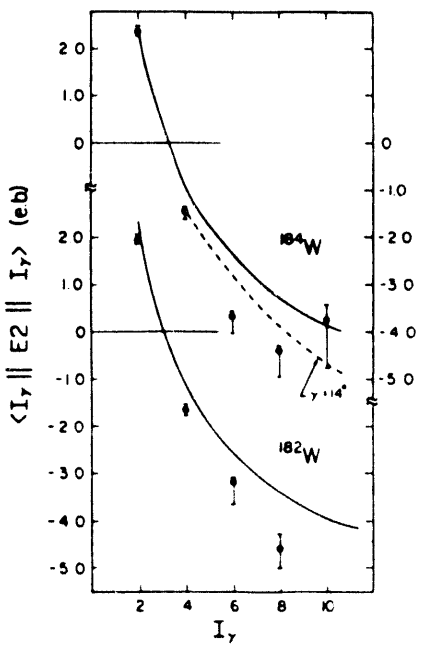

Fig. 1. Experimental static E2 matrix elements for the γ band and predictions of symmetric and asymmetric rotor models, labeled with solid and dashed curves, respectively.

Population of high-spin states in ^{234}U by heavy-ion-induced transfer reactions*

K. G. Helmer, C. Y. Wu, D. Cline, M. A. Deleplanque, R. M. Diamond, A. E. Kavka, W. J. Kernan, X. T. Liu, A. O. Macchiavelli, R. J. McDonald, J. O. Rasmussen, F. S. Stephens, M. A. Stoyer, and E. G. Vogt

We have performed the one-neutron pickup transfer experiments ^{235}U(^{58}Ni,^{59}Ni)^{234}U and ^{235}U(^{206}Pb,^{207}Pb)^{234}U at bombarding energies near the Coulomb barrier. The goal of this work was to compare the high-spin one neutron transfer populations in order to note any effects of the rotational excitation on the final spin population in ^{234}U. The grazing angle for each reaction as well as the total transfer cross section have been extracted. The cross section for the ^{206}Pb + ^{235}U reaction is compared to a prediction of a semi-classical model for transfer reactions involving ^{208}Pb and is found to fit the systematics nicely.

The initial experiment was performed at the Holifield Heavy Ion Research Facility using a 325 MeV beam of ^{58}Ni ions impinging on a 300-μg/cm^2 ^{235}U target with a 110-μg/cm^2 Ni backing. The scattered ions were observed in a parallel-plate avalanche counter (PPAC) in coincidence with γ-rays detected using the Spin Spectrometer plus 14 Ge detectors (12 Compton suppressed). Further experimental details can be found in Ref.[1]

The second experiment was done using a 1394 MeV beam of ^{206}Pb ions, from the SuperHILAC at LBL, to bombard a ^{235}U target on thin Ni backing.

Both the recoiling U and the scattered Pb ions were detected by the Rochester six-sided position-sensitive parallel-plate avalanche counter in coincidence with the deexcitation γ-rays by 14 Compton suppressed Ge detectors. The PPAC's covered an angular range of 300° - 360° in ϕ and 15° - 111° in θ relative to the beam direction. The beamlike and targetlike fragments were partially resolved by their time-of-flight difference and the measured scattering angles. The γ rays were corrected for Doppler shift on an event-by-event basis using the measured kinematics.

Fig. 1 shows a sample gated spectra of ^{234}U transitions for the two different projectiles. With the heavier projectile the transitions go to higher spin, but the resolution is degraded due to incomplete mass separation and consequently poorer Doppler shift corrections.

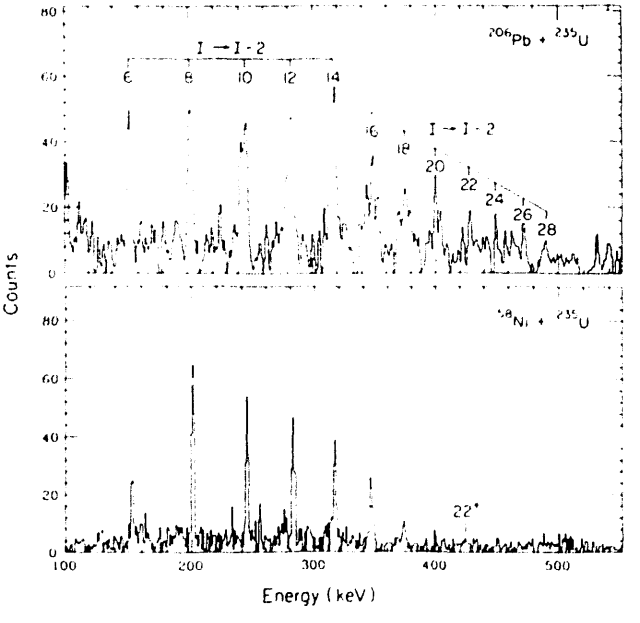

Fig. 1. Particle-gamma-gamma Coincidence spectra for the Pb (upper) and Ni (lower) projectiles. The spectra have summed gates on the $8^+ \rightarrow 6^+$, $10^+ \rightarrow 8^+$ and $12^+ \rightarrow 10^+$ transitions of ^{234}U.

Footnotes and References

*Published in *Phys. Rev. C* **44**, 2598 (1991).

[1] C. Y. Wu, X. T. Liu, S. P. Sorensen, R. W. Kincaid, M. W. Guidry, D. Cline, W. J. Kernan, E. Vogt, T. Czosnyka, A. E. Kavka, M. A. Stoyer, J. O. Rasmussen, and M. L. Halbert, *Phys. Lett. B* **188**, 25 (1987).

Plutonium Speciation at the Solubility Limit in Near Neutral Carbonate Solutions

M.P. Neu, H. Nitsche, R.J. Silva,† R.E. Russo, andD.C. Hoffman

We are measuring the solubility limited speciation of ^{242}Pu as a function of time in near neutral carbonate solutions to better understand the chemical behavior of Pu in groundwater. Because Pu is only slightly soluble under these conditions[1] we are using laser-induced photoacoustic spectroscopy, which is roughly 100 times more sensitive than conventional spectrophotometry, to identify and quantify Pu^{4+}, PuO_2^+ and PuO_2^{2+}. A remote system was assembled to measure spectra of radioactive samples in a glove box, thus avoiding the risk of exposure and contamination of the laser laboratory. The photoacoustic spectrometer, shown schemetically in Fig. 1, includes an optical fiber to deliver excitation laser light to the cuvette and is similar to a system previously reported[2] . A representative spectrum of Pu^{4+} in perchloric acid obtained using this spectrometer is shown in Fig. 2.

Solutions are prepared and monitored in a way similar to those used in solubility studies.[3] Pu of the desired oxidation state is prepared electrochemically and added to a pre-equilibrated carbonate solution. All experiments are performed at pH = 6.0, T = 30.0, P_{CO2} = 5.71%, with 0.100 M in sodium perchlorate as an electrolyte. A Pu^{4+} solubility/speciation experiment in which spectral absorbtion regions for Pu^{4+} and PuO_2^+ were scanned and liquid scintillation counting was performed has been completed.

To reduce the amount of Pu used in experiments, a smaller volume cuvette was placed in the glove box . The 10X microscope objective initially used to collimate the light from the fiber and direct it into the cuvette was replaced by a convex lens and an iris. There was no loss in sensitivity due to these modifications; however as expected photoacoustic signals from system have a different waveform.

Footnotes and References

†Permanent address: Lawrence Livermore National Laboratory, Livermore, CA 94550

1. H. Nitsche, M.A.T. Res. Soc. Symp. Proc. Vol. 212, 1991 Material Research Society,, 517-529 (1991).

2. R.E. Russo, D. Rojas, P. Robouch and R.J. Silva, Rev. Sci. Instrum. 61(12), 3729 (1990).

3. D.B. Tucker, E.M. Standifer, H, Nitsche and R.J. Silva Lanth. and Act. Res. 2, 279 (1988).

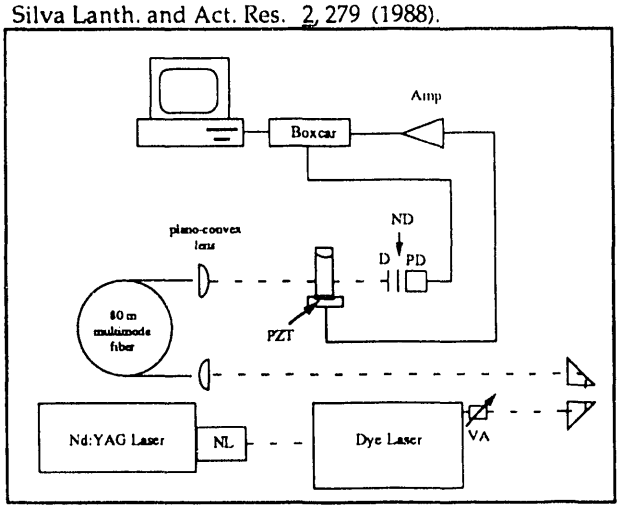

Fig. 1. Schematic of the optical fiber photoacoustic spectrometer. NL non-linear optics, PZT, piezoelectric transducer; D, diffuser; ND, neutral density filter; PD, photodiode; AMP, preamplifier and amplifer .

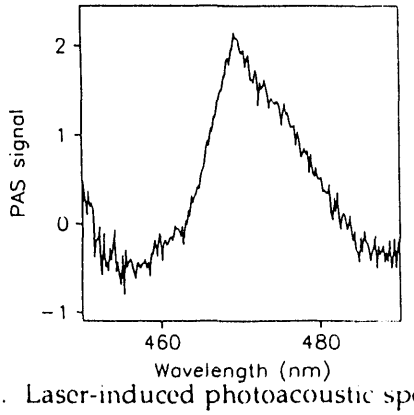

Fig. 2. Laser-induced photoacoustic spectrum of 2.0×10^{-5} M Pu^{4+} in 1.0 M $HClO_4$ using LD466 laser dye (Exiton).

New Apparatus for High Voltage Molecular Plating

K.E. Gregorich and B. Kadkhodayan

In our studies of the chemical and nuclear properties of the actinide and transactinide elements, we bombard targets containing near milligram quantities of highly radioactive actinide isotopes such as ^{248}Cm, ^{249}Bk, ^{249}Cf, etc. During bombardment with heavy-ion beams as intense as one particle microampere, these targets must withstand temperatures up to several hundred °C and extreme ionizing conditions without loss of any significant amount of target material. In addition, the targets must be physically strong enough to act as a vacuum window. We have found that high voltage molecular plating[1] onto beryllium backing foils fulfills all of these target requirements.

In the high voltage molecular plating method, a salt of the target material cation is dissolved in isopropanol. This isopropanol solution containing enough of the salt to form a 75 μg/cm^2 deposit is placed in a plating cell with the Be backing foil as the negative electrode at the bottom of the cell. Several hundred volts are then applied between the Be foil and a positive electrode about 1 cm above. After approximately 30 minutes, the foil is removed and heated in a furnace to 550 °C to convert the deposit to the oxide form. This procedure is repeated until a target of the desired thickness is obtained.

We have developed a new plating cell system to facilitate this multi-layer procedure and to comply with electrical safety requirements. A cross section exploded view is presented in Fig. 1. The plating cell is modular and all parts are held together with 10/24 socket head bolts to facilitate operation of the cell in an alpha glovebox. The positive electrode is made of a perforated paltinum foil and is confined between the top section and the mid ring. When mounting the target in the cell, the Be backing foil is placed in a shallow depression in the base plate and hald in place by bolting the clamp ring to the base plate. The combined mid ring/top section is then bolted to the clamp ring to complete the cell. After plating, the procedure is reversed to remove the target from the cell. Production of ^{147}Sm and ^{nat}Eu targets have been performed as an initial test of the plating cell.

References

1. D. Aumann, G. Mullen, *Nucl. Instrum. Meth.* **115**, 75 (1974).

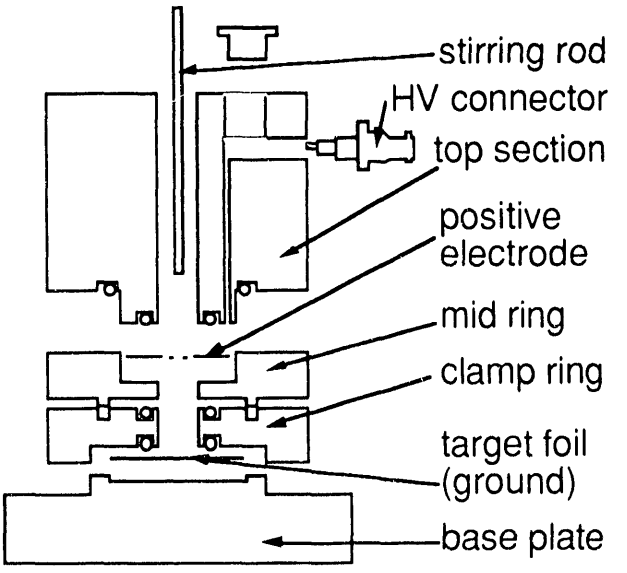

Fig. 1. Exploded cross section view of the plating cell.

Production of Actinides from the Interactions of ^{40}Ca, ^{44}Ca and ^{48}Ca with ^{248}Cm*

*A. Türler, H.R. von Gunten†, J.D. Leyba#, D.C. Hoffman, D.M. Lee, K.E. Gregorich, H.L. Hall**, R.A. Henderson††, and M.J. Nurmia*

In our systematic study of target-like transfer reaction products, we have measured excitation functions for production of isotopes of Th through Fm in bombardments of ^{248}Cm with 231- to 323-MeV ^{44}Ca ions and for the production of isotopes of Th through Cm in bombardments of ^{248}Cm with 230- to 291-MeV ^{40}Ca ions, respectively, using radiochemical methods. The experimental data were compared with the results of previous reaction studies in the systems $^{40}Ca + ^{248}Cm$ [1,2] and $^{48}Ca + ^{248}Cm$ [1,3]. The half-widths of the Gaussian isotopic distributions were about 2.5 mass numbers for above-target elements and 5 to 5.5 mass numbers for below-target elements in all three systems. The majority of the cross section for the production of above-target nuclides was assigned to predominantly quasi-elastic reactions, whereas below-target nuclides were formed in deeply inelastic and asymmetric quasi-fission reactions. The maxima of the isotopic distributions were shown[3] to closely follow the minimum of the potential energy surface (PES) in experiments with ^{48}Ca, whereas in reactions with ^{40}Ca and ^{44}Ca we found that a transfer of 4 to 5 protons in either direction was required to reach the minimum in potential energy (Fig. 1). The different neutron numbers of ^{40}Ca, ^{44}Ca and ^{48}Ca are only partly reflected in the target-like reaction products. Differences in the element yields of two orders of magnitude for the production of below-target elements were observed between the reactions of ^{40}Ca and ^{48}Ca ions with ^{248}Cm. The differences for above-target elements were largest between the reactions of ^{44}Ca and ^{48}Ca ions with ^{248}Cm. Differences in below-target yields have been attributed either to losses of reaction products due to prompt fission, and/or to dynamic effects due to fusion hindrance.

Footnotes and References

*submitted to Phys. Rev. C.

†Radiochemisches Laboratorium, Universität Bern, Switzerland.

#Westinghouse Savannah River Co., Savannah River Laboratory.

**Department of Chemistry and Material Science, LLNL.

††EG&G Rocky Flats, Inc., Rocky Flats Plant.

1. D.C. Hoffman et al., Phys. Rev. C 31, 1763 (1985)
2. M. Lerch, private communication
3. H.W. Gäggeler et al., Phys. Rev. C 33, 1983 (1986)

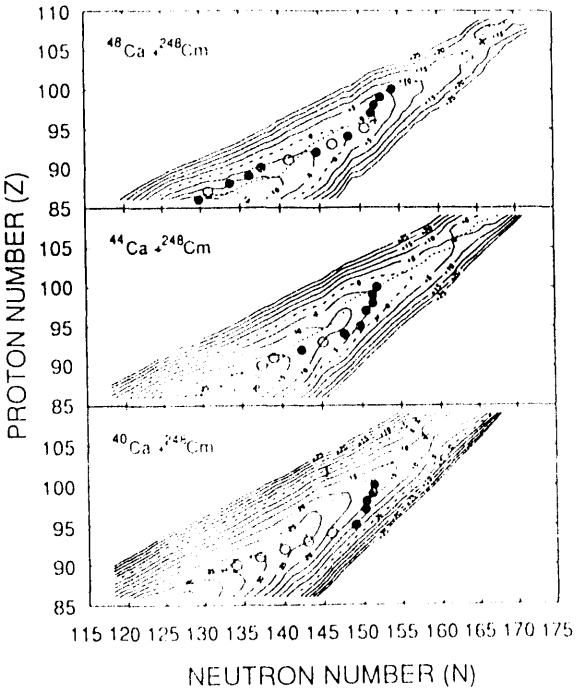

Fig. 1 Contour map representation of the calculated PES's for the reactions of $^{40,44,48}Ca + ^{248}Cm$ at an angular momentum of $l = 0\ \hbar$. The dashed lines denote the equipotential contour lines at 0 MeV. The injection points (^{248}Cm) are represented with +. The dotted lines connect the minima of the potential energies calculated for each Z. The saddle point is indicated with X. The closed circles represent the position of the experimentally determined maxima of the isotopic distributions, whereas the open circles represent estimated maxima.

Surface Sorption Technique For Separation Of Rutherfordium

C.D. Kacher, A. Bilewicz[*], *and D.C. Hoffman*

Rutherfordium-261 is produced in the nuclear reaction $^{248}Cm(^{18}O,5n)^{261}Rf$ at the 88-Inch Cyclotron, then separated from its constituents so its chemical properties can be studied. This isotope was chosen because it is the longest-lived of the known Rf isotopes. Because of the 65-s half-life of ^{261}Rf, however, it would be desirable to have a shorter procedure to separate ^{261}Rf than the current solvent extraction techniques that take approximately one half-life to perform. A new method of separation using cobalt ferrocyanide surfaces on glass plates has been devised that can be performed in 10 to 15-s. These surfaces have a high affinity for tetravalent metal cations and a low affinity for trivalent metal cations. Therefore, ^{261}Rf can be separated from the actinides that are also formed. In preliminary tests, these surfaces were used in a one-step procedure and gave excellent sources for measurement of ^{261}Rf. The chemistry can be done directly on the surface which is immediately measured with an alpha detector.

We have also performed tracer studies of the chloride complexation and hydrolysis of Zr, Hf, and Th using this technique.

Figs. 1 and 2 show the effects of HCl concentration on adsorption. Zr, Hf, and Th have a 4+ ionic charge. In Fig. 1, as the concentration of HCl increases, Zr and Hf continue to sorb while sorption of Th is decreased. This shows Th may be forming chloride complexes such as $ThCl^{3+}$ or $ThCl_2^{2+}$. Since these surfaces poorly adsorb 3+ species, Th adsorption then decreases. In Fig. 2, as HCl concentration decreases, adsorption of Hf and Zr also decrease while Th maintains an adsorption of nearly 100%. This may be due to the hydrolization of Zr and Hf to form species such as $Zr(OH)^{3+}$ and $Hf(OH)^{3+}$.

It will be of interest to see if Rf behaves more like its lighter homologs Zr and Hf or more like Th.

[*]Institute of Nuclear Chem., Warsaw, Poland

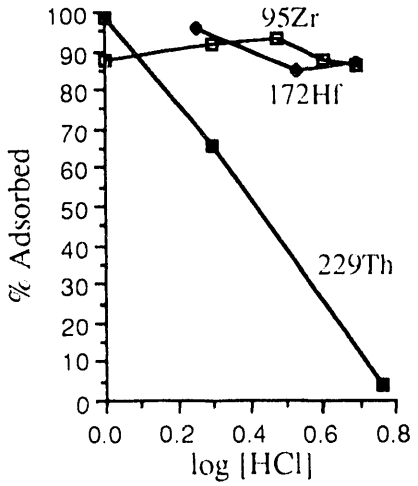

Fig. 1. Dependence of adsorption of ^{95}Zr, ^{172}Hf, and ^{229}Th on HCl concentration.

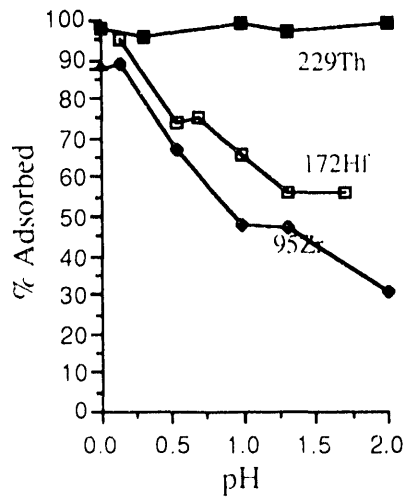

Fig. 2. Dependence of adsorption of ^{95}Zr, ^{172}Hf, and ^{229}Th on pH.

Extraction of Rf and its Homologs with TTA

K.R. Czerwinski, K.E. Gregorich, T.M. Hamilton, N.J. Hannink, C.D. Kacher, B.A. Kadkhodayan, S.A. Kreek, M.R. Lane, D.M. Lee, M.J. Nurmia, A. Türler, and D.C. Hoffman

The extraction of tetravalent Rf (element 104), Zr, Hf, Th and Pu by thenoyltrifluoroacetone (TTA) in benzene from acidic chloride solutions has been studied using 65-s ^{261}Rf produced at the LBL 88-Inch Cyclotron via the ^{248}Cm(^{18}O, 5n)^{261}Rf reaction and appropriate tracers. The HCl concentration was varied between 0.05 and 0.24 M. The TTA concentration was 0.5 M in benzene.

The extraction results are shown in Fig. 1. The tracers extracted in the order Zr > Hf ≈ Pu > Rf > Th. The extraction of Zr, Hf, Pu, and Th follows the values in the literature[1,2,3].

From the distribution coefficients derived from these extractions, the equilibrium constant (K_{eq}), hydrolysis constants and ionic radius for Rf were determined[4,5]. The log K_{eq} of Rf with TTA was determined to be 3.18 ± 0.90. (See Fig. 2). The hydrolysis constants for Rf are calculated to be: K_{11} = -2.6 ± 0.7; K_{12} = -5.9 ± 1.7; K_{13} = -10.2 ± 2.9; and K_{14} = -14.5 ± 4.1. These hydrolysis constants are lower than the values for Zr, Hf, and Pu, and slightly larger than the values for Th[4]. These results indicate that Rf will not hydrolyze under conditions which Zr, Hf, and Pu will. The ionic radius was calculated to be 9.1 ± 0.4 nm for the 6-coordinate species and 10.2 ± 0.4 nm for the 8-coordinate species.

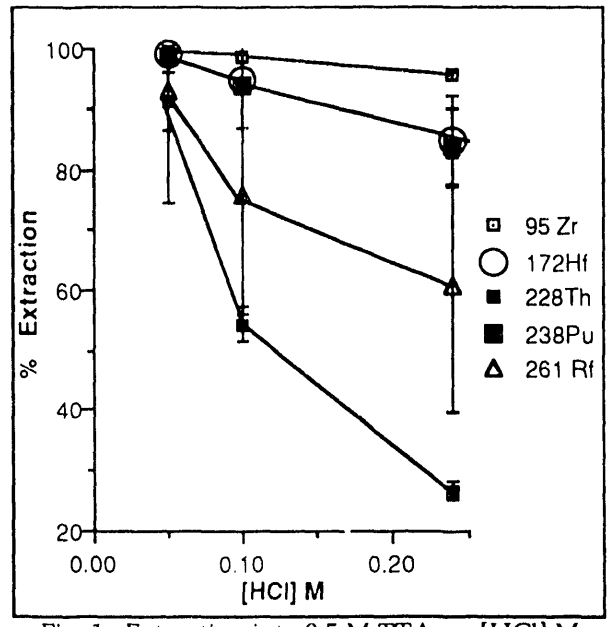

Fig. 1. Extraction into 0.5 M TTA vs. [HCl] M

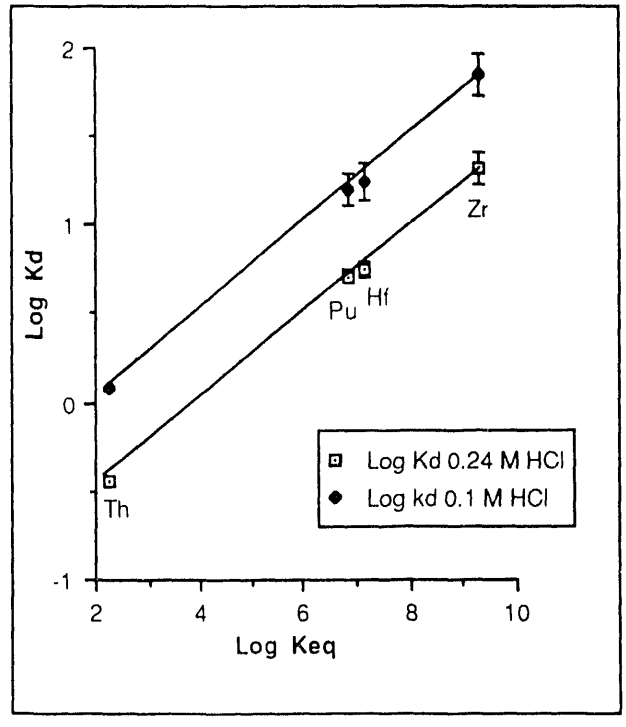

Fig. 2. Log K_d vs. Log K_{eq}

Footnotes and References

1. A. Ramanujam, *et.al.*, J. Radioanal. Chem. 42, 349 (1978).

2. S.V. Bagawde, *et.al.*, J. Inorg. Nucl. Chem. 38, 1339 (1976).

3. A.M. Poskanzer, *et.al.*, J. Inorg. Nucl. Chem. 16, 323 (1961).

4 . C.F. Baes, *et.al.* The Hydrolysis of Cations; Wiley Interscience, New York, p. 152-191 (1976).

5 A.E. Martell, and M. Calvin, Chemistry of the Metal Chelate Compounds; Prentice-Hall, New York, p. 191-202 (1952).

Extraction of Zirconium and Hafnium with TTA

K.R. Czerwinski, M.R. Lane, and D.C. Hoffman

The group 4 elements Zr and Hf are being studied for comparison with their heavier homolog, Rf (element 104). The liquid-liquid extractions of radioactive ^{95}Zr and ^{162}Hf tracer into thenoyltrifluoroacetone (TTA) from aqueous solutions were studied.

For the Zr experiments, a stock solution of ^{95}Zr in HCl was prepared at a concentration of approximately 10 μCi/50 μL. Two Zr extraction experiments were performed. In the first experiment, the HCl concentration was kept at 0.24 M while the TTA concentration was varied between 0.005 M and 0.5 M . In the second, the TTA concentration was kept at 0.25 M while the HCl concentration was varied between 0.25 M and 4 M (Fig. 1).

The Hf experiments were performed at the Lawrence Berkeley Laboratory 88-Inch Cyclotron. The isotope 162Hf was produced by the ^{147}Sm (^{20}Ne,5n) reaction. Two extraction experiments were performed. In the first, the HCl concentration was kept at 0.24 M while the TTA concentration was varied between 0.05 M and 0.5 M. In the second, the TTA was kept constant at 0.25 M while the HCl was varied between 0.05 M and 0.5 M (Fig. 1).

A comparison of the data for Zr and Hf shows three things. First, Zr generally extracts better than Hf as indicated by the higher K_d values. This result is consistent with the data in the literature[1,2]. Second, both Zr and Hf form similar complexes with TTA. This is shown by the fact that their slopes as a function of TTA concentration are similar (both approximately 1.2), which means they are similarly dependent on the TTA concentration. From these figures, it can be seen that a good choice for the range of TTA concentrations for rutherfordium extraction would be between about 0.25 M and 0.5 M. In addition, TTA is kinetically slow compared to triisooctylamine and tributylphosphate, two common organic ligands. A high TTA concentration is needed to overcome the slow kinetics. Therefore, 0.5 M TTA in benzene was the concentration chosen for rutherfordium extraction.

The effects of HCl concentration shows the need for a low acid (Fig. 1). This is especially true if Rf behaves more like Pu than the other group 4 elements. Previous work has shown that the group 4 elements have higher distribution coefficients than Pu under the same conditions[1]. In addition, the equilibrium constants for TTA complex formation of Pu are lower for Hf or Zr[3]. From these Zr and Hf results, conditions for extraction of rutherfordium were chosen.

Footnotes and References

1. A.M. Poskanzer, and B.M. Foreman, Jr., J. Inorg. Nucl. Chem. 16, 323 (1961).
2. R.E. Connick, and W.H. McVey, J. Amer. Chem. Soc. 71, 3182 (1949).
3. J. Stary, The Solvent Extraction of Metal Chelates; Macmillan Company, New York,p. 71-77 (1964).

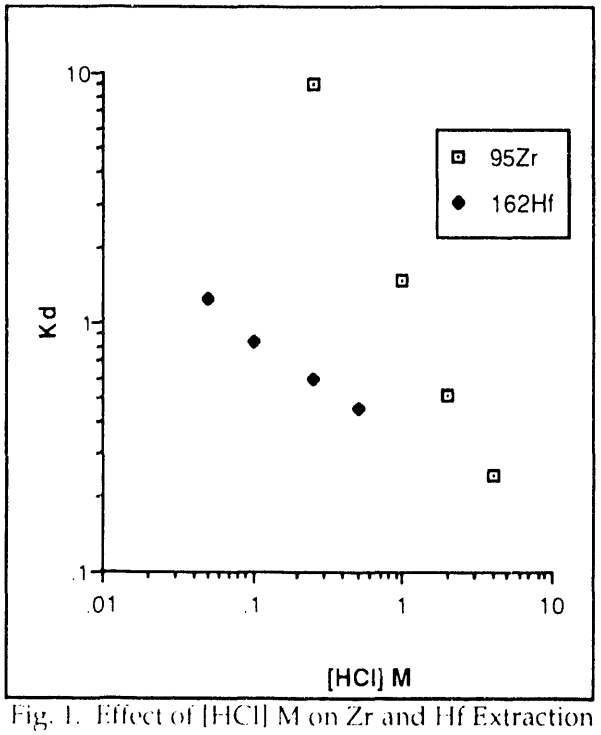

Fig. 1. Effect of [HCl] M on Zr and Hf Extraction

Extraction of Rf and its Homologs with Trialkylamines

K.R. Czerwinski, K.E. Gregorich, T.M. Hamilton, N.J. Hannink, C.D. Kacher, B.A. Kadkhodayan, S.A. Kreek, M.R. Lane, D.M. Lee, M.J. Nurmia, A. Türler, and D.C. Hoffman

The extraction of tetravalent Rf, Zr (a Rf homolog), Th and trivalent Eu (an actinide homolog) by trihexylamine, triheptylamine and triisooctylamine (TIOA) in organic diluent from aqueous HCl environments has been studied using 65-s ^{261}Rf produced at the LBL 88-Inch Cyclotron via the ^{248}Cm(^{18}O, 5n)^{261}Rf reaction and the appropriate tracers. The organic diluent examined were methylisobutylketone, benzene, hexanes, and dichloromethane. The Cl^-, and H^+ concentrations in the aqueous phase were varied. The effect of HF on extraction was also studied. The tracers were in a 12 M HCl solution at an activity of 50 nCi/50 µL. The tracers used were ^{95}Zr, ^{152}Eu and ^{228}Th.

TIOA was the superior trialkylamine extractant. Benzene had the highest extraction of the diluents examined. Addition of HF inhibited extraction. The results showed that an organic phase of 1 M TIOA in benzene and an aqueous phase of 12 M HCl had the best Zr extraction (Fig. 1). Tracer evaporation as a function of TIOA concentration was studied using ^{95}Zr (Fig. 2). This experiment showed an increase in tracer evaporation with an increase in TIOA concentration.

Based on the results, TIOA was used to study extraction of Rf from aqueous HCl solutions. The HCl solution was held constant at 12 M HCl. TIOA concentrations of 1 M and 0.1 M were used. The studies showed Rf extraction of 29.1 ± 6.5 % at 1.0 M TIOA and 117 ± 22.0 % at 0.1 M TIOA. The low extraction at 1.0 M is due to tracer loss during evaporation of the organic phase. These results showed that Rf behaves differently than Th and Eu and most similarly to Zr. This result is further evidence that both Rf and Zr are group 4 elements.

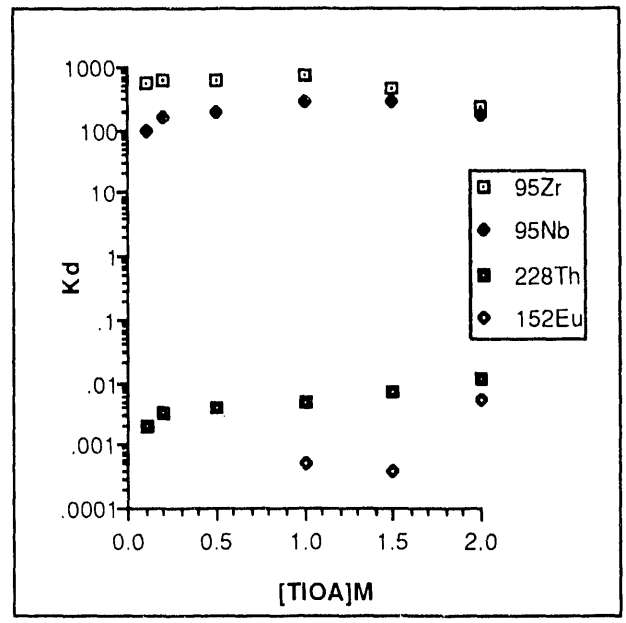

Fig. 1. Extraction from 12 M HCl into [TIOA]M

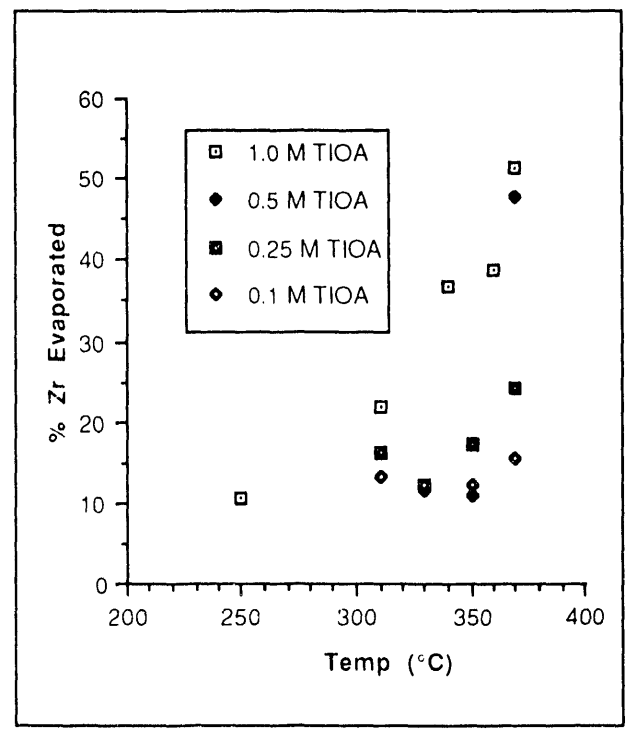

Fig. 2. Temperature Effect on Zr Loss with Varied [TIOA] M

Search for ^{263}Rf

K.R. Czerwinski, K.E. Gregorich, T.M. Hamilton, N.J. Hannink, C.D. Kacher, B.A. Kadkhodayan, S.A. Kreek, M.R. Lane, D.M. Lee, M.J. Nurmia, A. Türler, and D.C. Hoffman

An attempt was made to produce a new isotope, ^{263}Rf. The production reaction used was $^{248}Cm(^{18}O,3n)$ with a beam energy of 92 MeV. Utilizing mass tables[1,2], calculations were done for the alpha and electron capture. The spontaneous fission half-life was estimated from systematics[3]. The Rf was separated from the actinides using liquid-liquid extractions. The organic phase was 0.5 M thenoyltrifluoroacetone (TTA) in benzene and the aqueous phase was 0.05 M HCl. The collection time for each experiment was 3 minutes.

The cross section for the $^{248}Cm,(^{18}O, 3n)$ reaction was calculated using a modified SPIT code[4]. The peak of the excitation function is at 92.5 MeV with a cross section estimate of 300 pb. From the cross section estimate, the ^{263}Rf production rate is about 2 atoms per hour. Folding in the gas jet transport yield, chemical yield and detector efficiencies, the detection rate would be 1.3 events per hour for SF and 0.7 events per hour for alpha decay.

The half-life predictions are shown in Fig. 1. The alpha half-life estimate ranged from 100 seconds to 3500 seconds. These estimates were made using masses from Refs. 1 and 2 respectively. The electron capture half-life estimate was 3600 seconds. The spontaneous fission half-life estimate is 500 seconds.

Seven spontaneous fission events in the Rf chemical fraction were observed in 300 experiments. The observed events had a half-life of $500 \pm^{300}_{200}$ seconds. No alpha events were detected, preventing absolute identification of the production of ^{263}Rf. The cross section for the seven events is 140 ± 50 pb.

Footnotes and References

1. P. Möller, and J.R. Nix, At. Data Nucl. Data Tables, 39, 213 (1988)
2. L. Satpathy, and R.C. Nayak, Atom. Data Nucl. Data Tables 39, 241 (1988)
3. D.C. Hoffman, Spontaneous Fission Properties and Lifetime Systematics, LBL-26975, (1989).
4. J. Alonso, Gmelin Handbuch der Anorganishen Chemie. 7b, 28 (1974).

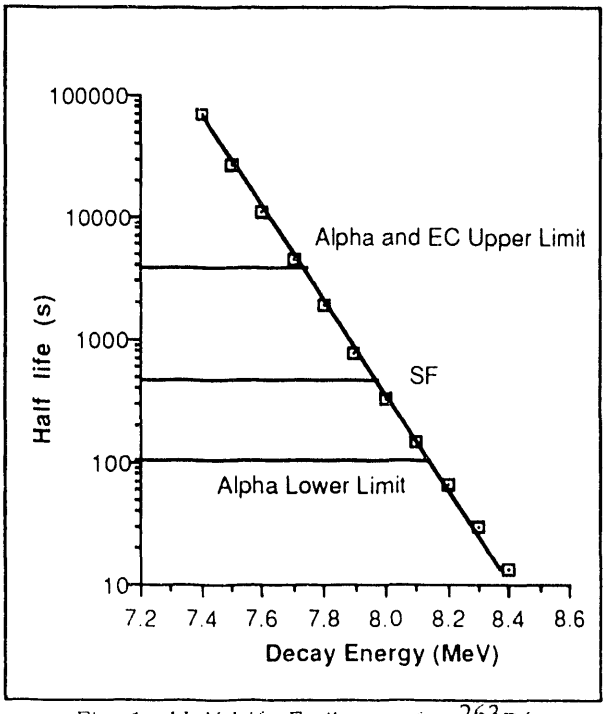

Fig. 1. Half-Life Estimates for ^{263}Rf

The Heavy Element Volatility Instrument (HEVI)

B. Kadkhodayan, A. Türler, K.E. Gregorich, M.J. Nurmia, D. M. Lee, and D.C. Hoffman

Experimental investigation of the chemical properties of the transactinide elements is extremely difficult. The longest lived known isotopes of the transactinide elements have half-lives of a minute or less. These elements have only been produced in heavy ion fusion reactions at rates of a few atoms per minute or less. Furthermore, actinide activities which are produced in high yields in these reactions interfere in the detection of the transactinides, which further complicates chemical studies. Due to the low production rates and short half-lives of these nuclides, very specific and unique chemical procedures have been devised. On-line isothermal gas chromatography is one of the most unique chemical procedures designed to investigate the properties of these elements. This method takes advantage of the high volatilities of the halides of the group 4, 5, and 6 transition elements to efficiently separate transactinide halides and their lighter homologs from the less volatile trivalent actinides. This chemical separation allows the investigation of nuclear and chemical properties of the transactinide elements.

We have constructed[1] the Heavy Element Volatility Instrument (HEVI), an on-line gas chromatography system which is used to continuously separate halides according to their volatility. Both gaseous HBr and HCl have been used as halogenating agents. A schematic of HEVI is shown in Fig. 1.

Footnotes and References

1. B. Kadkhodayan *et al.*, LBL-31645.

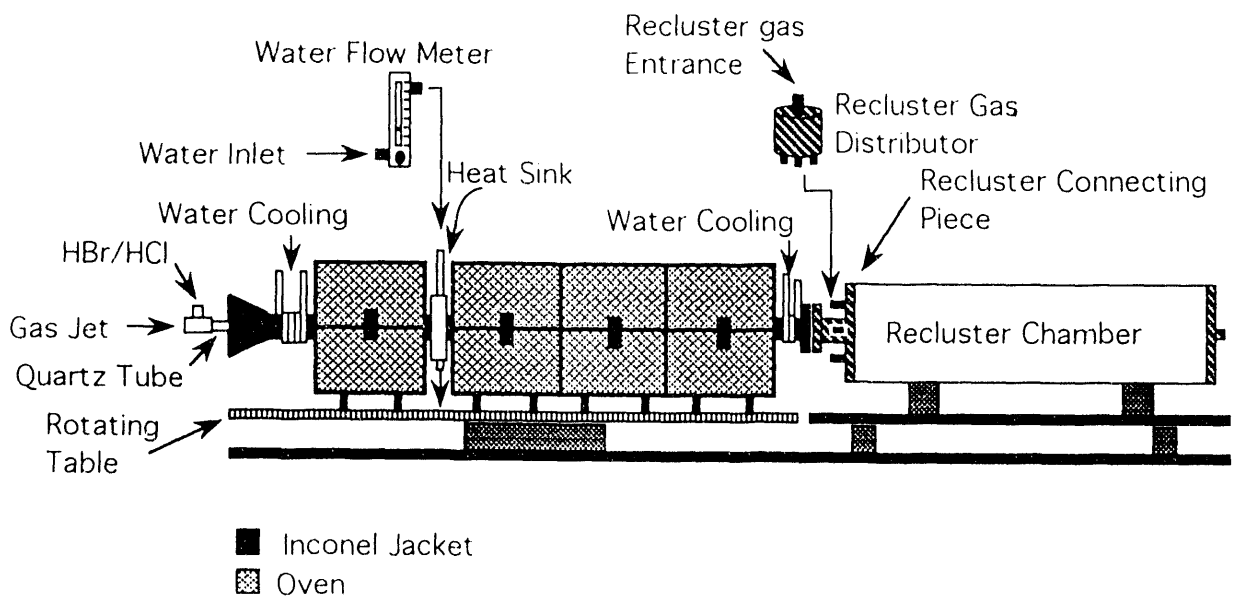

Fig. 1. Illustration of the Heavy Element Volatility Instrument (HEVI). Shown here is the side view of the chromatography and recluster segments.

A Simulation of Isothermal Gas Chromatography Using the Monte Carlo Method

*A. Türler, K.E. Gregorich, D.C. Hoffman, D.M. Lee, and H.W. Gaggeler**

Due to the very low production rates and the short half-lives of transactinide elements, chemical operations can be performed only on an atom-at-a time level. The significance of results obtained from a very small number of processed atoms is hard to assess in statistical terms. A discreet event simulation model, which adequately describes the properties observed for a vast number of processed atoms, i.e. for a homolog element in a given experiment, is therefore of great value. Using a simplified microscopic model to describe the downstream migration of a molecule through a column with a negative longitudinal downstream temperature gradient, Zvara[1] was able to simulate the profiles of thermochromatographic zones. In employing Zvara's model we could reproduce the experimentally observed yield curves in isothermal gas-solid chromatography experiments with OLGA II[2] and determine the adsorption enthalpy of the investigated species. Compared to analytical analyses methods[3], Monte Carlo calculations easily allow accounting for actual experimental conditions, such as the real temperature profile in the chromatography column.

Each molecule in the chromatography column experiences a series of discrete displacements and adsorption-retention sequences. The displacements are usually very short, since a recently desorbed molecule will very likely encounter the surface again after a flight of a few free path lengths. Occasionally, the molecule will diffuse far enough from the wall to be transported downstream over a much longer distance by the gas flow, before hitting the column surface again. In Zvara's model[1] the actual probability density distribution for the displacement of a molecule inside the chromatography column is replaced with an acceptable approximation, which assumes, that whenever the molecule encounters the surface a series of adsorption-desorption events occur without displacement. Then, a long downstream displacement takes place, before the molecule encounters the surface again. Thus the numerous displacements of a molecule are replaced by a much smaller number of effective downstream "jumps"[1]. This way a vast number of molecule histories can be calculated with a computer within a reasonable time.

In Fig. 1 the data measured for $^{167}TaBr_5$ ($T_{1/2}$ = 78 s), the calculated yield curves using the Monte Carlo simulation procedure and an analytical analyses method[3] for an adsorption enthalpy of ΔH_a = -95 kJ/mol are shown. The flow rate of He through the column was 2 l/min (STP). The Monte Carlo simulation procedure convincingly reproduces the data, whereas, due to the absence of long "jumps" the analytical calculations predict a zero yield for low isothermal temperatures.

Footnotes and References

*Paul Scherrer Institut, CH - 5232 Villigen, Switzerland

1. I. Zvara, Radiochim. Acta, 38, 95 (1985)
2. H.W. Gaggeler et al., Nucl. Instr. Meth., A309, 201 (1991)
3. H.W. Gaggeler et al., Radiochim. Acta, 38, 103 (1985)

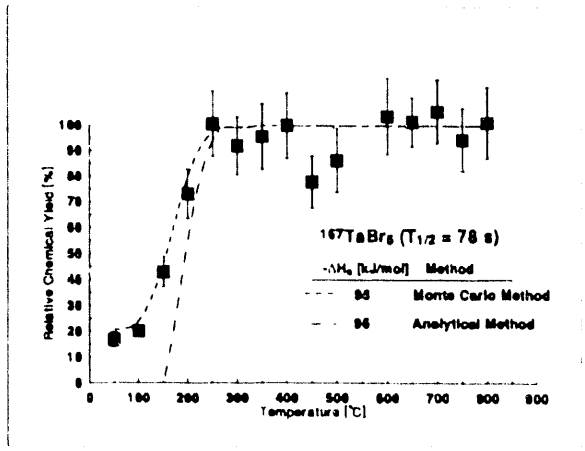

Fig. 2 Calculated yield curves using the Monte Carlo simulation - and an analytical calculation procedure.

Evidence for the new Isotopes ^{252}Bk and ^{253}Bk

S.A. Kreek, K.E. Gregorich, K.R. Czerwinski, B. Kadkhodayan, N.J. Hannink, M.P. New, C.D. Kacher, T.M. Hamilton, M. R. Lane, E.R. Sylwester, R.F. Gaylord, A. Turler, M.J. Nurmia, D.M. Lee, and D.C. Hoffman

The production of neutron-rich actinide isotopes is hampered by available target projectile combinations and reaction cross-sections. Previous attempts by our group to produce ^{252}Bk and ^{253}Bk were unsuccessful because the methods employed did not provide sufficient sensitivity.

We have recently obtained evidence suggesting that both ^{252}Bk and ^{253}Bk can be produced in bombardments of ^{248}Cm by ^{18}O. Preliminary data indicate that ^{252}Bk has a half-life of about 1 minute and ^{253}Bk has a half-life greater than 10 minutes. The half-lives were determined by alpha analysis of the ^{252}Bk and ^{253}Bk growth curves with increasing irradiation time in a method similar to that used[1] to discover ^{253}Md.

Isotopes of Bk were produced at the 88-Inch Cyclotron at LBL in bombardments of a 600 μg/cm^2 ^{248}Cm target with 99 MeV $^{18}O^{5+}$ at an intensity of 2.5 eμA. The recoils were transported with our He/KCl aerosol jet system and collected for varying times (1, 3 and 10 minutes). A bis-2-ethylhexyl-orthophosphoric acid separation was performed to isolate the Bk and the fractions were pooled according to the collection time. The samples were electroplated on Pt foil and analyzed by alpha pulse-height analysis. Fig. 1 is a raw alpha spectrum showing the ^{253}Es alpha peak at 6.6 MeV. These data were taken before the samples were electroplated. The ^{252}Cf peak is buried under the ^{250}Cf and ^{248}Cf peaks at 6.0 and 6.3 MeV. A plot of the amount of ^{252}Cf (daughter of ^{252}Bk) and ^{253}Es (grand-daughter of ^{253}Bk) versus the collection time was generated to determine the Bk halflives and is shown in Fig. 2. It is assumed that the Cf and Es in the samples originated from the decay of the Bk.

Because the chemistry was performed without a tracer, it is impossible to determine whether the observed ^{252}Cf and ^{253}Es were contamination from directly produced Cf/Es or were decay products of the Bk. The activity levels are consistent with a 10^{-4} contamination. Further study is required before discovery of the new isotopes can be claimed. Also of interest, in addition to the potential discovery of two new Bk isotopes, is the observation of ^{4}H and ^{5}H transfer reactions. This is useful for our understanding of transfer reactions.

References

1. B. Kadkhodayan *et al.*, LBL Report #30260, 1991.

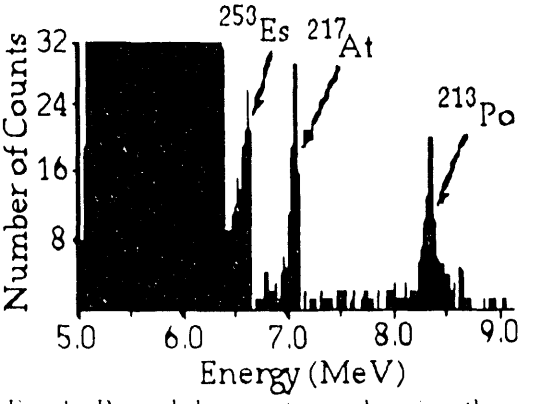

Fig. 1. Raw alpha spectrum showing the ^{253}Es alpha peak at 6.6 MeV.

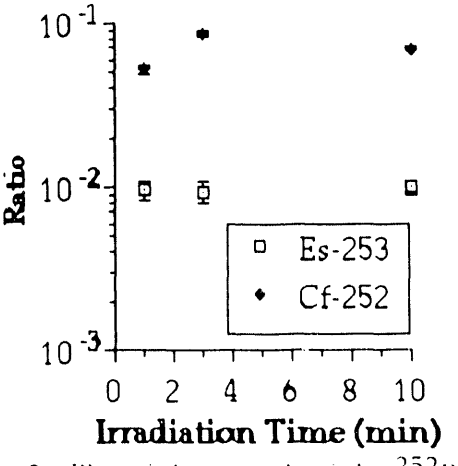

Fig. 2. Plot of the growth of the ^{252}Bk (^{252}Cf) and ^{253}Bk (^{253}Es) with time.

The Spontaneous Fission Properties of ^{259}Lr

T.M.Hamilton, K.E. Gregorich, K.R. Czerwinski, B. Kadkhodayan, N.J. Hannink, M.P.Neu, C.D. Kacher, M.R. Lane, R.F. Gaylord, A. Turler, M.J. Nurmia, D.M. Lee, and D.C. Hoffman

We have measured the spontaneous fission properties of ^{259}Lr at the LBL 88-Inch Cyclotron using an on-line rotating wheel system. The ^{259}Lr was produced via the ^{248}Cm(^{15}N,4n) reaction with a production cross section of 100 nanobarns for 81-MeV projectiles. The recoils were deposited on eighty 40 $\mu g/cm^2$ polypropylene foils equally spaced around the circumference of a horizontal wheel. The wheel was stepped at six-second intervals to position the samples sequentially between six pairs of charged-particle detectors. The kinetic energies and times of the coincident fission fragments and the alpha particles were recorded in list mode. From these data, the half-life and the mass and total kinetic energy (TKE) distributions were derived.

The mass and TKE distributions are shown in Figs. 1 and 2, respectively. The mass distribution was found to be broadly symmetric (full-width at half-maximum of about 40 mass numbers). The TKE distribution seems to consist of a single Gaussian component with a most probable pre-neutron TKE of 200±5 MeV. The ^{259}Lr half-life was determined to be 6.10±0.3 seconds by measuring the decay of the 8.439±0.010 MeV alpha particles. The spontaneous fission branch was measured to be 20±2 %. These values are consistent with those obtained for ^{259}Lr by K.E. Gregorich *et al.*[1] The mass distribution and most probable TKE are consistent with trends observed for other trans-berkelium isotopes.[2]

Footnotes and References

1. K.E. Gregorich *et al.*, LBL Nuclear Science Division Annual Report for 1989-1990, LBL-30798 UC-413, April 1991.

2. D.C. Hoffman, "Spontaneous Fission of the Heaviest Elements," Fifty Years with Nuclear Fission, Gaithersburg, MD, April 1989, (Am. Nucl. Soc., Inc., La Grange Park, Ill., USA) Vol. I, p. 83 (1989).

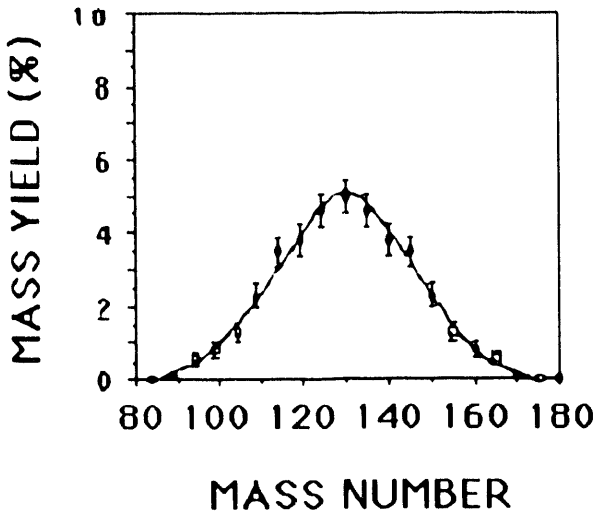

Fig. 1. Pre-neutron Emission Mass Yield Distribution for ^{259}Lr (457 events).

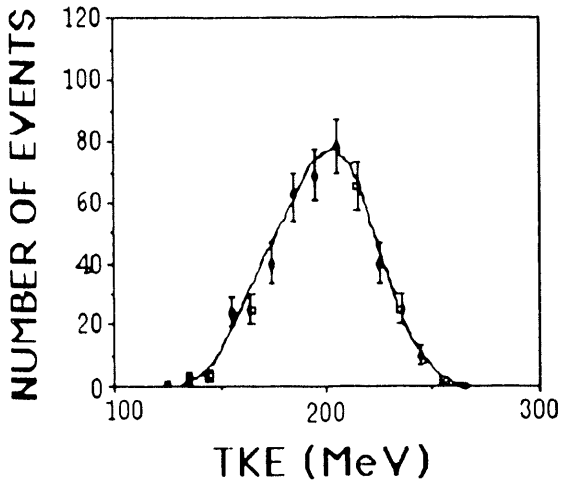

Fig. 2. Pre-neutron Emission TKE Distribution from SF of ^{259}Lr.

Central Collisions for $^{16}O + ^{12}C$ at 32.5 MeV per nucleon*

J.A. Scarpaci, Y. Chan, K.G. Stokstad and I. Sura

The decay mechanism for central collision products in $^{16}O + ^{12}C$ at 32.5 MeV/A has been studied. The experimental set up consisted of an array of 58 plastic phoswich detectors covering a total solid angle of 1 steradian at forward angles. The charge and energy of individual fragments up to carbon were identified. Central collision events were selected by requiring the detection of at least 6 light fragments. Maximum excitation energies of about 7 MeV per nucleon have been reached for the quasi-fusion primary fragments formed. The center of mass velocity of the detected fragments was calculated by using masses of the most tightly bound isotopes for each Z. A center of mass velocity analysis had been performed[1] in order to extract the contributions from various incomplete fusion channels. For instance, for events where 12 out of the total 14 charges are detected, most of the cross section (~80%) is due to the decay of ^{24}Mg.

The 5He+2H channel, interesting because of its homogeneity, was studied in detail to infer the decay mechanism. (In this case there is no large mass fragment to take away most of the energy.) Different ways of looking at the data have been used in previous work[2]. Here we have chosen to concentrate on the folding angles between each pair of particles. For seven fragments, 21 angles are calculated for each event.

Theoretical calculations have been performed to compare with the data. The code Gemini was used to model the sequential decay of ^{24}Mg into 5He+2H. For the multifragmentation part, the code of Lopez *et al.* was used[3]. This code gathers the final fragments in a sphere and lets them move away from each other under mutual Coulomb repulsion. A third calculation was performed by choosing particle angles randomly from an isotropic distribution. The data as well as the three calculations discussed above are presented in the figure. The data (points) agree remarkably well with the sequential decay calculation (curve) as well as the random orientation (histogram) calculation. The multifragmentation calculation (dashed histogram), on the other hand, does not fit as well and peaks at a somewhat lower average angle. In other words the meltifragmention shows more of a spherical pattern presumably due to the final state mutual coulomb repulsion. A similar result was also obtained in a previous experiment that dealt with the peripheral break up of an ^{16}O nucleus on heavy targets.

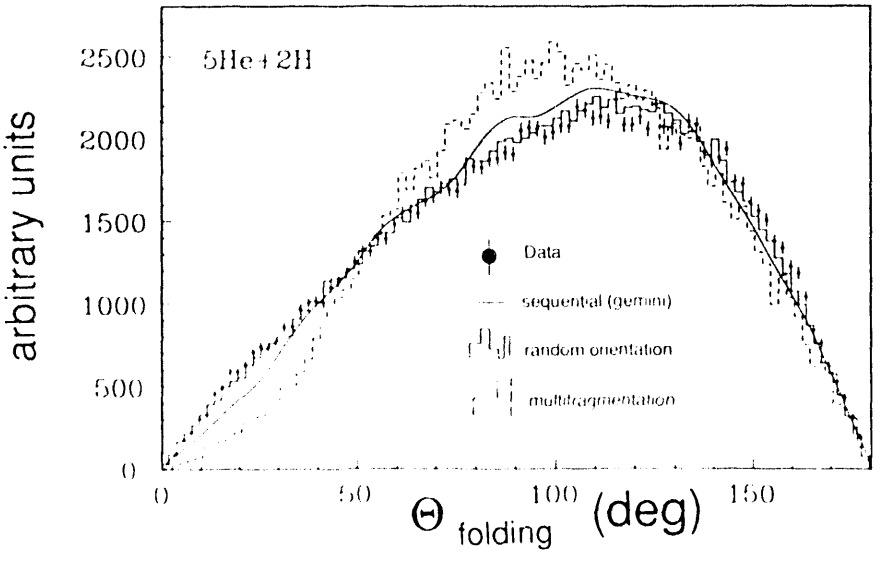

Footnotes and References

*Condensed from LBL report LBL-32047.

1. J.A. Scarpaci et al., *NSD annual report*, 135 (1991).
2. B.A. Harmon et al., *Phys. Lett.* B235, 234 (1990).
3. J. Lopez and J. Randrup, *Nucl. Phys.* A491, 477(1989).

Fission- and Neutron-Decay Time Scales in Deep-Inelastic $^{238}U + ^{238}U$ Collisions by K-Vacancy Production*

J. D. Molitoris[a], W. E. Meyerhof[b], Ch. Stoller[b], R. Anholt[b], D. W. Spooner[b], L. G. Moretto, L. G. Sobotka[c], R. J. McDonald, G.J. Wozniak, L. Blumenfeld[d], N. Colonna, M. A. McMahan, M. Nessi[e], and E. Morenzoni[e]

In 1962, Gugelot pointed out that one can calibrate the decay width Γ_c of a compound nucleus in terms of the K x-ray width Γ_x of the atomic electrons attached to this nucleus. One has only to prepare an atom with an excited nucleus and a K vacancy and then measure the branching ratio Γ_x/Γ_c. Using the same basic method, we have found a way to calibrate the fission-decay time of excited uranium (U)-like nuclei in terms of their K x-ray width.

The experiment was conceived as follows. Two ^{238}U nuclei are made to collide and undergo a deep-inelastic scattering. After the collision, the two U-like nuclei exit with a variable amount of excitation energy and some K vacancies. Due to their excitation energy, the U-like nuclei may emit neutrons and/or undergo fission. If the K vacancies are filled before fission occurs, uranium K x-rays are emitted. We consider three different classes of events: 1) both U nuclei survive fission; 2) one U nucleus undergoes fission and other survives; and 3) both U nuclei undergo fission. The uranium K x-rays were measured in coincidence with the above three classes of events. If the K x-ray emission time is much greater than the fission time (our first null hypothesis), the x-ray emission probability should be in the ratio P_2: P_3: P_4 = 1: 1/2: 0. On the other hand, if the K x-ray emission time is much smaller than the fission time, (our second null hypothesis), but greater than the collision time, the x-ray emission probabilities should be in the ratio P_2: P_3: P_4 = 1: 1: 1. If the ratios of the observed probabilities are intermediate between the values expected from the two null hypotheses, fission and x-ray times can be intercalibrated.

Our results show that the three probabilities are not in the ratios expected for either of our two null hypotheses. Clearly, some of the times, but not always, K x-ray emission precedes fission. Thus, this constitutes a proof of principle for the calibration of fission times in terms of atomic K x-ray times and is the major conclusion of this work.

Footnotes and References

[a]Lawrence Livermore National Lab, Livermore, CA 94550

[b]Dept. of Physics, Stanford Univ., Stanford, CA 94305

[c]Dept. of Chem., Washington Univ., St. Louis MO 63130

[d]DPE/SPEA, CE Saclay, 91191 Gif-sur-Yvette, France

[e]Eidgenossische Technische Hochschule, CH-8093 Zurich, Switzerland

Table I. 2-, 3-,and 4-body K x-ray production probabilities averaged over the TKEL spectrum.

Probability	Model $\tau_x >> \tau_f$	Model $\tau_f >> \tau_x$	Experiment
$<P_2>$	1	1	1.09 ± 0.03
$<P_3>$	0.5	1	0.91 ± 0.06
$<P_4>$	0	1	0.36 ± 0.08

Heavy-ion induced transfer reactions with spherical and deformed nuclei*

W. J. Kernan, C. Y. Wu, X. T. Liu, X. L. Han, D. Cline, T. Czosnyka, M. W. Guidry, M. L. Halbert, S. Juutinen, A. E. Kavka, R. W. Kincaid, J. O. Rasmussen, S. P. Sorensen, M. A. Stoyer, and E. G. Vogt

Extensive light-ion induced few-nucleon transfer experiments have been performed for four decades. One-nucleon transfer has been shown to be a selective probe of single-particle configurations and has been of great importance in establishing an understanding of spherical and deformed shell structure in nuclei. Two-nucleon transfer probes nucleon-nucleon correlations and has played an important role in understanding the pairing field in nuclei.

In this paper we report measurement of cross sections for the quasielastic channels at energies slightly above the Coulomb barrier using various Ni and Sn projectiles and various isotopic Sn and Dy targets. The deexcitation γ rays were detected in a 4π NaI array (the Spin Spectrometer of the Oak Ridge National Laboratory) in kinematic coincidence with both target-like and projectile-like particles, thus providing a measure of the total energy and multiplicity of the entry state. The reaction channels were identified by characteristic γ deexcitation transitions measured with Ge detectors substituted for array elements in the Spin Spectrometer. The angular distribution for inelastic cscattering is well described by both semiclassical and quantal calculations. Two general features for few-neutron transfer channels are observed; (i) the dependence of the total cross section on the ground-state Q-value, (ii) the "coldness" of the reaction mechanism indicated by the measured entry states. For one-neutron transfer the distorted-wave Born approximation seems to give a correct overall qualitative description of the reaction mechanism for spherical nuclei and reproduces the cross sections within a factor of two. The ground-to-ground two-neutron transfer probability for the reaction between Sn isotopes was deduced and found to be strongly enhanced ($F \approx 760$), which is consistent with the expectation of strong pairing correlations. Two-neutron transfer to the ground-state band in Dy was partially resolved from transfer to other intrinsic states by using the Spin Spectrometer. The oscillating radial dependence of the probability for populating the ground-state band was found to be related to the nuclear deformation. This leads to an explanation of the "slope anomaly," where the measured radial dependence of the total two-neutron transfer probability has too flat a slope compared to the prediction based on a simple binding-energy argument. The probability for two-neutron transfer to the ground-state band is found to be similar to the probability for ground-to-ground transfer in the Sn + Sn system, suggesting a comparable strength for pairing correlations in the two systems.

Footnotes and References

*Published in *Nucl. Phys. A* **524**, 344 (1990).

Source and Emission Velocities for the $^{63}Cu + ^{12}C$ Reaction*

D. N. Delis, Y. Blumenfeld[a], D. R. Bowman[b], N. Colonna, K. Hanold, K. Jing[c], M. Justice, J. C. Meng[c], G. F. Peaslee[b], G. J. Wozniak, and L. G. Moretto

Fragments with atomic numbers (Z) covering nearly the entire range of the mass-asymmetry coordinate were observed from the 5.0, 6.2, 6.9, 8.0, 10.2 and 12.7 MeV/A $^{63}Cu + ^{12}C$ reactions. Energy spectra and angular distributions show the presence of projectile- and target-like components along with an isotropic component. The isotropic component appears as a Coulomb ring in the invariant cross-section plots indicating the presence of binary-compound-nucleus decay which is confirmed by the coincidence data.

The source and emission velocities for each Z-value were obtained from its Coulomb ring by determining its center and average radius. For the four highest energies, the extracted source velocities versus fragment Z-values are shown in the upper portions of each quadrant of Fig. 1. The experimental source velocities show very little dependence on the fragment Z-value confirming that all fragments are emitted by the same source. These source velocities agree closely with the velocities expected for complete fusion V_{cf}, which are indicated by the horizontal lines.

The average radii of the Coulomb circles or emission velocities of the fragments are shown in the lower portions of each quadrant. The Coulomb nature of these velocities can be inferred both from their magnitude and from their nearly linear dependence upon atomic number. A calculation (solid line) of the Coulomb velocities based upon the Viola systematics generalized to asymmetric divisions is also shown. The dashed lines are the first moments of the emission velocity distributions calculated with the statistical code GEMINI which includes evaporation and angular momentums effects. The agreement between the data and the calculations is quite good and confirms that the emission velocities are Coulomb-like and consistent with statistical emission.

Footnotes and References

*Condensed from Nucl. Phys. A534 403 (1991)

[a]Institut de Physique Nucleaire, Orsay, France
[b]NSCL, MSU, E. Lansing, MI 48824
[c]Institute of Atomic Energy, Beijing, China

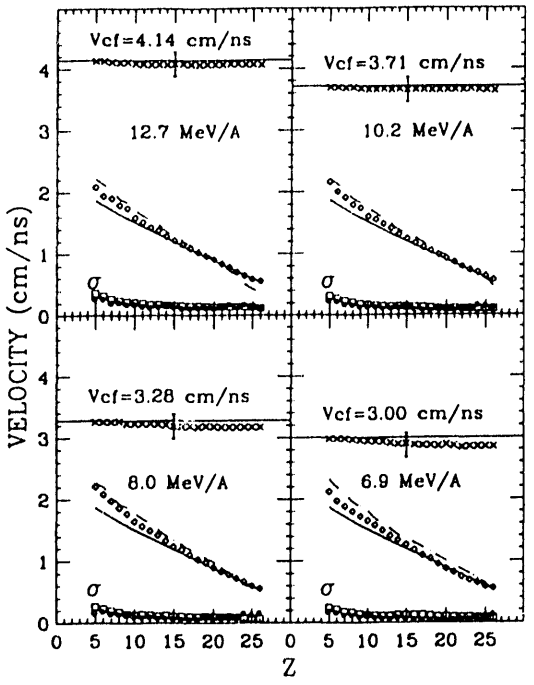

Fig. 1. In the upper part of each quadrant are shown the extracted source velocities (x) for each Z-species produced in the 6.9, 8.0, 10.2 and 12.7 MeV/A $^{63}Cu + ^{12}C$ reactions. The single large error bar for each data set indicates the possible systematic error due to the mass parameterization and energy calibrations. In the lower portion of each quadrant are shown the extracted Coulomb velocities (diamonds). For comparison, a calculation based on the Viola systematics (solid lines) and GEMINI (dashed lines) are shown.

The Transition From Complete to Incomplete Fusion in Asymmetric Reactions

K. Hanold, L.G. Moretto, G.F. Peaslee, G.J. Wozniak*
D.R. Bowman†, M.F. Mohar†, and D.J. Morrissey†

The study of complex fragment emission from very asymmetric systems in reverse kinematic reactions, e.g. ^{93}Nb,^{139}La+C,Al at 14 and 18 MeV/nucleon [1] [2] has shown, besides the quasi and deep inelastic component, a compound nucleus component associated with a sharp, well defined source at the complete fusion velocity. Recently the reaction of ^{139}La+Ni has been studied in reverse kinematics at 18 MeV/ nucleon. [3] The complex fragments from this more symmetric system are no longer associated with a single sharply defined source but rather are produced by a broad range of sources. This is thought to be a result of a broad distribution of mass transfers. The study of (^{129}Xe+C,Al,Ti,Cu) at 26 and 31 MeV/nucleon was carried out so that comparisons to the lower energy systems can be made and to examine the transition from complete to incomplete fusion at higher energies.

The center-of-mass velocity was reconstructed for each event of the binary coincidence data. The distributions of the perpendicular velocity component are very narrow. The distributions of the parallel velocity component ($V_{||}$) in the C and Al systems are also narrow. Only a peak corresponding to complete fusion or very near complete fusion velocity is seen. This result is identical to the results from lower energy (11.4 to 18 MeV/nucleon) reactions of ^{93}Nb+C,Al and to 14,18 MeV/nucleon ^{139}La+C,Al. In figure 1, the $V_{||}$ distributions for the 18 MeV/nucleon ^{139}La+Ni, 26 MeV/nucleon ^{129}Xe+Cu, and 31 MeV/nucleon ^{129}Xe+Cu systems are shown. The arrows at the bottom of each frame in figure 1 indicate the complete fusion velocity for each system. One can see the evolution of the distribution to include relatively greater amounts of incomplete fusion as the energy is increased. The tail that extends to low velocities in the figure is the result of events in which there were three or more fragments and only two were detected.

The modeling of these systems has been undertaken. These results and the rest of the experimental results will be described in a upcoming article.

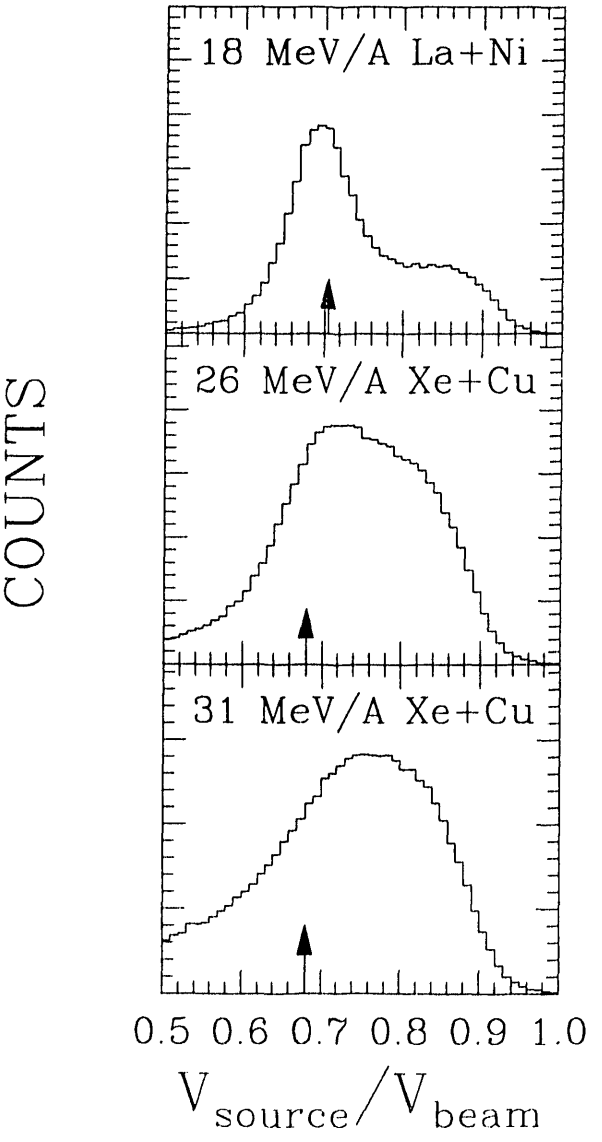

Fig. 1. The relative yield of coincidence events as a function of the extracted source velocity.

Footnotes and References

*present address; NSCL,MSU,East Lansing, MI 48824
†NSCL,MSU,East Lansing, MI 48824

[1] R.J. Charity, et al., Nucl. Phys. *A483*, 371 (1988).
[2] R.J. Charity, et al., Nucl. Phys. *A511*, 59 (1990).
[3] N. Colonna, et al., Phys. Rev. Let. *62*, 1833 (1989).

Projectile Breakup of ^{16}O at 32.5 MeV/A: Comparison of a Classical Dynamical Model with Experiment*

J. Suro, Y.D. Chan, J.A. Scarpaci, R.G. Stokstad, K. Möhringt and T.C. Schmidtt

The predictions of the classical dynamical model of Möhring, et al., [1] have been compared to the experimental data of Pouliot, et al., [2] for the reaction $^{16}O+^{197}Au$ at 32.5 MeV/A. The experimental apparatus detected the forward-angle fragments (up to 18 degrees) produced by the breakup of the projectile and enabled the full kinematic reconstruction of multiple breakup events having four fragments. The dynamical model, which considers the alpha-particle degrees of freedom only, was compared to the alpha-particle channels observed in the experiment. The angular range and energy thresholds of the detector system were used to select theoretical events for comparison to the data. Overall, rather good agreement was found in the 4 a channel for the cross sections, folding angle distribution (Fig.1), sphericity and coplanarity distributions, and the excitation energy spectrum.

Particle-particle correlations were not found to be very important in either the experiment or the dynamical theory. The present dynamical theory, statistical models for sequential decay, and the experiment all exhibit essentially identical folding-angle and sphericity/coplanarity distributions. This makes it impossible, on the basis of the present comparisons alone, to conclude that the measured folding angle distributions *require* an interpretation in terms of sequential decay. The experimental data, however, appear to rule out the particle-particle correlations corresponding to the mutual Coulomb repulsion of alpha particles from the multifragmentation [3] of an isolated ^{16}O nucleus.

Footnotes and References

*LBL-31597, Submitted to Nuclear Physics A.

† Hahn-Meitner-Institut Berlin, Germany

1. K. Möhring, T. Srokowski, D.H.E. Gross, and H. Homeyer, Phys. Letts. **B203** (1988) 210.

2. J. Pouliot, et al., Phys. Letts. **B223** (1989) 16.

3. J.A. Lopez and J. Randrup, Nucl. Phys. **A 491** (1989) 477.

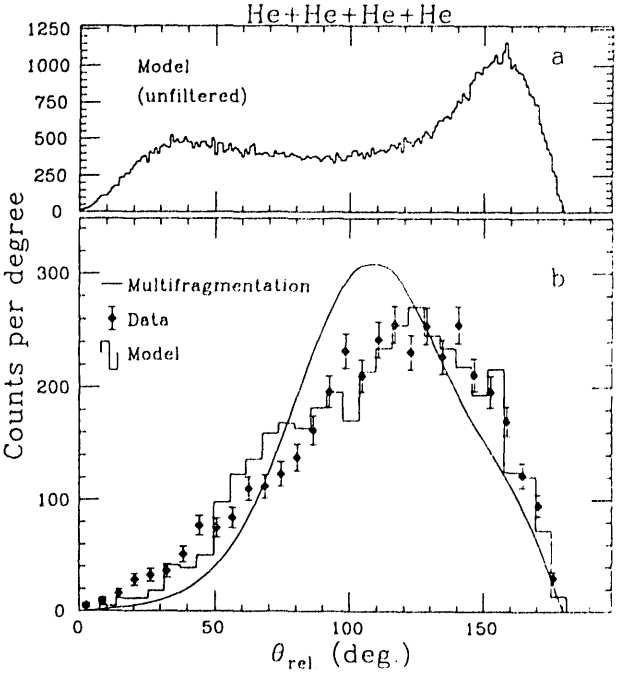

Fig. 1. The folding angle distribution in the rest frame of the 4 a system. The angle is the polar angle between alpha particles taken pair-wise. Each event contributes six counts to the spectrum. a) The theoretical distribution for all 4 a events. b) The filtered theoretical events (histogram), the experimental data (solid points), and the multifragmentation distribution from the kinematic model of ref. 3. (solid line).

Neon Radioactivity of Uranium Isotopes*

R. Bonetti†, A. Cesana‡, C. Chiesa†, A. Guglielmetti†, C. Migliorino†, P. B. Price, and M. Terrani‡

Because of the large branching ratio for neon emission from ^{232}U, the presence of ^{232}U impurities in sources consisting of other uranium isotopes may give rise to a background of neon emission that must be accurately known and accounted for. Given the factor-of-four discrepancy between the previous two measurements of B(Ne/α) for ^{232}U done in 1985 [1] and 1989 [2], we decided to make a new measurement of the neon emission rate of ^{232}U and to reevaluate the neon emission rate of ^{234}U and ^{235}U, both of which had been studied before, using sources containing a non-negligible amount of ^{232}U.

A 5cm x 5cm plate of PSK-50 phosphate glass track-etch detector was exposed to a (15±0.7) MBq ^{232}U source for 38 days, resulting in an exposure of 7×10^{12} alphas cm^{-2}, well below the point at which radiation damage affects detector performance (1×10^{14}). At this stage, the source activity was carefully measured by gamma-ray counting in two different geometries, with consistent results. The plate was then etched and scanned carefully for neon tracks by two independent observers, yielding 90 tracks with zenith angles between 0° and 65°. Due to ineffiency in track recording at large zenith angles and uncertainty in zenith angle measurement at small zenith angles, only the 82 events in the range $20° \leq \theta \leq 55°$ were selected; their distribution was consistent with a constant number per unit solid angle. Dividing the number of detected tracks in this interval by the fraction of solid angle covered [(cos20° - cos55°)/2], we obtained a branching ratio of $B(Ne/\alpha) = (9.16 \pm 1.1) \times 10^{-12}$, quite consistent with the 1989 result of 8.68×10^{-12}, but nearly a factor of 5 higher than the 1985 result; we believe that the most likely explanation for the discrepancy is that in the first experiment the source was from a commercial firm and the activity was assumed to be that specified by the manufacturer and not independently checked.

The above results imply a revision of rates previously reported for Ne radioactivity of ^{234}U and ^{235}U, where the subtraction of background from ^{232}U activity assumed the 1985 result for ^{232}U. The Ne emission rate goes down a factor of 4.8 for ^{234}U, and may have been marginally detected (1.9σ) for ^{235}U.

Footnotes and References

*Condensed from *Phys. Rev. C* **44**, 888 (1991).

†Istituto di Fisica Generale Applicata dell'Università di Milano, Istituto Nazionale di Fisica Nucleare, Sezione di Milano, Milano, Italy

‡Centro Studi Nucleari Enrico Fermi, Politecnico di Milano, Milano, Italy

1. S.W. Barwick et al., *Phys. Rev. C* **31**, 1984 (1985).

2. R. Bonetti et al., *Phys. Lett. B* **241**, 179 (1990).

A Complete Ridge-line Potential for Complex Fragment Emission*

D. N. Delis, Y. Blumenfeld[a], D. R. Bowman[b], N. Colonna, K. Hanold, K. Jing[c], M. Justice, J. C. Meng[c], G. F. Peaslee[b], G. J. Wozniak, and L. G. Moretto

Fission saddle points shapes for nuclei with a small fissility parameter (x<0.7) are strongly constricted at the neck, so that the nascent fission fragments are already well defined in mass. Therefore a physical significance can be assigned to the mass-asymmetry parameter in the neighborhood of the saddle. It is then possible to cut the potential energy surface of the nucleus with a line passing through the fission saddle point along the mass-asymmetry coordinate in such a way that each of its points is a saddle point if one freezes the mass-assymmetry coordinate. The locus of all these conditional saddle points, or conditional barriers is called the ridge line. This line controls the emission of complex fragments and can be determined from complex fragment excitation functions.

Complex fragment excitation functions were measured for the reaction $^{63}Cu + ^{12}C$ at six bombarding energies. The experiment was performed at the 88-Inch Cyclotron.

The excitation functions were analyzed by a means of a two parameter fit. One of these parameters was the conditional fission barrier and the other the ratio of the level density parameters at the saddle point (a_z) and at equilibrium (a_n).

The extracted zero-angular momentum barriers and ratio of level density parameters are shown in Fig. 1. The extracted barriers increase as a function of mass asymmetry, peak at symmetry and then fall off. This is the trend expected for a system with A = 75 whose fissility parameter x = 0.28 lies well below the Businaro-Gallone point. Theoretical barriers calculated with both the liquid-drop model and the finite-range model are also shown in the figure. The agreement between the experimental barriers and those calculated with the finite-range model is remarkably good while the liquid-drop barriers lie significantly higher than the data.

Footnotes and References

*Condensed from Z. Phys. A339 279 (1991)

[a]Institut de Physique Nucleaire, Orsay, France
[b]NSCL, MSU, E. Lansing, MI 48824
[c]Institute of Atomic Energy, Beijing, China

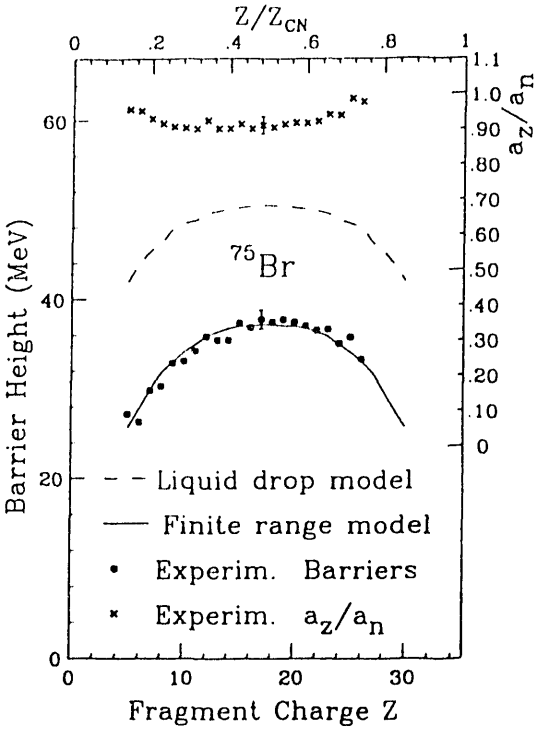

Fig. 1. The emission barriers and ratio of a_z/a_n extracted in fitting the excitation functions as a function of the fragment charge or asymmetry, Z/Z_{cn}. The data points are the extracted barriers (near the bottom) and ratios (near the top). The error bars arising from the χ^2 of the fitting procedure are smaller than the size of the symbols. The error bar represents an estimate of the possible systematic errors. The finite-range and liquid drop model barriers are shown by the solid and dashed lines, respectively.

Further Studies of the Spectra Observed from a ^{14}C-Doped Germanium Detector

*E. B. Norman, F. E. Wietfeldt, K. T. Lesko, R. M. Larimer, Y. D. Chan, M. T. F. da Cruz, A. Garcia, R. G. Stokstad, I. Zlimen, B. Sur[+], M. M. Hindi[++], P. N. Luke *, W. L. Hansen *, and E. E. Haller**

Over the past year we have continued to collect data from our first ^{14}C-doped germanium detector.[1] We have now accumulated approximately one year's worth of ^{14}C data and approximately 111 days worth of background data (using an undoped crystal). From analysis of all of this data, we find a "kink" in the spectrum which can best be explained by the emission of a neutrino with a mass of 17.1±0.6 keV and an emission probabilty of (1.2±0.3)%. This can be seen in Figure 1.

We have performed numerous tests of the response function of the detector and of the electronics to see if the "kink" could be some experimental artifact. To date, we have not been able to find any other explanation for the feature we observe in the beta spectrum of ^{14}C.

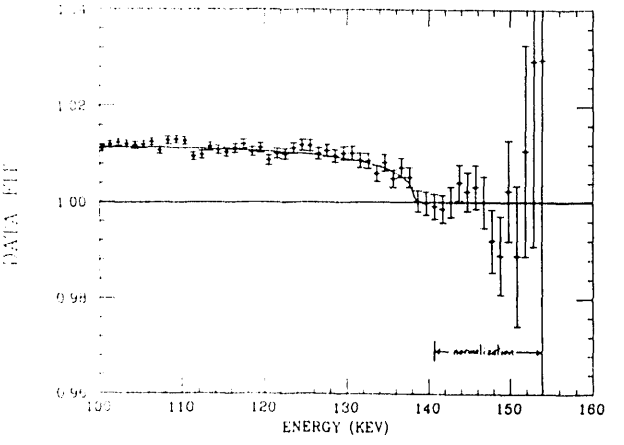

Fig. 1. The ratio of the data to a theoretical fit assuming the emission of only zero-mass neutrinos. The horizontal line is the shape expected for zero-mass neutrinos. The curve illustrates the shape expected from the best fit to the data.

Footnotes and References

+ Physics Department, Queen's University, Kinston, ON K7L 9N6, Canada

++ Physics Department, Tennessee Technological University, Cookeville, TN

* Engineering Division, LBL

1. B. Sur et al., Phys. Rev. Lett. 66, 2244 (1991).

Search for Evidence of Heavy Neutrino Emission in the Inner Bremsstrahlung Spectrum of ^{55}Fe

I. Zlimen, E. B. Norman, K. T. Lesko, R. M. Larimer, A. Garcia, R. G. Stokstad, Y. D. Chan, F. E. Wietfeldt, M. T. F. da Cruz

During the past year, the controversy surrounding the possible existence of a neutrino with a mass of 17 keV has grown. While three additional groups using solid-state germanium or silicon detectors have claimed to see evidence of this heavy neutrino, others using magnetic spectrometers claim not to see it. A common feature of all of these experiments is their relatively low statistics. This necessitates fitting a fairly wide energy interval and looking for a small departure from the expected smooth shape of a beta or an inner bremsstrahlung spectrum. We are attempting to gather enough data at the expected position of the "kink" so as to be able to perform a local analysis using the second derivative of the inner bremsstrahlung spectrum of ^{55}Fe.

The "kink" we are searching for is produced because the spectrum of inner bremsstralung photons (or electrons) accompanying the emission of a massive neutrino near its endpoint approaches zero with an infinite slope, while that associated with a massless neutrino goes to zero with zero slope. Thus, in the second derivative, the emission of a massive neutrino produces a narrow peak-like structure. Monte-Carlo calculations indicate that at least 10^7 counts per keV are required at the expected "kink" position in order to see this structure in the second derivative.

We are currently acquiring data from a 25 milliCurie ^{55}Fe source. The inner bremsstralung spectrum is observed in a 110 cm^3 high-purity Ge detector that is surrounded by a 12x12 inch NaI active shield. We expect to have the necessary statistics within a few months to perform the second derivative analysis for the presence of the massive neutrino.

Beta Plus Decay and Cosmic-Ray Half Life of ^{91}Nb

M. M. Hindi[+], K. L. Wedding[++], E. B. Norman, K. T. Lesko, B. Sur[*], R. M. Larimer, M. T. F. da Cruz, and K. R. Czerwinski

In the laboratory, ^{91}Nb decays by electron capture with a 680 year half life. However, with a Q_{EC} value of 1255 keV, it is energetically possible for it to also beta plus decay. As a high energy cosmic ray, with all of its atomic electrons stripped away, positron emission would be the only open decay channel for ^{91}Nb. Future observations of ^{91}Nb in the cosmic rays could be used to determine the age of the medium mass cosmic rays if the beta plus decay rate of ^{91}Nb were known.

We produced ^{91}Nb by bombarding a yttrium foil with 38 MeV alpha particles from the 88-Inch Cyclotron. The niobium fraction was then chemically separated from the target. We used an array of Ge and NaI detectors to measure 511-511 keV gamma ray coincidences as a signature of beta plus decay. By following the annihilation radiation over an extended time period, we were able to determine the beta plus branching ratios of both the 104-keV, 61-day isomer and the ground state of ^{91}Nb. For the isomer, $BR(\beta^+) = (2.8\pm0.2)\times10^{-5}$. For the ground state, $BR(\beta^+) = (1.38\pm0.25)\times10^{-4}$, leading to a β^+ partial half-life (and hence cosmic-ray half-life) of $(4.9\pm0.9)\times10^6$ years. Such a value of this half life makes ^{91}Nb an ideal candidate for determining the age or confinement time of this secondary component of the cosmic rays.

Footnotes and References

+ Physics Department, Tennessee Technological University, Cookeville, TN 38505

++ Carleton College, Northfield, MN

* Physics Department, Queen's University, Kingston, ON, Canada

Half-Life of ^{56}Ni

M. T. F. da Cruz, Y. D. Chan, R. M. Larimer, K. T. Lesko, E. B. Norman, R. G. Stokstad, F. E. Wietfeldt, and I. Zlimen

Discrepancies in measured values of the half-life of ^{56}Ni contribute to uncertainties in the expected shapes of supernova light curves. To help resolve this issue the ^{56}Ni half-life was redetermined by measuring the time-dependent yields of four ^{56}Ni gamma ray lines. The ^{56}Ni was produced by the ^{56}Fe(^{3}He,3n) reaction using a 50-MeV ^{3}He beam from the 88-Inch Cyclotron. Following the irradiation, a chemical separation was performed to remove the large amounts of ^{56,57}Co and ^{52,54}Mn also produced. The purified ^{56}Ni was then mixed with ^{207}Bi which provided an internal standard for the counting. Measurements were performed over a 38-day span. The yields of the ^{56}Ni gamma-ray lines were normalized to those of the lines from the ^{207}Bi. A weighted mean value of 6.077±0.12 days was found for the ^{56}Ni half life. This value is in good agreement with the most accurate previous measurement[1] of 6.10±0.02 days.

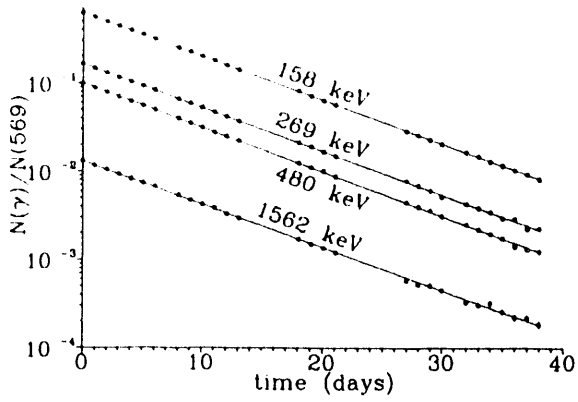

Fig. 1. Time dependent yields of ^{56}Ni gamma rays normalized to the observed yield of the 569-keV gamma-ray from the decay of the ^{207}Bi standard.

Footnotes and References

1. D. O. Wells et al., Phys. Rev. 130, 1961 (1963).

Beta-Delayed Two-Proton Decay of ^{39}Ti*

D.M. Moltz, J.C. Batchelder, T.F. Lang, T.J. Ognibene, J. Cerny, P.E. Haustein, and P.L. Reeder

Studies of nuclei near the proton drip line permit examination of very exotic decay modes and analysis of specific nuclear structure problems not addressable nearer stability. To date, only four examples of proton radioactivity have been discovered. Another decay mode which is theoretically possible at the drip line is ground state two proton radioactivity (where $S_p > 0$ and $S_{2p} < 0$). The most experimentally accessible candidate which could exhibit this decay mode is ^{39}Ti.

Initially we undertook several experiments to search for ground state two-proton emission in the 110 MeV $^3He^{2+}$ + ^{Nat}Ca reaction with our fast rotating wheel. The null results were in agreement with a concurrent experiment at GANIL[1] which also measured the half-life of ^{39}Ti to be 28 ms. We then chose to utilize our newly developed cubic array of triples telescopes[2] (gas-gas-Si) in conjunction with our standard helium-jet system to search for the beta-delayed two-proton decay branch from ^{39}Ti. All software gated-diproton events were then subjected to detailed analysis of the original raw event. The final two-proton sum-energy spectrum shown in Figure 1 was generated by individually summing the energies of each separate proton.

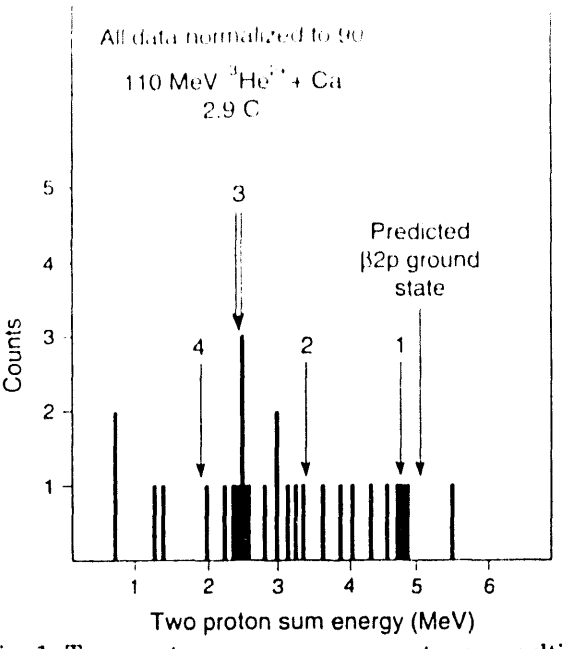

Fig. 1 Two-proton sum energy spectrum resulting from the bombardment of a ^{Nat}Ca target with 2.9 C of 110 MeV $^3He^{2+}$ beam.

Although the seven events at ~2.50 MeV correlate with two states in ^{37}K, the unknown nature of these states and their very close spacing forbid us from using them in the determination of the excitation energy of the isobaric analog state in ^{39}Sc. Thus, this determination was made solely with the peak labelled 1) in Figure 1 at 4.75 MeV. The measured energy of 4.75 ± 0.04 MeV is 0.23 MeV smaller than the predicted β2p energy. Because the calculated Coulomb displacement energy is unaffected by this measurement, this leads to a lower value of S_{2p} of -530 + 65 keV. This number is also consistent with the GANIL result[1] demonstrating that ^{39}Ti primarily beta decays.

*Condensed from D.M. Moltz *et al.*, Z Physik A, in press.

Footnotes and References

1 C. Detraz *et al.*, Nucl. Phys A 519 (1990) 529.

2 D.M. Moltz *et al.*, 1990-91 LBL Annual Report, p. 102.

Possible Evidence For The β-delayed Proton Emission of ^{65}Se

J.C. Batchelder, D. M. Moltz, T. J. Ognibene, M. W. Rowe, and Joseph Cerny

The decays of many proton-rich light nuclei near the proton drip line have been identified by their β-delayed proton emission. In the case of a strong proton emitter, the Isobaric Analog State (IAS) is unbound with respect to proton emission.

All members of the $T_z = -3/2$, A = 4n+1 series from ^{17}Ne to ^{61}Ge[1] are strongly delayed proton emitters. The next member of this series, ^{65}Se, has been predicted by the Kelson-Garvey mass relation coupled with a formula for the Coulomb displacement energies, to be bound to ground state proton emission, while the IAS in ^{65}As is unbound to proton emission by 3.7 MeV.

For this search, we have utilized our helium-jet system which has a transit time of around 25 ms. The activity was deposited on a moving tape (to remove long lived activity) directly in front of a Si ΔE-E telescope.

An 115 MeV (on target) $^{28}Si^{6+}$ beam was bombarded on a natural Ca target to produce ^{65}Se. Observation of this decay has proved to be more difficult due to a drop in predicted cross section and an omnipresent oxygen contamination in the targets used. The reaction of ^{28}Si on ^{16}O produces the well-known strong β-delayed proton emitter ^{41}Ti. ^{41}Ti has transitions at 3.69 MeV (15.5%), and at 3.75 MeV (31.0%), thereby creating a "background" peak precisely where it would interfere with the observation of ^{65}Se (refer to figure).

We have been able to partially solve this problem by using Ca targets as oxygen-free as possible. The result is a spectrum with 150% greater number of events at 3.7 MeV than can be explained as resulting from ^{41}Ti. This suggests that the extra counts may be due to ^{65}Se. (The counts at the higher energy of 4.1 MeV are believed to be due to ^{25}Si which is seen in large amounts at lower bombarding energies.) A second series of runs at a bombarding energy of 130 MeV on target also showed a large number of counts in the region of 3.7 MeV with respect to the main ^{41}Ti peak (in a different ratio than the data obtained at 115 MeV)

1) M. A. C. Hotchkis, *et al* Phys. Rev. C 35, 315 (1987)

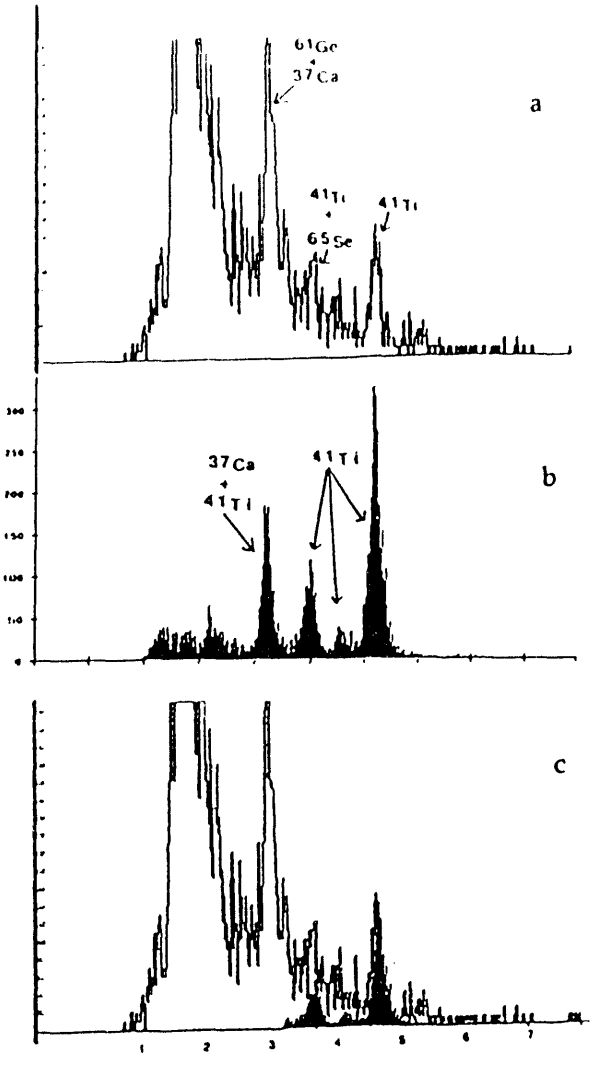

Fig. 1. a). Delayed proton spectrum arising from the compilation of several 115 MeV ^{28}Si + ^{nat}Ca bombardments.
b).β-delayed proton spectrum produced in the 40 MeV ^{3}He + ^{nat}Ca reaction.
c).^{41}Ti spectrum from b) normalized to the 4.7 MeV peak, and superimposed on spectrum a).

Alpha-Decaying Low-Spin Levels in ^{155}Lu and ^{157}Lu*

K.S. Toth†, K.S. Vierinen‡, J.M. Nitschke, P.A. Wilmarth, and R.M. Chasteler§

We have reinvestigated many α emitters above N=82 at the OASIS isotope separator on-line at the LBL SuperHILAC. In these studies, we have determined isomer excitation energies, more precisely determined a number of α-branching ratios, and have observed[1] fine structure in the α-decay spectrum of ^{153}Tm. Here we report on the α-particle decays of ^{155}Lu and ^{157}Lu.

The two isotopes were produced in (^{64}Zn, p2n) reactions on self-supported, 2 mg/cm^2 -thick, foils of ^{94}Mo and ^{96}Mo, respectively. The isobars of interest were selected by the separator, transported ionoptically to a fast cycling tape system, and periodically positioned between an array of detectors. A ΔE-E particle telescope and a planar HPGe detector faced the radioactive layer while a 52% Ge detector was located on the opposite side of the tape. A second 24% Ge detector was also placed at 90° relative to the other detectors.

Figure 1 shows the α spectrum recorded at A=155. Above the intense ^{155}Yb 5194-keV α peak are two weak α groups with energies of 5579(5) and 5648(5) keV. The higher energy group, presumedly the α decay of the $h_{11/2}$ state in ^{155}Lu, has been known[2] since 1965. Recently, Hofmann *et al.*[3] observed 5575-keV α-decay from a second ^{155}Lu level. Our data, therefore, confirm this new α-emitting level which we believe is either the $s_{1/2}$ or $d_{3/2}$ single-proton state. No half-life for this level was reported in Ref. 3; we measured a value of 140(20) ms. We also remeasured the half-life for the ^{155}Lu high-spin α decay and our value of 67(7) ms is in good agreement with previous measurements.[2,3]

At A=157, in addition to the known α lines from ^{149}Tb, ^{153}Ho, ^{157}Yb, ^{153}Er, ^{153}Tm, and ^{157}Lu ($h_{11/2}$ state), we were able to identify a new α group at 4924(20) keV. We assign this line to the previously unreported low-spin ($1/2^+$ or $3/2^+$) state in ^{157}Lu. Our data indicate a half-life of 5.7(5) s for this state rather than the 4.8(2) s for the $h_{11/2}$ state. From our data, a decay scheme for ^{157}Lu high-spin β decay could be constructed and an α-branching ratio of 18(5) % determined. This disagrees with an earlier 6(2) % α branching ratio measured by Hofmann, *et al.*[4] No α-branching ratio could be deduced for the low-spin decay.

Reduced widths were calculated for the 5648-keV (^{155}Lu) and 4988-keV (^{157}Lu) α groups and the values are comparable to those of nearby N=84, 86 even-even nuclei. Therefore, the α transitions are unhindered and most probably connect the $\pi h_{11/2}$ high-spin parent state to the corresponding $\pi h_{11/2}$ daughter ground state.

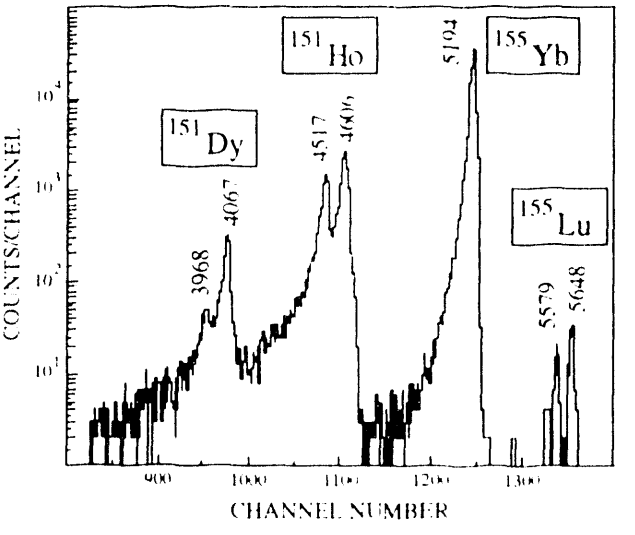

Fig. 1. Alpha-particle spectrum recorded at A=155. Energies are expressed in keV.

Footnotes and References

* Condensed from Z. Phys. A 340, 343 (1991).

† Physics Division, Oak Ridge National Laboratory, Oak Ridge, TN 37831

‡ Permanent address: University of Helsinki, SF-00170 Helsinki, Finland

§ Present Address: Department of Physics, Duke University and Triangle Universities Nuclear Laboratory, Durham, NC 27706

1. K.S. Toth, *et al.*, Phys. Rev. C 38, 1932 (1988).
2. R.D. Macfarlane, Phys. Rev. 137, B 1448 (1965).
3. S. Hofmann, *et al.*, Z. Phys. A 333, 107 (1989).
4. S. Hofmann, *et al.*, Z. Phys. A 291, 53 (1979).

Investigation of A=155 and A=151 Nuclides: Identification of the ^{155}Tm $s_{1/2}$ Isomer and of the ^{155}Yb β-Decay Branch*

*K.S. Toth†, K.S. Vierinen‡, M.O. Kortelahti§, D.C. Sousa†,**, J.M. Nitschke, and P.A. Wilmarth*

The decay properties of ^{155}Lu, ^{155}Yb, ^{155}Tm, and of the α-decay daughters ^{151}Er and ^{151}Ho were investigated at the OASIS isotope separator on-line at the LBL SuperHILAC. The A=155 products were produced in ^{64}Zn irradiations of ^{95}Mo, mass analyzed, transported to a fast-cycling tape system, and periodically positioned between an array of solid state detectors for spectroscopic studies. Both low- and high-spin α-decaying states in ^{155}Lu were observed and, for the first time, a half-life of 140±20 ms was determined for the low-spin state. The β-decay branch for ^{155}Yb was also identified in this study by observing six daughter γ rays and Tm K x rays decaying with the 1.75 s parent half-life. A parent spin of 7/2$^-$ was proposed and the six transitions placed in a decay scheme. From the observed β and α intensities, an α branching ratio of 90% was deduced. The α and β decays of ^{155}Tm had been previously studied but there existed a discrepancy in half-life values. From our K x-ray coincident γ-ray data, we were able to assign transitions with two different half-lives to ^{155}Tm decay. This can be explained by the existence of a heretofore unknown $s_{1/2}$ isomer with a half-life of 44±4 s in addition to the $h_{11/2}$ isomer which has a half-life of 21.6±0.2 s. The proposed decay scheme is shown in Fig. 1. A detailed study of the β decay of ^{151}Er yielded a more precise determination for the $s_{1/2}$ isomer energy (41.1±0.2 keV) in ^{151}Ho. From decay intensity balances, the α-branching ratios for ^{151}Ho and ^{151}Ho^m, 28±7 and 80^{+15}_{-20} %, respectively, could be determined.

Footnotes and References

* Condensed from Phys. Rev. C **44**, 1868 (1991).

† Physics Division, Oak Ridge National Laboratory, Oak Ridge, TN 37831.

‡ Permanent address: University of Helsinki, SF-00170 Helsinki, Finland.

§ Louisiana State University, Baton Rouge, LA 70803; Present Address: University of Jyväskylä, SF-40100, Jyväskylä, Finland.

** Permanent address: Eastern Kentucky University, Richmond, KY 40475.

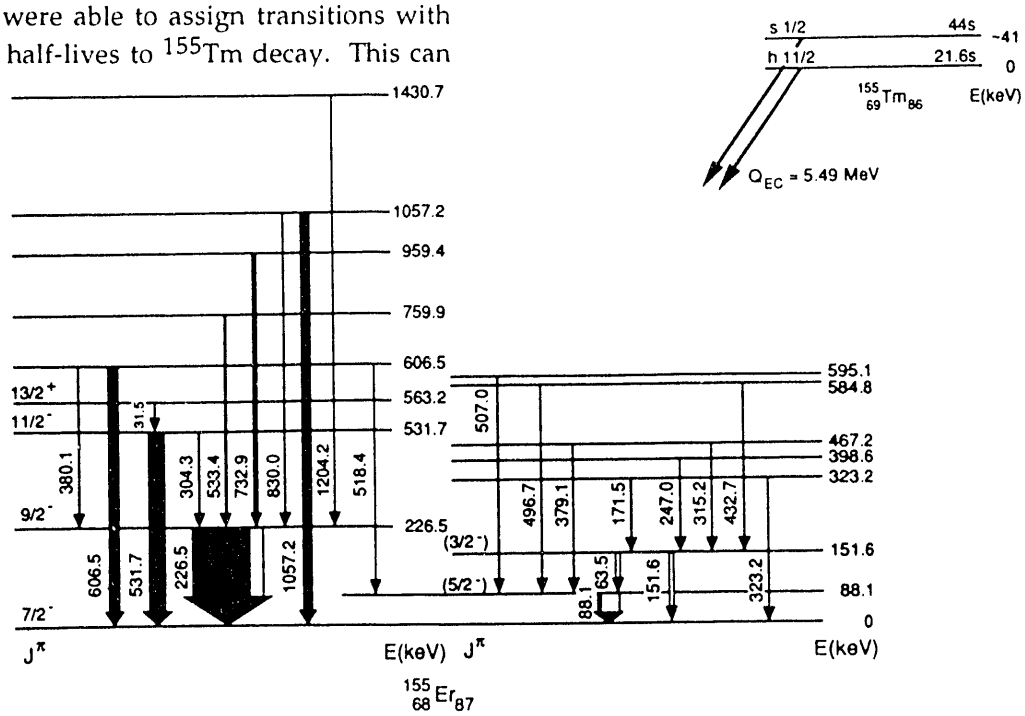

Fig. 1. Proposed decay schemes for the ^{155}Tm $s_{1/2}$ isomeric and $h_{11/2}$ ground states.

K X-Ray Multiplet Fitting

P.A. Wilmarth

To measure the ground-state to ground-state Electron Capture (EC) decay branching ratio in the Total Absorption Spectrometer (TAS) experiments, K x rays are measured both in and out of coincidence with γ-rays in TAS. TAS has a very large probability (>90% over an energy range from 0.05 to 12.0 MeV) for γ-ray interactions, so, to first order, the intensity ratio is a direct measurement of the ground state feeding. There are four major K x-ray transitions of known energy and relative intensity for each element, so a mixture of even a few elements will give rise to a very complicated spectrum. Many of the peaks will overlap and the correct intensities may be difficult to determine. While many γ-ray peak fitting programs exist, none make use of the known x-ray energies and intensities to constrain the fit. A program was written to perform x-ray peak fitting with the following assumptions: the background under the x-rays is specified by a second-order polynomial, each element is described by 4 Gaussians of fixed energy and relative intensity, the number of elements in the sample and the region of interest are specified, and the intensity of each element is varied until the best fit is found. Figure 1 shows the fit for a sample with 4 elements (16 transitions) present. A typical fitting program may vary positions and amplitudes for each peak, a single width, and a background function for a total of 37 parameters. However, if the fit is constrained by the known K x-ray information, the number of parameters is reduced to 11. The data in Fig. 1 were also fit with SAMPO[1] which gave comparable results for Cs and Xe but missed considerable intensity (factors of 2 to 3) for I and Te. Since the peak positions, determined from the literature energies, are fixed in this approach, uncertainties in the energy calibration may cause poor fits. An elegant solution to this problem is to vary the energy calibration coefficients as part of the fit. The program uses the MINUIT package for the minimization and runs under VMS.

Footnotes and References

1. J.T. Routti and S.G. Prussin, Nucl. Instum. Methods **72**, 125 (1969).

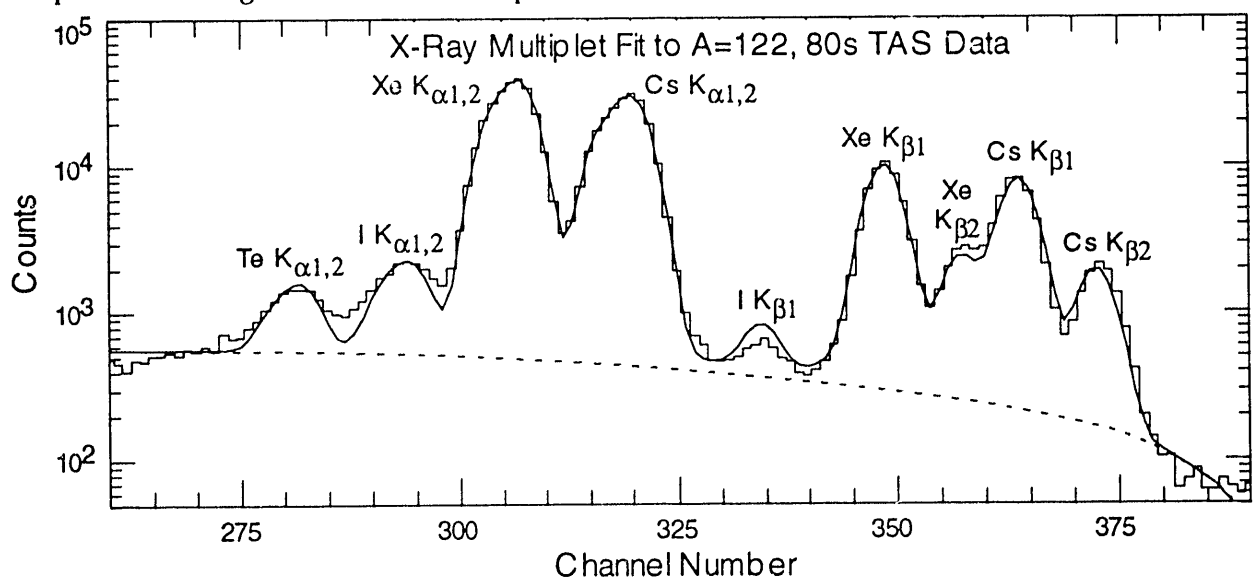

Fig. 1. Comparison between x-ray multiplet fit and data for 80s, A=122 TAS x-ray data; data (solid histogram), fit (solid curve), and background (dashed curve). Major x-ray transitions are labeled.

Laser Trapping of Radioactive Atoms

S.J. Freedman†, B.K. Fujikawa†, Z. Lu†, S. Shang†, K. Coulter†, and L. Young‡

A series of experiments exploiting the new techniques for trapping and manipulating neutral atoms was begun this year. We will use the technique to make high precision measurements of nuclear beta-decay properties. The first experiment is a measurement of the beta-asymmetry parameter in the mirror beta-decay of ^{21}Na to ^{21}Ne. This measurement could provide an interesting test of the handedness of the weak interaction. The Standard Model proposes that the weak interaction involves only the left handed helicities of fundamental quarks and leptons.

The ^{21}Na is produced with the ^{24}Mg(p,α)^{21}Na reaction with a 30 MeV proton beam from the 88-Inch Cyclotron. The beam is stopped inside of an atomic beam oven which is loaded with shavings of magnesium metal. In-beam tests of this procedure were begun this winter.

An argon-ion pumped dye laser and associated optics was recently set up in a laboratory in Building 19A. The required techniques of atom manipulation are now being developed with this apparatus. In recent experiments we successfully trapped stable Na contained in a simple cell at room temperature. Measurements of the atomic density and the other experimental parameters are in progress.

The experiments with radioactive atoms will require us to trap atoms from a laser slowed atomic beam. In the experiments with the 88-Inch Cyclotron we will transport laser light to the target area with a system of fiber optics. With this in mind we have begun to set up a laser laboratory in Building 88.

The basic techniques we are now developing will be useful for measurements of other beta-decay correlations that can be used to probe the detailed character of the weak interaction in nuclear systems. We are considering possible measurements of induced weak currents, possible time-reversal symmetry violating correlations, and neutrino mass.

Footnotes and References

† Lawrence Berkeley Laboratory, Berkeley CA 94720
‡ Argonne National Laboratory, Argonne IL 60439

A High-Pressure Ionization Chamber for Massive Neutrino Search

Y. Chan, M.T.F. da Cruz, A. Garcia, R.M. Larimer, K.T. Lesko, E.B. Norman, R.G. Stokstad, F.E. Wietfeldt and I. Zlimen

The possible existence of a heavy (17-keV) neutrino in nuclear weak decay has been suggested by several authors[1] from studying the shapes of either the β- or γ- (inner bremsstrahlung electron capture) energy spectra observed in Si or Ge detectors. Such claims, however, are not supported by magnetic spectrometer measurements. To see whether this could possibly be due to some unknown properties of crystalline solid state devices, it is desirable to make similar measurements with a gaseous detector.

A high-pressure ionization chamber (HPIC) has been constructed for this purpose. The detector is capable of handling both solid and gaseous radioactive sources. It has a cylindrical symmetry and is equipped with a Frisch grid. The field cage is made up of 8 concentric gold-plated conducting rings. The total resistance in the voltage divider circuit is 1 GΩ. The charge collecting anode consists of a central disk-like region and a concentric guard ring. The purpose of the guard ring is to veto events from β's that are not completely stopped within the central region of the detector. This provides a means of defining the source volume in the radial direction, which is essential for gaseous sources.

A transparent window with wavelength shifter for primary scintillation light detection is located at the top of the chamber. By recording the time difference between the phototube signal and the anode signal one can deduce the vertical position of the event vertex. Since electronic noise is a major factor in affecting the resolution of the detector, effort has been made to minimize the preamp noise with selected components.The detector can be operated up to a pressure of 22 atm.

The initial performance of the detector and its response to internal conversion electron sources have been examined. The energy resolution was 9.5 keV (FWHM) at 85 keV for a ^{109}Cd source. Further improvements in the resolution, stability tests and Monte Carlo simulations of the energy response are in progress.

Footnotes and References

1. J. J. Simpson et al., *Phys. Rev. Lett.* **54**, 1891(1985).
B. Sur et al., *Phys. Rev. Lett.* **66**, 2444 (1991).
I. Zlimen et al., *Phys. Rev. Lett.* **67**, 560 (1991).

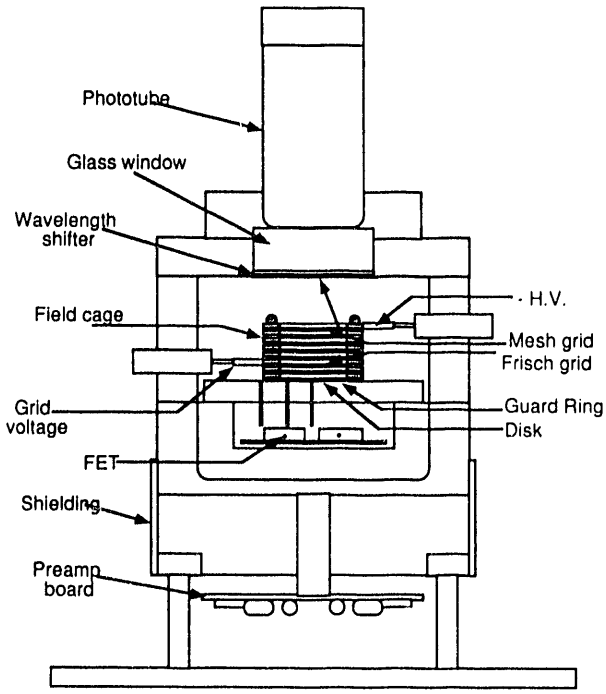

Fig. 1. A schematic drawing of the HPIC.

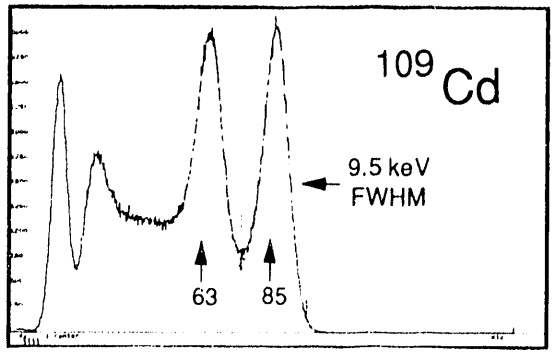

Fig. 2. ^{109}Cd internal conversion spectrum.

Antarctic Muon and Neutrino Detector Array (AMANDA)

S. Barwick‡, F. Halzen§, D. Lowder, T. Miller, R. Morse§, P.B. Price, A. Richards, D. Snowden-Ifft, S. Tilav§, and A. Westphal

Observation of the small fluxes of neutrinos expected at energies above 1 TeV requires much larger neutrino telescopes than exist today. An instrument of such large dimension (~ 1 km^2) requires a large naturally occurring detector medium, so that only photodetectors and electronics have to be built. One such medium is Antarctic ice. A neutrino telescope could be built by drilling holes in the ice and lowering strings of photomultiplier tubes (PMTs) to a depth of ~ 1 km. Neutrinos would be detected via the Cerenkov light emitted by upward-moving neutrino-induced muons. At these high energies, the direction of the muon produced is within 1 degree of the direction of the parent neutrino, so neutrino source observation is possible. Such a detector would have many advantages over other proposed neutrino telescopes. Although the technique's feasibility depends on the optical clarity of the ice, the transparency of South Polar ice should be good, as the ice cap has been shown to be bubble free at large depths (~ 1 km), and is known to be quite free of impurities in the interior of the continent. We have begun the AMANDA project to test the feasibility of this idea and ultimately to build such a large-scale detector at the South Pole.

During 13-16 August 1990, we conducted an initial investigation of the quality of *in situ* polar ice as a Cerenkov radiator at the GISP-II site in Greenland (72° N. 38° W.). The success of this trial[1] led to more extensive experiments at the South Pole during the 1991-1992 Antarctic summer. Preliminary examination of the results of these tests indicates that the ice at 800 m depth is of good optical quality, consistent with the absence of bubbles, and further work is in progress to determine more precisely the ice transparency. In addition, it was shown that PMTs survive deployment and freezing into the Antarctic ice cap and remain operational, and that radioactive backgrounds and light leakage from the surface are negligible. During the 1992-1993 season, we plan to begin construction of an array of nine strings of twenty PMTs.

Footnotes and References

‡Department of Physics, University of California, Irvine, CA 92717, USA
§Department of Physics, University of Wisconsin, Madison, WI 53706, USA

1. Lowder et al.,*Nature* 353, 331 (1991).

Sudbury Neutrino Observatory, Photomultiplier Tube Support Structure Geodesic Dome

Kevin T. Lesko, Yuen Dat Chan, Tiago de Cruz, Alejandro Garcia, Yoichi Kajiyama†, Gary Koehler† Milt Moebus† Alex Ozeroff†, Eric Norman, Peter Purgalis†, Alan Smith†, Robert Stokstad, Igor Zlimen and the Sudbury Neutrino Observatory Collaboration

The Sudbury Neutrino Observatory (SNO) will be a world class observatory for neutrino astrophysics. It will contribute to both astrophysics and particle physics by addressing the solar neutrino problem and neutrino oscillations.

The SNO detector is a large heavy water cherenkov detector designed to detect neutrinos in the 1000 ton D_2O target. The detector has sensitivity to the total neutrino flux, ν_x, regardless of family (x= e, μ, τ) and to the ν_e flux separately by measuring the elastic scattering, charged and neutral current signals. The D_2O is contained in a thin-wall acrylic sphere, 6 m radius, which is itself suspended in a cavity filled with 7000 tons of ultrapure light water. The detector is located in a mine 2 km below ground level near Sudbury, Ontario Canada. The mine is an active nickel mine operated by INCO, Ltd.

Lawrence Berkeley Laboratory is designing the Photomultiplier Tube Support Structure which will position and secure the ~10000 PMTs used to detect the cherenkov light generated by neutrino interactions in the D_2O. The experimental constraints on the design require an extremely low radioactivity contamination of detector components, submersion in ultrapure water for a period of > 10 years, restricted maintenance opportunities, and installation in an active nickel mine while simultaneously maintaining cleanroom conditions.

The PMT Support Structure load bearing structure (Figure 1) is based on a three-frequency icosahedron geodesic structure, 8.9 in radius. The structure is constructed of 270 stainless steel struts joined in 92 hubs. While weighing only 10000 kg it will support a maximum load of 66000 kg prior to filling the cavity with water. After filling the cavity the structure will support a buoyant load of 14000 kg for the 10 years of the experiment.

All components which make up the geodesic structure are specially selected to assure compatibility with the aggressive ultrapure water environment and to guarantee very low radioactive element contamination. The design and prototyping of the structure is nearing completion in 1992. Installation will commence in the Spring of 1993 and be completed in 1994.

Footnotes and References

† Engineering Division, Lawrence Berkeley Laboratory

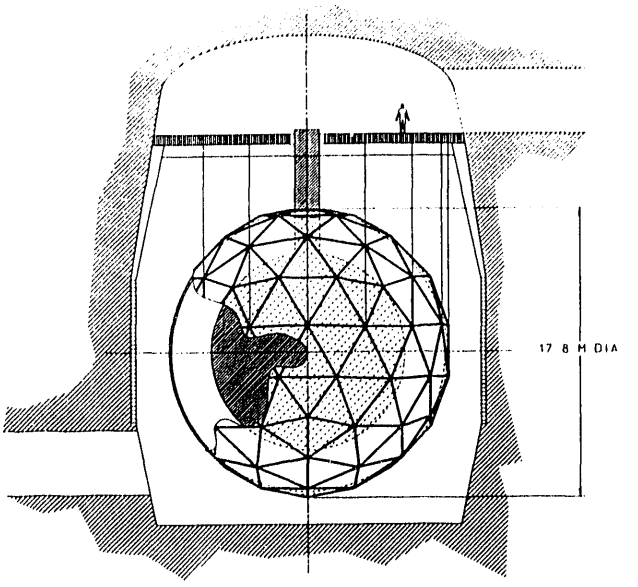

SUDBURY NEUTRINO OBSERVATORY

Fig. 1. This figure shows the three frequency icosahedron dome which makes up the principal load bearing structure of the SNO PMT Support structure. Also shown are the acrylic vessel which contains the 1000 tons of D_2O and the outline of the rock cavity. The cavity is situated 2 km below ground level.

Sudbury Neutrino Observatory, Photomultiplier Tube Support Structure Panel Assemblies

The Lawrence Berkeley Laboratory SNO Group and the Sudbury Neutrino Observatory Collaboration

To accurately align and secure the ~10000 PMTs required by the SNO experiment we have designed panel assemblies which tessellate the 8.5 m sphere defined by the geodesic structure described in the previous article. The PMT sphere is concentric with the D_2O acrylic vessel. Each spherical 8" diameter Hamamatsu PMT uses a non-imaging reflector to enhance the light collection efficiency by ~70%. This reflector while enhancing the PMT's light collection also effectively defines a light collection angle of 56°. Consequently, each PMT needs to be aligned with the center of the vessel within a few degrees of pointing accuracy.

Our design presently accommodates 9522 PMTs and reflectors and achieves a "packing fraction" of ~83%. This high density of PMTs simplifies the additional requirement that the PMT Support Structure serve as a water barrier separating the relatively contaminated water outside of the PSUP from the necessarily very clean water between the PMTs and the D_2O.

We have developed a design which uses five differently shaped panels. Each panel holds between 7 and 21 PMTs. There are a total of 751 panels. Each panel is constructed of identical right hexagonal cells bolted together to form flat panels. Each cell secures and aligns a PMT and its reflector.

We selected ABS plastic[1] for the cell material following our materials property test program. ABS was shown to be sufficiently strong and to resisted long term creep while submerged in ultrapure water. All materials used in the SNO detector are specially selected to be compatible with the aggressive ultrapure water environment and to be very low in radioactive element contamination ([U] and [Th] ≤ 20 ppb).

A cross section of a typical cell is shown in Figure 1. In Figure 2 we present a three-dimensional view of one of the smaller panels.

Footnotes and References

† Engineering Division, Lawrence Berkeley Laboratory

[1] ABS Plastic, G.E. Resin GPM 5600, Cycolac.

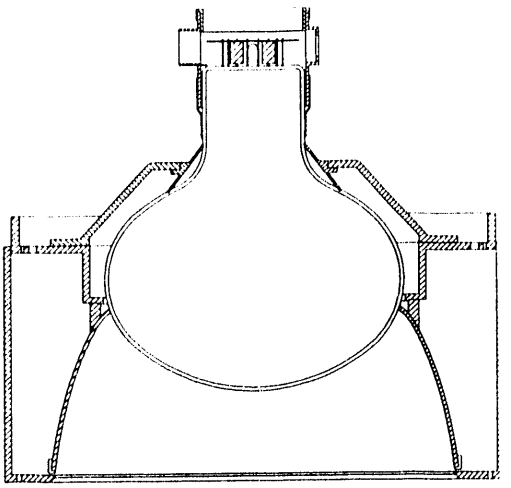

Fig. 1. This figure shows a cross sectional schematic of a hexagonal cell.

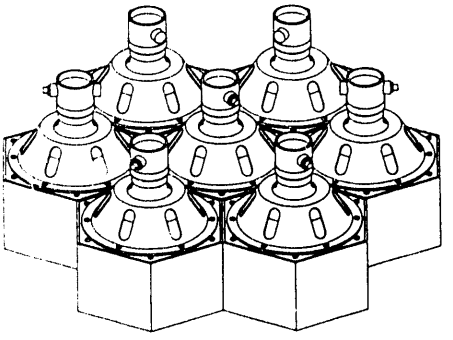

Fig. 2. This figure shows a three dimensional view of a panel assembly which holds seven PMTs.

Controlling U/Th Surface Radioactivity at SNO

LBL-SNO Group, with E. Kongt and Y. Huit

The Sudbury Neutrino Observatory will have the lowest background radioactivity of any place on earth. Achieving a low background requires detector materials with low intrinsic radioactive content *and* correspondingly contamination-free surfaces. The main surface contamination will be the dust that permeates the nickel mine hosting SNO. The local mineral is norite, which contains about 5 ppm of Th. By contrast, the Th in the acrylic vessel holding the D_2O is about 1 ppt, or 5000 times smaller.

All detector components, construction equipment, and personnel must pass along a 2.5 km long tunnel leading from the mine shaft to SNO. The tunnel floor is covered with several inches of mine dust or mud. During the 18-month construction period, workers and car-sized containers will pass through this tunnel into the clean laboratory 10,000 times and 600 times, respectively. Yet, at the end of this period, at most 50 grams of dust may be present in the 2200 m^3 sensitive region of the detector.

LBL has a major role in designing the program to control surface contamination.[1] This involves systems and procedures to prevent dust from entering the laboratory,[2] for purging the air of contamination, and for developing methods to measure particulate on surfaces.

Our R&D on particulate measurement has two objectives; to develop 1) a quantitative technique for measuring dust, sensitive to 0.1 $\mu g/cm^2$, and 2) semi-quantitative tests that are fast and do not require sophisticated equipment.

X-ray fluorescence (XRF) has proven to be an ideal technique for quantitative work (Fig.1). Norite contains 6% Fe and Fe is detectable at the level of 10 ng/cm^2. By using a thin adhesive tape, selected for its low Fe content, to remove the dust from the surface, this sensitivity can be attained in a counting time of 20 min. We are constructing an XRF spectrometer for use in the mine.

The semi-quantitative methods use calibrated samples with which an unknown can be compared. The first of these methods uses surfaces (plastic, glass, acrylic, steel) prepared with known amounts of mine dust from a few tenths to 10 $\mu g/cm^2$. Viewed under oblique light with a 50x field microscope, the amount of dust can be estimated to a factor of 2 or 3. The second method uses a tightly woven white cloth wrapped around a 90 degree edge. This edge is moved along the surface at a constant pressure for 15 cm, concentrating the dust by a factor of 100. Dust levels down to 0.5 $\mu g/cm^2$ can be seen with the unaided eye.

Footnotes and References

† UCB engineering undergraduates, Supported by LBL Engineering Division COOP program.

1. "Establishing a Cleanliness Program and Specifications for SNO," E.D. Hallman and R.G. Stokstad, Report No. SNO-STR-91-009.

2. "Delivering Clean Components to the Cavity," R. G. Stokstad, Ed., Report No. SNO-STR-91-066

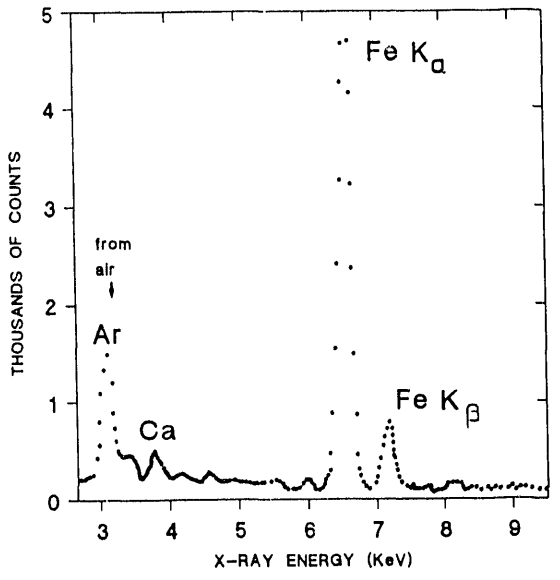

Fig. 1. X-ray fluorescence spectrum for 50 $\mu g/cm^2$ of norite on 7 mg/cm^2 of adhesive tape, obtained in 20 min. counting time. XRF analysis by R. Giauque, Applied Science Division.

An Interactive Photon Tracing Monte Carlo Package for SNO

LBL-SNO Group

We have developed an interactive ray tracing Monte Carlo package for the SNO (Sudbury Neutrino Observatory) detector project. This program runs on a DEC VAXstation platform. SNO is a Cerenkov D_2O detector designed to study neutrinos coming from the sun. The basic detector is made up of a spherical D_2O target (6m in radius) viewed by about 10,000 phototubes. The tubes are mounted on a geodesic structure at a radius of 8.5m. Detailed Monte Carlo information about how photons propagate through the different layers of media making up the detector and the effect of reflection-refraction at the interfacing surfaces is very important in determining the overall detector response and the acceptable level of background radioactivity.

The present program has the following features:

a. Electron and photon showers (based on EGS4[1])

b. Cerenkov light generation

c. Tracing the Cerenkov photons and source particles in realistic geometry, including reflection, refraction, and absorption on all target media/surfaces as well as the phototubes and reflectors.

d. Automated or guided reconstruction of Cerenkov vertices via time fitting routines.

The main interaction with the user is via a mouse-driven single event color display. In the manually guided analysis mode, the experimenter rotates the geodesic sphere and the phototubes interactively until the Cerenkov cone is facing the user directly. The time/cone fitter then takes this as the initial input for least square fitting.

A similar version using the X Window system is currently planned.

Footnotes and References

1. The EGS4 Code System, SLAC-Report-265.

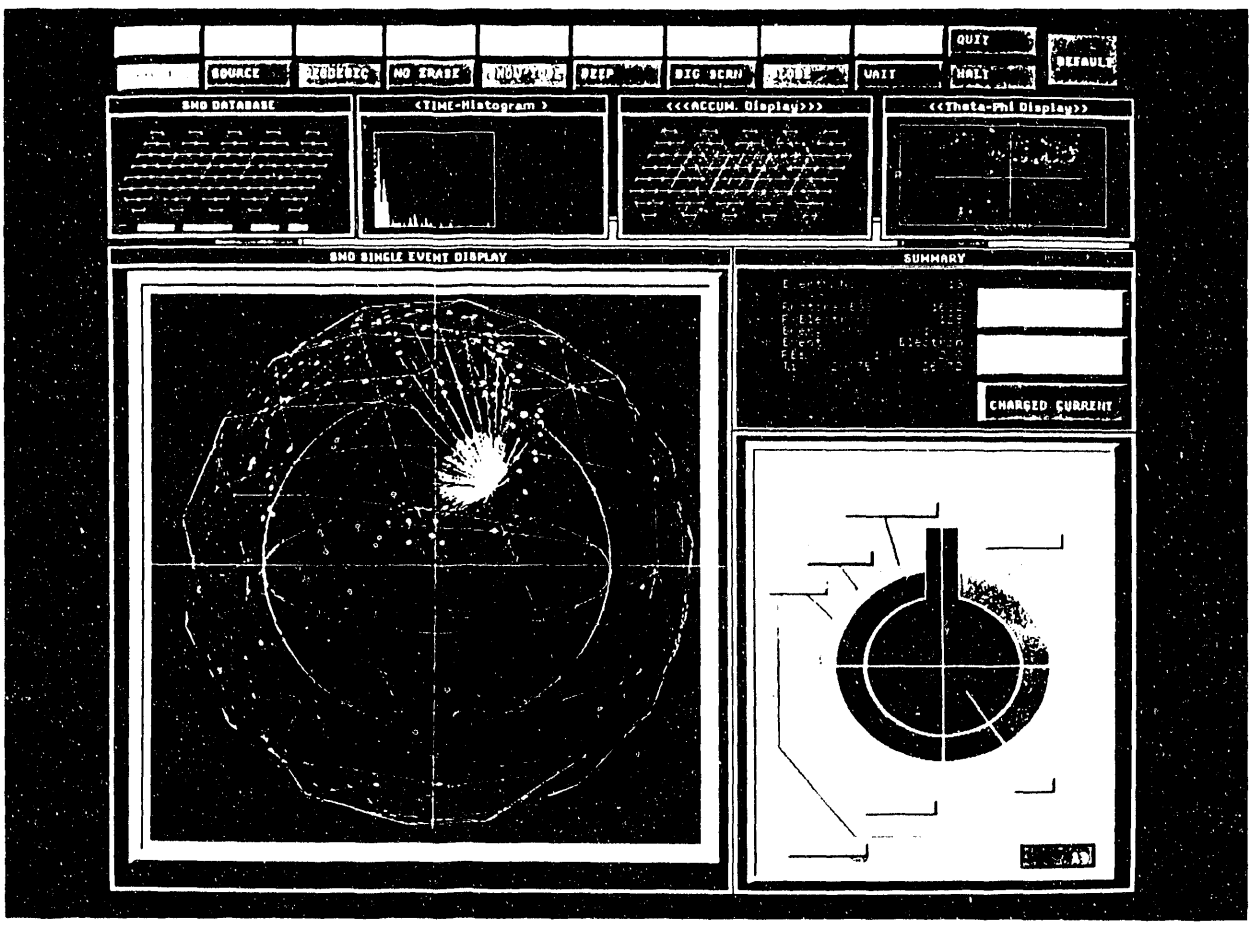

The IsoSpin Laboratory (ISL)

J.Michael Nitschke

After the First International Conference on Radioactive Nuclear Beams[1] (RNB) in Berkeley and the Workshop on the Science of Intense Radioactive Beams[2] hosted by LANL, several important events have occurred on the way towards the construction of a high intensity RNB facility in North America.

An ISL Users Group was formed that has presently over 400 members; the Second International Conference on Radioactive Nuclear Beams[3] convened in Louvain-la-Neuve, Belgium; several workshops were held in conjunction with APS meetings; and the ISL steering committee issued a White Paper[4] outlining the research opportunities with RNBs.

The White Paper addresses three major topics: (1) an overview of RNB science, (2) scientific opportunities with RNBs, and (3) the facility concept. Some highlights of the scientific case for the ISL stand out. Nuclei with extreme N/Z ratios will become available either directly from the ISL or in nuclear reaction induced by RNBs. On the neutron-rich side these nuclei may have neutron skins and neutron halos due to low neutron binding energies, with matter densities in the halo region between that of normal nuclear matter and free nucleons. Such nuclei may help to elucidate the properties of neutron matter. Projectiles with extreme isospin will give access to special nuclear regions, be it the important N=Z sequence from ^{80}Zn to ^{100}Sn, new phase transition regions, new subshells, new regions of stability among the heaviest elements, or new regions of deformation. Special states may become accessible in interactions of nuclei with extreme N/Z ratios. Very neutron rich nuclei may have their fission barriers raised and be able to support higher angular momenta. Regions of hyper deformation, oblate superdeformation, and exotic octupole shapes may be reachable only with radioactive projectiles.

Nuclear reaction studies will benefit from the extended neutron wave functions that may lead to neck formation in fusion reactions, neutron flow phenomena, multinucleon transfer, and cross section enhancements due to high Q-values.

Since the ISL will cover the entire beam energy spectrum from a few keV to ~10MeV/u, astrophysical processes can be explored that occur away from stability under conditions typically encountered in explosive stellar events. An understanding of the nucleosynthesis leading to the heavier elements via rp-, p-, r-, and s-processes requires the determination of such key nuclear parameters as reaction rates, half-lives, masses, and Q_{EC}-values, involving radioactive beams and targets.

In the atomic and material sciences many applications are envisioned based on probing the solid state environment with implanted RNBs.

In the White Paper the ISL Steering Committee makes the recommendation *that the North American nuclear physics community should seriously pursue the construction of a dedicated, flexible, broad range RNB facility that would provide intense beams of nearly all elements up to energies of ~10MeV/u for a program of studies in nuclear structure, low-energy nuclear reactions, astrophysics, and atomic and material science.*

References

1. *Proceedings of the First International Conference on Radioactive Nuclear Beams*, October 16-18, 1989, Berkeley, California, W.D. Myers, J.M. Nitschke, and E.B. Norman, Eds. (World Scientific, Singapore, 1990).

2. *Proceedings of the Workshop on the Science of Intense Radioactive Beams*, Los Alamos National Laboratory, April 10 -12, 1990, Los Alamos, New Mexico, LA-11964-C and UC-413.

3. *Proceedings of the Second International Conference on Radioactive Nuclear Beams*, August 19-21, 1992, Louvain-la-Neuve, Belgium, Th. Delbar, Ed., (Adam Hilger, Bristol, 1991).

4. *The IsoSpin Laboratory. Research Opportunities with Radioactive Nuclear Beams.* Los Alamos Report LALP 91-51, 1991.

Radioactive Beam Intensity Calculations for the ISL

J.M. Nitschke, G.G. Howes and J.I. McIntyre

Of crucial importance for the performance of the proposed IsoSpin Laboratory (ISL) are the intensities of the radioactive nuclear beams (RNB). The intensities published in the ISL White Paper[1] are corrected for ionization and stripping efficiencies and the transmissions through the isotope/isobar separators and the post-accelerator(s); they are, however, *not* corrected for radioactive decay losses because of the difficulties in estimating characteristic diffusion and desorption times for ~90 elements in many different target matrices. We have, therefore, engaged in a program of calculating RNB intensities for different targets and accelerator configurations, and made comparisons to experimental yields obtained at ISOLDE/CERN.[2]

As a starting point, we have taken cross sections calculated with a code developed by Silberberg and Tsao[3] that takes into account fission, spallation, peripheral-, and break-up reactions. Calculated target yields for comparison with ISOLDE data were obtained by multiplying the cross sections with the target thicknesses used in the ISOLDE experiments and the primary (proton) beam intensity. As shown in Fig. 1 for the case of Cs isotopes produced from a UC target, the agreement between calculation and experiment is satisfactory for isotopes near stability (^{133}Cs). However, deviations of several orders of magnitude occur for isotopes with short half-lives. These decay losses are mainly due to four mechanisms: bulk diffusion in the target material, surface desorption, delay in the transfer line to the ion source, and the hold-up time in the ion source itself. For solid targets the ISOLDE group has found that bulk diffusion through the target is the dominating step and that the ratio of observed to measured yield can be expressed by a simple relation between a global diffusion constant, the half-life of the isotope, and a parameter characteristic of the ion source. Using this prescription and an ionization efficiency of ~80% for Cs, a good fit to the measured yields can be obtained. For liquid targets the dominating delay is the surface desorption process.[4] We have verified this observation for targets like liquid La and Pb.

Our goal is to study as many combinations of radioactive species and target matrices as possible, extract the relevant diffusion parameters, and make reliable predictions for the expected beam intensities at the ISL. An understanding of the relevant delay processes will also aid in the development of "fast" targets. In the future contributions from secondary reactions, the decay of parent nuclei, and changes of the primary beam characteristics in the massive target have to be included in the model.

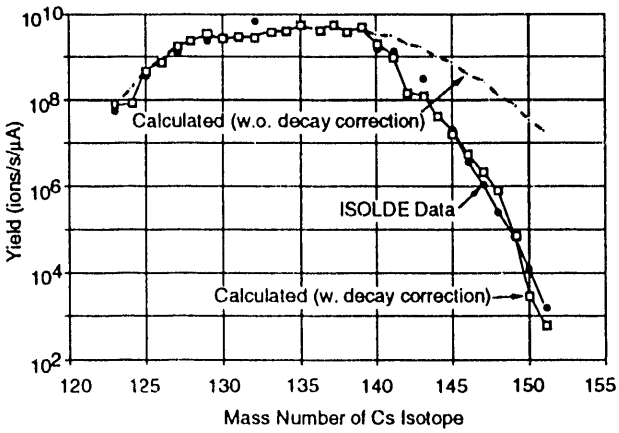

Fig. 1. This figure shows a comparison between the measured yields of Cs isotopes at ISOLDE and the decay-loss-corrected and uncorrected yields calculated as described in the text.

References

1. *The IsoSpin Laboratory. Research Opportunities with Radioactive Nuclear Beams.* Los Alamos Report LALP 91-51, 1991.
2. *ISOLDE User's Guide*, H.J. Kluge, Ed. CERN-86-05.
3. R. Silberberg and C.H. Tsao, Astrophysical Journal, Supplemental Series No. 220(I), **25**, 313 (19730
4. H.L. Ravn, Physics Report **54**, 201, (1979).

Muon Catalyzed Fusion Studies

T. Case, H. Bossy, K.M. Crowe, K. Lou, C. Petitjean*, P. Ackerbauer†, W.H. Breunlich†, M. Fuchs†, S. Fussy†, M. Jeitler†, P. Kammel†, J. Marton†, J. Werner†, J. Zmeskal†, D.V. Balin‡, V.N. Baturin‡, Yu.S. Grigoriev‡, A.I. Ilyin‡, E.M. Maev‡, G.E. Petrov‡, G.G. Semenchuk‡, A.A. Vorobyov‡, P. Baumann§, H. Daniel§, F.J. Hartmann§, P. Hofmann§, R. Huber§, R. Lipowsky§, and P. Wojciechowski§*

Our group has been involved in a long standing collaboration doing basic muon catalyzed fusion (μCF) research at PSI. In the past this collaboration has contributed some of the major results setting limits on this intriguing process and shedding light on the underlying physics.

In the past couple of years our efforts have concentrated on an experiment which directly measures the probability that the μ^- remains bound to the alpha particle from d-t fusion ("sticking")[1] This sticking probability limits the ultimate number of fusions which a single muon can catalyze. This value has been somewhat controversial, with measurements indicating a value significantly less than theory. Our experiment, based on a very high pressure ionization chamber surrounded with thick neutron detectors (see Fig. 1) will attempt to settle this question with final precision. The main data runs were in the fall of 1989 and the fall of 1991.

In between we have developed advanced signal analysis methods and a detailed Monte Carlo code which can answer efficiency and systematic error questions at the percent level. This analysis is nearing completion. Because this experiment uses a triple mixture of hydrogen, deuterium and tritium and it detects both the fusion neutrons as well as charged particle tracks, we have made measurements on many other side reactions and have been able to solve several other μCF puzzles. For instance, we detected a high energy resonance in dμt molecular formation which is an order of magnitude faster than the usual resonance mechanism responsible for the present record of 124 fusions per μ^-. There is also continuing progress in the attempt to make a high temperature target (2000 K) which can confirm the mechanism of these important resonances. This work has been in collaboration with LLNL also.

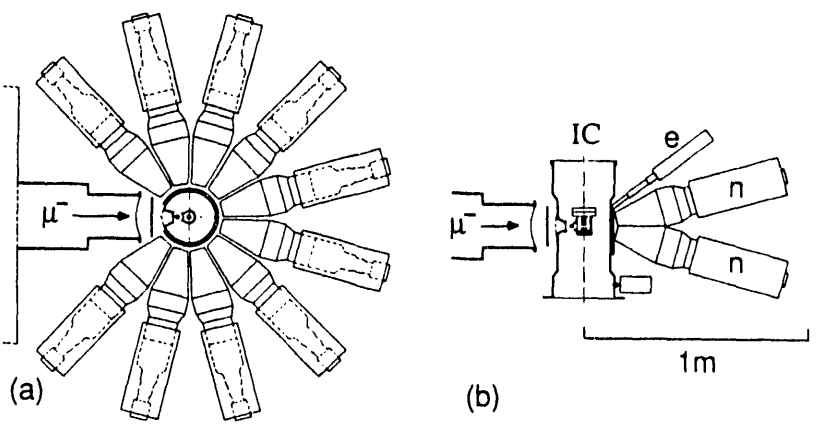

Fig. 1. Experimental arrangement (a) top view; (b) side view. 'IC' is the ionization chamber, the neutron counters are labelled 'n' and the electron counters are labelled 'e'.

Footnotes and References

*Paul Scherrer Institute (PSI), Villigen, Switzerland.
†Institute for Medium Energy Physics (IMEP), Austrian Academy of Sciences, A-1090, Vienna, Austria.
‡Leningrad Nuclear Physics Institute, Gatchina, USSR
§Technical University Munich, Garching, Germany.

[1] C. Petitjean *et al.*, Muon. Cat. Fusion 5/6 (1990/91)261.

Bevalac Experiments

Rayleigh–Taylor–like Surface Instabilities and Nuclear Multifragmentation*

L. G. Moretto, Kin Tso, N. Colonna, and G. J. Wozniak

In the simulated head–on collisions of two nearly symmetric heavy–ions using the Boltzmann–Nordheim–Vlasov (BNV) equation we noticed two interesting features. First, during the collision process a "disk" develops due to the side–squeezing of nuclear matter, whose thickness decreases and diameter increases monotonically with increasing bombarding energy. Second, if the disk becomes sufficiently thin, it breaks up into several fragments of a size commensurate with the thickness of the disk.

At high incompressibility and at 55 MeVu bombarding energy (see Fig. 1), a thick disk forms and some mottling develops at its maximum extension (incipient fragment formation). However, the mottling heals and the disk falls back to a more or less spherical blob. At higher bombarding energy, the disk becomes thinner, with a larger diameter than in the previous case. As the collision progresses, the mottling appears and develops rapidly into a beautiful crown of many fragments of approximately the same size, that slowly separate due to the residual kinetic energy of the disk and their mutual Coulomb repulsion.

The calculations were repeated for lower incompressibility in order to cover the range of nuclear incompressibility currently believed appropriate for nuclear matter. At 55 MeV/u and K = 200 MeV, a thin disk is formed and fragment formation occurs (see Fig. 1), in contrast to the high incompressibility case where fragment formation does not occur as yet. At higher bombarding energies, fragment formation is observed for both values of the incompressibility. Similar calculations have been performed for a range of central impact parameters and entrance–channel mass asymmetries with similar results.

The qualitative features associated with the disk fragmentation suggest immediately that it is caused by surface instabilities. *More precisely, the system escapes from the high surface energy of the disk by breaking up into a number of spherical fragments with less overall surface.* Thus, fragment formation, in this picture depends only on the presence of a surface energy term.

Footnotes and References

*Condensed from Lawrence Berkeley Laboratory preprint LBL–31812

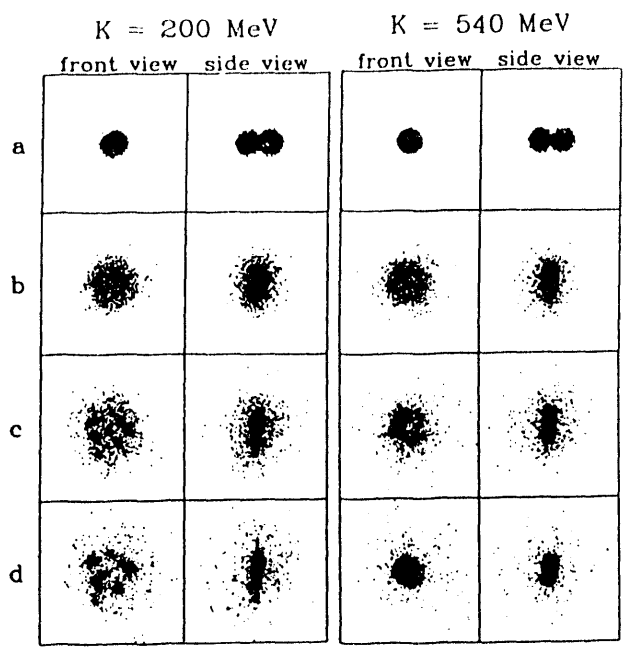

Fig. 1. BNV calculations for a head–on collision (b = 0) of the 55 MeV/u ^{90}Mo + ^{90}Mo reaction at time steps of (a) 20, (b) 60, (c) 120, and (d) 180 fm/c. The front and side–views of the colliding systems are given in columns 1 & 2, respectively for a value of the incompressibility constant, K = 200 MeV. Similar views are shown in columns 3 & 4 for K = 540 MeV.

A Modular Array to Detect Complex Fragments Produced in Intermediate-Energy Reverse-Kinematics Reactions*

W. L. Kehoe[a], A.C. Mignerey[b], A. Moroni[c], I. Iori[c], G. F. Peaslee[d], N. Colonna, K. Hanold, D. R. Bowman[d], L. G. Moretto, M. A. McMahan, J. T. Walton, and G. J. Wozniak

A segmented silicon-silicon-plastic array was constructed for studying complex-fragment production in heavy-ion reactions with incident energies of 35 - 100 MeV/u. The array was designed: (1) to measure the energy, position, and charge of fragments with $1 \leq Z \leq Z_{proj}$; (2) to have high efficiency for detecting fragments produced in reverse-kinematics reactions; (3) to detect events with two or more fragments; and (4) to have a flexible configuration.

Each array telescope consists of a 300 μm Si detector, a 5 mm Si(Li) detector and a 7.6 cm plastic scintillator. The elements of the telescope are held by interconnecting modular packages which allow the telescopes to be close packed about the beam direction. This modular array has been used in several different experimental configurations.

The Si-Si-Pl array has been used to study binary and multi-body decays of hot nuclear systems formed in a number of reverse-kinematics reactions. For 40 MeV/u ^{139}La-induced reactions on four targets, the total charge detected in the array is plotted in Fig. 1 for 2-, 3-, and 4-fold coincidence events. The very asymmetric ^{139}La + ^{12}C reaction forms a warm nuclear system with very little missing charge, presumably in the form of preequilibrium or evaporated light charged particles. These data show that this warm system decays into two or three large fragments, which contain a very large fraction of the total charge present in the entrance channel ($Z_{entrance}$ = 63). For the hotter ^{139}La + ^{27}Al system, more charged particles are emitted and a smaller fraction of the entrance-channel charge is contained in these 2-, 3- and 4-fragment events. For the very hot ^{139}La + ^{51}V, ^{nat}Cu systems, only about 50% of the entrance-channel charge is measured when four fragments are detected. These very hot systems emit several complex fragments and a large number of light charged particles for which the array is not very efficient.

Footnotes and References

*Condensed from Nucl. Instr. and Meth. **A311** (1992) 258

[a]LNS, 26-402, MIT, Cambridge, MA 02139
[b]Univ. of Maryland, College Park, MD 20742
[c]Univ. of Milano, 20133, Milano, Italy
[d]NSCL, MSU, E. Lansing, MI 48824

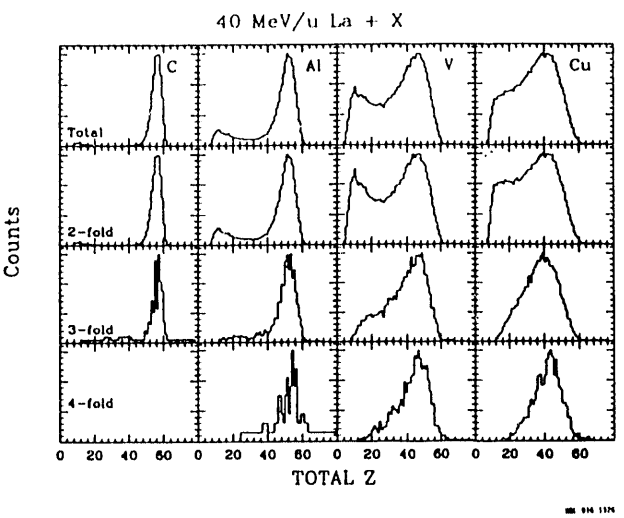

Fig. 1. For 2-, 3-, and 4-fold events, the total charge detected in the array is plotted for the 40 MeV/u ^{139}La + ^{12}C, ^{27}Al, ^{51}V and ^{nat}Cu reactions. Each column and row contain data from a different target and for different n-fold events, respectively.

Decay of Hot Nuclear Systems as a Function of Neutron Multiplicity

D.N. Delis, N. Colonna, Q. Sui, K. Tso, K. Hanold, M. Justice, G.J. Wozniak, L.G. Moretto, B. Libby[+], A. C. Mignerey[+], A. Pantaleo[++], G. D'Erasmo[++], V. Paticchio[++], L. Fiore[++], E.M. Fiore[++], I. Iori[+++], and A. Moroni[+++]

In the past we have been able to correlate, within the incomplete fusion model, the measured source velocity with the excitation energy of the hot nuclear system formed in asymmetric-entrance-channel reactions. The main objective of the present work is to provide, a probe that would determine the excitation energy of the source independent of any assumption made about the reaction mechanism. In our experiment such a probe was the neutron multiplicity.

Complex fragments were detected in a 20-telescope array. Each telescope consisted of a ΔE Si(.30 mm) and a E Si(5 mm). The array was placed at 50 cm from the target and covered an angular range of $\pm 16^0$. The neutrons were detected in 16 NE110 plastic modules (neutron calorimeter) placed behind the array at a distance of 200 cm from the target. The neutron calorimeter covered an angular range in the lab of $\pm 20^0$.

The data collected in this experiment are currently under analysis. Preliminary results have shown that a relationship exists between the total charge detected in the array and the total light output from the neutron calorimeter. Figure 1 shows the total charge for the binary events as a function of the neutron light output. At low values of the neutron light output (0-12 MeVee), one clearly sees the fission peak of Au ($Z_1 + Z_2 = 79$) which is associated with the peripheral reactions (large impact parameters). For larger values of the the neutron light output, the fission peak diminishes in intensity. This is due to the fact that these events arise from more central collisions with more excitation energy.

The five reactions studied in this experiment were 60 MeV/A $^{197}Au + ^{12}C, ^{27}Al, ^{51}V, ^{63}Cu, ^{197}Au$.

Footnotes and References

[+]University of Maryland, College Park, MD

[++]Instituto Nazionale di Fisica Nucleare, Bari, Italy

[+++]Instituto Nazionale di Fisica Nucleare, Milano, Italy

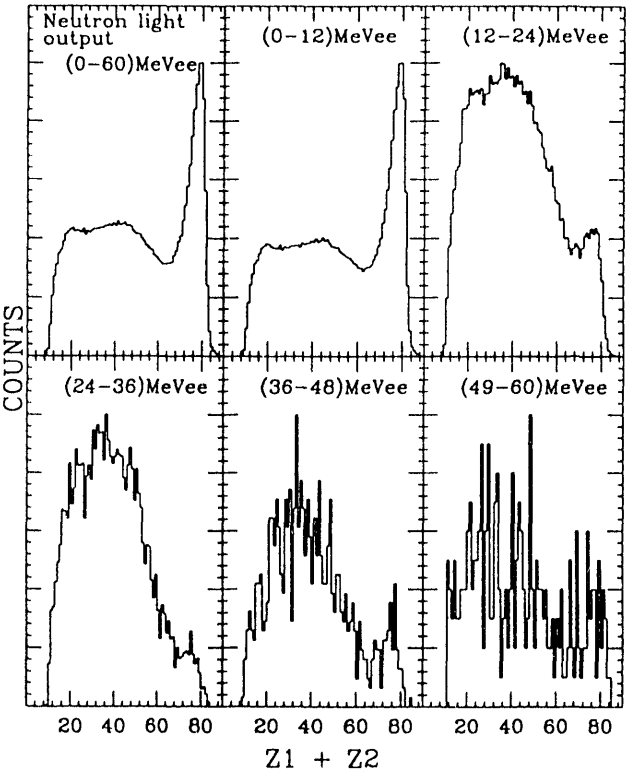

Fig. 1. Total charge detected for binary events for different gates on the neutron light output. The numbers in parentheses indicate the range of each gate. The smaller values correspond to the more peripheral reactions.

Multifragment Disintegration of the ^{129}Xe + ^{197}Au System at E/A = 50 MeV*

D. R. Bowman[a], G. F. Peaslee[a], R. T. de Souza[a] N. Carlin[b], C. K. Gelbke[a], W. G. Gong[a], Y. D. Kim[a], M. A. Lisa[a], W. G. Lynch[a], L. Phair[a], M. B. Tsang[a], C. Williams[a], N. Colonna, K. Hanold, M. A. McMahan, G. J. Wozniak, and L. G. Moretto

To date, very few experiments have been performed with sufficient phase-space coverage to allow the extraction of intermediate-mass-fragment (IMF) multiplicities. Thus it is still uncertain under which conditions multifragment emission becomes a dominant decay channel. In order to search for experimental conditions which produce multifragment final states and to test predictions for different fragment production models, we have measured charged-particle and IMF (Z = 3 - 20) multiplicities for the ^{129}Xe + ^{197}Au reaction at $E_{c.m.}$ = 3.9 GeV.

The ^{129}Xe beam was extracted with an intensity of 10^7 particles/s from the K1200 cyclotron of the National Superconducting Cyclotron Laboratory and impinged upon a 1.05-mg/cm^2 gold target. Reaction products were detected with 171 elements of the Michigan State University Miniball phoswich-detector array which covered polar angles of $16^o \leq \theta \leq 160^o$, corresponding to approximately 87% of 4π. The most forward angles were covered by a 16-element hodoscope, each element of which consisted of two position-sensitive solid-state detectors (0.300 and 5 mm thick) and a 7.6-cm-thick plastic scintillator. This forward hodoscope covered approximately 64% of the solid angle at $2^o \leq \theta \leq 16^o$.

Experimental multiplicity distributions (uncorrected for detector acceptance) are shown Fig. 1. The upper panel shows the probability distribution of N_C, the detected total charged-particle multiplicity. The lower panel shows probability distributions of N_{IMF}, the number of detected IMFs, for various gates on N_C. The average number of detected IMFs increases with N_C. For the most central gate, $N_C \geq 33$, it reaches a value of $\langle N_{IMF} \rangle$ = 6.5, which is the largest value yet observed in any nuclear collision. Events with N_{IMF} up to 14 are observed.

Footnotes and References

*Condensed from Phys. Rev. Lett. 67 (1992) 1527

[a]NSCL, MSU, E. Lansing, MI 48824

[b]Instituto de Fisica, Univ. de Sao Paulo, Sao Paulo, Brazil

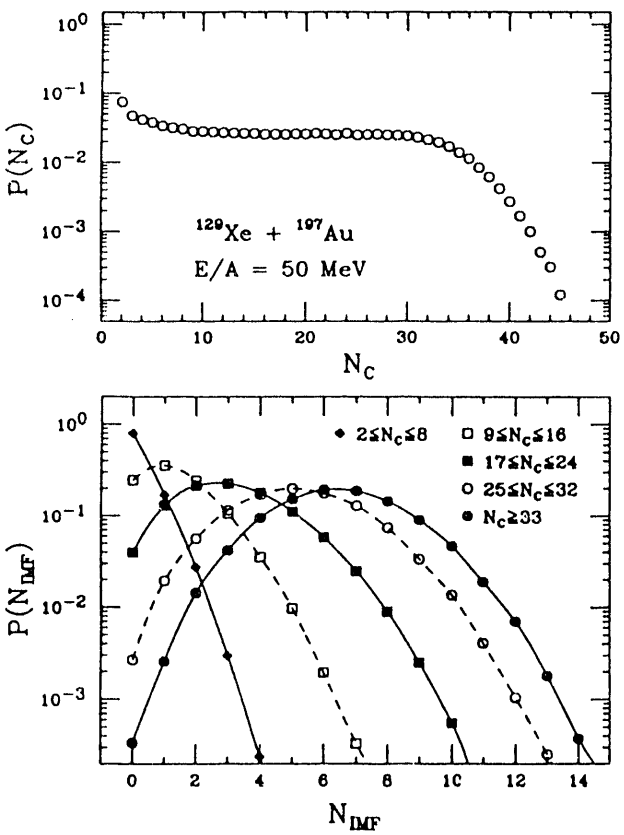

Fig. 1. Upper panel: Measured charged-particle multiplicity distribution, N_C, for the 50 MeV/u ^{129}Xe + ^{197}Au. Lower panel: Measured IMF multiplicity distributions for the indicted gates on N_C.

Sources and Characteristics of Complex Fragments in La-induced Reactions*

P. Roussel-Chomaz[a], Y. Blumenfeld[b], R. Charity[c], M. Colonna[d], N. Colonna, B. Libby[e], K. Hanold, L. G. Moretto, G. F. Peaslee[f], and G. J. Wozniak

To compare our experimental data on complex fragment emission with model predictions, we have utilized a self-consistent transport equation approach (Blotzmann-Nordheim-Vlasov). The two fundamental ingredients that enter the BNV equation are the self-consistent mean field and the in-medium nucleon-nucleon cross section σ_{NN}. In the code we used, the mean field is given by the Coulomb interaction between protons plus a nuclear density dependent part of Skyrme type with parameters chosen to get a nuclear compressibility value K = 200 MeV. The value of σ_{NN} was assumed to be the free nucleon-nucleon cross section with an energy dependence parametrized from experimental data.

An example of the time evolution of the collision between ^{139}La and ^{27}Al nuclei at 55 MeV/u is presented in Fig. 1. For the most central collisions, "complete fusion" occurs, accompanied by pre equilibrium emission. At the end of the collisions only one heavy residue exists which is very elongated and will probably undergo fission (b = 3 fm). For intermediate impact parameters, incomplete fusion occurs, where the target breaks into two pieces and part of the target is absorbed by the projectile. For larger impact parameters, the two incident nuclei merge together, but two centers can always be distinguished and, after a time depending on the impact parameter, the system separates into two fragments close in mass to the target and the projectile. Although this process is again accompanied by pre equilibrium emission its features are reminiscent of deep inelastic collisions as they are observed at low incident energies. For heavier systems e.g. ^{139}La + ^{51}V and ^{139}La + ^{nat}Cu at 55 MeV/u, these BNV calculations show the presence of a participant zone in addition to the projectile-like and target-like remnants for impact parameters between 5 and 7 fm, and therefore indicate the occurrence of participant-spectator type reactions.

Footnotes and References

*Condensed from LBL-30294

[a]SEPN, CEN Saclay, 91191 Gif-sur-Yvette,France
[b]Institut de Physique Nucleaire, Orsay, France
[c]Washington Univ., St. Louis, MO 63130
[d]INFN, L.N.S., 95129 Catania, Italy
[e]Univ. of Maryland, College Park, MD 20742
[f]NSCL, MSU, E. Lansing, MI 48824

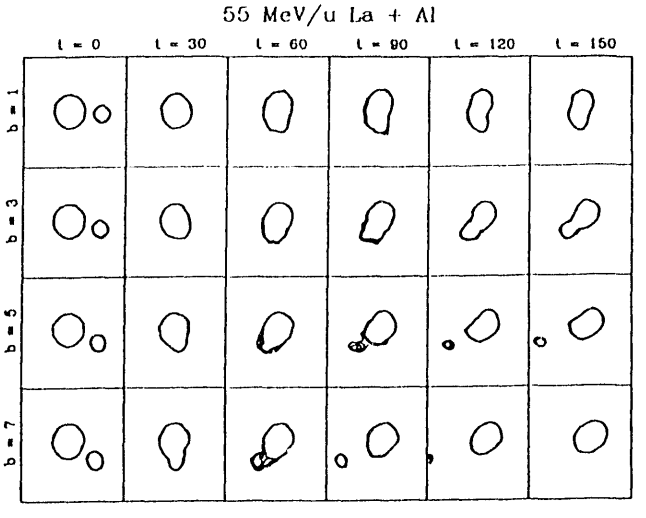

Fig. 1. ^{129}La + ^{27}Al collisions at 55 MeV/u calculated with the BNV equation for several impact parameters (expressed in fm). The initial velocity axis (z) is horizontal and the impact parameter axis (x) is vertical. The times are expressed in fm/c. The lines represent equal density level in the (x,z) plane.

Interaction Cross Section of ^{11}Li + p and ^{11}Li + d Reaction

K. Yoshida, T. Kobayashi,* T. Suzuki,* I. Tanihata,* S. Shimoura,† K. Sugimoto,‡ K. Matsuta, T. Minamisono,‡ O. Testard,§ W. Christie, D. Olson, and H. Wieman*

Here we report the new measurement of interaction cross sections (σ_I) for ^{11}Li + p and ^{11}Li + d reactions at 790 *A* MeV. The matter density distribution of ^{11}Li is determined from these data combined with σ_I for Be, C, Al targets at same energy.[1]

Liquid proton and deuteron targets of 10 cm thickness were used at Berkeley BEVALAC. The targets were operated at the temperature below the boiling points to avoid bubbling. The σ_I were measured by a transmission method using HISS magnetic spectrometer system; the same system used for previous measurements.[1] The interaction cross section of ^{11}Li + p and ^{11}Li + d reactions have been determined to be (276 ± 10) mb and (465 ± 5) mb, respectively.

Nuclear interaction radii determined from σ_I of reaction between neutron rich nuclei and nuclear targets (Be, C, and Al) show the separability of the interaction radii of a projectile and a target. However, if we use p+ p total cross section and d+ d reaction cross section, the σ_I's expected are 456 mb and 567 mb, for ^{11}Li + p and ^{11}Li + d reactions, respectively, and they are much larger than what observed. The separability is thus broken in these reactions. Therefore if we combine these data, it is possible to determine the density distribution in ^{11}Li.

The Glauber type model of the interaction cross section is employed to determine the density distribution of ^{11}Li. It is assumed that the density distribution of ^{11}Li has core and a halo. The density distribution of the core is assumed to have harmonic oscillator density. The halo nucleons are assumed to be orbiting in the potential with the same shape as the core distribution. The density of the halo, which is calculated as the amplitude of the wave function, is added to the core density to form a ^{11}Li density distribution. In this density distribution, the width parameter of the harmonic oscillator, the number of halo nucleon, and the binding energy of the orbital for the halo nucleon are used as parameters for fitting the σ_I's. The density distributions that give the best fit are shown in Fig. 1. As seen in the figure, a long extended tail is necessary to reproduce the cross sections consistently.

Footnotes and References

*RIKEN, Wako, Saitama 351-01, Japan
†Univ. of Tokyo, Hongo, Tokyo 113, Japan
‡Osaka Univ., Toyonaka, Osaka 560, Japan
§Saclay, 91191 GIF-sur-YVETTE, Cedex, France

1. I.Tanihata et al., Phys. Rev. Lett. 55 (1985) 2676; I.Tanihata et al., Phys. Lett. B206 (1988) 592.

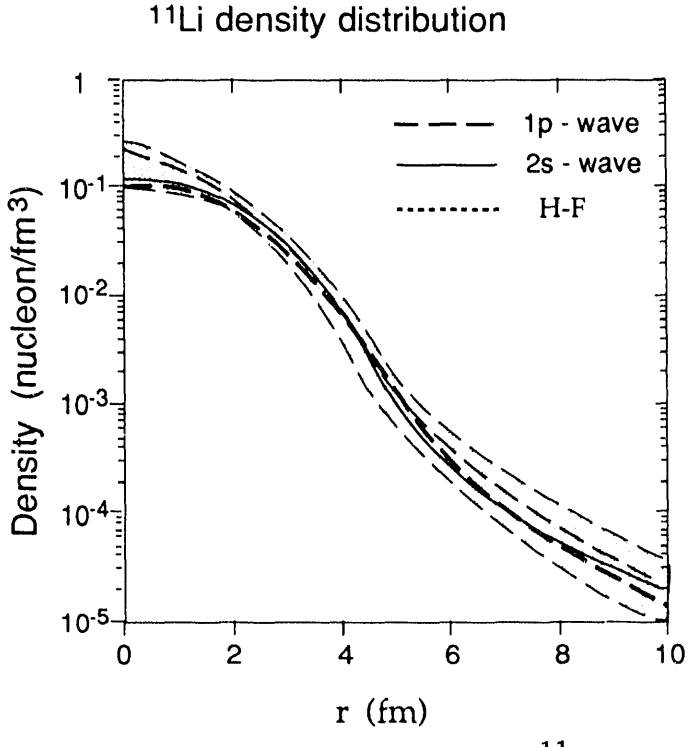

Fig. 1. Nucleon density distribution of ^{11}Li determined from the interaction cross sections. Selection of the orbital makes little difference in the results.

Momentum Correlation of Halo Neutrons in ^{11}Li

I. Tanihata, T. Kobayashi,* S. Shimoura,† T. Suzuki,* K. Yoshida,* K. Matsuta, T. Minamisono,‡ K. Sugimoto,‡ O. Testard,§ W. Müller, D. Olson, and H. Wieman*

The transverse momentum (P_t) distribution of ^{9}Li fragment from 800*A* MeV ^{11}Li on p, d, and C targets are measured with high statistics at the LBL Bevalac. Improvements of the intensity of primary ^{18}O beam and the beam optics enabled us to use about 300 ^{11}Li per pulse. The experimental system is essentially the same one as already reported in previous publications except the target system for liquid hydrogen and deuterium.[1,2] The thickness of the target was about 12 cm.

The widths of ^{9}Li and neutron fragment distribution were used to deduce the correlation term between two halo neutrons. The momentum balance at the fragmentation of ^{11}Li->^{9}Li+n+n gives

$$\langle P_9^2 \rangle = \langle (P_1+P_2)^2 \rangle = 2\langle P_1^2 \rangle + 2\langle P_1 \cdot P_2 \rangle \quad (1)$$

where P_9 is the internal momentum of ^{9}Li and P_1 and P_2 are those of neutrons. It was found that the correlation term $\langle P_1 \cdot P_2 \rangle$ has a large positive value (300 ± 43) (MeV/c)^2. This suggests that these neutrons are moving in same direction on an average. It presents quite a contrast to normal nucleon correlations, in which the correlation has negative value. Present analysis, however, depends on the simple qualitative reaction model. Therefore we need a detailed realistic reaction model to confirm this correlation. Also we need high statistic data of the neutron distribution at high energies because they were measured only at a low energy (30 *A* MeV) where final state interactions may be important.

This work is supported by the US Department of Energy under the contract No. DE-AC03-76SF0098, by the LBL-RIKEN collaboration program, and by the Japan-US Cooperative Program from the Japan Society for the Promotion of Science.

Footnotes and References

*RIKEN, Wako, Saitama 351-01, Japan
†Univ. of Tokyo, Hongo, Tokyo 113, Japan
‡Osaka Univ., Toyonaka, Osaka 560, Japan
§Saclay, 91191 GIF-sur-YVETTE, Cedex, France

1. I. Tanihata, T. Kobayashi, O. Yamakawa, S. Shimoura, K. Ekuni, K. Sugimoto, N. Takahashi, T. Shimoda, and H. Sato, *Physics Letters* B **206** (1988) 592.

2. T. Kobayashi, O. Yamakawa, K, Omata, K. Sugimoto, T. Shimoda, N. Takahashi, and I. Tanihata, *Phys. Rev. Letters* **60** (1988) 2599.

Two-Pion Correlations and Multiplicity Effects in La on La Collisions*

H. Bossy, J. A. Bistirlich, R. R. Bossingham, A. D. Chacon, K. M. Crowe, M. Justice, J. O. Rasmussen, A. A. Shihab-Eldin, M. A. Stoyer, and K. D. Wyatt

We studied Bose-Einstein correlations of negative pions in heavy ion collisions for the reaction ^{139}La +^{nat} La $\rightarrow 2\pi^- + X$ at 1.26 GeV/nucleon at two acceptances, centered at laboratory observation angles of approximately 0° and 45° with respect to the beam axis. The spectrometer was described in Ref[1] except for addition of a scintillation counter array downstream of the target. This array was used to sample the charged particle multiplicity of each event and hence distinguish between peripheral and central collisions. Including results from previous experiments, space-time dimensions of the pion source are now available for mass-symmetric collisions in the mass range of $A = 40$ to 139. As can be seen in Fig. 1 an oblateness of the source region generally persists for all systems, although La + La central collisions viewed near 45° in the lab. (90° in the center of mass) are spherical. The perpendicular radius $R_\perp$ is never less than 4 fm, regardless of the centrality of the La + La collision. Furthermore, $R_\perp$ seems independent of the mass of the collision system.

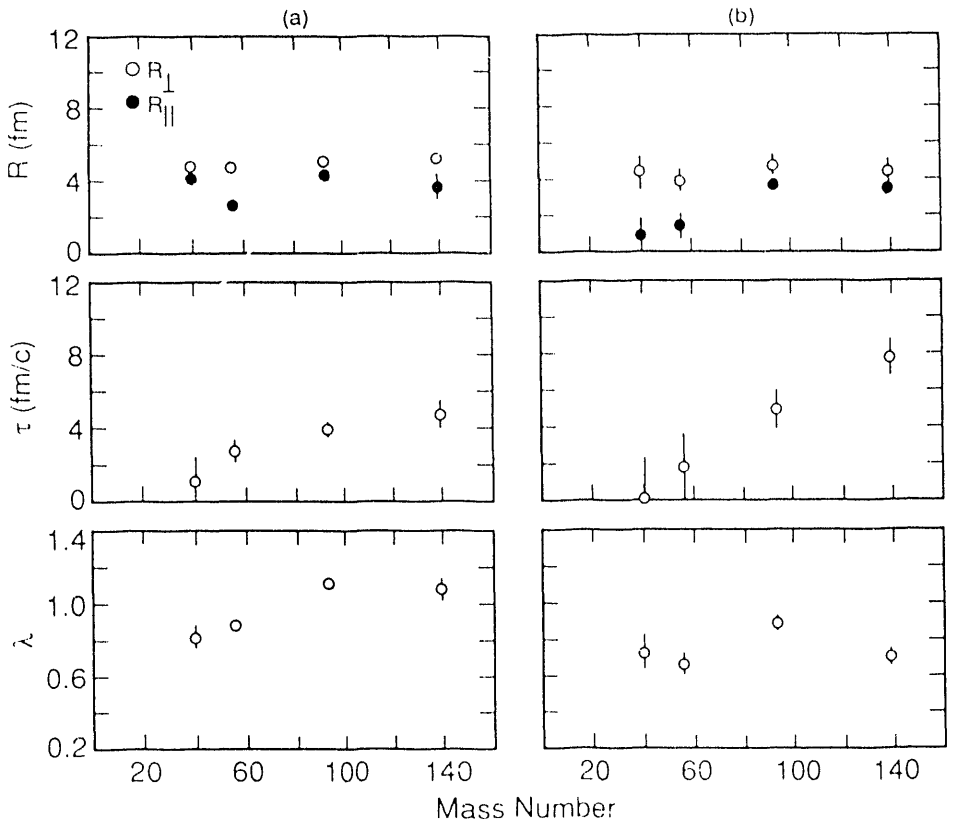

Fig. 1 Gaussian source shape parameters as a function of the mass number of the projectile (= target) for (a) 0° and (b) 45° measurements.

Footnotes and References

*to be submitted to *Phys. Rev. C*

[1] A. D. Chacon *et al.*, *Phys. Rev. C* **43**, 2670 (1991).

Astrophysically Important Fragmentation Cross Sections*

Craig E. Tull, the Transport Collaboration

The Transport Collaboration is an international collaboration concentrating on the interpretation of the heavy ion component of the Galactic Cosmic Ray (GCR) spectrum measured at Earth. We have conducted an experiment at the HISS beamline at the Bevatron to measure the elemental and isotopic production cross sections from the fragmentation of relativistic heavy ions on Hydrogen.

The heavy ion component of the GCR detected at the Earth's upper atmosphere has traveled through a significant thickness of interstellar material (mostly Hydrogen and Helium) since its generation at some source object (such as a Wolf-Rayet Star) within our galaxy. In order to extrapolate back to the isotopic composition of GCRs at their source, we need fragmentation cross sections of many systems over a wide energy range.

Currently, the most common method of predicting these fragmentation probabilities is to use a semi-empirical code such as that of Silberberg & Tsao[1] for those cross sections that have not been measured in experiment. However, these type of cross section codes have been notoriously unreliable for predictions of reactions outside a limited range of initial conditions.

We have conducted measurements of the elemental and isotopic production cross sections from the fragmentation of 20 different beam-energy combinations on a liquid hydrogen target (see Table for a list of systems).

For each beam-energy system, we have measured fragments with charge and mass resolutions of $\Delta Z = 0.2$ e and $\Delta A = 0.2$ u for all isotopes with $Z_f \geq Z_b/3$ and with production cross sections ≥ 5 millibarns.

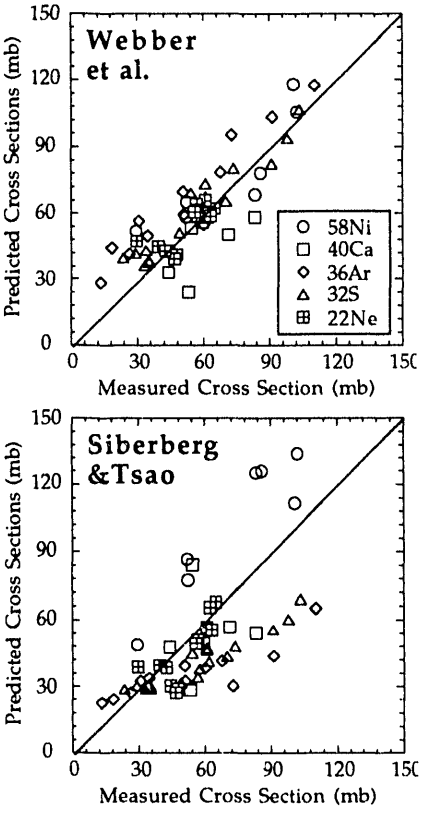

Our preliminary cross sections indicate that the parametric model of Webber, et al[2] is a better predictor of our measured cross sections than is the Silberberg & Tsao semi-empirical model.

The included figures show measured elemental production cross sections for ten of our twenty beam-energy combinations compared to the predictions of Webber's parametric model (upper plot) and Silberberg & Tsao's semi-empirical model (lower plot). The predictions of Webber's model are more highly correlated with our experimental data than are the Silberberg & Tsao values.

---

* Condensed from contributions to the 22nd International Cosmic Ray Conference, Dublin, Ireland, (1991).

[1] R. Silberberg & C. H. Tsao. Phys. Reports, 191(6): 351-408, (1990).

[2] W.R. Webber, J.C. Kish, & D.A. Schrier, Phys. Rev. C41: 520,533,547,556 (1990).

Beam	^{4}He	^{22}Ne	^{26}Mg	^{32}S	^{36}Ar	^{40}Ar	^{40}Ca	^{52}Cr	^{56}Fe	^{58}Ni
Energy	400	400	400	400	400	393	400	400	400	400
(MeV/A)	600	600	600	600		600				800
		910		800	800		800			

NMR on Projectile Fragment ^{43}Ti

K. Matsuta, A. Ozawa, Y. Nojiri,† T. Minamisono,† M. Fukuda,† S. Momota,†
T. Ohtsubo,† S. Fukuda,† K. Sugimoto,† I. Tanihata,‡ K. Yoshida,‡ K. Omata,§
J.R. Alonso, G.F. Krebs and T.J.M. Symons

Nuclear Magnetic Resonance (NMR) has been observed on beta-emitting ^{43}Ti produced through projectile fragmentation process to investigate nuclear structure of mirror nuclei and reaction mechanism of the process.

The present experimental method is similar to the previous measurement of fragment polarization[1]. A 260(480) mg/cm^2 thick C(Au) target was bombarded with a ^{46}Ti primary beam at an effective energy of (108 ± 12) *A* MeV. The fragment ^{43}Ti produced in the target was then purified by a fragment separator set at B44 in the Bevatron and implanted into a cooled Pt foil. The polarized ^{43}Ti nuclei were obtained by selecting deflection angle and fragment momentum.

The production cross section observed for the ^{43}Ti with Au target was significantly smaller than that with C target. The target mass dependence of the cross section cannot be reproduced by simple fragmentation models like Abrasion-Ablation model, where the production cross section increases with the target mass. The present result suggests that the electromagnetic dissociation of the produced ^{43}Ti during the collision may play an important role in fragment production.

The fragment polarization of ^{43}Ti produced from ^{46}Ti on C collision showed a reversed tendency in its momentum dependence compared with the previous results[1] on the fragment polarization of ^{39}Ca and ^{37}K produced through ^{40}Ca on Au collision. So, it is suggested that the contribution from far-side collision is the main component in the case of light target like C.

NMR effects on the ^{43}Ti nucleus were observed through the beta-decay asymmetry as a function of rf frequency at an external magnetic field H_0= 6.878 kOe. As shown in the figure, we found a resonance at the frequency f= (1.27 ± 0.03) MHz. From the observed resonance frequency, the magnetic moment of ^{43}Ti was deduced to be $|\mu|$= (0.85 ± 0.02) μ_n. The observed magnetic moment significantly differs from the single particle value 1.91 μ_n, showing a strong effect resulted from meson exchange currents and configuration mixing. The isoscalar moment of the mass A= 43 mirror pair deduced from the sum of the measured magnetic moment of ^{43}Ti and the known moment of ^{43}Sc, however, was in agreement with the single particle value. Thus, the effects from meson exchange currents and/or configuration mixing are of the isovector type.

The spin expectation value (0.29 ± 6) deduced from the sum moment vividly shows the difference from the single particle value 0.5. A certain simple shell-model calculation explained the magnetic moment fairly well, but failed to reproduce the spin expectation value correctly.

Footnotes and References

† Osaka Univ., Toyonaka, Osaka 560, Japan
‡ RIKEN, Wako, Saitama 351-01, Japan
§ INS, The Univ. of Tokyo, Tanashi, Tokyo 188, Japan

1. LBL-30798, p. 165

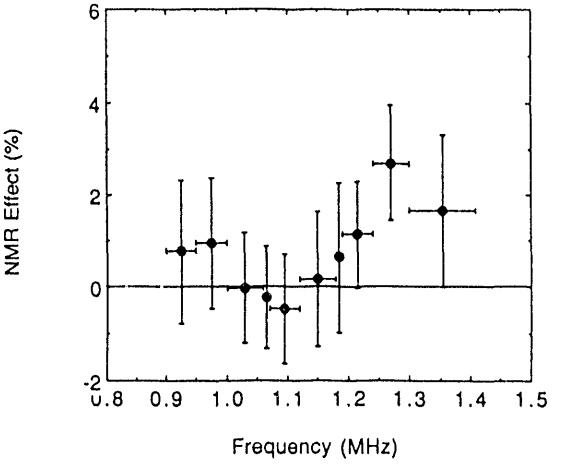

Fig. 1. NMR spectrum of ^{43}Ti

Excitation curve for pd/pp dielectron production

C. Naudet, S. Beedoe*, M. Bougteb†, J. Carroll*, L. Heibronn, T. Hallman*, H. Huang, G. Igo*, P. Kirk‡, G. Krebs, L. Madansky§, F. Manso†, H. Matis, D. Miller**, J. Miller, J. Porter, G. Roche†, L. Schroeder, P. Seidl, W.K. Wilson, Z.F. Wang‡, R. Welsh§, and A. Yegneswaran††

The study of low-mass electron-positron pairs ($0.2 < M < 1.0$ GeV/c^2) in proton-proton and proton-deuteron collisions has been of considerable theoretical and experimental interest. The DLS collaboration has performed a series of dielectron measurements from Dec 1986 until Sept. 91 in an effort to to characterize dielectron production.[1] Although theoretical calculations have been performed and compared with the DLS data in the hopes of understanding the dominate mechanism of dielectron production; large ambiguity still exists in the relative contributions of bremsstrahlung, Δ and η Dalitz decay and $\pi^+\pi^-$ annihilation.[2]. To help disentangle the relative contributions of the various processes the DLS has performed a series of dielectron measurements in pp and pd collisions. This will allow an estimate of the relative contributions of the sources in proton-neutron and proton-proton dielectron production.

The dielectron production in pp and pd collisions was measured at four different values of kinetic beam energies. The yield above an invariant mass of 200 MeV/c was then integrated to obtain a total yield for both the pp and pd collisions. The ratio of pd to pp total yields at four kinetic beam energies is shown in Figure 1 (squares). At the highest kinetic beam energy measured (5 GeV) the dielectron pd/pp ratio has a value of 1.67, much lower than the predicted value of 10 for a Bremsstrahlung dominate source and even less than 3 the prediction for a hadronic dielectron source. As the beam energy drops the ratio gradually increases until at 1.6 GeV beam energy a large enhancement is seen. The additional data (crosses) shows the ratio of the $\pi^0 0$ (dalitz decay) electron pairs which are a smooth function without any enhancement at 1.6 GeV, illustrating that systematics are an unlikely source for the enhancement. The large enhancement in the pd/pp dielectron pair excitation curve at 1.6 GeV was not predicted and we hope will lead us to a deeper understanding of the primary source of dielectron production.

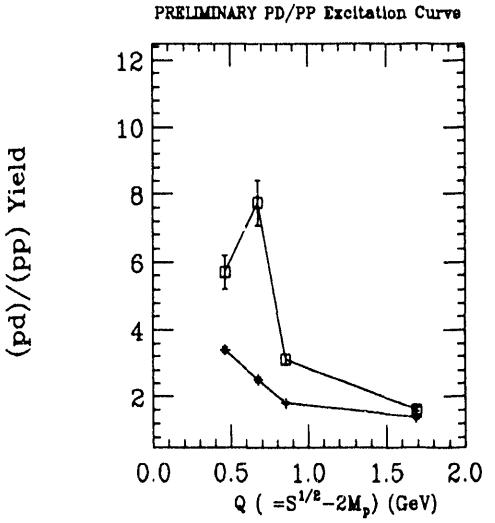

Figure 1: The excitation curve for the pd/pp dielectron production.

Footnotes and References

*Department of Physics, University of California at Los Angeles, Los Angeles, CA 90024

†University of Clermont, Aubiere, France

‡Louisiana State University, Baton Rouge, LA 70803.

§Department of Physics, The Johns Hopkins University, Baltimore, MD 21218.

**Department of Physics, Northwestern University, Evanston IL 60201.

††CEBAF, Newport News, VA 23606.

[1] G. Roche, et. al. Phys. Rev. Lett. 61, 1069 (1988). C. Naudet et. al. Phys. Rev. Lett. 62, 2652 (1989).

[2] Gy. Wolf et. al. Proceedings of the 4Th Journees des Theoriciens at Saturne, Nov 22-23,1990

Dilepton Invariant Mass Spectra Produced In p+p Collisions

W.K. Wilson, S. Beedoe, M. Bougteb, J. Carroll, T. Hallman, L. Heilbronn, H. Huang, G. Igo, P. Kirk, G. Krebs, F. Manso, H. Matis, J. Miller, C. Naudet, J. Porter, G. Roche, L. Schroeder, P Seidl, and R. Welsh

During September of 1991, the Dilepton Spectrometer (DLS) was used to investigate p+p and p+D collisions at 1.0, 1.6, and 2.1 GeV beam kinetic energy. These data were measured as part of our ongoing program to study the production of electron-positron pairs in elementary collisions. This report will focus on the results of a preliminary analysis of the p+p collisions; the relationship between the p+p data and p+D data will be presented in another report.[1]

Electron-positron pairs are produced through the decay of massive virtual gamma rays. The production of gamma rays with masses up to several hundred MeV in collisions at Bevalac energies was established by the DLS collaboration in 1988.[2] The original motivation of this study was the possibility of using virtual gamma rays as a penetrating probe of the early stages of nucleus-nucleus collisions.[3] However, comparison of the initial DLS p+nucleus[4] and nucleus+nucleus[5] data with the theoretical predictions current at the time failed to produce a clear picture of the basic sources of virtual gamma rays in these complex collisions. The DLS group has therefore embarked on a study of p+p and p+D collisions in order to shed light on the elementary processes leading to dilepton production.

The gamma rays that decay into electron-positron pairs can be produced in three different ways: radiation of charges accelerated in the collision (bremsstrahlung), π-π annhillation, and the decay of unstable particles such as the η and the Δ resonance. Simple p+p collisions allow one to untangle the contributions from these sources if measurements are made immediately below and above the absolute energy threshold for a given process. For example, at 1.0 GeV p kinetic energy one is above the Δ production threshold, while at 1.6 GeV one is also above the η and the two π production thresholds.

Fig. 1 shows the preliminary invariant mass spectra of dileptons observed in 1.0, 1.6, and 2.1 GeV p+p reactions. The combinatoric background has been removed, and the error bars include only statistical uncertainties. Note that the slope of the yield near 300 MeV changes dramatically as the threshold for η and two π production is crossed.

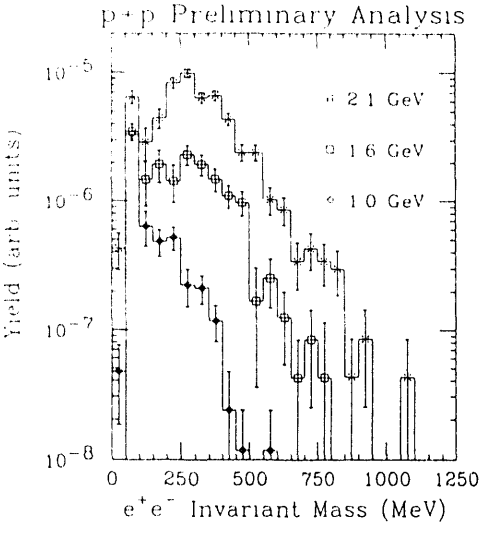

Fig. 1. This figure shows dilepton yield as a function of invariant mass for three different beam kinetic energies.

We are currently evaluating simulations of the DLS response to various sources of dileptons. These simulations, along with a more complete analysis of the result depicted in fig. 1, should provide the understanding of basic dilepton production in p+p collisions needed to interpret our nucleus-nucleus data.

Footnotes and References

[1] See the contribution by C. Naudet et al. in this volume.

[2] G. Roche et al., *Phys. Rev. Lett.* **61**, 1069 (1988).

[3] C. Gale and J. Kapusta *Phys. Rev. C* **35**, 2107 (1987).

[4] C. Naudet et al. *Phys. Rev. Lett.* **62**, 2652 (1989).

[5] G. Roche et al. *Phys. Lett. B* **226**, 228 (1989).

Performance of the EOS TPC

EOS Collaboration

The EOS TPC is now completely instrumented, the construction project has been officially finished. The first experimental run has been completed. We selected the systems 800 MeV/n Ne + NaF, Nb, and Au, for which there is a large body of existing inclusive data for comparison. Several thousand central events were taken for these systems and the data are currently under analysis. Prior to the first experimental run, we had test runs to optimize the trigger, to test the electronics and acquisition system, and to study the response of the TPC to highly ionizing particles (gold).

Before and after the experimental run the laser calibration system was operated. This performed two functions; it allowed testing to take place prior to the delivery of experimental beams and an analysis of the performance of the TPC. Preliminary analysis of the data taken from the laser calibration runs indicates that the drift velocity, positional resolution, and field distortions have magnitudes comparable to that expected from the simulations.

The off-line analysis chain has been completely integrated in a single shell which interfaces with the user through the popular PAW package. This analysis chain includes gain correction, distortion correction, hit reconstruction, track reconstruction, and particle identification. The user is free to add analysis modules to handle any physics analysis of interest. Fig. 1 displays a top view of an analyzed TPC event.

The EOS TPC is the first pad-readout TPC to successfully perform particle identification through dE/dx. Fig. 2 displays a scatter plot which shows the bands of protons, deuterons, alphas, and other species up to beam particles (neon).

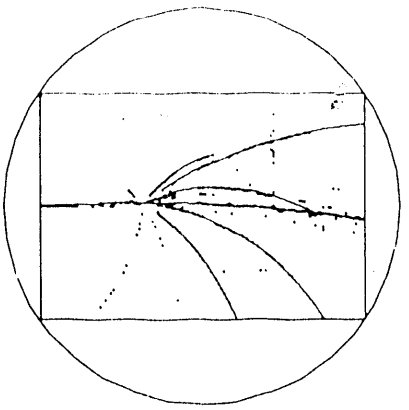

Fig. 1. This figure displays the results of a first attempt to track data from an event in which the interaction occurred between an 800 MeV/n Ne beam particle and an argon nucleus of the TPC gas. The small crosses correspond to reconstructed hit centroids while the thin lines correspond to found tracks. The large rectangle indicates the active region of the EOS TPC and the circle indicates the pole face of the HISS dipole.

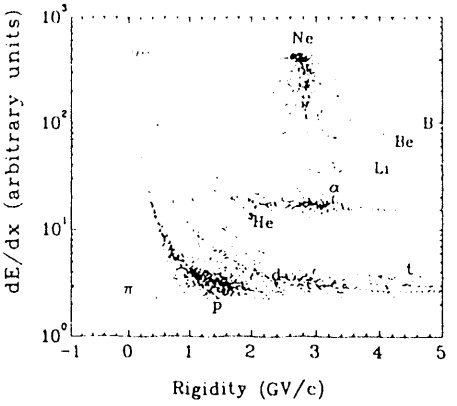

Fig. 2. Scatter plot of ionization density (dE/dx) against rigidity. Each point corresponds to a single track. The data are from a set of 350 reactions of 800 MeV/n Ne + NaF. Superimposed on this scatter plot are dotted lines which correspond to the predicted curves for several particle species.

Proton-like Production Cross Section from 0.8 GeV/n La on La Collisions

J. Bistirlich, R. Bossingham, H. Bossy, A. Chacon, T. Case,
K. Crowe, Y. Dardenne, W. McHarris, J. Rasmussen, M. Stoyer

There exist discrepancies between experimental results[1] and theoretical calculations[2] (Fig.1). for the p-like production cross section from 0.8 GeV/n La on La collisions. The theoretical calculations were for six models, with the results all in general agreement with each other, but not with the experimental result. Since these models have varied assumptions, it was thought that the problem might lie in the experimental results. For this reason the experiment was repeated on a different spectrometer (Janus, Beam 30).

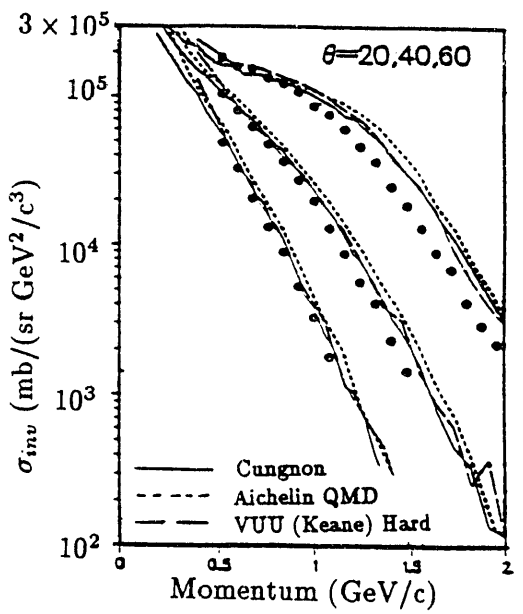

Fig. 1. The invariant production cross section of p-like particles from 0.8 GeV/n La on La collisions and three models, at three angles. Notice the large discrepancy at 20 degrees.

Figure 1 shows the invariant p-like (p-like refers to H, ^{2}H, ^{3}H, ^{3}He, and ^{4}He) cross section as a function of momentum per nucleon at three angles. The invariant p-like cross-section is defined as

$$\sigma_{inv} = \sum_{i=1}^{n} Z_i \, E_i \frac{d^3\sigma_i}{d^3k_i}, \qquad (1)$$

where Z_i is the charge of the particle, while E_i and k_i are the energy and momentum per nucleon, respectively.

The results so far obtained can be seen in Fig. 2. This figure compares the 40° proton cross-sections with the previous experimental results. The 40° data seem to agree well with the previous experimental results; however, there is no disagreement at this angle between experiment and theory. Obtaining the 20° measurement is a bit more complicated as it involves reverse kinematics; this analysis is in progress.

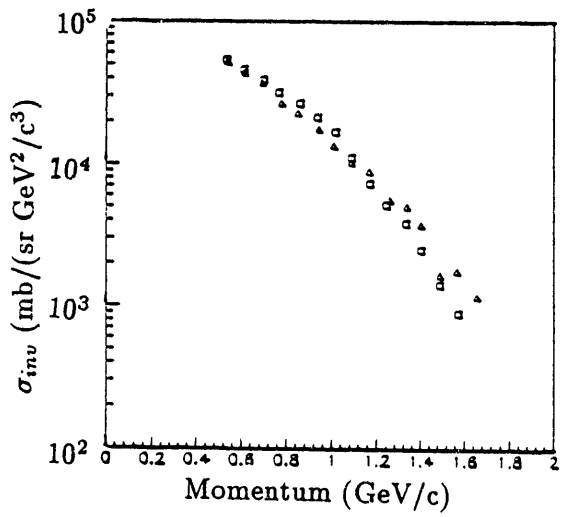

Fig. 2. The invariant production cross-section of protons from 0.8 GeV/n La on La collisions in the Janus spectrometer (squares) together with previous results (triangles).

Footnotes and References

[1] S. Hayashi et al Phys. Rev. C 38, 1229(1988).
[2] J. Aichelin et al Phys. Rev. C 62, 1461(1989).

Ultrarelativistic Experiments

Strangeness Production in Central S+Ag Collisions at 200 GeV/N.

G.Odyniec, S.I.Chase, J.W.Harris, H.G.Pugh, G.Rai, L.Teitelbaum, S.Tonse and the NA35 Collab.*

The production of neutral and charged strange particles (K^0_s, Λ^0, $\overline{\Lambda}^0$, K^+,K^-) in S+Ag central collisions at 200 GeV/Nucleon, was studied in the NA35 streamer chamber at the CERN-SPS. The trigger cross section was 0.09 barn, corresponding to a fraction of 0.03 of the total inelastic cross section. The NA35 streamer chamber was modified in order to reduce the high track density and to extend the acceptance to higher rapidity intervals and lower p_T values. 2445 events were scanned visually for the decay of neutral particles (V^0) and 1411 of them also for the charged particle (kink and tau) decays. 3365 V^0, 596 two body and 29 three body decays of the charged particles were measured. The neutral candidates were kinematically fitted for the K^0_s, Λ^0, $\overline{\Lambda}^0$ and γ hypothesis and the charged ones for the K^+, K^-, Σ^+, Σ^- and Ξ^- hypothesis.

The identification of the particles was based on the fit results (fit probability $\geq$ 1%). For the neutral particles an additional cut on their life time, on the isotropy of the V^0 decay in its rest frame, and on the symmetry between negative and positive decay products for K^0 and γ was imposed. The contamination of the charged kaons by Σ^+, Σ^-, Ξ^-, π^+ and π^- was partially removed by an angle cut of 2^o, and a life time cut for the ambiguities between Ξ^-, Σ^+, Σ^- and kaons [2].

The identification result was 521 Λ^0, 58 $\overline{\Lambda}^0$ and 356 K^0_s in the sample of the 2445 events, and 232 K^+ and 119 K^- in the sample of the 1411 events. In order to compare with our previous data from S+S central collisions at 200 GeV/Nucleon [1], we determine the ratios of the mean multiplicities for the kaons,lambdas and antilambdas in S+Ag and S+S collisions, in the acceptance of the S+S sample (Table 1). The mean lambda and kaon multiplicity increases by about a factor of two going from S+S to S+Ag system, while the antilambda multiplicity appears to change less. The ratio of S+Ag/S+S for lambdas (Fig. 1) shows no significant change within errors when comparing the rapidity intervals 1–2 and 2–3, the same ratio for the antilambdas versus rapidity seems to be constant too (not shown).

Table 1: Ratios of mean Multiplicities in the S+S acceptance

	Λ^0	K^0_s	$\overline{\Lambda}^0$
$\frac{S+Ag}{S+S}$	2.06 ± 0.23	2.4 ± 0.5	1.5 ± 0.5

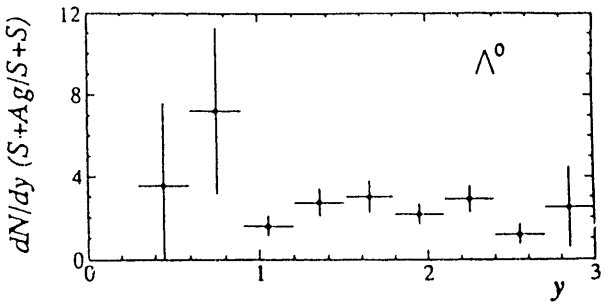

Figure 1: Ratio of lambdas in S+Ag and S+S collisions versus rapidity, in the S+S acceptance.

Footnotes and References

* Deceased

[1]J.Bartke et. al., Z. Phys. C - Particles and Fields 48,191-200(1990)

[2]M. Kowalski, Talk presented at Quark Matter 1991, Gatlinburg, to appear in Nucl. Phys. A

CERN Experiment NA-36

D. E. Greiner, C. R. Gruhn, P. Jones and I. Sakrejda

The NA36 experiment at CERN has begun publication of the results obtained in its 1990 data taking run. The data for 200 GeV/c S + Pb has shown some very interesting effects. Although the temperatures measured for the strange particles were much like those seen by experiment NA35 for S + S collisions (Figure 1), the rapidity distributions were very different, especially for the Λ particles. There was a very considerable excess production of all strange neutral particles in the mid-rapidity region. The data are shown in Figure 2.

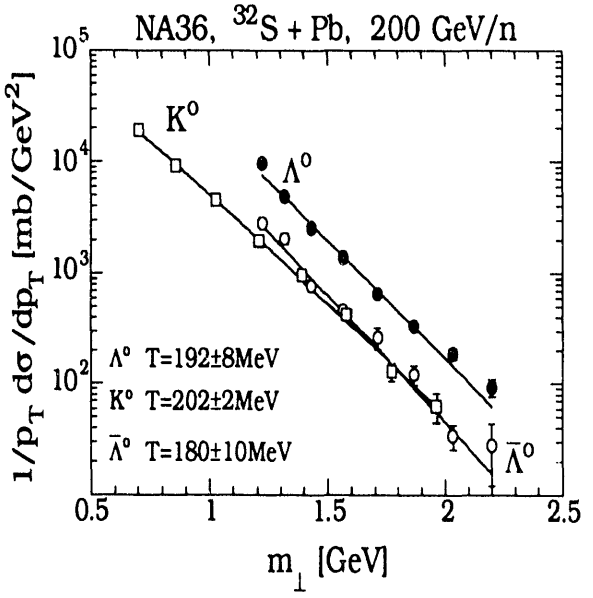

Fig 1. Transverse mass distributions for Λ, $\bar{\Lambda}$ and K°.

This enhanced production cross section region also exhibits a very high anti-baryon abundance. The ratio of $\bar{\Lambda}/\Lambda$ is .64 for this signal. This fact is a strong indication that the source is a quark-gluon plasma and not a hot hadronic gas. Further evidence is the fact that the percent of the enhanced flux increases with event multiplicity.

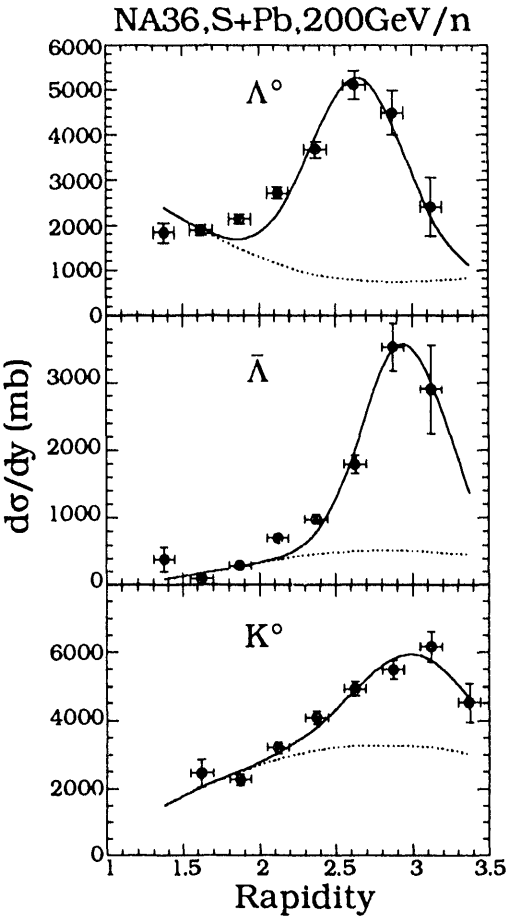

Figure 2. Rapidity distributions for Λ, $\bar{\Lambda}$ and K°. The dotted curves correspond to FRITIOF 1.7 monte carlo predictions scaled to pass through the points in the region 1.5 <y <2.0. The solid curves are the sum of the FRITIOF curves and the gaussians describing the "enhanced" production.

These results have been presented at a CERN ion seminar and are currently being prepared for publication.

Intermittency in ^{32}S+S and ^{32}S+Au Collisions at the CERN SPS

M.A. Bloomer, P. Jacobs, A.M. Poskanzer and the WA80 Collaboration

The presence of mixed phases of QGP and hadronic matter in high energy heavy ion collisions might produce "intermittent" fluctuations of charged particle density in small regions of phase space[1]. This collaboration previously reported a strong intermittency signal for ^{16}O+Au collisions[2], but that analysis needs to be redone due to an error in the track reconstruction algorithm.

The data for this intermittency analysis were taken during August 1990 at the CERN SPS with the WA80 Streamer Tube Detector. A "horizontal-vertical" factorial moment analysis was performed using tracks within the intervals $2.12 \leq \eta \leq 2.57$ and $-110° \leq \phi \leq 110°$. A full Monte Carlo simulation of the detector and surrounding material was also implemented using FRITIOF v1.7 and GEANT v3.14.

Figure 1 displays the dependence of $\langle F_2 \rangle$ on $\delta\eta$ and $\delta\phi$ for both data (solid circles) and the Monte Carlo simulation (open circles). The panels on the left are for a 1D analysis in η, while the panels on the right are for a 2D analysis in both η and ϕ. The slopes of the 1D data are consistent with zero or less than zero; the "sagging" of the moments for small values of $\delta\eta$ is a known detector effect discussed below. This sagging is even more pronounced for the 2D analysis. The 2D peripheral ^{32}S+S data show a significant increase with decreasing $\delta\eta\delta\phi$, but this trend disappears for the central ^{32}S+S and ^{32}S+Au data. In all cases, the *trends* of the moments are reproduced fairly well by the Monte Carlo simulation.

A two-dimensional extension of the alpha model[3] for simulating intermittency in both η and ϕ was developed in order to study how detector response and limited acceptance impede the measurement of intermittency. When the two-track resolution of $\simeq$ 5 cm of the WA80 multiplicity detector is included in the alpha model simulation, the moments for small values of $\delta\eta\delta\phi$ "sag" in the same manner as in the data. Separately varying the detector efficiency or η-ϕ acceptance has little or no effect on the calculation of the moments. Hence the single most important detector effect is the finite two-track resolution.

Based on the agreement of the data with our Monte Carlo, we conclude that no "new" physics beyond that contained in FRITIOF is needed to explain the measured scaled factorial moments.

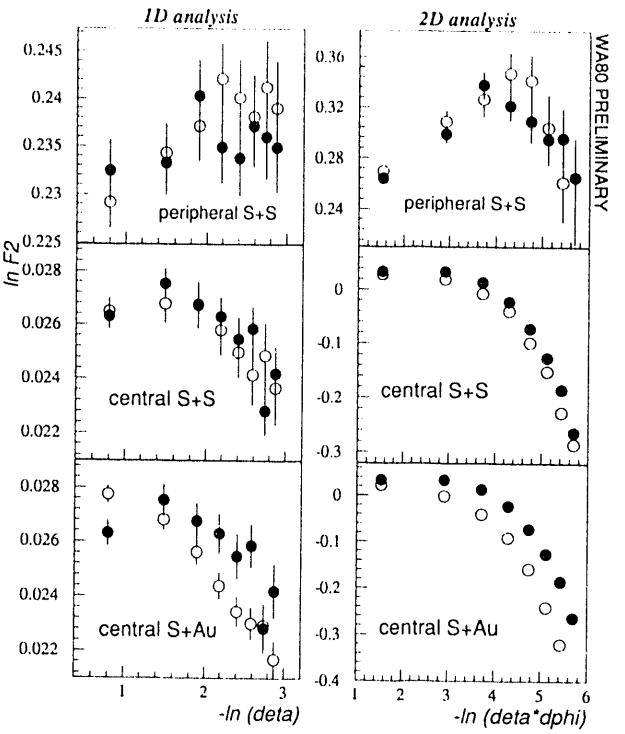

Figure 1: $\ln\langle F_2 \rangle$ versus $-\ln(\delta\eta)$ (left panels) and $-\ln(\delta\eta\delta\phi)$ (right panels) for various systems and triggers. Solid circles: data. Open circles: Monte Carlo.

Footnotes and References

[1] A. Bialas and R. Peschanski, Nucl. Phys. **B273** (1986) 703; L. Van Hove, Z. Phys. **C27** (1985) 135.

[2] R. Albrecht et al. (WA80 Collaboration), Phys. Lett. **B221** (1989) 427.

[3] P. Desvallées, R. Ouziel and R. Peschanski, Phys. Lett. **B235** (1990) 317.

Simulations of a Large Acceptance Hadron Detector for Pb Beams at the CERN SPS

M.A. Bloomer and the NA49 Collaboration

The full utility of high energy heavy ion collisions for creating very hot and dense hadronic matter is reached only for symmetric collisions of very heavy nuclei (e.g. Pb or Au). For this purpose, a large acceptance hadron spectrometer was proposed for use in the Pb beams which will become available at the CERN SPS in early 1994. This experiment (recently approved as experiment NA49) will consist of two dipole magnets in series followed by several large volume TPCs. Its goal is to study the production of charged hadrons ($\pi^{\pm}$, $K^{\pm}$, p, $\overline{p}$) and neutral strange particles (ϕ, K^0_s, Λ, $\overline{\Lambda}$) in a search for the deconfinement transition predicted by QCD lattice gauge calculations. The very large number of particles produced in central Pb+Pb collisions enables the **event-by-event** analysis of observables such as the temperature of pion spectra, strangeness production, the rapidity-loss of projectile nucleons, and Bose-Einstein correlations.

To fully exploit the physics potential of such collisions it is necessary to have a detector which identifies and measures the momenta of $\approx$ 1000 hadrons per central event. Large volume TPCs are ideally suited to accomplish this goal. A GEANT simulation was undertaken to study the acceptance of the TPCs for various configurations. Events were generated for central Pb+Pb collisions at 180 AGeV/c in the laboratory using FRITIOF v1.7. All particles from FRITIOF were fed into GEANT and tracked through the detector. All processes were turned off except for energy-loss and particle decays. A particle was accepted if 1) its path length in one of the TPCs was sufficient for tracking; 2) it could be identified using dE/dx information in the relativistic rise region; and 3) its trajectory was not obscured by a nearby track in the same detector.

Shown in Figure 1 is the acceptance of NA49 for protons, antiprotons, π^- and K^- for opposing dipole magnet field polarities. The open histograms are the initial rapidity distributions from FRITIOF; the shaded regions correspond to the fraction of the initial distribution which is measured by the detector. As can be seen, NA49 accepts most of the protons and almost all other hadrons forward of midrapidity (y = 3). The momenta of negative pions can be measured below midrapidity using TPCs within the magnet volumes (hatched region); however, these pions cannot be particle identified. About 900 charged particles per central event are measured within the acceptance, which is adequate for event-by-event determination of the interesting physics observables.

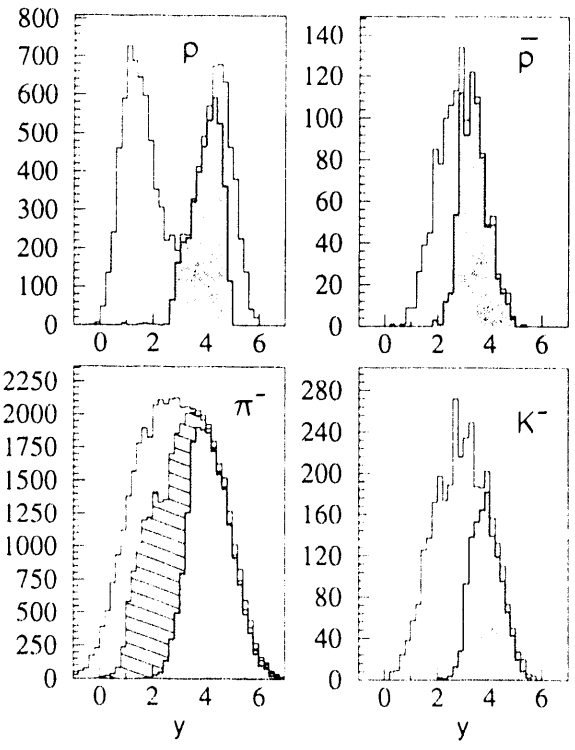

Figure 1: Rapidity (y) acceptance of NA49 for various species of particles. Open histograms: initial rapidity distribution. Shaded region: particle identified tracks. Hatched region: π^- detected by TPCs within magnet volumes.

Multi-strange particle reconstruction in STAR: a simulation.

S. Margetis, D. Cebra, W. Christie, C. Naudet, G. Odyniec, W. Wilson and the STAR Collab.

One of the physics goals of the STAR experiment at RHIC is the measurement of strange particles[1]. Particles with short mean life times ($\sim$ few cm) require good vertex and track reconstruction capabilities in order to be succesfully recovered from the thousands of background tracks. A combination of a large TPC and a vertex detector (SVT) has been proposed for that purpose; the SVT having an excellent position and two track resolution.

A simulation of the detector was set-up in order to study its response to Ξ^- and its antiparticle[2],[3]. These particular particles have decay modes into only charged particles ($\Xi^- \rightarrow \pi^- + \Lambda$ [100%] and $\Lambda \rightarrow p + \pi^-$ [64%]). Fritiof generated events were passed through GEANT and the produced 'tracks' were properly 'smeared' for effects like position, momentum and angular resolutions according to the characteristics of each detector. A reconstruction routine loops over all tracks and after reconstructing the Λ combines it with the remaining π^- looking for Ξ^- candidates. A set of cut parameters eliminated most of the combinatorial background. These are spatial cuts like: a) the distance at the point of closest approach of the combined tracks (checks for common vertex), b) the impact parameter of the reconstructed Ξ^- from the main vertex (primary particles should emanate from the vertex), and c) the distance of the decay vertex from the main vertex (avoids the confusion area due to vertex tracks).

Fig. 1 shows the invariant mass distribution of Ξ^- for a sample of 900 central Au + Au events at $\sqrt{s}$ = 200 GeV/nucleon. The simulation suggests that a very good signal to noise ratio could be achieved with the combination of the tracking capabilities of the TPC + SVT. A test of the stability of the results through a life-time fit was successful. Preliminary simulations with only the TPC detector in the apparatus showed that the very small signal (in that case) virtually disappears in a much higher background.

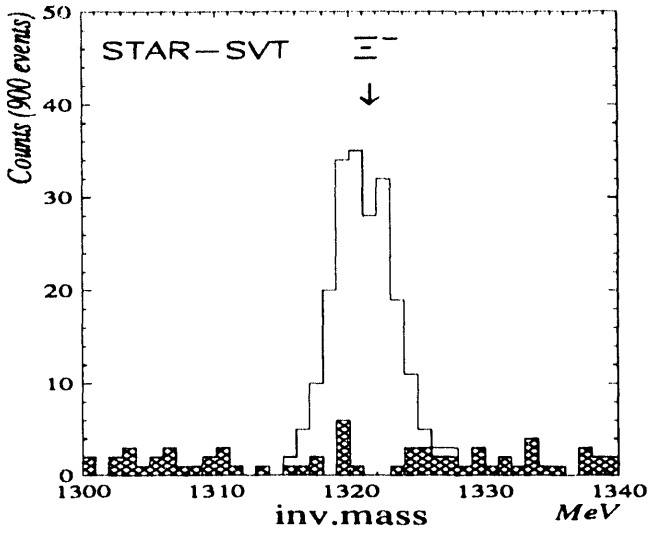

Figure 1: Invariant mass distributions of Ξ^-. Shaded area represents the contribution of the combinatorial background.

The clean TPC + SVT sample allows for a further investigation of the physical parameters (like rapidity and pt spectra) of the reconstructed particles (see ref. 3). The estimated (optimized) overall efficiency would be in the range 15 - 25% in the $\eta = \pm 1$ region, and we have observed that it extends to the low pt region. The reasons for this efficiency are branching ratios and (rejected) decays very close to the vertex.

An effort to establish a full scale simulation folding in more accurate estimates of the response of the detector is under way. It will allow us to optimize the arrangement of the detector, study the effect of different configurations on physics parameters and accurately calculate the efficiency for each particle species.

Footnotes and References

[1] The STAR Collaboration, LBL - 31040.
[2] G. Odyniec et al., LBL - 31773.
[3] STAR Coll. meeting, BNL Nov. 1991.

Pion Correlations in Relativistic Heavy Ion Collisions at HISS

W. Christie, D. Olson, P. Brady, J.Chang, Y. Dardenne, S. Fung, G.Grim, J. Kang, D. Keane, J. Osbourne, M. Partlan, J. Romero, C. Tull, S. Zhang
UCD, UCR, LBL, Kent State, MSU

Presented here is a brief summary of the results of a pion correlation experiment performed at HISS. The beam and target used were 1.2 GeV/nucleon Lanthanum on Lanthanum.

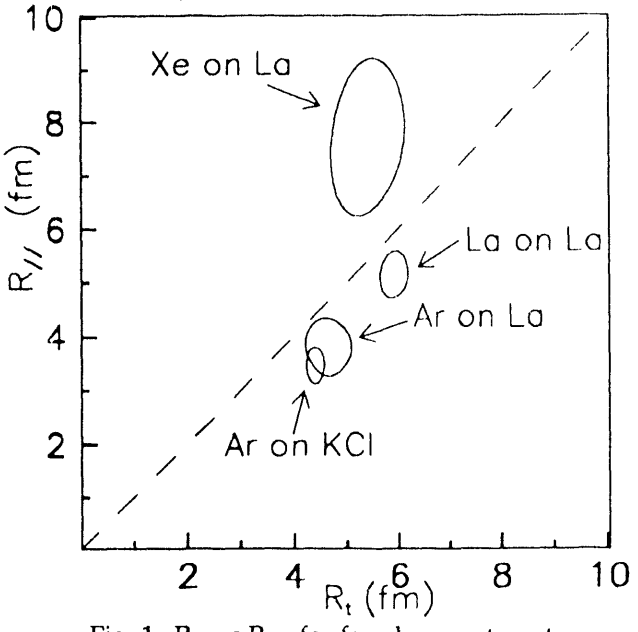

Fig. 1. $R_\perp$ vs $R_{//}$ for four beam - target combinations. Shown are one sigma error contours.

The analysis technique used is commonly known as the Hanbury-Brown, Twiss (HBT) or Goldhaber, Goldhaber, Lee, and Pais (GGLP) method.

The acceptance for the π^-s was centered about 0° in the center of mass system. Central events were selected by triggering on events which had little or no charge in the projectile fragment region. The trigger selected ≈ 37% of the geometric cross section.

The experimental data was fit using the forms:

$$C_2(q,q_0) = N[1 + \lambda e^{(-q^2R^2/2 - q_0^2\tau^2/2)}],$$

$$C_2(q_\perp q_{//} q_0) = N[1 + \lambda * e^{(-q_\perp^2 R_\perp^2/2 - q_{//}^2 R_{//}^2/2 - q_0^2\tau^2/2)}]$$

The quantities q, q_0, $q_\perp$ and $q_{//}$ refer to the relative three momentum, energy, perpendicular and parallel momentum relative to the beam direction, respectively. The fit parameters $R_\perp$ and $R_{//}$ are thus interpreted as measures of the source radius in these two directions. N is a normalization constant and λ, commonly referred to as the chaoticity parameter, allows for correlations due to effects other than the Bose Einstein (BE) statistics. The fitted values are:

R (fm)	τ (fm/c)	λ	$\frac{\chi^2}{NDF}$
5.93 ± 0.25	0.0 + 2.0	0.77 ± 0.06	$\frac{763.98}{661}$

with 94,812 correlated π^- pairs. and

$R_\perp$ (fm)	$R_{//}$ (fm)	τ (fm/c)	λ	$\frac{\chi^2}{NDF}$
5.91 ± 0.21	5.15 ± 0.35	$3.43 \pm^{1.0}_{1.2}$	0.77 ± .05	$\frac{1742.2}{1669}$

with 93,036 correlated π^- pairs.

The fits given are with systematic corrections applied for the Gamow Coulomb effects, the DC tracking efficiency, and for Background correlations. The one σ errors are given for the parameters. Also listed are the χ^2 and the number of independent degrees of freedom (NDF) for the fit.

Shown in figure 1 are the one sigma error contours for this new data (La on La) as well as those from a previous HISS experiment[1]. The motivations for this experiment were to check the apparent change from prolate to oblate source shapes observed in the earlier experiment, and to get a more precise measurement for a large system. Note that the results of the present experiment show a prolate source shape for the La on La system, with an aspect ratio very similar to that for Ar on KCl.

Analysis of the dependence of the fitted source size on the mean momentum of the π^- pairs is still in progress.

---

[1] W.B.Christie, Ph.D. Thesis, LBL Report #LBL-28986, 1990. (submitted to Phys.Rev.C)

Electronics for the NA35 TPC

A.A. Arthur, F. Bieser, W. Cwienk, V. Eckardt*, P. Jacobs, R. Jones, S. Kleinfelder, K. Lee, M. Nakamura, T. Noggle, W. Pimpl*, A.M. Poskanzer, W. Rauch*, J. Schambach, J.Seyerlein*, J. Zhu†, and the NA35 Collaboration*

We have constructed 6600 channels of modified EOS electronics for the NA35 TPC, for use during the heavy ion beam time at CERN in April 1992 and for the NA49 experiment in 1994. The modifications include a new board layout, a shortening of the shaping time, expansion of the SCA (switched capacitor array), and an increase in the clock speed to 12.5 MHz. The project will double the number of instrumented channels on the NA35 TPC. In addition, it is serving as a test bed for developments necessary for the NA49 experiment. It is a collaborative effort between LBL, MPI Munich, University of Frankfurt, GSI, and the University of Washington.

The modification of the EOS "stick" entailed splitting the EOS structure between the shaper amplifier and the SCA. This was necessary because the layout of the NA35 TPC pad connectors is irregular and does not allow a simple stick geometry. The preamplifiers and shaper amplifiers are contained on small printed circuit boards ("PA/SA boards") containing four EOS preamp chips (each chip contains four readout channels) and sixteen sub-boards, each containing a single shaper amplifier. Each PA/SA board therefore services 16 readout channels, corresponding to the geometry of the NA35 TPC pad plane connectors. The shaping circuit was modified to have FWHM of 180 ns in order to increase the two-track resolution in the time direction, and the clock speed was increased from 10 MHz to 12.5 MHz accordingly. The PA/SA boards are connected via a 40-pin flat ribbon cable to the "readout board". Each readout board contains eight SCAs, two ADCs, memory, optical fiber link circuitry, and multiplexing and logic chips to handle the data flow between these elements. The SCAs, which are 16 channels wide, were modified to be 512 time buckets deep, compared to 256 for EOS. The readout boards service 128 channels (one pad row), with each SCA connected to one PA/SA board. All 128 channels are multiplexed into a single optical fiber, connected to an EOS quad receiver module resident on a 9U VME card.

The NA35 TPC requires only 8 bit accuracy, compared to 12 for EOS, and this truncation allowed us to double the number of time buckets while still using the EOS receiver without major modifications. The packing of the data in the data stream was therefore different, with two pixels occupying a single word in the receiver memory. Custom DSP code was developed to unpack the data and perform pedestal subtraction, zero supression and gain correction.

The PA/SA boards were constructed at MPI Munich, using the EOS shaper amplifier design and EOS preamp chips supplied by LBL. The readout board power supplies were also constructed at MPI. The readout boards and receiver boards were designed and constructed at LBL. In the course of this project, two test stands at LBL were also built. The first was the SCA test stand, whose hardware and software were closely based on the EOS SCA test stand. The yield of the modified SCA chips, demanding low pedestals and good linearity in all channels, was about 50%. The second test stand, for the completed readout boards, utilized the EOS Test Manager (developed by C. MacParland) for control of the boards, and the NA35 Pad Monitor (developed by J. Schambach) for display of the data.

Footnotes and References

*MPI Munich

†University of Washington

Reconstruction of K^0_s, Λ and $\bar{\Lambda}$ particles in STAR: a simulation.

W. Wilson, D. Cebra, W. Christie, S. Margetis, C. Naudet, G. Odyniec and the STAR Collab.

The measurement of neutral strange particles in a heavy ion experiment is an indispensable tool in the search of a phase transition in nuclear matter[1,2]. In the very high multiplicity environment of RHIC ($\sim$ 3000 particles in $|\eta| < 1$), very good tracking capability is necessary for a virtually background free signal (so that the specific properties of the species can be further studied; e.g. spectra and even K^0_s HBT interferometry[2,3]). The combination of the tracking and vertex capabilities of a large TPC and a vertex detector (SVT) has been proposed as an adequate solution.

A simple simulation demonstrated the ability of these detectors to deliver a clean sample of strange particles. Fritiof generated events were passed through GEANT and the spatial resolution of the SVT as well as interactions between particles and many of the elements of the detector environment are taken into account. Fritiof produces $\approx$ 240 K^0_s and $\approx$ 60 (35) Λ ($\bar{\Lambda}$) particles per central Au+Au event at $\sqrt{s}$ = 200 GeV/nucleon. About one out of five particles is potentially reconstructible. The remainder are lost due to branching to non-reconstructible secondaries, geometrical inefficiencies, interactions, and detector resolution. Due to the finite spatial resolution at the main vertex, a very large number of random track crossings occur within a sphere of only a few centimeters radius. These crossings create a formidable background in the invariant mass spectra of the reconstructed primaries. We employ two cuts to separate out the true secondary vertices. First, the number of random crossings is reduced by rejecting vertex candidates less than 1-2 cm from the main vertex. This is effectively a combined lifetime/p_T cut which eliminates part of the signal. Second,

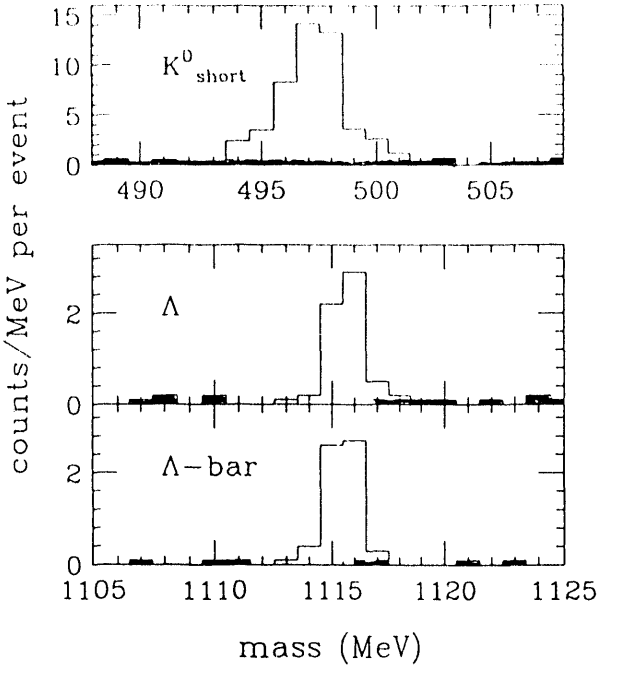

Figure 1: Invariant mass distributions of K^0_s, Λ and $\bar{\Lambda}$. Shaded area represents the contribution of the combinatorial background.

we demand that the sum of the closest approach of the two secondaries and the deviation of the reconstructed primary from the main vertex be less than 2 to 3 mm. This cut rejects few more particles from the signal. The values of these cuts were determined by optimizing the relationship between the yields of the true secondaries and the random background vertices in the invariant mass spectra. The figure shows these results averaged over 10 events, the plain histogram representing all the reconstructions and the shaded histogram representing only the random background.

We can conclude that the spatial resolution of the SVT will allow for the reconstruction of strange particles with an estimated efficiency of 15 - 20% in $|\eta| < 1$.

Footnotes and References

[1] The STAR Collaboration, LBL - 31040.

[2] G. Odyniec et al., LBL - 31773.

[3] D. Keane, STAR Coll. meeting, LBL March 1992.

Production of Charged Kaons in Central S+S and O+Au Collisions at 200 GeV/N.

G.Odyniec, S.I.Chase, J.W.Harris, H.G.Pugh, G.Rai, L.Teitelbaum, S.Tonse and the NA35 Collab.*

Production of charged kaons in central S+S and O+Au collisions (0.02 and 0.07 of the total cross section, respectively) at 200 GeV/N has been studied in the NA35 Streamer Chamber experiment.

The events were scanned for 2-body-like decays with one charged secondary (kink topology) and for 3-body decays into charged secondaries (tau topology). These decays were measured and run through a kinematical fit. The contaminations due to the 2-body decays of charged hyperons and due to decays into 1 charged and 2-neutral secondaries were found to be negligible. Corrections due to the contamination by the decay and elastic scattering of pions and due to scanning losses were applied to the data. Analyzed samples were restricted to the following phace space regions: $0.6 < y < 2.4$ and $0.2 < y < 2.0$ for S+S and O+Au respectively with a high p_T cut of 1.1 GeV/c.

Fig.1 shows the comparison of the transverse mass distribution $1/m_T dN/dM_T$ for neutral and charged kaons in S+S interactions. Agreement between the slopes and cross sections of charged and neutral kaons, as expected from isospin symmetry, proves the consistency of the analysis. Transverse mass distributions for K^+ and K^- in both reactions show an exponential behavior (Table 1). Comparisons with the spectra predicted by Fritiof [1] and Venus [2] models show that Venus describes the K^+ distribution relatively well, while its predictions for the K^- spectra are too steep [3]. Fritiof fails to describe the data [3]. In Table 2 the multiplicities within the limited phase space region of our analysis are presented and compared with models. It appears that none of the models give satisfactory predictions for the data.

Table 1. Fits of the form $1/m_T dN/dM_T = c\cdot\exp(-A\cdot m_T)$ to the transverse mass.

	A_{K^+}	A_{K^-}
S + S 0.6 - 2.4	4.4±0.3	3.7±0.5
O + Au 0.2 - 2.0	4.7±0.4	4.0±0.7

Table 2. Multiplicities of K^+, K^- in S + S collisions. $0.6 < Y < 2.4$

	$\langle K^+\rangle$	$\langle K^-\rangle$	$\frac{\langle K^+\rangle}{\langle K^-\rangle}$
DATA	3.31±0.17	1.69±0.14	1.98±0.19
VENUS	2.98	2.03	1.47
FRITIOF	2.67	1.89	1.41

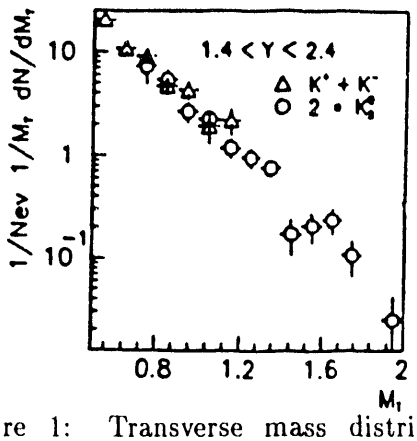

Figure 1: Transverse mass distribution for charged and neutral kaons in S + S interactions.

Footnotes and References

* Deceased

[1] K.Werner Phys.Rev.Lett.62(1989)2460 (version 3.07)

[2] B.Anderson et al., Nucl. Phys. 281(1987) 289 (version1.6)

[3] M.Kowalski, Talk presented at Quark Matter 1991, Gatlinburg, to appear in Nucl. Phys. A

Charged Particle Spectra in Central S + S Collisions at 200A GeV

L. Teitelbaum, S.I. Chase, J.W. Harris, G. Odyniec, H.G. Pugh, G. Rai, S. Tonse and the NA35 Collab.*

The transverse momentum distributions of negatively charged hadrons and protons have been measured in central S + S collisions at 200 GeV/nucleon in the NA35 streamer chamber. The visible trajectories of charged particles were imaged and recorded by a novel data acquisition system[1] which employed high resolution CCDs to capture directly-digitized images. The data reduction procedure was also new, relying on computer tracking and computer image matching to accelerate track measurement by a factor of $\sim 3-5$. Outside of a central beam pencil at forward laboratory angles, 216 events were fully measured and the momenta of all charged particles determined by stereoscopic reconstruction.

A track-by-track weighting procedure was used to correct the spectra for geometrical inefficiencies. The negatively charged particles were also corrected for electron contamination, for secondary production from the weak decays of neutral strange particles, and for secondary hadronic production from hA interactions in the target. The proton distributions were deduced from the excess of positively over negatively charged particles. Because S + S is isoscalar, the yield and phase space distributions of π^+ and π^- must be the same. The proton spectra were corrected for the asymmetrical production of K^+ and K^-, for protons from Λ decay, and for the intrinsic charge excess resulting from nuclear fragmentation in secondary hA interactions.

Figure 1 shows the transverse momentum distributions $1/p_T\, dN/dp_T$ as a function of p_T. The pion spectrum can be fit to a two-component superposition of the thermal expression $A\, m_T\, K_1(m_T/T)$. The high temperature component contains 78% of the p_T-weighted, integrated yield. Although the yield increases at

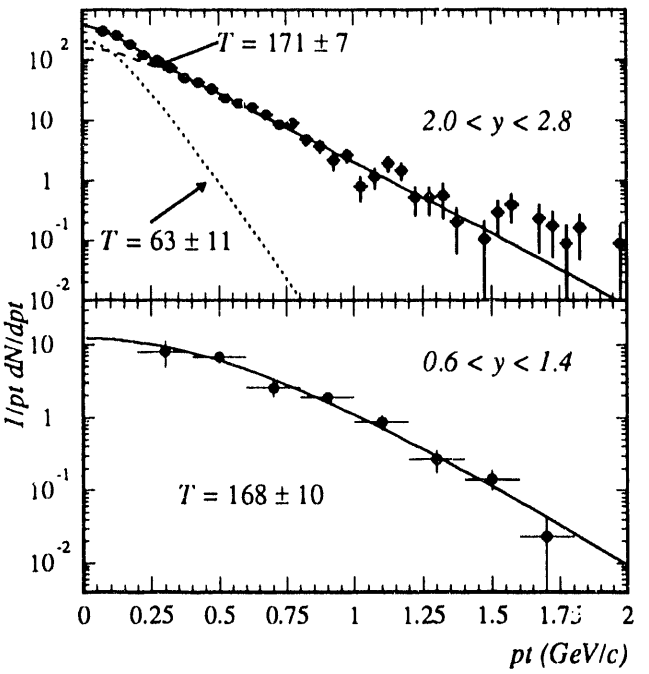

Figure 1: Transverse momentum distributions. The upper panel is for negative hadrons, the lower for protons. The temperatures are in MeV

low p_T, a comparison of the AA data to pp data[2] at the same $\sqrt{s}$ showed no evidence for a low-p_T enhancement. The proton spectrum can be fit to a single-component form of the same expression. Note that the proton temperature is the same as the high temperature component of the negative hadron spectrum. Both spectra are consistent with a simple model[3] which assumes a hadron resonance gas in thermal and chemical equilibrium at a single temperature T. The rise at low p_T is a consequence of the decay kinematics of the many produced resonances which decay into pions at high energy.

Footnotes and References

*Deceased

[1] M.L. Tincknell et al., Opt. Eng. **26**, 1067 (1987).

Footnotes and References

[2] B. Alper et al., Nucl. Phys. **B100**, 237 (1975)

[3] J. Sollfrank et al., Phys. Lett. **B252**, 256 (1990)

A sub 65 pS Time-of-Flight System using Silicon Avalanche Diodes

G. Rai, A. Haugert, A.S. Hirscht, N.T. Porilet, R.P. Scharenbergt, M.L. Tincknellt

A generic research program is underway to establish a proof of principle for the application of Silicon Avalanche Diodes (AVD)‡ in ultra fast time-of-flight systems. This new technology could also be of considerable value to other scientific and commercial fields which use conventional high performance photomultiplier tubes (PMT). Our effort is, in part, directed by the proposal (called STAR) to construct a large tracking detector capable of doing experiments at the Relativistic Heavy Ion Collider facility at BNL. The time-of-flight component is highly segmented (10^4 pixels) and must operate in a magnetic field. A time resolution of $\sigma < 100$ps is needed to extend the particle identification capability of the Time Projection Chamber.

We are currently exploring two concepts: the large pixel array detector and the AVD phototube. In the first scheme, a self sufficient module comprising four 0.5x0.5 cm (or possibly 1x1cm) AVDs would be used to form a larger patchwork panel. The AVDs are readout by custom integrated electronics located directly on the opposite side of the panel. In the second concept, an AVD is used as an active dynode placed behind a planar photocathode. The combination of internal gain and the large number of electron-hole pairs created per incident photo electron should provide for an attractive low cost miniature device with a timing performance potentially superior to the PMT.

We have made time resolution studies using suitably modified AVDs purchased from EG&G (Canada). Each AVD was supplied with a 100Mhz bandwidth transimpedance amplifier mounted adjacent to each AVD and both parts enclosed in a light tight beryllium/aluminium package. The mechanical test arrangement is shown in Figure 1. Electrons from a beta source passes through two AVD diodes and are stopped in a scintillator trigger counter. The entire assembly sits in a faraday shield which in turn is sealed in a temperature controlled container. The external chain of electronics was very carefully setup using commercially available high speed components. With this system the coincidence time measurement dispersion per channel was determined to be 5.4 pS.

Preliminary results indicate a time resolution of σ=65 pS. Still, with further optimization of the electronics and the AVD diode parameters, better performance is expected. We have also measured the gain of the AVDs as function of applied bias and temperature.

In summary our findings so far suggest that AVDs could be exploited in fast timing applications and developed into practical detectors.

Footnotes and References

† Purdue University, Physics Dept.

‡C.R. Gruhn, IEEE Trans. Nucl. Sci., Vol.23,(1976),145
P.P. Webb, R.J. McIntyre and J. Conradi,
RCA Review, Vol. 35,(1975),234

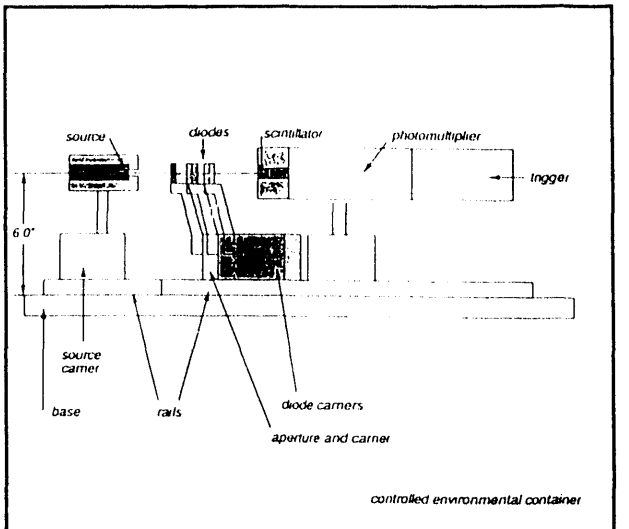

Fig. 1. Experimental test layout for coincidence time resolution studies.

A Radial Drift TPC for use in STAR

D. Cebra, F.P. Brady[1], J. Chance[1], J. Draper[1], K. Foley[2], E. Platner[2], J. Romero[1], I. Stancu[3], and the STAR Collaboration

The STAR experiment attempts to characterize relativistic collisions as completely as possible on an event by event basis. Of the roughly ten thousand charged particles that are produced in a central Au + Au event, more than four thousand are emitted with $5.0 > |\eta| > 2.0$, these can be detected in an external radial TPC. The primary particle distributions in the forward regions can be analyzed to look for regions of enhanced particle emission, signs of intermittency, and remnants of the projectiles. TPCs employing radial drift are ideal for this region because they allow vectoring for rejection of secondaries and have a reduction in effective pixel size with radial distance which matches the increased particle flux.

The response of a radial TPC has been simulated in detail to determine if the naive expectation of reduced effect pixel size with radius is actually achievable. These simulations have considered the effects of diffusion, non-uniform drift field, and fringe magnetic fields from the main solenoid. Fig. 1 displays the separation of the detected ionization clouds of two tracks that were initially 1 cm apart for both a radial and conventional TPC. It is clear that the radial TPC separates the two tracks better. The effect of the magnetic fringe field is to azimuthally distort the drift trajectories. For the expected strength of the fringe field this is a small effect. Simulations have also addressed the ability to find tracks; 95% of the tracks from primary particles and 75% of the tracks from secondaries are correctly found. The primary tracks that are lost are of the lowest rigidities. Vectoring back to the interaction vertex successfully distinguishes most primaries from secondaries as well as allowing a rough momentum and charge determination.

A conventional TPC employs an electric field that is uniform in both strength and direction, this is not true for a TPC employing radial drift. The field strength varies as a function of radius and thus the drift velocity of the ionization is not uniform. The challenge of the radial TPC is to keep the drift velocity as uniform as possible, the diffusion as low as possible, and the position resolution as high as possible. The technical innovations that make this possible are the manufacture of curved pad and wire planes and the orientation of the wire planes parallel to the long axis of the pads. We are currently constructing a prototype sector to determine if the curved wire and pad planes can be manufactured to enough precision to maintain the required performance.

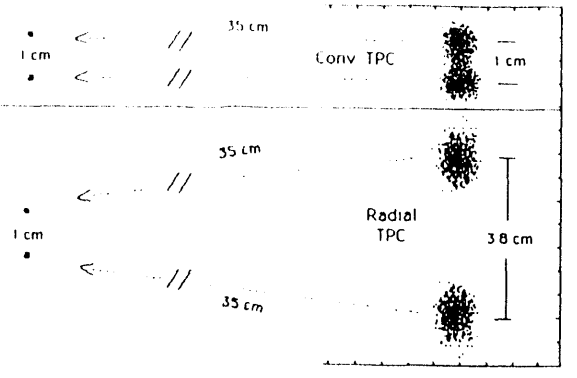

Fig. 1. This figure illustrates the advantage of radial drift. It displays the expected initial ionization clouds from tracks separated by 1.0 cm (left) and then the final cloud after 35 cm of drift (right). During this drift the intial ionization clouds are spread by diffusion and by the drift field. The bottom portion indicates the detected ionization distributions for two tracks in a radial TPC while the top portion is for drift in a conventional TPC.

Footnotes and References

1. U.C. Davis, Davis, CA, USA
2. Brookhaven National Lab, Upton, NY, USA
3. Rice University, Houston, TX, USA

Testing of Silicon Drift Detectors

C. Naudet, D. Cebra, W. Christie, S. Margetis, G. Odyniec, W.K. Wilson and the STAR Collab.

The relativistic heavy ion collider (RHIC) is presently under construction at Brookhaven National Laboratory (BNL). The STAR (Solenoidal Tracker at RHIC) collaboration has been approved to build an experiment at RHIC to measure particle and jet production at midrapidity. The Silicon Vertex Tracking group (SVT) has the charge of developing a tracking device which, when coupled with the time projection chamber, will yield the position of the primary interaction vertex with high accuracy and precision, improve the momentum resolution, and locate secondary vertices with a positional resolution better than 50 microns.

The SVT group has designed a detector to meet these goals. The detector is arranged in three cylindrical layers at radii of 5, 8 and 11 cm. Each layer is formed by connecting ladders (40 cm by 6 cm) together in a hexagonal pattern. Each ladder is composed of six silicon drift detectors (SDD) [1] each 6.8 cm by 5.8 cm by 300 microns.

The SDD's are fully depleted silicon wafers which have a second electrical field superimposed to transport the charge carriers towards the segmented anode. A minimum ionizing charged particle will deposit approximately 25K electrons in the wafer. Since the transport time is linearly related to the distance from the anode, the position in the drifting dimension is obtained by measuring the arrival time of the electron cluster. In the transverse dimension the position is obtained by charge division using segmented anodes. The positional resolution has been measured to be better than 10 microns in each dimension.[2]

During the last two months at LBL we have been developing a SDD testing laboratory. This lab consists of a SDD test station with readout electronics and a Macintosh based data aquisition system. The SDD test station consists of a computer controlled X-Y table (.5 micron step), a xenon flash lamp with a band-pass filter and 50 micron diameter fiber optic cable. This allows a precise injection of charge at a know location on the silicon wafer, allowing a method to measure the positional resolution and linearity of the device over it's entire surface. The electron pulses which arrive on the SDD anode pads are amplified, shaped, and then processed by a 50 mhz waveform digitizer. Shown in Figure 1 is the digitized waveform from a 60 KeV gamma ray which closely simulates a minimum ionizing particle. An integration of this spectra for many pulses yields the energy spectrum of the 60 KeV source, we observe a energy resolution (sigma/mean) of 3%. Two track resolution measurements and magnetic field effects will be studied in the near future.

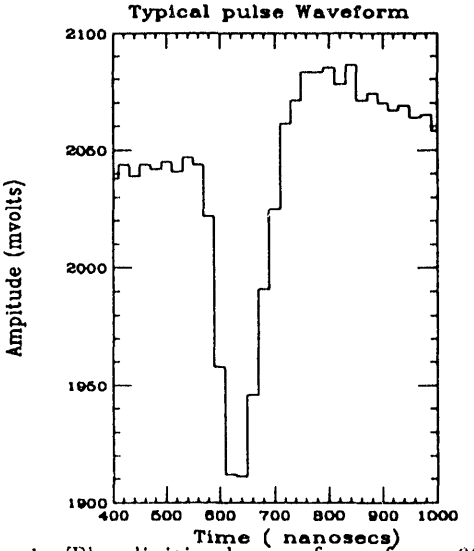

Figure 1: The digitized waveform for a 60 KeV gamma ray.

Footnotes and References

[1] P. Rehak and E. Gatti NIM 225 (1984) 608

[2] P. Rehak and E. Gatti NIM 226 (1984) 129

Simulations of Si Drift Detectors

W.K. Wilson, W. Christie, S. Margetis, C. Naudet, G. Odyniec, J. Walton and the Star Collab.

The Si drift detector (SDD) is a low noise solid state detector which can supply two dimensional position information with an accuracy down to a few microns.[1] Only recently developed, these devices do not suffer from the left/right ambiguity of traditional drift chambers, and they provide a high density of effective pixels using a modest number of readout channels. Due to these qualities, the the STAR (Solenoidal Tracker at RHIC) collaboration has based the design of its SVT (Silicon Vertex Tracker) on SDDs. The SVT will form the inner layer of the STAR detector, allowing accurate primary and secondary vertex reconstruction in the high multiplicity environment expected in Au+Au collisions at RHIC.

The line of electrons freed by the passage of a charged particle through the 300 μm thick SDD is compressed into the central plane of the chip and transported to a row of anode pads at the edge of the detector. The time of the arrival of the electrons at the anode pads (up to 6 μs in the SVT design) is proportional to the drift distance, providing position information along the drift direction. As the cloud drifts toward the row of anodes, diffusion causes it to spread over several anode pads. The centroid of the observed charge distribution across the anodes provides position information along the axis perpendicular to the drift direction.

The evolution of the electron cloud with time can be found by converting the continuity equation into a difference equation and using it to propagate the electron density on a 3 dimensional grid. We have rejected this approach due to the prohibitively large arrays needed to represent a SDD chip, and because the solution of the second order non-linear difference equation is unstable. Instead, we individually track the motions of the electrons, separating the drift due to the electric field and the diffusion into separate steps.

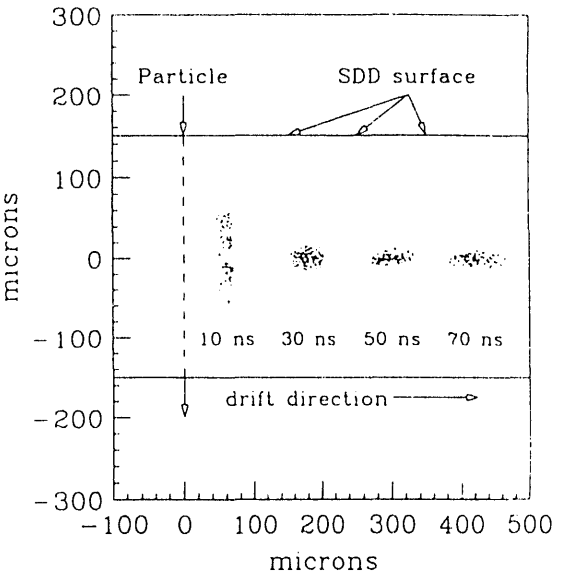

Fig. 1. This figure shows the results of a SDD electron cloud simulation in different time snap-shots after the passage of a charged particle along the dashed line.

A sample simulation is shown in fig. 1 for a 6 μm/ns drift velocity. The electron cloud is rapidly compressed into the central plane of the detector and transported towards the anodes on the right (not shown).

The next step is to use the simulations to parameterize the current induced on the anode pads due to tracks at different distances from the pad rows and different angles of incidence. These calculations will provide a detailed understanding of the position resolution of the SDD chips. Thus we will be able to set the sampling frequency, drift voltage, and chip overlap (if any) to meet the resolution dictated by the STAR physics objectives.

Footnotes and References

[1] Gatti et al., *Nuc. Instr. and Meth.* 226, 129 (1984).

An Online Monitoring System for the NA35 TPC

J.J. Schambach and the NA35 collaboration

We have developed a program for online monitoring of the performance of the NA35 time projection chamber (TPC), which was used for the October 1991 run. This program, called "Pad Monitor", was developed on a SUN SPARCstation using the X-Windows based "XView" toolkit by SUN Microsystems. XView was chosen because of its simplicity and because it is a toolkit available in public-domain, which should make the portability of the Pad Monitor program to a different workstation easier. The NA35 Pad Monitor program is a significant expansion of the orginal EOS TPC pad monitor program developed by Howard Wieman and Yiping Shao.[1] The motivation for developing this program was to provide a tool with an easy, MacIntosh like interface, which can show problems in any of the (currently about 12,000) pads at a glance.

The Pad Monitor program provides a graphical representation of the TPC pad plane. The program associates a user-selectable amplitude (such as mean ADC value — averaged over time-buckets — , rms over time-buckets, maximum ADC value, etc.) with each pad.

A slider bar controlled cut affects the display of the pad rectangles in the display with pad rectangles appearing in one color for amplitudes above the cut and another color for pads with amplitudes below the cut. This cut is also illustrated with a histogram of all the active pad amplitudes using the same colors to indicate the location of the cut. This histogram displayed in a popup window on the display.

The current version of the Pad Monitor can read a NA35 event file, or gets its input from the NA35 data acquisition processor or from the test station for the LBL electronics via Ethernet.

The ADC versus time spectra in the pads for 2 pads are displayed in another popup window. These pads are selected with the mouse and indicated with a color marker on the display. A message box of matching color contains information about the selected pad. The limits of the spectra can be manipulated with the mouse buttons, which makes it easy to magnify a region of interest. By dragging the mouse over a time region in this spectrum, a time slice can be selected, which will be used in calculating the above mentioned amplitudes for all pads.

There is a provision to read in events from two separate sources to enable comparison between events. The difference of the ADC spectra for each pad between these two events can be displayed in another popup window.

Another popup window displays drifttime versus pads in one padrow. Each timebucket is represented by a green rectangle, where the intensity reflects the pulse height. Overflowed timebuckets are shown as red rectangles. This display provides a quick overview of the hit distribution in the plane perpendicular to the beam direction. A region of interest in this display can be magnified for a more detailed inspection. The padrow to display can be chosen with a slider.

Recently, the Pad Monitor has been used in testing the new NA35 electronics developed at LBL For this purpose additional windows to control the test stand and to histogram the test results were added. To document the tests, selected histograms can be printed on a laserprinter.

This tool proved useful in debugging the detector and electronics as well as to provide a quick overview of the topology of an online event. The program is easily adaptable to new detector geometries and will be used again in the April 1992 run of NA35.

Footnotes and References

[1] H. Wieman, private communication, February 1991

Interactions of 15 A GeV Au at $\theta < 15$ mrad Leading to Composites with $|Z|/\beta \geq 60$

Y.D. He and P.B. Price

Five stacks of detector/target combinations will be exposed to defocussed beams of 15 A GeV Au in the run of April 1992 at AGS. A new type of detector – BP-1 phosphate glass – will be used in these exposures. A single sheet of BP-1 can achieve a charge resolution of 0.2e and several sheets stacked together can achieve a charge resolution as low as 0.05e, which is good enough to enable a search for fractional charged nuclei. The most extraordinary aspect of this detector is that , in a sampling distance of only 30 μm, it can measure the instantaneous ionic charge state of ions as heavy as uranium. By using one of three different etchants, the sensitivity of any particular sheet can be tuned after the exposure, which enables us to zero in on a particularly interesting kind of process in mid-investigation.

These three unique advantages of BP-1 glass allow us to study various processes taking place when a 10 A GeV Au beam passes through various targets. Examples include the following phenomena:

- Projectile fragmentation, both nuclear and electromagnetic spallations
- Nuclear charge pickup process
- Ionic charge state distribution
- Possible production of fractional charges
- Dependence of detector response on velocity (β=0.996 compared to 0.87)
- Possible production of exotic composites (e.g., Lee-Wick matter) with $Z > 79$ and $\tau \geq 10^{-10}$ sec in central collision

Search for Fractional Charge States in High-Energy Heavy Fragments Produced in Collisions of 14.5 A GeV ^{28}Si with Pb and Cu Targets*

Y.D. He and P.B. Price

We used nuclear track detectors to construct the trajectories of interactions and to measure with high resolution the charge of the beam and of heavy nuclear fragments produced in interactions. A null result of our search for fractional charge states in high-energy fragments with charges $8 \leq Z \leq 13$ produced in collisions of 14.5 A GeV ^{28}Si nuclei with Pb and Cu targets leads us to conclude that the upper limits for the probability of production of a fragment with charge $\frac{23}{3}, \frac{25}{3}, \frac{26}{3}, \frac{29}{3}, \frac{31}{3}, \frac{32}{3}, \frac{34}{3}, \frac{35}{3}, \frac{37}{3}$, or $\frac{38}{3}$ charge unit in Pb and Cu at 90% confidence level are 1.9×10^{-4} and 3.9×10^{-4}, respectively. We set a similar limit on the relative number of particle-stable fragments with $8 \leq Z \leq 14$ created in the central rapidity region.

Footnotes and References

*Condensed from *Phys. Rev. C* **44**, 1672 (1991).

Search for Particles with $|Z| \geq 3$ and Negative Charge or Large A/Z Produced in Central Nucleus-Nucleus Collisions at AGS

P. B. Price, Y. D. He and D. M. Lowder

We will be performing two experiments that will use CR-39 plastic track-recording detectors to study production of multiply charged composites in central collisions, and in particular to search for both positively and negatively charged mid-rapidity particles with $|Z| \geq 3$, especially those with anomalously large A/Z. Three features unique to these experiments and important for strange quark matter searches are their sensitivity to particles with lifetimes as short as 10^{-9} sec, their sensitivity to particles with unusually large transverse momenta, and their huge coverages in phase space region.

In the first experiment, scheduled for the AGS run in March 1992, we will expose a 3-cm thick Pb target to ~ 10^{12} Si ions of 14.5 A GeV without collimators and magnet. Downstream 75-cm from the target, 17 detector modules – each consisting of 12 repeating units (1 unit = 3 0.75-mm sheets of CR-39 + 0.67-cm of Pb absorber) will be mounted on a plus-sign shaped frame. For particles with $|Z| \geq 3$ produced in a large forward cone, ~ 0.015 rad $\leq \theta \leq$ 0.3 rad, $|Z|/\beta$ and A will be determined by measuring the etchpit size and its rate of change with distance as the particles slow. The plus-sign shaped frame and 17 detector modules have been constructed. To increase the sensitivity, new CR-39 plastics that contain 100 ppm naugard additive have been made and their sensitivities have been evaluated in a calibration at the LBL Bevalac. After the AGS run, we expect up to 10^5 particles to be identified in one year of automated track-measurement and off-line data analysis.

In the second experiment, we will search for negatively charged objects with $|Z| \geq 3$ produced in central collisions of 10^{11} Si ions in a Pb target. Three tracking chambers inside a magnet with BDL = 1~2 T-m – each consists of 25 rigidly mounted sheets of CR-39 separated by 2-cm air gaps with no Pb absorbers – will record the curvature of objects at mid-rapidities with $|Z| \geq 3$ and identify their charges. This experiment will be a ideal detector for strangelet searches, because for negatively charged particles with $|Z| \geq 3$, there is no intrinsic background expected; also, Greiner and Stocker [1] have calculated that, for a reasonable choice of parameters, negatively charged strangelets may be more likely than positively charged strangelets. This experiment will be scheduled for a run in 1993.

References

1. C. Greiner and H. Stöcker, *Phys. Rev. D* **44**, 3517 (1991).

Upper limit on the cross section for nuclear charge pickup by relativistic uranium ions*

Andrew J. Westphal, Buford Price and Daniel P. Snowden-Ifft

We have recently discovered that BP-1, a track-etch detector of remarkably high sensitivity which we developed several years ago [1], exhibits extremely good charge resolution, about 0.16e, in measurements of uranium ions down to energies as low as 500 MeV u^{-1} . Such resolution enables us to make direct measurements of the mean free paths for electron capture and loss in the glass detector [2], to measure cross sections for charge-changing fragmentation, and to search for nuclear charge pickup.

We have searched for examples of nuclear charge pickup by relativistic uranium ions in targets of both uranium and phosphate glass. We find none, which allows us to set an upper limit of 7.7 mb per target atom at the 90% confidence level on the cross section for this process. An extrapolation of the approximately quadratic dependence on projectile charge of the cross section for charge pickup predicts a cross section which would be ~10 times larger. Fig. 1 shows the dependence of the cross section for nuclear charge pickup on projectile charge for relatistic beams.

We infer from measurements [3] of the relative rates of neutron emission Γ_n and of fission Γ_f from excited nuclei that an excitation energy no more than a factor of five higher than the neutron evaporation energy $E_{evap} \simeq 8$ MeV would be sufficient to ensure that most of the hot nuclei fission before they reach their ground states. That the projectile nucleus should have an excitation energy greater than 40 MeV after the charge-pickup process is likely. Thus the observed scaling violation can be understood in terms of the propensity of the actinides (in this case, neptunium) to fission upon the deposition of even a small amount of excitation energy.

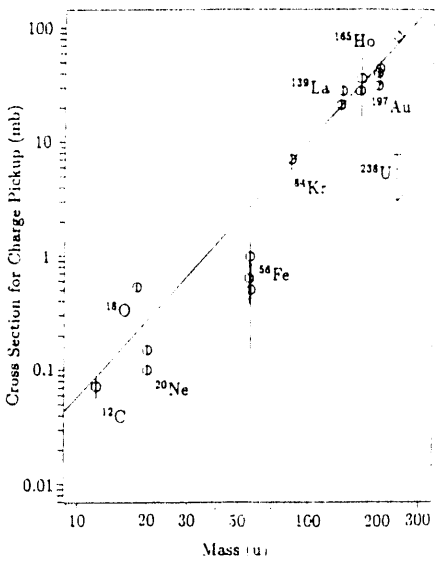

Fig. 1. The dependence of the cross section for nuclear charge pickup on projectile charge for relatistic beams. References are found in our paper. [4]

Footnotes and References

*Accepted by Physical Review C

[1] Shicheng Wang *et al.*, Nucl. Instrum. Meth. **B35**, 43 (1989).

[2] R. Anholt, Phys. Rev. A **31**, 3579 (1985); W. E. Meyerhof, *et al.*, Phys. Rev. A **32**, 3291 (1985)

[3] A. Gavron *et al.*, Phys. Rev. C **13**, 2374 (1976)

Footnotes and References

[4] Westphal *et al.*, Upper limit on the cross section for nuclear charge pickup by relativistic uranium ions, accepted by Phys. Rev. C.

The Crystal Barrel Spectrometer at LEAR

K.M. Crowe, D.S. Armstrong, J. Bistirlich, R.R. Bossingham, H. Bossy, T. Case, and the Crystal Barrel Collaboration

The Crystal Barrel spectrometer is a detector optimized for the study of low-energy $\bar{p}p$ and $\bar{p}n$ annihilations at the Low Energy Antiproton Ring (LEAR) facility at CERN. The study of low-energy antiproton annihilations is of interest primarily for two reasons. The first is to study the annihilation process itself, by measurement of branching ratios and cross sections of the primary reactions, with the aim of testing various theoretical descriptions. These descriptions can be either conventional meson/baryon exchange models or quark/gluon approaches; the latter is of particular interest as a test of QCD in the low-energy domain. The second motivation is the spectroscopy of light meson resonances and the search for non-$q\bar{q}$ (exotic) states. $p\bar{p}$ annihilations are a rich source of ordinary $q\bar{q}$ mesons such as π, η, and ω. QCD, however, predicts the existence of a host of exotic particles such as multi-quark states ($q\bar{q}q\bar{q}$), states of pure glue (glueballs) and hybrids ($q\bar{q}g$). The definitive observation of such states would provide a dramatic confirmation of the validity of QCD. While low-energy $p\bar{p}$ annihilations have been studied for decades, the roughly 60% of annihilations that proceed via channels containing more than one neutral particle have been almost unexplored. This is the motivation for the Crystal Barrel detector which provides almost 4π solid angle for the detection of both photons and charged particles (*i.e.* $\pi^{\pm}$, $K^{\pm}$). This allows a kinematically complete reconstruction of complicated final states with several particles decaying into photons (e.g. $\pi^0 \rightarrow \gamma\gamma$, $\eta \rightarrow \gamma\gamma$).

Fig. 1 shows a cutaway view of the detector, which is located in a magnet producing a 1.5 T field. Surrounding the liquid hydrogen or deuterium target are two cylindrical multiwire proportional chambers, which provide fast trigger information on the charged particle multiplicity of the event and rϕ coordinates for charged particles close to the annihilation point. Surrounding these chambers is the main charged-particle tracking detector, a cylindrical Jet Drift Chamber (JDC). The JDC, which was designed and built at LBL, is described elsewhere in this report. Outside the JDC is the barrel-shaped electromagnetic calorimeter, which consists of 1380 individual CsI(Tl) crystals, with each crystal pointing to the detector center. The calorimeter covers polar angles of 12° to 168° with almost complete coverage in the azimuthal angle, for a total solid angle of 95% of 4π. The photon energy resolution is about 2.5% (σ) at 1 GeV with an angular resolution of 28 mrad (σ) for isolated showers. To date, approximately 4.6×10^7 events have been recorded, mostly with a stopping $\bar{p}$ beam. Data analysis is well underway, and more data will be obtained over the next few years, largely to be taken in flight at up to 1.8 GeV/c.

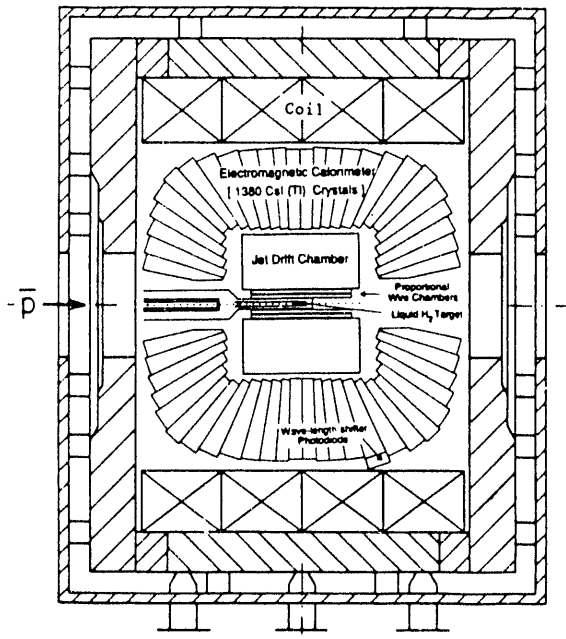

Fig. 1. Cutaway view of the Crystal Barrel detector.

The Crystal Barrel Jet Drift Chamber

K.M. Crowe, D.S. Armstrong, J. Bistirlich, R.R. Bossingham, H. Bossy, T. Case, and the Crystal Barrel Collaboration

The Jet Drift Chamber (JDC) for the Crystal Barrel spectrometer at LEAR was designed and constructed at LBL. It has a jet-chamber type of drift cell, and is divided into 30 azimuthal sectors and 23 radial layers with 8 mm spacing. The inner (outer) wires are at a radius of 63 mm (239 mm), with a sensitive length of 399 mm, giving a detection solid angle of 95% of 4π. The azimuthal segmentation keeps drift times relatively short, and the radial segmentation allows sufficient ionization samples to provide dE/dx resolution adequate to distinguish $\pi^{\pm}$ from $K^{\pm}$ for momenta up to about 500 MeV/c.

The 690 sense wires are 20 μm diameter stainless steel (Elgiloy) and are strung axially. A resistive (29.7 Ω/cm) wire is used so that the z-coordinate of each hit can be determined by charge division. The anode sense wires in each sector are staggered in the azimuthal direction by ± 200 μm to resolve the right-left ambiguity. The grounded sense wires are alternated on the sector midplane by cathode guard wires to control the gas gain. The guard and field wires (2430 in total) are 152 μm diameter gold-plated aluminum. Aluminum was used to minimize energy loss and multiple scattering in the wires. The wires were crimped into gold-plated brass pins, around which are molded Delrin bushings. The bushings were glued directly into holes in the aluminum end plates, yielding an overall wire position accuracy of $\pm 40\mu$m.

The signals from each end of the sense wires are amplified by 24-channel AC-coupled surface mounted preamplifier cards[1] mounted on each endplate of the JDC. Outside the detector the signal wires are regrouped from a sector to a layer configuration to distribute the load on the readout processors evenly. The differential signals are sent to Struck DL300V amplifier boards and are digitized by Struck DL305 and DL310 100 MHz flash ADC's, used in a non-linear mode to enhance the dynamic range to an effective 8 bit resolution. Signals from selected layers of wires are separately discriminated and summed to provide a fast charged-multiplicity trigger decision which is available after 4 μs.

The JDC was designed as a relatively low-mass device to minimize losses due to charged and neutral particle interactions before the calorimeter. The inner cylinder is made from 0.73 mm thick carbon fiber, corresponding to 0.0025 of a radiation length (X_0). The outer shell, made of 2.0 mm of Al, contributes 0.03 X_0. The gas and the wires contribute 0.0010 and 0.0007 X_0 respectively; the chamber endplates and electronics are relatively massive and represent about 0.20 X_0 for particles intersecting them. The "slow gas" used is a 90:10 mixture of CO_2/isobutane at atmospheric pressure. For a 1000 V/cm drift field in a 1.5 T magnetic field the electron drift velocity is 8.4 μm/ns and the Lorentz angle is 7.2°. The drift velocity in such an unsaturated gas is strongly dependent on temperature, gas mixture and pressure. For a maximum position error of 30μm, the temperature of the JDC must be known to ± 0.36°C, the CO_2 content to $\pm 0.15\%$ and the absolute pressure to $\pm 0.12\%$. The first two parameters are controlled and monitored, while the pressure is recorded for offline correction during data analysis.

The JDC has performed very successfully to date. The position resolution achieved is 125 μm (σ) in the r-ϕ plane and 7-9 mm (σ) in the z-coordinate.

Footnotes and References

[1] C.C. Lo, S. Olson, and J. Bistirlich, IEEE Trans. on Nucl. Sci. 36(1989)462.

Observation of a tensor resonance at 1515 MeV in proton-antiproton annihilation at rest*

K.M. Crowe, J. Bistirlich, R.R. Bossingham, H. Bossy, T. Case, and the Crystal Barrel Collaboration

An analysis of 1.2×10^6 all-neutral $p\bar{p}$ annihilation events obtained with the Crystal Barrel detector at CERN has been made to select the $3\pi^0$ final state (this represents 10% of the total all-neutral statistics now on tape). Events with 6γ and no charged particles were selected, and an initial kinematic fit to total energy and momentum balance was made. 104K events were selected that satisfied these fits with > 10% probability. Kinematic fits were then made to each of the hypotheses $p\bar{p} \rightarrow \pi^0\pi^0\pi^0$, $p\bar{p} \rightarrow \pi^0\pi^0\eta$, $p\bar{p} \rightarrow \pi^0\eta\eta$, and $p\bar{p} \rightarrow \pi^0\pi^0\gamma\gamma$ (from $\omega\omega$) via the decays $\pi^0 \rightarrow \gamma\gamma$, $\eta \rightarrow \gamma\gamma$ and $\omega \rightarrow \pi^0\gamma$. Selecting events which satisfy the first hypothesis with > 10% probability yields 55K events with < 1% background from ambiguous events which satisfy more than one hypothesis. A partial wave analysis was made to the $3\pi^0$ Dalitz plot, and indicates the existence of a resonance at 1515±10 MeV with width 120±10 MeV, decaying into $\pi^0\pi^0$, with quantum numbers $J^{PC} = 2^{++}$; we label this state $X_2(1515)$. The projection of the Dalitz plot onto the $\pi^0\pi^0$ invariant mass axis is shown in Fig. 1. The $X_2(1515)$, along with the $f_2(1270)$, is apparent at high mass; the enhancements at low mass are due to the $\pi^0\pi^0$ s-wave interaction and reflections from the high-mass resonances. The $X_2(1515)$ is also clearly seen in preliminary analysis of annihilation in deuterium with a spectator neutron.

The $X_2(1515)$ cannot be identified with the well-known $f_2'(1525)$ which has the same quantum numbers and is nearly degenerate in mass because we do not see the dominant decay mode into $K\bar{K}$ characteristic of this meson. We cannot determine the isospin of the $X_2(1515)$ from these data alone, but if it is identified with either the 1565 MeV 2^+ state observed previously at LEAR by the ASTERIX group[1] or with the isoscalar two-pion resonance postulated by Gray *et al.*,[2] then the I=0 assignment is favoured. The $X_2(1515)$ is unlikely to be the first radial excitation of the $f_2(1270)$ since this is predicted to lie around 1.82 GeV, making the $f_2(1810)$ the preferred candidate. Therefore it appears probable that this particle is an exotic (non-$q\bar{q}$) state. It is unlikely to be a glueball, since it is not observed in radiative J/ψ decays, so it appears likely to be a four-quark state or an N-$\bar{N}$ state.

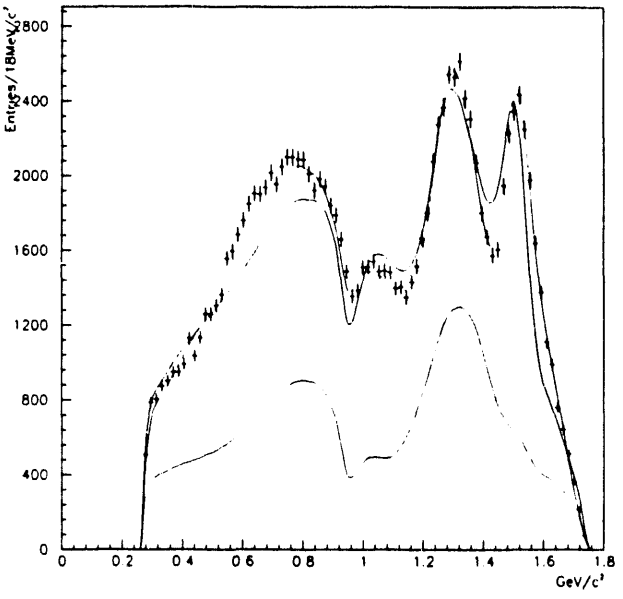

Fig. 1. The $\pi^0\pi^0$ invariant mass spectrum (projection of the $3\pi^0$ Dalitz plot). The solid line shows the final fit. The dashed line shows the fit including an X(1515) but with J=0, the dotted line shows the fit without the $X_2(1515)$ and the dash-dotted line shows the contribution of the $\pi^0\pi^0$ s-wave interaction to the final fit.

Footnotes and References

*E. Aker *et al.* , Phys. Lett. B260(1991)249.

Footnotes and References

[1]B. May *et al.* , Phys. Lett . 225B(1989)450.
[2]L. Gray *et al.* , Phys. Rev. D27(1983)307.

Theory

Gravity Wave Limits on Rotating Neutron-stars

Norman K. Glendenning and Fridolin Weber

Motivated by the increasing discovery rate of fast pulsars in globular clusters, we have undertaken a broad study of the structure and stability of rotating neutron stars. Since the numerical solution of Einstein's equations in the case of rotation is very cumbersome we have investigated a perturbative method, pioneered by Hartle and Thorne, and improved upon by us, by incorporating a self-consistency condition when computing the Kepler frequency, which is an absolute bound on rotation, since it is the frequency at which mass will be shed at the equator[1] [2]. We established the accuracy of the improved method to periods $\sim 1/2$ ms. As it turns out, this is about as small a period as a neutron star can have, since there are additional constraints, namely stability to gravitational radiation-reaction modes. Having established the method, we have selected a large number of equations of state based on both relativistic many-body theory, and the non-relativistic results of Wiringa et al. to include in a study of the physical properties of rotating stars[3] [4]. Another important facet of the investigation included the calculation of stability of rotating neutron stars to unstable vibrational modes which radiate the angular momentum of the star in gravity waves[5] [6]. These modes are strongly effected by the viscosity of the star and so depend sensitively on its temperature. For a pulsar that remains isolated, the limiting frequency is set in its very early history when it is hot and its viscosity is low. We find that these modes are unstable at frequencies that are higher than about 60-70 % of the Kepler frequency, and so set the true limits on rotation. For cold stars that have been spun up by accretion from a companion, the gravity wave limitations are less severe, and amount to 80-90 % of the Kepler frequency. Effectively what this means is that the shortest stable period for a neutron star is about a millisecond (see Fig. 1). If shorter period pulsars are found, they would be difficult to understand as gravitationally bound neutron stars.

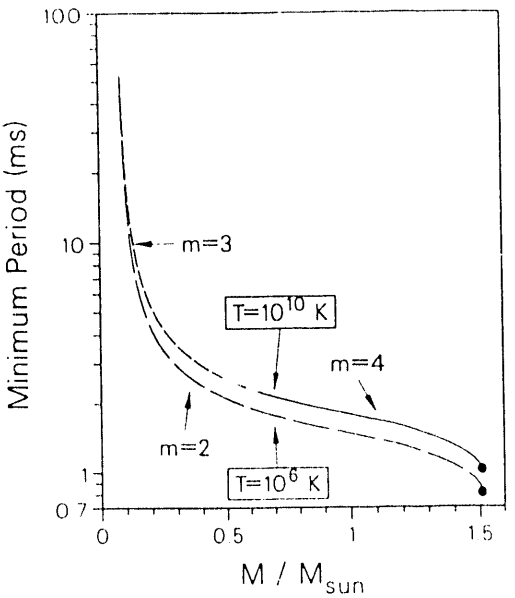

Fig.1 Minimum stable period against gravity-wave viscosity-moderated instability for a sequence of stars as a function of their mass at two temperatures corresponding to young and old stars.

Footnotes and References

[1] F. Weber and N. K. Glendenning, Phys. Lett. **265** (1991) 1.

[2] F. Weber and N. K. Glendenning, Astrophys. J. in press May 1992.

[3] F. Weber, N. K. Glendenning and M. K. Weigel, Invited paper in Proceedings of Second International Conference on Medium and High Energy Physics, Part A, p. 309, Taipei, May, 1990, (North Holland, Amsterdam, 1991).

[4] F. Weber and N. K. Glendenning, in *Proc. Int. Workshop on Unstable Nuclei in Astrophysics*, June 7-8, 1991, Tokyo, (World Scientific, in press) LBL-30726, June 1991.

[5] F. Weber and N. K. Glendenning, Astrophys. J. **373** (1991) 579.

[6] F. Weber and N. K. Glendenning, Z. Phys. A **339** (1991) 211.

First Order Phase Transitions with More than One Conserved Charge

Norman K. Glendenning

We extended the discussion of first order phase transitions to the general case that there is more than one conserved charge in the system[1]. Compared to the well known case of a single conserved charge, the differences are dramatic. The constancy of the pressure at all proportions of phases in equilibrium in the latter case is peculiar to there being but one conserved 'charge'. When there is more than one, the mixed phase has degrees of freedom that are otherwise not available: The charges are conserved over all, but not necessarily separately or in proportion to the phases in equilibrium. The internal forces will optimize the $n-1$ concentrations of the charges in the mixed phase, a degree of freedom available only for complex systems ($n > 1$). We show that nothing else is compatible with equilibrium in the mixed phase. We show the phase diagram in Fig. 1 for a system haveing two independent components.

Many systems in physics and astrophysics that undergo phase transitions are complex but have been fitted into the mold of a simple one by approximation. Consequences in the case that we have examined, the transition from the hadronic phase to quark-matter in a neutron star, are drastic. To assess whether neutron stars are likely to have quark cores, many authors approximated both phases as the equivalent of pure neutron matter. But neutron matter is beta unstable and the corresponding quark phase especially so. This latter fact leads to an estimate of the density at which neutron stars convert to quark matter of $\sim 10\rho_0$ and therefore beyond their densities, whereas when beta-equilibrium is accounted for we find $\sim 3\rho_0$. Furthermore, there are structural differences in the star model that result from the treatment of the phase transition as if it occurred in a simple body. The mixed phase in a simple body cannot exist in the presence of gravity. This causes a discontinuity in the density distribution in the star occurring at the radius where Gibbs criteria are satisfied. When beta equilibrium is properly treated, involving as it does both the conserved baryon and electric charge, the transition region is smoothed out; the density distribution is continuous. The mixed phase occupies a finite region of the star, the the inner sphere of seven kilometers radius. Quarks dominate within the central 5 km radius[2]. We expect the mixed phase to consist of a Coulomb lattice of regions of hadronic matter interspersed with quark matter, both electrically charged, and to evolve as a function of proportion of phases through a variety of geometrical shapes.

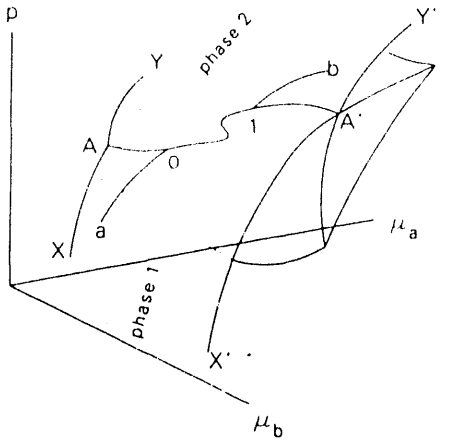

Fig.1 For a system having two conserved charges, the physical path of pressure in phase 1 is 'a0', in the mixed phase is, '01', and in phase 2 is '1b'.

Footnotes and References

[1] N. K. Glendenning, *Phase Transitions with More than One Conserved Charge: Consequences for Neutron Stars.* LBL-30295, March 1991.

[2] N. K. Glendenning, in *Proceedings Workshop on Strange Quark Matter in Physics and Astrophysics*, Aarhus, Denmark, May 1991, ed. by J. Madsen and P. Haensel, Nuclear Physics B (Proc. Suppl.) **24B** (1991).

Hypernuclei and Neutron-star Mutual Constraints

N K. Glendenning and S. A. Moszkowski

It was conjectured as early as 1960 that neutron stars would contain a population of hyperons, and many papers have computed their presence based on various idealizations of the interaction of the hyperons. It has remained a vexing problem how to convincingly constrain the strength of the interactions and hence the extent of the populations, and the degree to which the hyperons soften the equation of state and reduce the limiting mass of neutron-stars. We[1] have solved this problem by combining information on (1) neutron star masses, (2) the Λ binding in saturated nuclear matter, and (3) the positions of hypernuclear levels in finite nuclei. The Λ binding is expressible in terms of the strength of scalar and vector fields at saturation, S and V, and the ratio of the hyperon to nucleon scalar and vector couplings x_σ and x_ω, as in the equation:

$$-28 \text{ MeV} = x_\omega V - x_\sigma S.$$

The effect of all three constraints are show by the boxed area in Fig. 1. Taken together, these constrain the hyperon couplings sufficiently that it is possible to deduce that the limiting neutron star mass is reduced by the presence of hyperons by $0.71 \pm 0.15 M_\odot$ and that neutrons consitute only a *slight* majority population in neutron stars, 59 %, with hyperons being the next largest group, 24 %, followed by protons, 17 %. This is in strong contrast with the much of the astrophysical literature that evaluates the effect on cooling rates and transport properties of neutron stars based on very old early estimates of neutron stars as being almost purely neutron with a few percent admixture of protons.

While not directly observable, the presence of hyperons have been shown to influence appreciably the cooling of neutron stars, and they are likely to effect the electrical conductivity, which in turn determines the decay rate of the magnetic field.

The simple relation written above should be of use in future analysis of hypernuclei for such as have been made to date show a large correlation error when x_σ and x_ω are treated independently. The above equation shows that they are strictly correlated by the inferred binding of the Λ in nuclear matter and this relation should be employed to reduce the parameters by one.

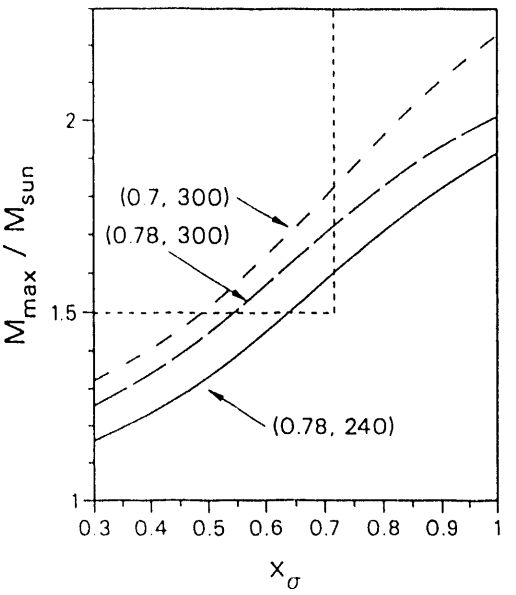

Fig.1 Curves of Maximum mass stars labeled by several values of nucleon effective mass at saturation and compressibility. Their segments in the box are the allowed values according the the constraints discussed.

Footnotes and References

[1] N. K. Glendenning and S. A. Moszkowski, Phys. Rev. Lett. **67** (1991) 2414.

Neutron-stars in the Derivative Coupling Nuclear Field Theory Model

N K. Glendenning, F. Weber and S. A. Moszkowski

By employing a point and derivative coupling of baryons to meson fields, with only two coupling constants we are able to account very well for the four bulk nuclear properties $\rho_0, B/A, K, m^*$. Encourage by this we have employed the theory to compute a wide range of neutron-star properties, perhaps the largest collection of properties computed for a single model[1]. The baryon and interaction part of the Lagrangian are;

$$\mathcal{L} = \sum_B \Big[\Big(1 + \frac{g_{\sigma B}\,\sigma}{2m_B}\Big) \Big\{ \overline{\psi}_B [i\gamma_\mu \partial^\mu - g_{\omega B}\gamma_\mu \omega^\mu - \tfrac{1}{2} g_{\rho B}\gamma_\mu \boldsymbol{\tau}\cdot\boldsymbol{\rho}^\mu]\psi_B - \Big(1 - \frac{g_{\sigma B}\,\sigma}{2m_B}\Big) m_B \overline{\psi}_B \psi_B \Big] \quad (1)$$

The sum on B is over nucleons and hyperons. The hyperon to nucleon coupling ratios satisfy a relation relating to the Λ binding in nuclear matter[2]. From the Weisskopf relation at saturation between the Fermi energy and the energy per nucleon of a self-bound system, $e_F = (\epsilon/\rho)_0$, which is a special case of the Hugenholtz-Van Hove theorem, we obtain for the binding energy of the lowest Λ level in nuclear matter,

$$\Big(\frac{B}{A}\Big)_\Lambda = x_\omega V + m_\Lambda^\star - m_\Lambda = x_\omega V - \frac{x_\sigma S}{1 + x_\sigma S/(2m_\Lambda)}, \quad (2)$$

where S, V are the scalar and vector strengths at saturation of nuclear matter and the x's are the ratios of hyperon to nucleon couplings for scalar and vector mesons.

Among the properties that we compute are the stable modes against gravitational radiation as moderated by viscosity. The critical frequency of the $l = m$ mode is the values of Ω that solves (eg. Lindblom),

$$\Omega_m = \frac{\omega_m}{m}\Big[\alpha_m(\Omega_m) + \gamma_m(\Omega_m)\Big(\frac{\tau_{G,m}}{\tau_{V,m}}\Big)^{\frac{1}{2m+1}}\Big]. \quad (3)$$

where the various quantities are defined in ref. 1. The gravitational wave instability effectively limits the period of neutron stars to $P > 1$ ms unless, as cold stars, they have been spun up by accretion. Then the period can be slightly smaller. The period of the fastest pulsar known so far, $P = 1.56$ ms, is easily accommodated by the theory of dense matter discussed here whether or not a phase transition to quark matter has occurred.

We also computed additional properties such as the masses, baryon populations, effects of beta equilibrium on these, the relativistic Kepler frequency, moment of inertia, surface redshift, mass-radius relations.

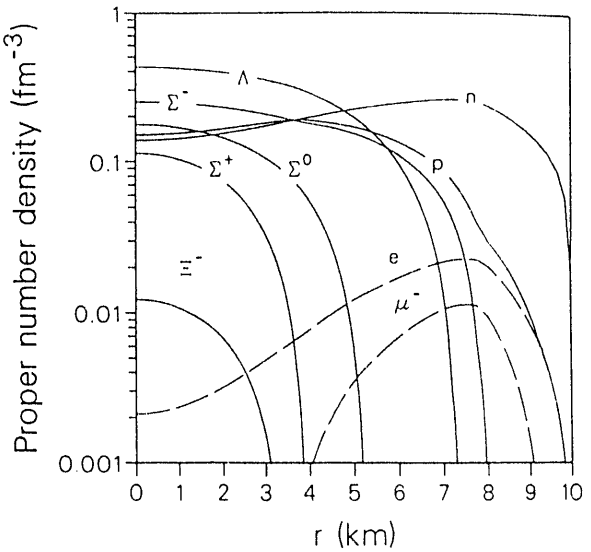

Fig.1 Populations in the limiting-mass neutron-star.

Footnotes and References

[1] N. K. Glendenning, F. Weber and S. A. Moszkowski, Phys. Rev. in press

[2] N. K. Glendenning and S. A. Moszkowski, Phys. Rev. Lett. **67** (1991) 2414.

Variational Limit on the Rotation Period of Gravitationally Bound Stars

N K. Glendenning

Limits are frequently of interest as a means of distinguishing between alternative descriptions of an observed phenomenon. For example, Rhoades and Ruffini (Ruffini 1974) derived an upper bound on the mass of a neutron star. It is $\sim 3.2M_\odot$. Several compact objects whose inferred mass is larger than this have been identified as candidates for moderate mass black holes on this basis. In this note we derive a lower limit on the rotational period of a gravitationally bound star[1]. Our purpose here is to provide a decisive means, based on their rotational periods and masses, of distinguishing between pulsars that *can* be neutron stars, or more generally gravitationally bound stars, and pulsars that *cannot*. It is timely that such a limit be established for the period of rotation. Since the discovery of the first millisecond pulsar in 1982 the discovery rate of fast pulsars has quickened, culminating in the recent observation (summer 1991) of ten in a survey of the globular cluster 47Tucanae by Manchester and Lyne. The minimum possible period of rotation of a neutron star is established on the basis of (1) Einstein's theory of relativity, (2) causality, (3) Le Chatelier's principle, (4) the existence of a neutron star of at least $1.442M_\odot$, and (5) a low density equation of state, uncertainties in which can be evaluated as to their effect on the result. We also examined the effect on the minimum period of a first order phase transition and of neglecting causality. The uncertainty in the period introduced by any of the above effects is less than 10 %. The minimum possible Kepler period, which is an absolute limit on rotation below which mass-shedding would occur, is 0.33 ms within the above uncertainty of about ± 0.03 ms. We also obtained a limit on the rotational period based only on the assumption that Einstein's equations of stellar structure hold. It is,

$$P > 0.15(M/M_\odot) \text{ ms} \qquad \text{(any star)}.$$

Our limit provides a decisive method of distinguishing neutron stars from stars (if they exist) which consist of stable self-bound matter of sufficiently large equilibrium density. Examples of the latter are strange-stars and Q-stars. Neutron-stars (or in general any gravitationally bound star) can lie only on or above the solid line in Fig. 1, while self-bound stars can also lie between the solid line and the GR forbidden region.

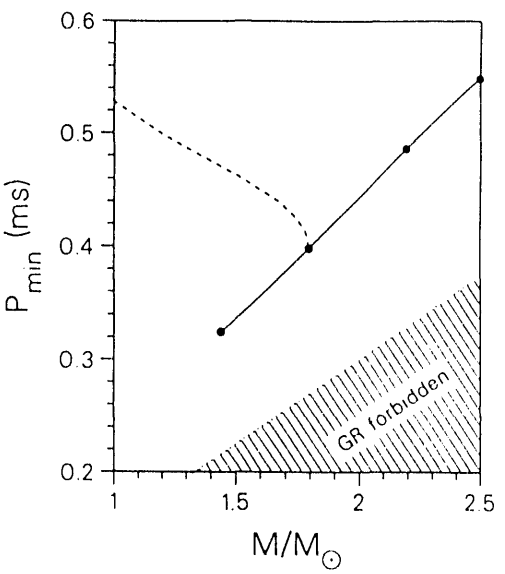

Fig.1 Minimum rotational periods of neutron-stars (solid line). Periods of a star sequence of limiting mass $1.8M_\odot$ (dashed line). Region forbidden by general relativity (shaded region).

Footnotes and References

[1] N. K. Glendenning, *Variational Limit on Rotation Period of a Neutron Star* LBL - 31511, Dec 1991.

N-Body Collisions in High-Energy Nuclear Reactions*

G. Batko, J. Randrup, and T. Vetter†

We have developed a treatment that incorporates many-body scattering processes in a dynamical BUU-type simulation of a nucleus-nucleus collision.

We have first made a detailed study of the three-nucleon scattering. The corresponding differential distribution has been calculated on the basis of a simple pion-exchange graph, with an off-shell intermediate baryon between two sequential pion exchanges. For a spatially uniform system, we have studied the evolution in momentum space for initial distributions describing interstreaming gases corresponding to the kinematics of high energy nuclear collisions. Particular attention has been paid to the yield in the backwards direction. Using statistical three-nucleon scattering in the idealized scenario, we have found that the backwards region is indeed more favored, but only early on in the reaction; subsequent collisions drive the momentum distribution towards the equilibrium distribution, which is independent of the specific collision mechanisms employed.

The inclusion of N-body collisions in a realistic dynamical simulation has been based in a BUU transport equation with an extended collision integral that allows the description of higher order scattering processes. We have examined the role of the particles situated in the proximity of two given collision partners. Using the energy-dependent interaction distance between two baryons, we have established a criterion for determining how many baryons in the environment may affect a given two-body collision, which provides a mean for classifying each collision event according to its cluster size N. Then, invoking the assumption of complete statistical sharing between the particles in a collision cluster, we have formulated a general treatment of the many-body scattering for any value of N. On this basis, we have examined the effect of N-body collisions for the collision of two calcium nuclei at bombarding energies ranging from 200 to 1000 A MeV. Overall, there is little effect in the commonly employed global observables, such as the flow tensor, the transverse momentum distribution, even though about half of the collision clusters contain more than two particles.

We have given special consideration to the effect of the many-body scattering on the subthreshold production of particles, since one might expect that such processes would be enhanced because of the larger amount of energy present of a many-body cluster, relative to the ordinary binary situation. We generalized the statistical model to particle production, assuming that the additional particles in a given cluster share their energy statistically with the two primary particles responsible for the production. This leads to a relatively simple and general model and we have applied it to kaon production in Ca-Ca collisions. Remarkably, despite the fact that about half the kaon are produced from clusters with $N > 2$, the net effect is rather small. This can be qualitativerly understood by realizing that the additional particles in a given cluster act as a reservoir that may not only contribute energy but also drain energy away from the producing particle pair. The determining feature is then the effective temperature of the clusters and this quantity is not very dependent on the cluster size N, since all the clusters are drawn from the same system.

In conclusion, then, we find that the results of the standard BUU dynamical simulations are not appreciably affected by the incorporation of many-body collisons. This simplifying feature supports this model as a quantitatively useful tool for nuclear reactions at relativistic energies.

Footnotes and References

*Preprint LBL-31031; Nucl. Phys. A536 (1992) 786.

†Institut für Theoretische Physik, Justus-Liebig-Universität Giessen, Germany.

Effect of N-Body Collisions on Subthreshold Kaon Production in High-Energy Nuclear Reactions*

G. Batko, J. Randrup, and T. Vetter†

As a supplement to our recent incorporation of N-body collisions into BUU simulations of nuclear reactions[1] we have considered the differential production cross section of subthreshold kaons. The general assumption of microcanonical exchange of energy between the colliding baryons and their neighbors has been augmented by the assumption that the produced particle has a momentum distribution reflecting the corresponding final three-body phase space. The resulting model then provides a conceptually simple, yet very general, scheme for taking account of the proximity of additional baryons in the nuclear medium.

We have specifically addressed the sensitivity of the differential kaon production cross sections to the inclusion of the N-body effects. The kaon is assumed to be produced in an elementary process of the form $B_1B_2 \rightarrow BYK^+$, where B denotes the final baryon and the hyperon Y is either a Λ or a Σ, and it is furthermore assumed that the corresponding differential cross section $d^3\sigma_{K^+}(\epsilon_{12})/d\boldsymbol{p}$ is known as a function of the relative energy ϵ_{12} of the two initial baryons B_1 and B_2. As a simple approximation, we assume that the momentum distribution of the kaon is proportional to the phase space associated with the three particles in the outgoing channel. In each such elementary process, the branching ratio $P_{K^+}(\boldsymbol{p})$ for producing a kaon with the specified momentum $\boldsymbol{p}$ is then given by the ratio between the associated differential production cross section and the elementary total interaction cross section,

$$P_{K^+}(\epsilon_{12};\boldsymbol{p}) = \frac{1}{\sigma_{B_1B_2}(\epsilon_{12})} \frac{d^3\sigma_{K^+}(\epsilon_{12})}{d\boldsymbol{p}} \,. \quad (1)$$

When N-body collisions are incorporated, the total energy available in the cluster, E^*, is first shared microcanonically between the N baryons in the cluster, before the two primary baryons produce the kaon. The resulting effective branching ratio is then obtained by averaging the elementary branching ratio (1) over all the microcanonical momentum configurations of the N-body cluster.

We have applied the model to head-on collisions of ^{40}Ca+^{40}Ca, ^{93}Nb+^{93}Nb, and ^{197}Au+^{197}Au. In these calculations we have ignored the rescattering of the produced kaons by the other hadrons in the system. The results suggest that, at least within the scope of the present model, the inclusion of N-body collision does not lead to a significant enhancement of the production of energetic kaons in the subthreshold energy regime. Of course, in the extreme tails of the spectra the relative enhancement will be large, but the associated absolute cross sections are then so small that the effect will probably be of little practical import.

We wish to emphasize that the model developed represents a very simple extreme in which there is full equilibration between the two primary baryons and their cluster partners. Generally speaking, the kaon yields are affected only rather little, and we understand this in a general way as a result of the statistical sharing of the energy between the kaon and the other baryons involved in its production.

Footnotes and References

*Preprint LBL-31828; submitted to Nucl. Phys. A

†Institut für Theoretische Physik, Justus-Liebig-Universität Giessen, Germany.

[1] G. Batko, J. Randrup, and T. Vetter, this report.

Spin-Orbit Coupling in Semiclassical Approximation*

Hans Frisk and Thomas Guhr

In quantum mechanics, the physical concept of spin is well incorporated into the theory, at least from a technical viewpoint. The spin and its $SU(2)$ character are intrinsic properties of the Dirac equation. The non-relativistic limit of this is the Pauli equation, i.e. the Schrödinger equation including a spin-orbit interaction. On the other hand, on a more figurative level, the question, how to imagine spin is often asked and not really satisfacorily answered since a direct and obvious classical analogue of spin is lacking. The probably closest classical picture for the concept of a quantum particle with spin is the motion of a top or a gyroscope with an intrinsic angular momentum besides the orbital one. This and similar interpretations give indeed a very instructive picture and are useful in many applications, although special features of spin like half-integer values, have disappeared. A detailed review can be found in Corben's book [1].

However, those approaches do not apriori address problems linked to the fundamental relation between classical and quantum mechanics since they are a somewhat ad hoc replacement of a quantal concept by a classical one. To go a step further, one has to ask the question, what happens to spin if one tries to derive classical equations from a given Schrödinger equation for a particle with spin by some semiclassical procedure. Apparently, the most natural idea is the attempt to keep the gyroscope like picture [2].

Nevertheless, we go a different way. We abandon the gyroscope like picture and try to construct a direct semiclassical approximation to a quantal Hamiltonian with spin-orbit interaction. Using WKB techniques [3] for multicomponent wave equations, we are able to preserve the discrete nature of spin by treating only the orbital motion semiclassically. Hence, we do not have to discuss an extended phase space, the effect of spin is just an additional force on the orbital motion. This implies enormous simplifications for our numerical studies. We focus attention on a spin-orbit interaction in a deformed system. The nuclei provide an obvious physical motivation.

Employing the theory of trace formulas we compare our classical results to quantum mechanical calculations which we also perform. The agreement is very good in most cases. We conclude that our semiclassical approach gives a clear and helpful new insight in the physics of spin and spin-orbit coupling.

We would like to emphasize that our system although motivated by nuclear physics is more the object of a general discussion to shed light on the role of the spin in semiclassical theories. At this stage of our investigations we do not intend to perform something like quantitative nuclear structure calculations. However, in rotating nuclei with extreme, superdeformed shapes an integer, or half-integer, quantization of the rotational angular momentum has been reported recently [4]. This remarkable observation encourages a careful study of the spin properties in these systems. Hence, at a further stage, our approach might be of some relevance in concrete applications.

Footnotes and References

*To be submitted to Annals of Physics (N.Y.)

[1] H.C. Corben, **Classical and Quantum Theories of Spinning Particles**, Holden-Day, San Francisco, 1968

[2] B. Milek and J. Reif, Z. Phys. **A339** (1991) 231; R. Arvieu, P. Rozmej and M. Ploszajczak, preprint University of Grenoble, 1991

Footnotes and References

[3] R.G. Littlejohn and W.G. Flynn, Phys. Rev. **A44** (1991) 5239

[4] F.S. Stephens et al., Phys. Rev. Lett. **64** (1990) 2623; F.S. Stephens et al., Phys. Rev. Lett. **65** (1990) 301

Fourier-Bessel Analysis in the Space of Ordinary and Graded 2×2 Hermitean Matrices*

Thomas Guhr

The scalar product of two vectors in arbitrary dimensions depends only on the lengths and the enclosed angle. Taking the exponential of the imaginary unit times this scalar product yields the plane wave. The Fourier-Bessel expansion of this plane wave in arbitrary dimensions is given by the generalized spherical Bessel functions for the radial and by the Gegenbauer polynomials for the angular part. The expansion is equivalent to finding the eigen functions of the Laplacian.

This concept can be transferred to the space of ordinary Hermitean matrices. The trace of the product of two matrices relpaces the scalar product that now depends on the eigenvalues and diagonalizing angles. The plane wave is the exponential of the imaginary unit times this trace. The corresponding Fourier-Bessel analysis of those problems is in general of higher rank. In the special case of 2×2 matrices, however, the problem can be reduced to a one rank problem. The radial part of the expansion of the plane wave is proportional to the spherical Bessel functions and the angular part is given by the spherical harmonics. The theory of the Laplacian can be generalized to the matrix case.

The next step is to consider graded Hermitean 2×2 matrices. A graded matrix contains commuting and anticommuting, i.e. Grassmann, variables as elements which satisfy

$$\eta_i \eta_j = -\eta_j \eta_i , \qquad i,j = 1(1)N \quad .$$

In particular, this means $\eta_i^2 = 0$. Consequently, all function of Grassmann variables are terminated power series. Integration and differentation can be defined consistently. In matrix space, an invariant graded trace and graded determinant can be constructed. A theory on groups, especially graded Lie groups is developed [1]. In our paper, the corresponding plane wave is expanded in graded Bessel functions and graded spherical harmonics. The latter depend only on anticommuting angles, they span a kind of Hilbert space and fulfil orthogonality and completeness relations. The index of the graded Bessel functions is a product of two anticommuting variables and thus commuting. Although the expansion itself is very analogous to the ordinary case, there are remarkable differences. The graded Bessel functions do not form a countable infinity of functions because of the structure of their index. Hence, shift operators do not exist. A gradient in the space of these graded Hermitean matrices is constructed and a theory of the Laplacian is designed. The graded spherical harmonics are eigen functions of the angular part and the graded Bessel functions are eigen functions of the thereby defined hybrid Laplacian.

In addition, a non canonical parametrization of the graded group $U(1/1)$ in the spirit of the Euler angles is introduced. The generators are evaluated and the Casimir operator is expressed in these coordinates. The corresponding Wigner functions, i.e. the matrix elements of the representation are derived

Further investigations and applications to high energy physics and random matrix theory are in progress.

Footnotes and References

*To be submitted to Journal of Mathematical Physics

Footnotes and References

[1] F.A. Berezin, **Introduction to Superanalysis**, MPAM vol. **9**, D. Reidel Publishing, Dordrecht, 1987

Evaluation of the GOE Level Density Using Graded Matrices*

Thomas Guhr

Random matrix theory reached a new culminating point when Efetov observed a connection to graded matrices [1]. Recently, it was shown that the use of graded matrices is something like an irreducible representation of random matrix ensembles and the calculation of the whole set of Dyson's correlation functions for the Gaussian Unitary Ensemble (GUE) was considerably simplified [2].

It is highly desirable to extent these methods to the Gaussian Orthogonal (GOE) and Symplectic Ensembles (GSE). Unfortunately, severe mathematical obstacles occur on this way. The reason is that the Itzykson-Zuber integral in the orthogonal and symplectic case can not be evaluated by the same means as in the unitary case. A closed solution is still lacking. Hence, in order to attack this problem, we perform a direct calculation for the simplest case, the level density of the GOE. This requires an explicit parametrization of the graded group $O(2/2)$ and a somewhat brute force evaluation of the Grassmann integrals. The result should give some insight in the structure of the Itzykson-Zuber integral in the non-unitary cases.

Footnotes and References

*In prepration

[1] K.B. Efetov, Adv. Phys. **32** (1983) 53

[2] T. Guhr, J. Math. Phys. **32** (1991) 336

Thomas-Fermi Fission Barriers*

W.D. Myers and W.J. Swiatecki

We have developed a model of average nuclear properties that can be used to discuss nuclear binding energies, sizes and charge distributions. The nuclear optical model potential, including its energy and isospin dependences can also be calculated. The interested reader should consult Parts I[1] and II[2] for a detailed description of this approach.

The binding properties of nuclei were fitted[3] (approximately) under the assumption that r_0 has the value 1.13, 1.16 or 1.19 fm. The resulting three sets of parameters were used to confront the predictions of the present model with measured nuclear fission barriers and charge distributions.

Fig. 1 shows three barrier calculations for $Z = 93$, $N = 136$ using the parameter sets for $r_0 = 1.13, 1.16, 1.19$. By taking $r_0 = 1.16$ fm the calculated barriers for the heaviest elements can be made to agree with measurements. However, the choice $r_0 = 1.16$ fm is unacceptable when the corresponding calculated charge distributions are compared with measurements.

The calculated charge distributions, for $r_0 = 1.16$, for a number of nuclei are systematically too low in the bulk. When the $r_0 = 1.13$ fm parameter set is used the bulk density and radius are in fair agreement with the measured values.

The integrity of the model, the accuracy of the unparameterized solutions and the amount of data brought to bear on the determination of the model's parameters are such that we are inclined to consider this discrepancy as the signal of a relatively small but definite piece of physics that is missing in the Thomas-Fermi treatment of average nuclear properties. We regard this as one of the principal conclusions of this work.

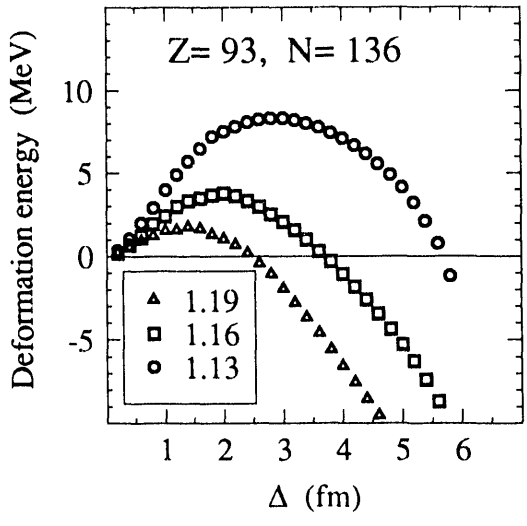

Fig. 1. This figure shows the fission barrier plots for the nucleus ^{229}Np. It illustrates the effect on the barrier height of changing the radius parameter r_0 while (approximately) preserving the fit to ground state masses.

The Thomas-Fermi treatment works well in the bulk region of the nucleus but becomes less accurate in the surface in the sense that it allows no penetration of the particles into classically forbidden regions of space. In heavy nuclei a significant fraction of the matter forms a quantal halo of material contributing positive density but negative kinetic energy density. One consequence of the presence of a fringe of negative kinetic energy in the outer layers of the surface is that such a surface should be easier to deform. As a result, the calculated fission barriers should be lowered by the presence of the halo, possibly removing the above mentioned discrepancy.

Footnotes and References

*Prepared for presentation at "Eighth Winter Workshop on Nuclear Dynamics,Jackson Hole, Wyoming, January 18-25, 1992."

1. W.D. Myers and W.J. Swiatecki, *Ann. Phys. (N.Y.)* **204**, 401 (1990).

2. W.D. Myers and W.J. Swiatecki, *Ann. Phys. (N.Y.)* **211**, 292 (1991).

3. P. Moller, private communication, March 1990.

The Coulomb Redistribution Energy as Revealed by a Refined Study of Nuclear Masses*

P. Möller†, J.R. Nix†, W.D. Myers and W.J. Swiatecki

The Macroscopic-microscopic approach to the calculation of nuclear masses has been further refined through the inclusion of ε_3 and ε_6 shape degrees of freedom. Most of the systematic discrepancies that previously existed for heavy nuclei have been eliminated. The agreement is so close that the effect of turning on and off the Coulomb redistribution terms in the Finite-Range Droplet Model can be clearly discerned, thus confirming the contribution of this physical effect to nuclear stability. Models without the higher-order terms of the Finite-Range Droplet Model that we investigate here, are clearly inferior in the heavy-element region.

Footnotes and References

*Abstract of LANL Preprint LA-UR-91-2999, Sept. 10, 1991. To be published in Nuclear Physics

† Los Alamos National Laboratory

Droplet-Model Electric Dipole Moments*

W.D. Myers and W.J. Swiatecki

In the recent review article by A. Aberg, H. Flocard and W. Nazarewicz[1], experimental and theoretical information on nuclear dipole moments is discussed in Section 6.3 in terms of a sum of microscopic and macroscopic contributions. The authors conclude as follows:

"The macroscopic contribution to the dipole moment has been estimated within the droplet model by Dorso et al. and has turned out to be negligible. This conclusion, however, has recently been questioned by Denisov whose result is consistent with the previous estimate of Strutinski. On the other hand, the values extracted from experiment are much smaller. From this point of view the question of the magnitude of the liquid drop dipole moment is still open. The shell-correction calculations provide an overall agreement with experimental data."

In the present paper we hope to have shown that Denisov's[2] criticism of the result of Dorso et al.[3] is not justified. This should help clarify the relation of experimental and theoretical aspects of nuclear dipole moments.

Footnotes and References

*Conclusion section of the paper published in *Nucl. Phys.* **A531** (1991) 93-96

1. S. Aberg, H. Flocard and W. Nazarewicz, *Ann. Rev. Nucl. Part. Sci.* **40** (Dec., 1990)

2. V. Denisov, *Yadernaya Fizika* (Journal of Nuclear Physics) **49** (1989) 644.

3. C.D. Dorso, W.D. Myers and W.J. Swiatecki, *Nucl. Phys.* **A451** (1986) 189.

A Modified Thomas-Fermi Treatment of Nuclei*

W.J. Swiatecki

An improved nuclear Thomas-Fermi theory is studied in which, rather than adding density-gradient corrections to the standard expression for the kinetic-energy density (proportional to $\rho^{5/3}$, where ρ is the density) one simply modifies this $\rho^{5/3}$ function to reflect the fact that the kinetic energy density becomes negative for small values of ρ when, in a typical nuclear problem, one is dealing with the outer fringes of the surface region. The net result of this study is simply stated: in order to find the density associated with a given nuclear potential, one exponentiates this potential instead of raising its depth with respect to the chemical potential to the three-halves power, as in the standard treatment. An improved description of the nuclear surface profile is obtained, including the quantal halo in the classically forbidden region. But since density derivatives are not involved, there is no need to solve a partial differential equation in order to find the density.

Footnotes and References

*Abstract of LBL Preprint LBL-31582, August 30, 1991. Submitted to Nuclear Physics

Order, Chaos and Nuclear Dynamics*

J. Blocki,† J.-J. Shi‡ and W.J. Swiatecki

The relation between the order-to-chaos transition in the dynamics of independent classical particles in a container, and the transition from an elastic to a dissipative response of the container to shape changes, is studied by means of computer simulations. The validity of the wall formula for energy dissipation is confirmed in the case of containers whose surfaces are rippled according to Legendre Polynomials P_3, P_4, P_5, P_6, in which case the particle trajectories are largely chaotic, as revealed by Poincaré sections in phase space. The opposite limit of an elastic response is illustrated by means of spheroidal containers of various eccentricities, for which the particle trajectories are integrable and the phase space is foliated by tori. Fission-like deformations are also considered, for which the response of the container changes from elastic to dissipative with increasing deformation. Idealized giant-dipole oscillations of the gas are studied for spherical as well as deformed containers. A generalization of the wall formula valid for long times (i.e., for arbitrarily large excitations of the gas) is constructed. The principal lesson of these studies is that a gas of independent particles in a time-dependent container does not behave at all like a gas.

Footnotes and References

*Abstract of LBL Preprint LBL-31563, July 1987, revised November 1991.

†Institute for Nuclear Studies, Swierk, Poland

‡Institute of Atomic Energy, Beijing, China

A Universal Asymptotic Velocity Distribution for Independent Particles in a Time-Dependent Irregular Container*

C. Jarzynski and W.J. Swiatecki

We show that the velocity distribution f(v) for a gas of non-interacting particles bouncing around in a deforming irregular container of fixed volume tends to a universal function independent of its original form and of the container's shape or time evolution. This function turns out to be the *exponential* velocity distribution $f(v) \propto e^{-v/c}$. This may be contrasted with the *gaussian* Maxwell-Boltzmann distribution appropriate in the case of a gas of *interacting* particles.

Footnotes and References

*Abstract of LBL Preprint LBL-31771, January 9, 1992.

From Ground State to Fission Fragments: A Complex, Multi-Dimensional Multi-Path Problem*

P. Möller,† J.R. Nix‡ and W.J. Swiatecki

Experimental results on the fission properties of nuclei close to ^{264}Fm show sudden and large changes with a change of only one or two neutrons or protons. The nucleus ^{258}Fm, for instance, undergoes symmetric fission with a half-life of about 0.4 ms and a kinetic-energy distribution peaked at about 235 MeV whereas ^{256}Fm undergoes asymmetric fission with a half-life of about 3 h and a kinetic-energy distribution peaked at about 200 MeV. Qualitatively, these sudden changes have been postulated to be due to the emergence of fragment shells in symmetric-fission products close to ^{132}Sn. Here we present a quantitative calculation that shows where high-kinetic-energy symmetric fission occurs and why it is associated with a sudden and large decrease in fission half-lives. We base our study on calculations of potential-energy surfaces in the macroscopic-microscopic model and a semi-empirical model for the nuclear inertia. For the macroscopic part we use a Yukawa-plus-exponential (finite-range) model and for the microscopic part a folded-Yukawa (diffuse-surface) single-particle potential. We use the three-quadratic-surface parameterization to generate the shapes for which the potential-energy surfaces are calculated.

We present the results of the calculations in terms of potential-energy surfaces and fission half-lives for heavy even nuclei. The surfaces are displayed in the form of contour diagrams as functions of two moments of the shape. They clearly show the appearance of a second fission valley, which leads to scission configurations close to two touching spheres, for fissioning systems in the vicinity of ^{264}Fm. Fission through this new valley leads to much shorter fission half-lives than fission through the old valley.

Footnotes and References

*Prepared for submission to Specialists' Meeting on Physics and Engineering of Fission, Kyoto University Research Reactor Institute, Kumatori-cho, Osaka, January 7, 1992.

†P. Möller Scientific Computing and Graphics, P.O. Box 1440, Los Alamos, NM 87544, USA

‡Theoretical Division, Los Alamos National Laboratory, Los Alamos, NM 87545

Alder-Winther-DeBoer Method applied to Diabolical Two-neutron Transfer*

L. F. Canto, R. Donangelo M. W. Guidry A. R. Farhan, J. O. Rasmussen, P. Ring, and M. A. Stoyer

Nikam *et al.*[1] showed that the two-neutron transfer matrix elements between yrast states in deformed heavy-ion transfer reactions might cross zero and become negative for higher spins.

In this paper we improve the computational methods of calculating the actual effect on final rotational state population.

First, we adapt the Alder-Winther-deBoer semiclassical method of integrating time-dependent Schroedinger equations in the amplitudes of the various rotational states, allowing for transfer by a transformation matrix on the amplitudes at the distance of closest approach. In this method we can put in realistic nuclear rotational energies and take into account the adiabaticity of the collision process; the departures from sudden approximation are seen to be great for Pb on rare earths, and they mean that the diabolic phase effects manifest themselves in lower-spin rotational states than expected.

Second, we use much more detailed information on the structure of the intrinsic wavefunction of the target in the diabolic region, by considering angular form factors.

Third, we take into account in the calculation of the transfer process not only the diagonal transition not changing spin, but also the off-diagonal transitions which change spin during transfer.

To simplify the calculation we specialize to a direct head-on collision, which means only $M = 0$ values enter.

Subsequent to the publication of this paper in May, 1990, Dasso and Winther [2] showed that the introduction of the two lowest bands in both initial and final nuclei was important and reduced the size of the diabolic interference effect. Our refined calculations, also taking all these bands into account, are reported in the accompanying Annual Report "Diabolic Effects on Nuclear Rotational State Population in Two-Neutron Transfer."

Footnotes and References

*Prepared for *Phys. Lett. B* **241**, *295 (1990)*.

[1] R. S. Nikam et al. Z. Phys. A **234**, 241 (1986).

Footnotes and References

[2] C. H. Dasso, and A. Winther, Phys. Lett. **242b**, 323 (1990).

Diabolic Effects on Nuclear Rotational State Population in Two-Neutron Transfer*

L. F. Canto, P. Ring, Y. Sun, J. O. Rasmussen, S. Y. Chu, and M. A. Stoyer

Recently, Dasso and Winther[1] improved the theoretical treatment of two-neutron transfer between heavy ions. The population of rotational band structures in the spheroidal target nucleus using a spherical projectile was considered. Their enhancement over previous theoretical work was the inclusion of the yrare along with the yrast band in the spheroidal A and $A+2$ nuclei. That is, they included the aligned band in addition to the ground band in the calculations. In earlier publications[2] [3] [4], an interference in the heavy-ion two-neutron transfer was noted and associated with a Berry phase[5] that manifests itself when two-neutron transfer paths lie on both sides of a diabolic point in the plane of particle number vs. angular momentum. Theoretical estimates of rotational state population patterns for such systems as Pb on rare earth nuclei indicated a substantial dependence on this interference, but our earlier theoretical work[6] only included the lowest (*i.e.*, yrast) levels in initial and final nucleus.

In this paper we calculate 2n transfer with ground and aligned bands. Fig. 1 shows our predicted gamma intensities in ^{154}Gd for the ^{206}Pb + ^{156}Gd $\rightarrow$ ^{208}Pb + ^{154}Gd reaction at 180° at the barrier energy. We qualitatively agree with Dasso and Winther that Berry-phase effects in 2n transfer are more subtle than first thought. Inclusion of the yrare band in theory is essential. There are features of their bandmixing model though that need further study. We now know that Berry interference effects are best sought where initial and final nuclei lie on opposite sides of a diabolic point but neither nucleus is too close to diabolic. The Hf cases that we first calculated have that appeal, but they have other experimental difficulties.

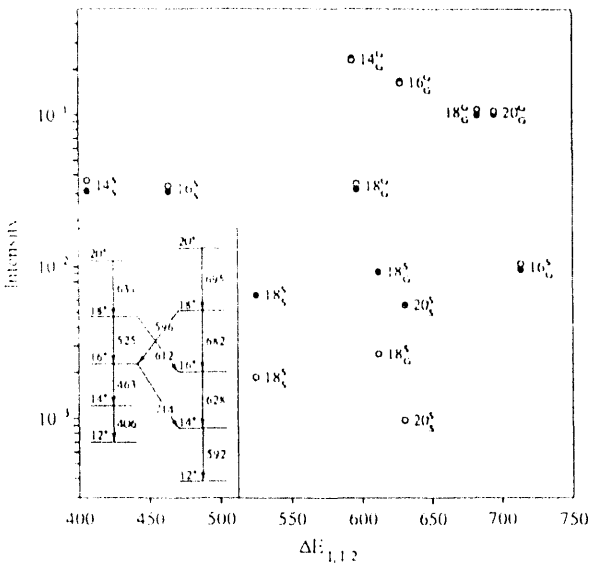

Fig. 1. Our theoretical relative intensities of gamma rays depopulating ^{154}Gd in the diabolic (•) and non-diabolic(o) cases. The points are labeled with the initial-state spin I and superscripts and subscripts for initial and final states, respectively. The letters G and S represent the ground and super band, respectively. The energy level inset is from the paper of Morrison, *et al.*, [7] with the ground band on the right and the superband (aligned band) on the left.

Footnotes and References

*Prepared for *Phys. Rev. C*, submitted Feb 18, 1992.

[1] C. H. Dasso, A. Winther, *Phys. Lett.* **242B**, 323 (1990).

[2] R. S. Nikam, P. Ring, L. F. Canto, *Z. Phys. A* **324**, 241 (1986).

[3] C. Price, H. Esbensen, S. Landowne, *Phys. Lett. B* **197** 15 (1987).

[4] Y. Sun, P. Ring, R. S. Nikam, *Z. Phys. A* **339**, 51 (1991).

[5] M. V. Berry, *Proc. R. Soc. (London) A* **392** 45 (1984).

[6] L. F. Canto, R. Donangelo, J. O. Rasmussen, P. Ring, M. A. Stoyer, *Phys. Lett. B* **248** 10 (1990).

Footnotes and References

[7] J. D. Morrison, J. Simpson, M. A. Riley, P. D. Forsyth, D. Howe, J. F. Sharpey-Schafer, *J. Phys. G: Nucl. Part. Phys.* **15**, 1871 (1989).

Relativistic Transport Theory for Hadronic Matter*†

Shun-Jin Wang, Bao-An Li, Wolfgang Bauer, and Jorgen Randrup

We have derived a set of coupled kinetic equations for nucleons, deltas, and pions, which are the main constituents of the hadronic matter formed in relativistic nuclear collisions. These equations reflect the physics of relativistic nuclear collisions in an instructive manner. Moreover, the approximate solution of the equations is possible with present computers. Our derivation is rather similar to the approach taken in Ref.[1], but we go beyond that work by including both delta-resonances and dynamical pions, which are expected to be significant at relativistic energies. The framework for describing nuclear reactions is extended from the baryon dynamics to the hadron dynamics level.

First, we construct the Hamiltonian for the hadronic matter, starting from the effective Lagrangian density containing $\Delta-$, $\sigma-$, $\omega-$, and $\pi-$mesons, as well as the minimum coupling between them. We reduce the dynamics to the baryonic level, by treating the pions as contributing to the potentials only, and we derive the equations of motion for the density matrix and the correlation functions for nucleons and deltas. Then we extend the baryon dynamics to hadron dynamics by introducing an independent dynamical pion field, and we obtain equations of motion for the density matrix of nucleons, deltas, and pions, as well as the pion-baryon interaction vertex function. Subsequently, we make Wigner transformations of these equations and obtain a set of transport equations for the phase-space distribution functions for baryons and dynamical pions. These equations contain a Vlasov term of the usual form and baryon-baryon, baryon-pion collision terms. The coupled transport equations are as follows:

$$\partial_t f_b(x,p) + (\Pi^i/E_b^*(p))\nabla_i^x f_b(x,p) - (\Pi^\mu/E_b^*(p))\nabla_i^x U_\mu(x)\nabla_p^i f_b(x,p) + (M_b^*/E_b^*(p))\nabla_i^x U_s \nabla_p^i f_b(x,p)$$
$$= I_{bb}^b(x,p) + I_{b\pi}^b(x,p).$$

$$\partial_t f_\pi(x,k) + \left(k\cdot\nabla^x/E_\pi(k)\right) f_\pi(x,k) = I_{b\pi}^\pi(x,k).$$

Footnotes and References

*Published in *Ann. Phys.*, **209**, 251 (1991)

†permanent address of S. J. Wang, Dept. of Modern Phys., Lanzhou Univ., Lanzhou, 730000, P. R.China

[1] S. J. Wang, and W. Cassing, Nucl. Phys. A**495**, 371c (1989); W. Cassing, and S. J. Wang, Z. Phys. A**337**, 1 (1990)

Many-Body Correlation Dynamics Within a Green's Function Formalism*†

Shun-Jin Wang and Wei Zuo

We have generalized the method used in the correlation dynamics of density matrix and established a set of equations of motion for many-body correlation green's functions in the non-relativistic case. These non-linear and coupled equations of motion describe the dynamical evolution of correlation green's functions of different order, and reflect how interactions produce many-body correlations and how different kinds of correlations interweave. The advantage of the present formalism resides in that it is expanded not in terms of the interaction strength but in terms of the many-body correlations, and therefore it is a non-perturbative approach providing a natural truncation scheme with respect to the order of correlations. It is shown that the non-perturbative results of the conventional green's function theory are included in the present formalism as two limiting cases (the so-called ladder diagram limit and ring diagram limit). In general, the correlation dynamics of green's function provides a unified and systematic method to treat quantum many-body problems in a non-perturbative manner. The correlation dynamics of green's function is a multi-time generalization of the correlation dynamics of density matrix and contains the latter as an equal time limit. For an interacting fermion system, the Hamiltonian can be written as Eq.(1). The n-body green's function $G^{(n)}$ is defined as usual and the correlation green's function is defined by the separation equation, Eq.(2). The equations of motion for correlation green's functions are Eq.(3). Under the equal time limit, the correlation dynamics of green's function reduces to the correlation dynamics of density matrix. The lowest order truncation is simply to neglect all many-body correlations and leads to Dyson equation in the mean field approximation. A better approximation is to keep two-body correlations and neglect more than three-body correlations. This truncation leads to the two-body dynamics which has two limits. The ladder diagram limit yields Bethe-Salpeter equation: $\hat{\Gamma} = \hat{V} + i\hat{V}GG\hat{\Gamma}$. And the ring diagram limit results in the equation of motion for polarization effect: $D = D^0 + D^0\hat{V}D$, $\hat{U}_r = \hat{V} + \hat{V}D\hat{V}$. [1] [2] [3]

$$\hat{H} = \int \psi^\dagger(\mathbf{x},t)\hat{t}(\mathbf{x})\psi(\mathbf{x},t)d^3\mathbf{x} + \int\int \psi^\dagger(\mathbf{x},t)\psi^\dagger(\mathbf{x}',t)\hat{v}(\mathbf{x},\mathbf{x}')\psi(\mathbf{x}',t)\psi(\mathbf{x},t)d^3\mathbf{x}d^3\mathbf{x}' \tag{1}$$

$$G_c^{(n)}(1,...n;1',...n') = G^{(n)}(1,...n;1',...n') - \hat{A}p_{(1'...n')}\hat{S}p_{(2,...n;2',...n')}\sum_{k=1}^{n-1} G_c^{(k)}G^{(n-k)} \tag{2}$$

$$\begin{aligned}
&[i\partial_{t_1} - \hat{t}(1)]G(1;1') = \delta^{(4)}(1,1') - i\int d2\hat{V}(1,2)[G(1;1')G(2;2^+) - G(1;2)G(2;1') + G_c^{(2)}(1,2;1',2^+)], (n=1)\\
&[i\partial_{t_1} - \hat{t}(1)]G_c^{(n)} = -i[Tr_{(n+1)'=(n+1)^+}\hat{V}(1,n+1)AS_{(n+1)}\sum\sum\sum_{k\geq l\geq m=0} G_c^{(k)}G_c^{(l)}G_c^{(m)}\delta_{k+l+m,n+1}]_L, (n\geq 2)
\end{aligned} \tag{3}$$

Footnotes and References

*Prepared for *Ann. Phys.*, submitted Mar 3, 1992

†Permanent address, Dept. of Modern Phys., Lanzhou Univ., Lanzhou, 730000, P. R. China

Footnotes and References

[1] P. C. Martin and J. Schwinger, *Phys. Rev.*, **115** (1959),1342; J. Schwinger, *J. Math. Phys.*, **9** (1961), 407.

[2] S. J. Wang and W. Cassing, *Ann. Phys.*, **159** 328 (1985).

[3] S. J. Wang, B. A. Li, W. Bauer and J. Randrup, *Ann. Phys.*, **209** 251 (1991).

Nuclear Stopping Power at the AGS

Scott Chapman and Miklos Gyulassy

Recently, there have been many claims in the literature that full nuclear stopping is realized in 15 AGeV central Si+Au collisions at the AGS[1]. However, we have pointed out[2] that the published E802 spectrometer data[3] cast doubt on this belief, since in fact none of the present models can reproduce the spectrometer normalization (fig. 1). Moreover, if the spectrometer dN/dy are normalized correctly, then these data are more indicative of a surprising degree of nuclear transparency.

We developed a model independent fit to the spectrometer data[4] which showed that if systematic errors do not cause more than a 30% suppression of proton and pion yields, then 4-momentum and baryon conservation laws imply that at least 11 out of 28 projectile nucleons suffer less than one unit of rapidity loss during a central Si+Au collision. We also developed a double firestreak and a multicomponent model in order to quantify the degree of transparency needed to reproduce the spectrometer data, and nuclear stopping lengths of 17-26 fm were found. On the other hand, the high rapidity data from E810[5] and E814[6] as well as preliminary $dN/d\eta$ data from E802[7] and E814[8] are consistent with models incorporating the expected degree of nuclear stopping. Until the discrepancies between all data sets are resolved, conclusions about full nuclear stopping remain premature.

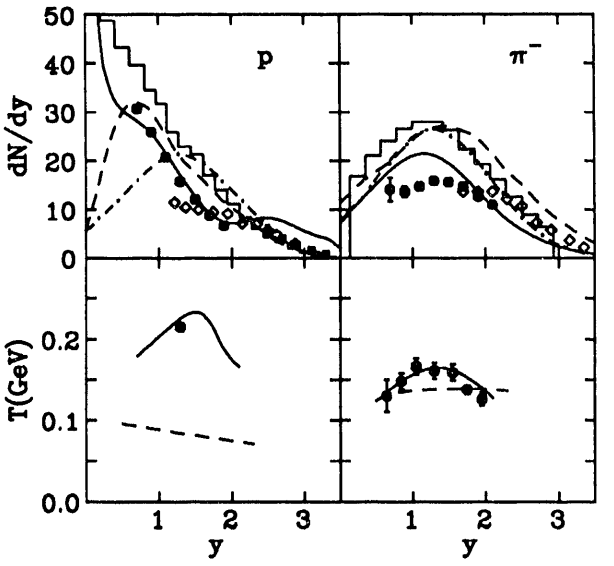

Fig. 1. Attila[9] (dashed), RQMD[10] (histogram), Landau fireball[11] (dot-dashed) and a multicomponent model with a stopping length of 26 fm (solid) are compared to E802 (solid dots), E810 (diamonds), and E814 (open circles).

Footnotes and References

[1] For a good list see N. Amelin et al, PRC**44** (1991) 1541.
[2] S. Chapman and M. Gyulassy, PRL**67** (1991) 1210.
[3] T. Abbott et al (E802 collab), Phys. Rev. Lett. 64 (1990) 847; Phys. Rev. Lett. 66 (1991) 1567.
[4] LBL preprint 31475 submitted to PRC.
[5] W. A. Love et al (E810 collab), Nucl. Phys. A525 (1991) 601c.
[6] J. Barrette et al (E814 collab), Phys. Rev. Lett. 64 (1990) 1219; P. Braun-Munzinger, Proc. QM91.
[7] F. Videbaek, Proc. of HIPAGS (1990), BNL-44911 and priv. comm.
[8] W. E. Cleland et al., Nucl. Phys. A525 (1991) 91c.

Footnotes and References

[9] M. Gyulassy, CERN-TH.4794 (1987), Proc. Balatonfured Conf. on Nuclear Physics (1987).
[10] H. Sorge et al., Phys. Rev. Lett. 68 (1992) 286; UFTP preprint 263 (1991).
[11] J. Stachel, and P. Braun-Munzinger, Phys. Lett. B216 (1989) 1; Nucl. Phys. A498 (1989) 577c.

Quark Damping and Energy Loss in the High Temperature QCD*

M.H. Thoma and M. Gyulassy

The energy loss per unit length of high energy quarks in a quark-gluon plasma is calculated via PQCD. Unlike the damping rate, the energy loss is infrared, finite and surprisingly small.

Footnotes and References

*Abstract of Nuclear Physics B351 (1991) 491-506

High P_T Probes of Nuclear Collisions*

M. Gyulassy, M. Plumer[1], M. Thoma[2], and X.N. Wang[3]

Jet quenching in high energy nuclear collisions is shown to provide new information on the energy loss mechanisms in dense matter near the quark-gluon plasma transition. In addition it is shown that A dependence of the inclusive p_T spectra in $p + A$ provides novel constraints on gluon shadowing in nuclei.

Footnotes and References

*Abstract of LBL Preprint LBL-31002, July 1991, submitted to Nuclear Physics A.

[1]Department of Physics, Universitat Marburg, D-3550 Marburg/Lahn, Germany.

[2]Department of Physics T-30, Technical Universitat Munchen, D-8046 Garching, Germany.

[3]Department of Physics, Duke University, Durhan, NC 27706.

High Resolution Multiparticle Tracking without Preprocessing via Elastic Tracking*

M. Gyulassy and Magnus Harlander[1]

Elastic Tracking (ET) is applied to the problem of tracking noisy overlapping tracks in visual and electronic detectors. The method avoids the necessity of local preprocessing to find track centroids and utilizes global information provided by the detector to resolve small momentum differences between multiple overlapping tracks for applications such as pion interferometry.

Footnotes and References

*Abstract of LBL Preprint LBL-31276, November, 1991.

[1]Department of Physics T-30, Technical Universitat Munchen, D-8046 Garching, Germany.

Nuclear Transparency in 15 AGeV Si+Au Reactions*

S. Chapman and M. Gyulassy

Recent data on central Si+Au collisions at 15 AGeV are shown to imply an unexpected high degree of nuclear transparency. The paucity of observed midrapidity protons and pions suggests that up to one half of the projectile nucleons may lose less than one unit of rapidity after traversing 5-10 fm of nuclear matter.

Footnotes and References

*Abstract of Phys. Rev. Lett 67, 1210 (1991).

Elastic Tracking and Neural Network Algorithms for Complex Pattern Recognition*

M. Gyulassy and Magnus Harlander[1]

A new Elastic Tracking (ET) algorithm is proposed for finding tracks in very high multiplicity and noisy environments. It is based on a dynamical reinterpretation and generalization of the Radon transform and is related to elastic net algorithms for geometrical optimization. ET performs an adaptive nonlinear fit to noisy data with a variable number of tracks and is more efficient numerically than the traditional Radon or Hough transform method because it avoids binning of phase space and the costly search for valid minima. Spurious local minima are avoided in ET by introducing an iteration time dependent effective potential. The method is shown to be very robust to noise and measurement error and extends tracking capabilitities to much higher track densities than possible via local road finding or even the novel Denby-Peterson (DP) neural network tracking algorithms. A possible neural network implementation of ET is also discussed.

Footnotes and References

*Abstract of Comp. Phys. Comm. 66, 31 (1991).

[1]Department of Physics T-30, Technical Universitat Munchen, D-8046 Garching, Germany.

Pion Interferometry and Resonances in pp and AA Collisions*

S.S. Padula[1] *and M. Gyulassy*

We study the sensitivity of pion interferometry in *pp* and *p-bar p* collisions at ISR energies to the resonance abundance. We show that those data are not compatible with the full resonance fractions predicted by the Lund model. The preliminary S+S and O+Au data at 200 A GeV are, however, not incompatible with the Lund predictions, although their sensitivity to resonances is significantly weaker than in the *pp/p-bar p* case.

Footnotes and References

*Abstract of LBL preprint LBL-31607, December 10, 1991.

[1]Instituto de Física Teórica, UNESP, Rua Pamplona, 145-01405 São Paulo - SP, Brazil.

An Approach to the Relativistic Extended Thomas-Fermi Expansion for Green's Functions, Phase-Space Densities and Densities*

M.K. Weigel, S.Haddad † and D.Von-Eiff ‡

Since the pioneering work of Wigner [1] semiclassical approaches have been applied with great success. Generally the advantage of the semiclassical approach is the avoidance of wave function calculations by utilizing densities, which in many cases makes the calculations easier.

In recent years much interest has been put toward describing the nucleus as a relativistic system [2]. In this case one expects several complications due to the Dirac structure of the approach, which make the formalism more difficult than in the standard nonrelativistic theory.

In this contribution we present a pure algebraic method, which resembles the standard nonrelativistic scheme as described, for instance, by Grammaticos and Voros [3]. It involves only straightforward but tedious algebraic methods and the residuum calcules.

The basic quantity for the semiclassical expansion is the Wigner transform of the one-particle propagator, defined as

$$G(R,p) = \int d^4r e^{\frac{ipr}{\hbar}}(-i) * \\ < N|T(\psi(R+\frac{r}{2})\bar{\psi}(R-\frac{r}{2}))|N >$$

which obeys the Dyson equation in the mixed position-momentum representation. The relevant expansions of the G-functions, phase-space densities and densities are given by the following scheme:

$$G(\vec{R},p) = \hbar^4 \sum_{j=0}^{\infty} \hbar^j G^{(j)}(\vec{R},p),$$

$$n(\vec{R},\vec{p}) = \hbar^3 \sum_{j=0}^{\infty} \hbar^j \int \frac{dp_0}{2\pi i} e^{ip_0\eta} G^{(j)}(\vec{R},p),$$

$$n(\vec{R}) = \sum_{j=0}^{\infty} \hbar^j \int \frac{d^3p}{(2\pi)^3} n^{(j)}(\vec{R},\vec{p}).$$

These expansions are given explicitly up to second order in $\hbar$.

Footnotes and References

*LBL-31614, submitted to Physical Review C

†Sektion Physik der Ludwig-Maximilians-University of Munich, Am Coulombwall 1, W-8046 Garching, Germany

‡Fellow of the Deutscher Akademischer Austauschdienst

[1] E.Wigner, *Phys. Rev.* **40**, 749 (1932).

[2] L.S.Celenza and C.M.Shakin, "Relativistic Nuclear Physics", World Scientific, Singapore (1986).

[3] B.Grammaticos and A.Voros, *Ann. Phys. (N.Y.)* **123**, 359 (1979) and **129**, 153 (1980)

Neural network approach to process jet fragmentation information *

D.W. Dong and M. Gyulassy

An application of neurocomputing techniques of potential interest for RHIC experiments is to jet finding. In [1] [2] we developed a new method of jet analysis based on high pass neural filters which are much more robust to low p_T "noise" than conventional calorimetric methods.

Our motivation was two fold. First, conventional methods of jet analysis developed for pp collisions begin to fail in pA collisions due to the nuclear enhance background of low p_T particles and are expected to fail completely for future applications to nuclear collisions where up to 10^4 low p_T particles may be produced per collision. Nevertheless, jet analysis may be of special interest for AA reactions as a novel tool for probing the energy loss mechanisms and infrared correlation scales in ultra-dense matter. Second, recent advances in neurocomputing techniques for complex pattern recognition problems suggest a novel approach to this problem.

In particular, we apply Feed Forward Network (FFN) methods to jet analysis. We show that a high pass linear neural filter can be trained using Monte Carlo event generators or pp data to provide a nearly bias free estimator of the jet energy distribution even in the presence of a very high level of low p_T "noise". In addition, we show that knowledge of the neural response function allows us to deconvolute the filtered jet distribution and recover the primordial jet distribution to a surprising high degree of accuracy.

Shown in Fig. 1 is the optimal neural filtered jet distribution (dotted) compared to the input QCD distribution (solid line). We see that below 20 GeV, the neural filter significantly underestimates the QCD distribution, but that the distortions become small above that energy (long dotted). The filter noise (dashed) is assumed to be the square root of the number of counts. The square symbols indicate the result of deconvoluting the filter response. The statistical errors (long dashed) of the deconvolution are 1% to 7% and the deconvoluted network response is within 10% of the desired input. We see that the deconvolution method accurately corrects for the distortions caused by the neural filter.

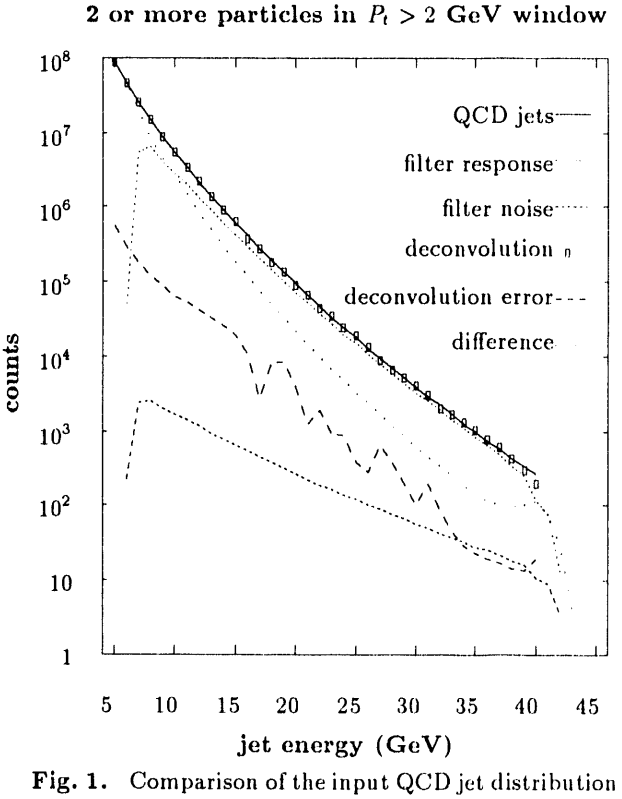

Fig. 1. Comparison of the input QCD jet distribution (solid) to the network response distribution (dotted) and the final deconvoluted network response (boxes).

Footnotes and References

*Submitted to IJCNN92

[1] D.W. Dong and M. Gyulassy (1991) Neural Filters for Jet Analysis. *LBL-31560*

[2] M. Gyulassy, D.W. Dong, and M. Harlander (1991) Neurocomputing Methods for Pattern Recognition in Nuclear Physics *Proc. 2nd Int. Workshop on Software Eng., A.I., and Expert Sys. for High En. and Nucl. Phys., L'Agelonde, France*

Seminars

Nuclear Science Division

Dr. L. Frankfurt University of Illinois	Color Screening from Nuclear Shadowing from eA to AA Collisions	January 8, 1991
Sidney Bludman University of Pennsylvania	Astrophysical Constraints on Neutrino Masses and Lifetimes	March 11, 1991
Dieter Fick University of Marburg	Nuclear Interaction with Polarized Heavy Ions	March 13, 1991
Salvador Gil TANDAR, Buenos Aires	Spin Distributions in Near-Barrier Fusion Reactions	March 15, 1991
Kevin Coulter Argonne National Laboratory	Optical Trapping of Radioactive Sodium: A Proposed Search for Right-Handed Currents	March 29, 1991
Helmut Bokemeyer GSI, Darmstadt	Positron Lines in Heavy Ion Collisions Observed in EPOS Experiments	May 6, 1991
Song Quan Shang SUNY, Stony Brook	Sub-Doppler Laser Cooling of Rb Atoms	May 10, 1991
Juha Äystö University of Jyväskylä	Symmetric Fission and Study of Extremely Neutron-Rich Nuclei	May 15, 1991
Pavel Povinec Comenius University Bratislava	Cosmogenic Radionuclide Variation	May 28, 1991
Peter Braun-Munzinger SUNY Stony Brook	Experimental Results on Nuclear Stopping and Transparency in Relativistic Nuclear Collisions from Experiment 814 at the AGS	May 28, 1991
Patricia Roussel-Chomaz SEPN, Centre D'Études Nucleaires, Saclay	Complex Fragment Emission in 139 La-Induced Reactions at Intermediate Energy	July 15, 1991
Ramon Wyss Oakridge National Laboratory	Bandcrossings in Superdeformed Nuclei	July 19, 1991

Roy Lemmon Australia National University Canberra, Australia	Experimental Determination of the Fusion Barrier Distributions for the $^{154}Sm + ^{16}O$ and $^{186}W + ^{16}O$ Reactions	July 23, 1991
Marina Galmarini University of Milano, Italy	Nonequilibrium Complex Fragment Emission in Heavy Ion Reactions	July 24, 1991
Rainer Hasse GSI, Darmstadt	Coulomb Crystals in Accelerator Beams	July 26, 1991
John Bigelow Oak Ridge National Laboratory	The Advanced Neutron Source	July 29, 1991
Peter Moller Lund University, Sweden	New Mass Predictions and their Importance for (Super) Heavy Elements	July 31, 1991
Stefan Frauendorf Niels Bohr Institute	Tilted Cranking	August 5,1991
Peter Seyboth Max Planck Institute, Munich	Recent Results from NA35 on Strangeness, HBT and Intermittency in 200 GeV/N Nucleus-Nucleus Collisions	August 7, 1991
Johann Rafelski University of Arizona	Strange Anti-Baryons from the Quark-Gluon Plasma	August 9, 1991
Paul Doll Kernforschunszentrum Karlsruhe, Germany	Status of the Karlsruhe Air-Shower Experiment: KASCADE	August 23, 1991
Declan Keane Kent State University	High Order Multiparticle Correlations in Heavy Ion Collisions	August 26, 1991
Daniel Bes Comision Nacional de Energia Atomica, Argentina	The BRST Treatment of Collective Coordinates	September 11,1991
Davor Palle Ruder Boskovic Institute Zagreb, Yugoslavia	Non-Contractible Space as the Symmetry Breaking Mechanism Collisions	September 17,1991

Hans Specht Heidelberg	Lepton Pair Production in High Energy Hadron and Nuclear Collisions	September 24, 1991
Klaus Dietrich Technical University of Munich Garching, Germany	Giant Diapole Vibrations of Fission Fragments and Emitted Electromagnetic Radiation	September 30, 1991
John Simpson Daresbury Laboratory, England	Towards Unpaired Nuclear Spectroscopy with Large Gamma-ray Arrays	October 7, 1991
I-Yang Lee Oakridge National Laboratory	High-Fold Coincidence Experiments and the Impact of New Detector Arrays	October 14, 1991
Jose Bacelar Kernfysisch Versneller Institute The Netherlands	The Decay of the Giant Dipole Resonance Built on Excited Nuclear States	October 16, 1991
Augusto Machiavelli Lawrence Berkeley Laboratory	Superdeformed Nuclei at High Spins	October 28, 1991
Paul Fallon Oliver Lodge Laboratory University of Liverpool, UK	From Superdeformation to Super Rigidity	October 30, 1991
Chang-Hong Yu University of Tennessee	High Spin Phenomena and Nuclear Shapes in the Rare Earth Region	November 4, 1991
Christoph Ender University of Heidelberg	From Eurogram to Euroball: Rethinking the Electronics	November 15, 1991
Steve Koonin Caltech	Environmental Fine Structure in Low Energy Beta Spectra and 17-keV Neutrinos	December 2, 1991
Homer E. Conzett Lawrence Berkeley Laboratory	A Sensitive New Test of Time-Reversal Invariance	December 9, 1991
Isao Tanihata RIKEN	Study of the ^{8}Li (a, n) ^{11}B Reaction at Energies Relevant to Astrophysical Interests (Big Bang Nucleosynthesis)	December 12, 1991

Fan Zhu Michigan State University	Two-Particle Correlation Function and Multiplicity-Selected Excited State Populations	December 16, 1991

Nuclear Theory

Antje Hoering Max-Planck Inst. Heidelberg	Gamma Decay of Giant Resonances in Pre-Equilibrium Nuclear Reactions in a Statistical Approach	10 Oct 90
Wolfgang Bauer NSCL/MSU	Decay of Ordered and Chaotic Systems	15 Oct 90
Thomas Guhr Max-Planck Inst.	Isospin Mixing, Breaking of Quantum Numbers and Fluctuation Properties	17 Oct 90
Gyuri Wolf Univ. of Giessen	Dilepton Production in Heavy-Ion Collisions	24 Oct 90
Markus Thoma Munich/LBL	Summary of the First Month of the Nuclear Theory Institute Fall '90	7 Nov 90
Thomas Hoch TH Darmstadt	Study of Nuclear Ground State Properties in the Framework of a Relativistic Point Coupling Model	9 Nov 90
Matthias Grabiak LBL	Report on the Nuclear Theory Institute, November 1990	11 Dec 90
Werner Köpf Tech. Univ., Münich	Y-Scaling in the Deuteron	11 Jan 91
Steve Tomsovic Univ. of Washington	A Test of Time Reversal Non-Invariance in Nucleon-Nucleon Interactions	15 Jan 91
Matthias Grabiak LBL	Interacting Nielsen-Olesen Vortices	18 Jan 91
Per Dahlquist NORDITA	Symbolic Dynamics in the XY-Potential	21 Jan 91
Fridolin Weber Munich/LBL	Part I: Equation of State Hadronic Matter and Neutron Stars	24 Jan 91

Fridolin Weber Munich/LBL	Part II: Neutron Stars	25 Jan 91
Massimo di Toro Univ. of Catania	Giant Resonances in Hot Nuclei	6 Feb 91
Norman Glendenning LBL	Phase Transitions of the Second Kind (not order): Consequences for star structure and for the quark transition in laboratory experiments	7 Feb 91
C. Yannouleas VA Commonwealth Univ., Richmond	From the Supported to the Unsupported: How Metal Clusters Absorb Light	15 Feb 91
Markus Thoma LBL/Munich	Energy Loss of a Heavy Fermion in a Hot QED Plasma	19 Feb 91
Xin-Nian Wang LBL	Aspects of Jets in Relativistic Heavy Ion Collisions	26 Feb 91
Andreas von Keitz Univ. of Frankfurt	High Density Matter at RHIC	6 Mar 91
Dirk H. Rischke Univ. of Frankfurt	The Nuclear Matter Equation of State for Interacting Hadrons with Finite Eigenvolume	7 Mar 91
Philippe Chomaz LBL/IPN, Orsary	Lattice Calculation of the Fluctuations in Nuclear Dynamics	19 Mar 91
Gil Gatoff Oak Ridge	Chromodynamics in the Quark-Gluon Plasma	14 May 91
Biswarup Banerjee Tata Institute	Diffusion of Neutrinos in Presupernova Stars	13 June 91
José A. Casado	Pion Interferometry as a Probe of Time Varying Sources	2 July 91

Markus Thoma Technical University, Munich	Interaction Rate and Energy Loss of High Energy Patron in the QGP and Viscosity of the QGP	8 July 91
Francois Chapelle LBL/Ecole Polytechnique	Fluctuations in Nuclear Dynamics: Criticism of the Different Available Methods	10 July 91
Thomas Vetter LBL/Univ. Giessen	N-Body Interactions in High Energy Reactions	15 July 91
Sidney Bludman LBL	Role of the Nuclear Equation of State in Supernova Explosions	24 July 91
Georg Peilert Universität Frankfurt	QMD + SMM: A Hybrid Model for the Description of Multi-fragmentation in Heavy Ion Collisions	29 July 91
Xi-Jun Qiu Institute for Nuclear Research PRC	Rho Meson in Dense Matter	20 Aug 91
Steve Moszkowski UCLA	Identical Bands in Superdeformed Nuclei	21 Aug 91
Detlef Von-Eiff Ludwig-Maximilian Universität, Munich	Relativistic Extended Thomas-Fermi Description of Finite Nuclei	27 Aug 91
Dawei Dong, LBL	Linear Neural Predictor for Estimating Jet Energies from Leading Particle Spectra	29 Aug 91
Avraham Rinat Weizmann, Inst. Israel	Inclusive eA Scattering in the Few GeV Range	16 Sep 91
Prof. W. Nörenberg GSI	On Quatum Chaos in a Many-Body System	23 Sep 91

Author Index

Author Index

END

DATE FILMED

12/9/92